UNIVERSITÄT BERN

Graduate School for Cellular and Biomedical Sciences

University of Bern

Towards unidirectional reconstitution of membrane proteins into liposomes

PhD Thesis submitted by

Andrea Marco Amati

from **Worb BE**

for the degree of

PhD in Biochemistry & Molecular Biology

Supervisor

Prof. Dr. Christoph von Ballmoos

Department of Chemistry and Biochemistry

Faculty of Science of the University of Bern

Co-advisor

PD Dr. Manfred Heller

Department for BioMedical Research

Faculty of Medicine of the University of Bern

Accepted by the Faculty of Medicine, the Faculty of Science and the Vetsuisse Faculty of the University of Bern at the request of the Graduate School for Cellular and Biomedical Sciences

Bern, Dean of the Faculty of Medicine

Bern, Dean of the Faculty of Science

Bern, Dean of the Vetsuisse Faculty Bern

Everything should be made as simple as possible, but not simpler.
— *Albert Einstein*

— *To my loved ones.*

I Acknowledgements.

Even though there's just my name written on the front page, this thesis was a team effort. Without the great help and support of numerous people throughout my PhD I would have ruefully failed.

First of all I thank Christoph von Ballmoos for having faith in me and delegating this straight-forward-project to me. At least that's what we were thinking until we had started. Anyway, we were proven horribly wrong – the perfect definition of science. Nevertheless, we never surrendered, and I am really grateful that your faith in me never fainted, even though we found ourselves quite frequently in bad, strange or puzzling situations concerning my project. We've had a damn funny start into our collaboration on a trip to Stockholm in fall 2014, and our relationship was probably also shaped later on by that start. I really appreciated your open-door policy and your advice, which certain times went ways beyond scientific questions. You taught me lots about membrane proteins, and your inner fire for science and your curiosity were inspiring, even in the most complicated moments. It was an honour to work in your lab!

Second, I thank all my coworkers within the notorious CvB group. When I came to this lab, there were only a few people working in Christoph's group, them being Linda Näsvik Öjemyr, Olivier Biner, Thomas Schick and Axel Meyrat. However, the group size eventually literally exploded and I've luckily got to know some very great folks.

Our first postdoc Linda was almost omniscient and not rarely my first contact for biochemical questions. Thank you for being patient with me, and probably even more important, for introducing the tradition of Fika in your lab. You may have left – but Fika has not!

Oli, Herr Schick, Axel and me became a conspiring unit on the trip to Stockholm already mentioned in the very beginning of my PhD (or even before). Oli and Schick I had already known from our mutual time during our bachelor's and master's studies. Unforgotten is our spontaneous trip to Marrakech, where we were accompanied also by Simone Graf and Stephan "Stifu" Kammer.

Thank you Dr. Oli the Üsserschwiizer for lots of hints concerning membrane proteins, but even more importantly, for being a good and reliable friend and for all our numerous discussions outside of any scientific field. It was also you who dragged me up to that damn Mönchsjochhütte just a few months after my back injury. I remember

how damn grateful I was for that Gipfelschnapps you offered me. Unforgotten is also your affection for funny names of beautiful places in the surroundings of Bern or the Emmental, as e. g. Lüderenalp, Gurnigel, Lueg or Chemmeribodä(-Bad).

Herr Schick, damn, where shall I start? Thank you for being a friend with lots of similar thoughts and interests. There would be lots of anecdotes to tell about our relationship, however, most of them we probably both can't recall anymore (whyever), or they would be too humiliating for one or both of us to be discussed in detail here, e. g. I just faintly remember a pool party or putatively dead bodies on the floor of a ship's lounge. Having you sitting next to me in the office was a guarantee for lots of fun. Not only was I always kept up-to-date regarding tennis, alpine skiing, or ice hockey, but you also promoted my skills in table tennis and beer pong.

Sensei Axel "Le Welsch", thank you for many funny late-night discussions concerning politics, literature (especially concerning Marquis de Sade), welsch mentality, or whatever topic we decided to philosophize on. Keep on fighting using your Shinai – we both know that once you will conquer the world.

Many thanks also to our former lab technician Sandra Schär. Thank you for helping me out with some very nasty stuff as e. g. cloning and other totally weird things. I will always be grateful to you for temporarily taking over and driving on my project during my absence. I am sure that we will meet again, either at some music or trucker festivals or at one of your dreaded girons.

I thank Simone Graf for all the time and fun as well as lots of (sometimes silly) discussions from the moment we first consciously met at the conference in Stockholm until Schick and me were promoted to be your personal bodyguards (Limited Inc.) in Marrakech and all the time thereafter. I always admired your omniscience in the fields of oxidases, transhydrogenases and many other damn fancy enzymes. Thank you for being my first place to go for questions regarding such enzyme's mechanisms, especially during the writing of my thesis.

Further, I thank Roman Mahler for first being an excellent bachelor's student and later for being an awesome new neighbour in the office after Oli and Herr Schick had left. You are really an awesome dude and quite a geeky genious! Thanks for your support regarding PyMOL-related questions. Many thanks also to our lab police officer Nicolas Dolder for his duty and his service to our entire lab. Next, thanks to Sabina Deutschmann for being a neat bench neighbour in the lab. Thank you also for all your help regarding your field of expertise; you were the one to put in order the mess in my brain regarding cloning. For Abbas Abou Hamdan, let me just switch to German: Vielen Dank für die gemeinsame Zeit und unsere spannenden Diskussionen.

Ich bewundere deinen Ehrgeiz und dein Tempo beim Erlernen der deutschen Sprache. Thanks to Meike Wieser for being my master's student; despite all the challenges we mastered it together. Many thanks to Philipp Müller for his competitiveness and for being an excellent bachelor's student for two weeks, to Lukas Rimle for being flabbergasted after lots of patter from my side, and thanks to Sarah Krummenacher for bringing some more lovely craziness to our lab (not that we would not have had enough thereof before you joined us, but anyway...). I am also thankful to our two latest master's students Stephan Berger and especially Stefan "Stony" Moning, whom I've supervised at least in the beginning of his time in our lab. I also thank the former lab members Aymar Ganguin, Martin Schori (fiiix!) and Tobias Blatter for being awesome enrichments to my time in the von Ballmoos lab.

Not only I could always rely on help of coworkers of my lab, but also from colleagues from other labs. Therefore, I thank Prof. em. Dr. S. Decurtins for hosting me in his lab to synthesize our trisNTA. Further, many thanks to Prof. Dr. J.-L. Reymond who welcomed me in his lab for the syntheses of Spy-peptides and trisNTA-Spy under the supervision of Dr. Sacha Javor. I would have had a very hard time without your help Sacha, thanks a lot for your patience, your advice and your tenacity. Next, many thanks to Prof. Dr. Achim Stocker for letting me use several devices. Many thanks also to his associates Stephan "Stifu" Kammer, Andreas "Andi" Hemmerle and John Sigrist, it was always a pleasure to discuss with you. John, thank you for proofreading my cover letters for job applications.

I further thank our in-house analytics services, i. e. the MS service provided by Prof. Dr. Stefan Schürch and his group and the NMR service provided by PD Dr. J. Furrer and his group. Special thanks there go to the crew of the MS service, namely Claudia Bühr, Urs Kämpfer and Simon Marti, for all their help.

Many thanks to Dr. Denis Maier for introducing me to the document preparation system LaTeX and for his patient help whenever I faced problems concerning the use of LaTeX during the writing of my thesis.

Next, many thanks to Dr. Oliver Birkholz from the lab of Prof. Dr. J. Piehler at the university of Osnabrück, Germany, for providing a sample of their version of trisNTA, and to Dr. Andrew Lees (Fina Biosolutions LLC, USA), for providing various samples of functionalized dextrans.

I also thank Prof. Dr. C. Largiadèr and PD Dr. M. Heller for being my mentor and my co-advisor at the GCB, respectively. Furthermore, my thank goes to Prof. Dr. Klaas Martinus Pos for assessing my thesis as external referee.

Further, working in an institute as the time-honoured DCB would not be as comfortable without the associates of the Werkstatt, Hausdienst and Materialausgabe. Thank you for providing your help and services, regardless of whatever crazy ideas I approached you with.

I also thank Christina Schüpbach and Beatrice Thönen for all their help regarding administrative questions during my PhD.

I am grateful to my former supervisors at Novartis, Dr. Steffen Renner and Dr. Pierre Farmer, for carrying on the work on the project in which I was involved prior to my PhD, eventually resulting in an awesome publication.

Special thank goes to the legendary Erich "Fuessbaugott" Hänzi for being a source of inspiration for persistence.

A big thank you to all the members of Burri's Ziegle, who were always there when I needed them in order to free my head from scientific thoughts and to get distracted.

Last but definitely not least at all, I wish to express my deep gratefulness to my family (Doris & Giancarlo, Sara) as well as to my beloved girlfriend Nicole, for always being there for me, for constantly supporting me during my PhD, and sometimes also for simply enduring me and my moods. Without all of you, I just really do not know how I would have managed to get to where I am right now. I love you all from the bottom of my heart!

II Abstract.

Investigating functions of membrane proteins (MPs) in their natural environment, i. e. in the membranes of various cellular compartments, is not straight forward, as these are packed with many other components which disturb direct measurement of the MP of interest, complicating the quantitative analysis. A common strategy to circumvent this dilemma is a *bottom-up* approach, in which the protein of interest is isolated, purified, and reconstituted into synthetic vesicles. Reconstitution is necessary as after successful expression, extraction from their native environment, and purification, isolated MPs display increased flexibility and reduced stability. Further, a wide variety of MPs, especially such with a vectorial function, can only execute their correct natural function in a membrane. Reconstitution into membrane mimetic systems (symmetric or asymmetric) resolves these problems.

Functional investigations on MPs with vectorial function require compartment-based model membrane systems, the most common of which are liposomes. Detergent-mediated reconstitution of MPs into liposomes however constitutes a difficult task, requiring optimization for every individual MP.

Orientation of the reconstituted MP in the liposomal membrane is influenced by various factors. Consequently, reconstitution scarcely ever results in homogeneous orientation of the MPs in liposomes, raising difficulties in evaluation of functional assays, which are even further tightened if investigating on consecutive processes of several different MPs coreconstituted in the same vesicle.

The aim of my PhD thesis was therefore to develop a tool kit to unidirectionally reconstitute MPs in a predefined orientation into liposomes, notwithstanding all other factors influencing orientation.

As a basis for our approach we decided to focus on reconstitution of MPs into preformed, detergent-destabilized liposomes, since other reconstitution methods appeared to be less promising. The paradigm of our strategy is the F_1F_0 ATP synthase, which was reported to unidirectionally reconstitute into liposomes with its F_1 part facing outwards, the size and the hydrophilic nature of F_1 disabling it from passing the hydrophobic core of membranes. Hence, MPs were modified by attachment of large soluble units (LSUs) purposed to guide unidirectional orientation into liposomes, similarly as the F_1 part for the ATP synthase.

To link the LSUs to the MP, we generally followed two different approaches. On one hand, two model MPs (cytochrome bo_3 ubiquinol oxidase, bo_3 oxidase; green light-absorbing proteorhodopsin, pR) were genetically modified to introduce different

linker tags, and on the other hand, a more generally applicable approach was pursued exploiting the His-tag used for purification.

In the former approach, as linker systems between the MP of interest and the LSU, either the interaction between biotin and streptavidin via *in vitro* biotinylation of an AviTag, or covalent bonding of the recently reported SpyTag-SpyCatcher system were employed. In the more generally applicable approach, for the specific interaction with His-tagged MPs the high affinity interaction between His-tags and trisNTA moieties coupled to LSUs were exploited.

In this thesis, unidirectional reconstitution of pR in a predefined manner is reported by using the SpyTag-SpyCatcher system. Application of the same system and additionally the AviTag system to bo_3 oxidase resulted in promising trends, however orientation of bo_3 oxidase seems to be much more difficult to be influenced than orientation of proteorhodopsin. Further, a dendritic version of trisNTA was synthesized, characterized, and coupled to different LSUs. Since direct coupling of trisNTA to LSUs was not particularly successful, trisNTA was coupled to a synthesized SpyTag peptide (trisNTA-Spy), offering the possibility to couple SpyCatcher-containing LSUs indirectly to trisNTA.

These approaches to unidirectionally orientate MPs are not easy to be implemented, however they are very promising. The most promising of the developed approaches are the SpyTag-SpyCatcher-based and the trisNTA-Spy-based systems. However, further investigation to optimize reconstitution of MPs into preformed, detergent-destabilized liposomes is required. It is further very important to have at hand a method to analyze the orientation of reconstituted MPs in the liposomal membrane, which is not depending on the function of the MP. Such a method is currently being developed in our lab.

Contents

1 Introduction.

1.1 Membranes.

The external boundaries of cells, the basic units of life, are defined by the cell or plasma membrane. These membranes primarily serve as barriers to prevent loss and mixing of the cell contents and the aequous interior, the cytoplasm, with the surrounding medium. Thus, membranes protect the cell from exterior influences, and most importantly, retain important biomolecules in reasonable concentrations. This compartmentalization through membranes reaches from molecular to macroscopic scale and allows for the spatiotemporal control of biochemical reactions.[1] While bacteria only have either one (gram positive) or two (gram negative) membranes, inside eukaryotic cells, this compartmentalization continues, as cellular organelles – such as mitochondria, endoplasmatic reticulum, Golgi apparatus and many others – are separated from the cytoplasm by lipid membranes again. Membranes themselves are ideal structures to organize and control biochemical reactions, and many important cellular processes as e. g. signalling and sensing, energy conversion, and metabolism take place at membranes.[1]

A very important characteristic of biological membranes is that they are so-called semi-permeable, which means, that they are permeable to nonpolar compounds, but impermeable to most polar or charged solutes.[2] Therefore, according to the chemiosmotic theory introduced by Peter Mitchell in 1961 [3], membranes can store energy in forms of chemical or ion gradients. Transmembrane differences in proton concentration are the reservoir for the energy extracted from biological oxidation reactions (e. g. during oxidative phosphorylation), which are the basis for the synthesis of adenosine triphosphate (ATP), the universal biological energy currency; consequently, these transmembrane differences in proton concentration across membranes are the driving force of life.[2]

Because of the mentioned attribute of membranes to be impermeable to most polar or charged solutes, cells need a system to selectively transport such solutes accross their membranes with high efficiency. Thus, membrane proteins (MPs) are embedded in the membrane, facilitating the exchange of solutes accross the membrane. Such MPs can be different kinds of transporters (coupled, passive, active, exchanger), channels (water, ion) or pumps. Additionally, not only MPs facilitating exchange of solutes are embedded in the membranes, but also MPs with other important

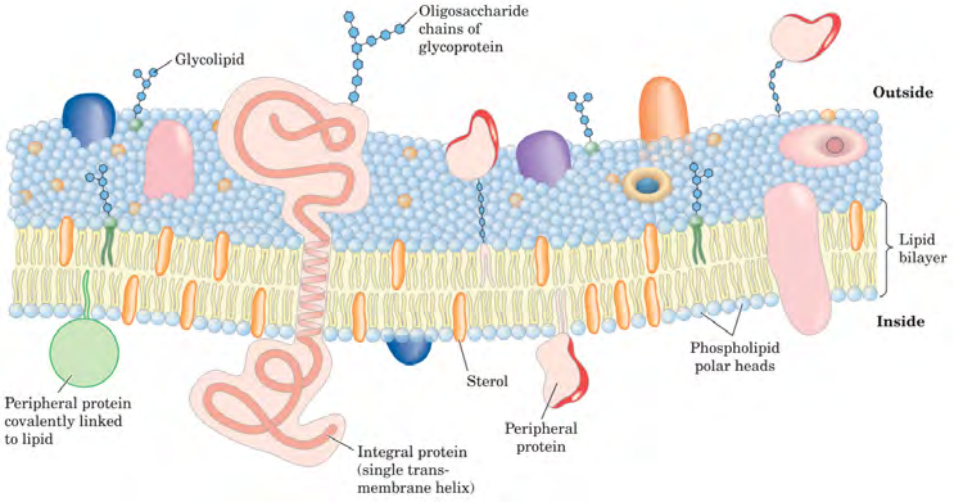

Figure 1: Fluid mosaic model for membrane structure. The fatty acyl chains in the interior of the membrane form a fluid, hydrophobic region. Integral proteins float in this sea of lipids, held by hydrophobic interactions with their nonpolar amino acid side chains. Both proteins and lipids are free to move laterally in the plane of the bilayer, but movement of either from one leaflet of the bilayer to the other is restricted. The carbohydrate moieties attached to some proteins and lipids of the plasma membrane are exposed on the extracellular surface of the membrane. Figure and description from [2]

physiological tasks, as e. g. MPs facilitating cell adhesion, translocases and receptors for signalling pathways, are present in or at membranes.

In 1972, Singer and Nicolson proposed the fluid mosaic model of the structure of cell membranes (see figure 1), where the structure of the plasma membrane is described as a mosaic of components containing phospholipids, cholesterol, MPs and carbohydrates, giving the membrane a fluid character.[4] The phospholipids form a bilayer, in which the nonpolar, hydrophobic fatty acid residues of the lipid molecules of both layers face each other in the center of the membrane, while their polar headgroups face outwards and interact with the aequous cytoplasm or the extracellular space, respectively. Lipid molecules are able to switch from one side of the lipid bilayer to the other, in a process called flip-flop. However, the rate of this process is rather low due to the polarity of the lipids' headgroups, helping to maintain a lipid asymmetry between the inner and the outher membrane leaflets.[5]

1.2 Membrane Proteins.

At or in biological membranes, a variety of MPs is located, specialized for promoting or catalyzing various vital cellular processes.[2] Most biologically active MPs are complex structures containing several polypeptides, cofactors and various active sites.[6] MPs located at the cell surface for example can be adhesion molecules holding neighboring cells together, receptors sensing extracellular signals and thus triggering molecular changes in the cell, or transporters moving specific organic solutes or ions across the membrane.[2]

Interestingly, MPs make up approximately 23 % of the human proteome [7], and an analysis performed in 2006 by Overington *et al.* [8] concluded that MPs constituted more than 60 % of drug targets.[9] Therefore, one of the main motivations to investigate on MPs of course is applying the generated knowledge in the development of new drugs.[10] Apart from drug discovery, investigations on MPs are motivated by the interest in designing novel devices in synthetic biology, as e. g. an artificial respiratory chain, the generation of which is a focus in our research group.

There are three types of MPs differing in their association with the membrane. Integral MPs are embedded in the membranes in a way that their hydrophobic domains are shielded from the aequous phases by the hydrophobic part of the phospholipids in the membrane. Thus, integral MPs are hard to remove from the lipid bilayer. To do so, agents which interfere with hydrophobic interactions have to be used, such as detergents or organic solvents.[2] If the functionality of the MPs shall be preserved, MPs are usually extracted from the membrane by solubilization of the latter by high concentrations of detergents (see section 1.4). Next to integral MPs there are also peripheral MPs associated with the membrane through electrostatic interactions and hydrogen bonding, or peripheral MPs that are covalently linked to a lipid with which they are anchored in the membrane. Last but not least, amphitropic proteins can be found both in solution in the cytosol and associated with the membrane through noncovalent interactions.[2]

As mentioned, one function of MPs is to facilitate transport of organic solutes or ions across the membrane by exhibiting vectorial function. Additional to a chemical gradient, ions of opposite charge separated by membranes generate a transmembrane electrical gradient called membrane potential. Together, the chemical gradient and the membrane potential are referred to as electrochemical potential or gradient.[2] MPs can either facilitate diffusion of a solute down its concentration gradient or it can occur against a gradient of concentration, electrical charge or both, in which cases

the transport process requires energy.[2] There are different types of MPs facilitating transport of solutes or ions across the membrane, a summary of which is illustrated in figure 2 on the next page. Channels allow transmembrane movement of substrates at rates approaching the limit of unhindered diffusion. Carriers on the other hand bind their substrates with high stereo-specificity, catalyzing transport at rates below the limits of free diffusion, and are saturable.[2] Carriers are subclassified: Passive transporters facilitate diffusion down a concentration gradient, while active transporters drive substrates across the membrane against a concentration gradient. Carriers can be uniporters, transporting just one type of substrate, or cotransporters, where two substrates are transported simultaneously either in the same (symport) or in opposite direction (antiport) (see figure 3A). As illustrated in figure 3B, transport against a concentration gradient requires energy, which can be provided directly by a chemical reaction (primary active transporters), i. e. the hydrolysis of ATP, or by coupling uphill transport of one substrate with downhill transport of another (secondary active transporters). Very prominent examples for primary active transporters are F-type ATPases (see section 1.2.3).[2]

Investigations on vectorial function of MPs facilitating transport of of organic solutes or ions across the membrane can be assessed by various transport assays. Such assays employ for example radioactively labeled substrates, or fluorophores specific for the transported substrate, as e. g. the pH-sensor pyranine to study transport of protons (see section 3.4) or Ca^{2+}-sensitive fluorophores [11]. Further techniques are reviewed in [12] or will be introduced in the respective sections of this thesis.

Knowing about the importance of MPs, in the following, three integral MPs used in this thesis are briefly introduced.

1.2.1 Proteorhodopsin.

Proteorhodopsin is a retinylidene MP, i. e. a MP of a family of proteins using retinal as chromophore for light reception. It is found in many species of marine proteobacteria in the photic zone of the oceans.[13–15] According to Wang, Sineshchekov, *et al.* [16], many hundred variants have been found. While sharing 80 % sequence identity, they show different absorption maxima, shifted by up to 35 nm between green and blue.[13, 16] Especially the green light-absorbing form from uncultured *Gammaproteobacterium EBAC31A08*, sharing a 30 % sequence identity with bacteriorhodopsin (bR) of *Halobacterium salinarum*, has been in the focus of numerous studies. Green

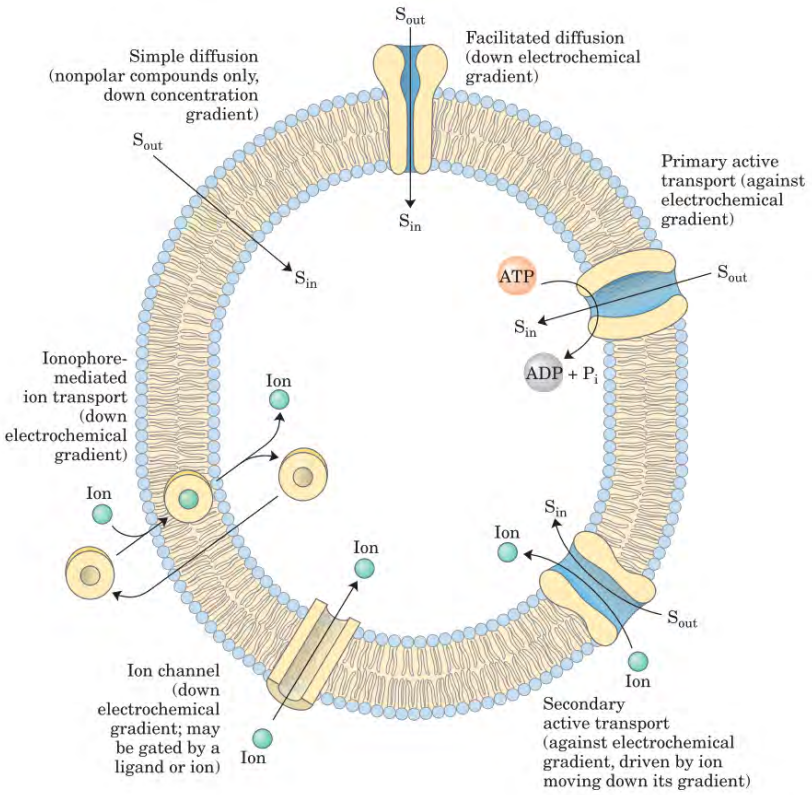

Figure 2: Summary of transport types. Apart from simple diffusion and ionophore-mediated ion transport, in all other transport types, MPs play a key role. Figure from [2].

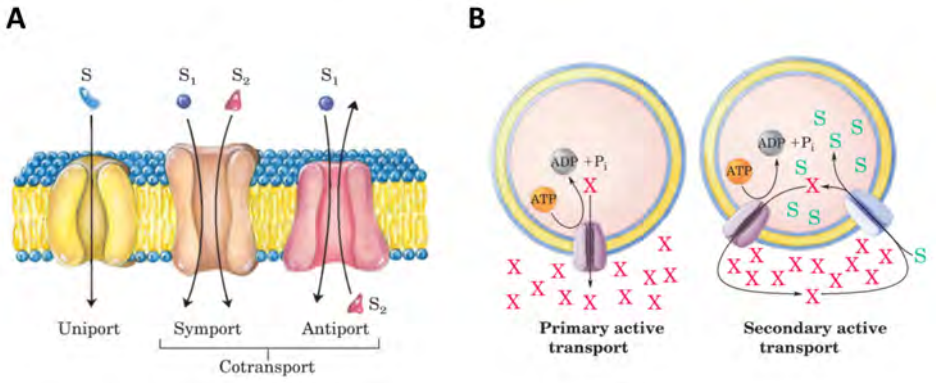

Figure 3: Further characterisation of transport systems. (A) Three general classes of transport systems. Transporters differ in the number of solutes (substrates) transported and the direction in which each solute moves. This classification does not tell whether these are energy-requiring (active transport) or energy independent (passive transport) processes. Figure and description from [2]. (B) Two types of active transport. In primary active transport (left), the energy released by ATP hydrolysis drives solute movement against an electrochemical gradient. In secondary active transport (right), a gradient of ion X has been established by primary active transport. Movement of X down its electrochemical gradient now provides the energy to drive cotransport of a second solute (S) against its electrochemical gradient. Figure and description from [2].

proteorhodopsin (in the following abbreviated as pR; see figures 4A and 4B) has a molecular weight of roughly 27 kDa and a λ_{max} around 520 nm.

pR, consisting of seven transmembrane helices, works as a light-driven proton pump. Its cofactor, the chromophore retinal, is covalently bound to the apoprotein through a protonated Schiff base to a lysine residue in the seventh transmembrane segment (Lys231).[13, 17, 18] Induced by light excitation of the retinal, the protein undergoes conformational changes, eventually resulting in the translocation of a proton across the membrane. The chromophore retinal exhibits a high spectral sensitivity towards its environment, enabling monitoring of the photocycle by transient absorbance changes at different wavelengths.[19] In more detail, in the first step of the photocycle, retinal by illumination undergoes an isomerization from all-*trans* to 13-*cis* upon transition from pR's ground state to the so-called K-intermediate. Subsequently, the Schiff base is deprotonated, while the primary proton acceptor Asp97 is protonated upon formation of the M state, possibly consisting of two substates M_1 and M_2. The M-intermediate decays by reprotonation of the Schiff base giving rise to the formation of late intermediates, the first of which is termed N.[18, 19] Finally, the retinal isomerizes back to the all-*trans* configuration by thermal relaxation.[18] The described photocycle is schematically depicted in figure 4C.

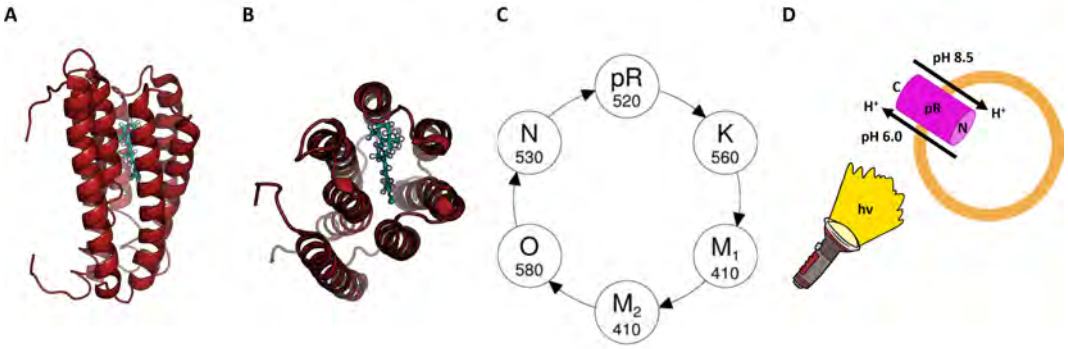

Figure 4: Green light-absorbing pR. (A) Structure of green light-absorbing pR (PDB: 2L6X; [20]), side view. N-terminus on the top left, C-terminus on the bottom left. The cofactor retinal is represented in cyan. (B) Top view of (A). (C) Simplified photocycle of pR. Numbers denote the absorbance maximum of the respective state. The photocycle starts with excitation of the ground state of pR which is named pR 520 in the scheme. Figure and description from [18]. (D) pH-dependency of reconstituted pR. pR exhibits bidirectional transport of protons, strongly depending on the pH of the surrounding environment. When illuminated, pR exports protons at pH 6.0, while protons are being imported at pH 8.5.

Interestingly, pR shows bidirectional transport. The net transport direction is strongly depending on the pH. As shown figure 4D, pR reconstituted in liposomes exports protons at pH 6.0, while it imports protons at pH 8.5.[13, 19] This effect was explained by Friedrich, Geibel, *et al.* [19] as a result of slight differences in the photocycle at high (10) or low (5) pH.

1.2.2 Cytochrome bo_3 Ubiquinol Oxidase.

During oxidative phosphorylation, ATP synthesis from ADP and inorganic phosphate by ATP synthases requires a proton electrochemical gradient which is maintained by proton transporters and pumps of the respiratory chain (see figure 5 on the following page). The final stage of the respiratory chain is catalyzed by heme-copper oxidases. Heme-copper oxidases can be divided into three subclasses, A, B, and C. The oxidases of type A include the cytochrome *c* oxidases in mitochondria and some bacteria (e. g. as *Paracoccus denitrificans* and *Rhodobacter sphaeroides*) as well as quinol oxidases as the cytochrome bo_3 ubiquinol oxidase of *E. coli*.[21–23] The B- and C-type heme-copper oxidases are exclusively found in archea and bacteria.[21].

Heme-copper oxidases are redox-driven proton pumps which use the free energy released by oxidation of the oxidase's substrate (cytochrome *c* or quinol) to reduce O_2 to water, coupled to vectorial translocation of protons across the inner mitochondrial

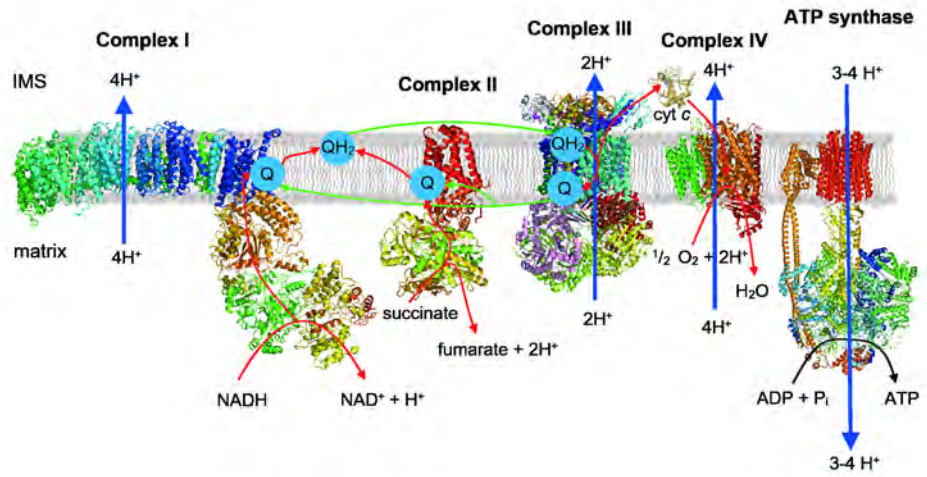

Figure 5: Schematic representation of the respiratory chain in mitochondria. Complex I (PDB: 4WZ7) oxidizes NADH to NAD^+ to reduce ubiquinone (Q) to ubiquinol (QH_2). The electron transfer is coupled to the transport of four protons from the mitochondrial matrix to the inner membrane space (IMS). Complex II (PDB: 2WDV) oxidizes succinate to fumarate and reduces Q without proton translocation. The electrons are then transferred from QH_2 to cytochrome *c* via complex III accompanied by the translocation of two protons. Finally, four molecules of cytochrome *c* are used to reduce oxygen to water in complex IV coupled to the transport of four protons. Overall, a total of ten protons are translocated across the mitochondrial membrane per NADH oxidized. The electrochemical proton gradient is dissipated by the ATP synthase to generate ATP. Electron and proton transfer processes are depicted with red and blue arrows, respectively. Figure and description from [24].

or the bacterial cell membrane.[21, 25, 26] The thereby induced transmembrane proton electrochemical gradient, consisting of a proton gradient (ΔpH) and a membrane potential ($\Delta\psi$), is called proton motive force (*pmf*). The *pmf* generated by heme-copper oxidases and the other members of the aerobic respiratory chain is used by the energy conserving system ATP synthase to store energy in the form of ATP, the universal currency of energy in biological systems.[26]

The *pmf* is generated by heme-copper oxidases in two different mechanistic means, which are linked to one another. First, since the electrons (*p*-side) and protons (*n*-side) used for O_2 reduction are taken from opposite sides of the membrane, this process leads to a separation of charges across the membrane, which is equivalent a net transfer of one positive charge from the more negative (*n*-) side to the more

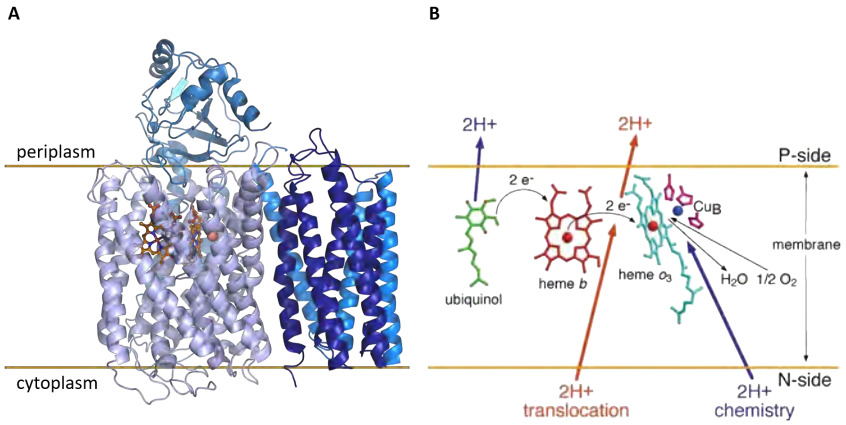

Figure 6: Cytochrome *bo₃* ubiquinol oxidase. (A) Crystal structure of the *E. coli* enzyme including bound hemes *b* (left) and o_3 (right) and Cu_B. Subunits I to IV are coloured in shades of blue; hemes *b* and o_3 are shown as balls and sticks; Cu_B is depicted as orange sphere. (PDB: 1FFT; [26]). (B) Schematic representation of electron and proton transfer. All redox centers are located within the largest subunit (subunit I), with a low spin protoheme (heme *b*) acting as the electron donor to a binuclear center composed of an O-type heme (heme o_3) and a copper ion (Cu_B) in close proximity of a redox-active tyrosine residue (Y288). Figure (B) and description thereof adapted from [26].

positive (*p*-) side of the membrane.[2, 21, 25] In addition to this vectorial arrangement of the oxygen reduction chemistry, heme-copper oxidases pump up to one proton per transferred electron across the membrane from the *n*- to the *p*-side, increasing the stoichiometry to two charges transferred across the membrane per electron transferred to O_2.[2, 21, 25]

The mentioned mentioned heme-copper oxidase cytochrome bo_3 ubiquinol oxidase from *E. coli* (from here on referred to as bo_3 oxidase; see figure 6A), consists of four subunits (subI: 74 kDa, apparent mass in SDS-PAGE: 55 kDa; subII: 33 kDa; subIII: 23 kDa; subIV: 12 kDa. [27]). Three of its subunits (core subunits) are homologous to the three mitochondrially encoded subunits of the eukaryotic cytochrome *c* oxidases.[28] All redox centers are located in the largest subunit (subunit I). A low spin protoheme (heme *b*) acts as the electron donor to a binuclear center composed of an O-type heme (heme o_3) and a copper ion (Cu_B).[26] The electron donor for the bo_3 oxidase is membrane-bound ubiquinol. First, the electrons are delivered to the intermediate electron acceptor heme *b*, and subsequently tunneled to the catalytic site composed of the Cu_B ion in close proximity to heme o_3 and a redox-active tyrosine residue (Y288) [29–34] (see figure 6B). Upon this stepwise reduction of the

catalytic site by two electrons, the heme o_3 binds O_2, which is subsequently almost instantaneously reduced to water by four electrons.[21, 25]

1.2.3 ATP Synthase.

Transmembrane ATPases are primary active MP transporters using ATP hydrolysis to drive transport of ions across a membrane. There are several different types (F, P, V, A, E) of transmembrane ATPases differing in function, structure and type of ions transported.

F-ATPases catalyze the transmembrane passage of protons against the electrochemical gradient driven by ATP hydrolysis. This reaction however is reversible; a proton (or sodium) gradient can supply the energy to drive the reverse reaction and synthesize ATP, giving the F-type ATPases a more appropriate name: ATP synthases.[2] Because of their structure, ATP synthases are also termed F_1F_0 ATP synthases. They consist of two opposing rotary motors connected in series as described in figure 7A. The F_1 motor is a water-soluble protein complex consisting of five different subunits designated in order of decreasing size and number of subunits as α_3, β_3, γ, δ and ε [35], with masses for the *E. coli* ATP synthase (figure 7B) of approximately 55, 50, 31, 19, and 14 kDa, respectively [36], resulting in a total mass of ∼379 kDa. The F_1 motor catalyses ATP synthesis or hydrolysis by a rotary mechanism.[35] The simplest F_0 part is held by the *E. coli* ATPase, with subunits and stoichiometry designated as a, b_2, and $c_{9\text{-}12}$, with masses of approximately 30, 17, and 8 kDa, respectively.[36] The F_0 motor is membrane-embedded and catalyses ion (*E. coli*: proton) translocation across the membrane coupled to rotation of the c ring versus the stator subunits a and b_2.[35] The two motors F_1 and F_0 are physically connected by two stalks composed of subunits from both parts. The central stalk contains γ- and ε-subunits and the peripheral stalk involves the δ- and b-subunits.[35, 36] Efficient rotation requires a *pmf* ($\Delta\psi + \Delta\,\mathrm{pH}$) as well as a high proton concentration at the source *p*-side.[35] As mentioned in section 1.2.2, the *pmf* is provided by the enzymes of oxidative phosphorylation, enabling ATP synthesis from ADP and inorganic phosphate by the synthase (see also figure 5 on page 8). Each 360° rotation of the central γ subunit leads to synthesis and release of three molecules of ATP. Hence, depending on the number of c subunits (n_c) in the F_0 motor synthesis of each molecule of ATP requires the transport of $n_c/3$ protons. The *E. coli* F_1F_0 ATP synthase contains 9 to 12 c subunits in its c ring, consequently requiring transport of

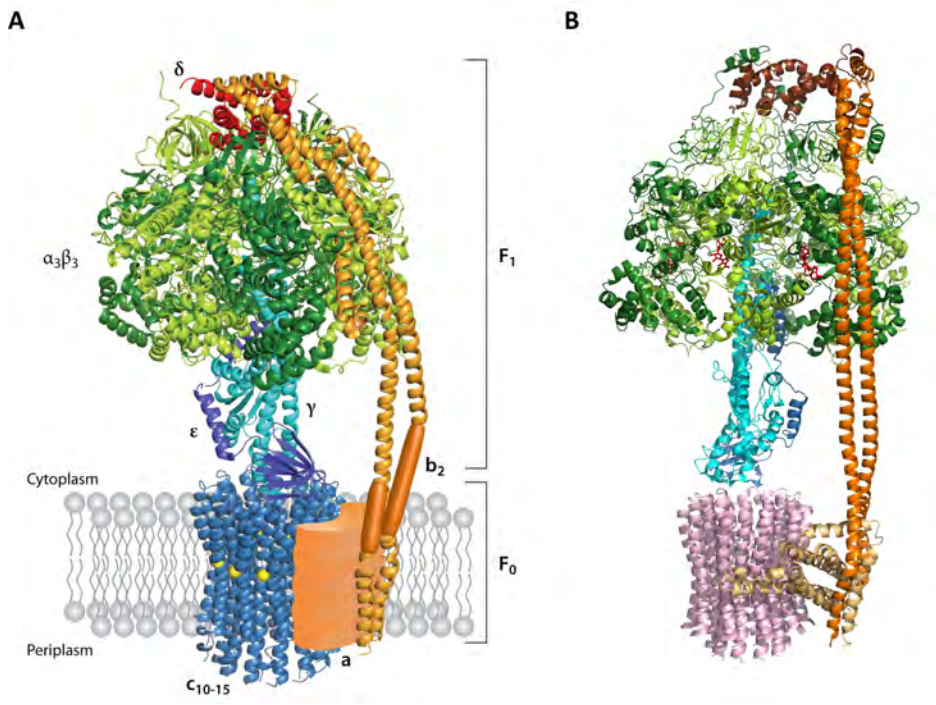

Figure 7: The structural organization of an F_1F_0 ATP synthase. (A) The F_1F_0 ATP synthase is a miniature engine composed of two opposing rotary motors. The F_1 motor is a water-soluble protein complex with the subunit composition $\alpha_3\beta_3\gamma\delta\varepsilon$ which catalyses ATP synthesis or hydrolisis by a rotary mechanism, while the F_0 motor is membrane embedded and in its simplest bacterial form has the subunit composition $ab_2c_{10\text{-}15}$. The F_0 part catalyses ion translocation across the membrane that is coupled to rotation of the c ring versus the stator subunits a and b_2. The two motors are physically connected by two stalks, a central one containing the γ- and ε-subunits and a peripheral one involving the δ- and b-subunits. Figure and description from [35] (B) Structure of the *E. coli* F_1F_0 ATP synthase. (PDB: 5T4P; [41]).

3 to 4 protons across the membrane per molecule of ATP synthesized.[35, 37] For further information on ATP synthases, consider [35, 38–40].

1.3 Lipids.

The definition of the term "lipids" is usually rather broad. According to Nelson *et al.* [2], biological lipids are a chemically diverse group of compounds, the common and defining feature of which is their insolubility in water.[2] A similar definition is given by the International Union of Pure and Applied Chemistry (IUPAC), saying that "lipids" is a loosely defined term for substances of biological origin that are soluble in nonpolar solvents. Further, lipids consist of saponifiable lipids (lipids with an ester

Table 1: Overall macromolecular composition of an average *E. coli* cell. *E. coli* in aerobic balanced growth at 37 °C in glucose minimal medium, with doubling time of 40 min and 1 pg cell wet weight (≈0.9 µm^3 cell volume). Under different growth rates the volume and mass per cell can change several fold. The relative composition changes with growth rate but not as significantly. For a given cell volume and growth rate, the uncertainty in most properties is expected to be on the order of 10 - 30 % standard deviation. Original values refer to B/r strain, but to within the uncertainty expected, the values reported here are considered characteristic of most common *E. coli* strains. Composition metabolites & cofactors pool, rules of thumb: carbon atoms $\sim 10^{10}$; 1 molecule per cell gives ∼1 nM conc.; ATP required to build and maintain cell over a cell cycle $\sim 10^{10}$; glucose molecules needed per cell cycle $\sim 3 \times 10^9$ (2/3 of carbons used for biomass and 1/3 used for ATP). Table and description adapted from [44].

macromolecule	percentage of total dry weight	weight per cell [fg]	characteristic molecular weight [Da]	number of molecules per cell
protein	55	165	3 x 10^4	3'000'000
RNA	20	60		
23 S rRNA		32	1 x 10^6	20'000
16 S rRNA		16	5 x 10^5	20'000
5 S rRNA		1	4 x 10^4	20'000
tRNA		9	2 x 10^4	200'000
mRNA		2	1 x 10^6	1'400
DNA	3	9	3 x 10^9	2
lipid	9	27	800	20'000'000
lipopolysaccharide	3	9	8'000	1'000'000
peptidoglycan	3	9	$(1'000)_n$	1
glycogen	3	9	1 x 10^6	4'000
metabolites & cofactors pool	3	9		
inorganic ions	1	3		
total dry weight	100	300		
water (70 % of cell)		700		
total cell weight		1'000		

functional group, hydrolyzable under basic conditions), such as glycerides, glycolipids, sphingolipids and phospholipids, as well as nonsaponifiable lipids, principally steroids.[42] Interestingly, eukaryotic cells invest substantial resources in generating a wide variety of different lipids, using approximatively 5 % of their genes for their synthesis.[43] Membrane lipids make up 5 % to 10 % of the dry mass of most cells.[2] In *E. coli*, lipids make up 9 % of the dry weight of a cell. A more detailed compilation on the overall macromolecular composition of an average *E. coli* cell can be found in table 1.

Lipids have three general functions in biological systems. First, they serve as principal storage form of energy in many organisms because of their relatively reduced state.[2, 43] Usually, this energy storage occurs in the form of triacylglycerol and steryl esters in lipid droplets.[43] Secondly, polar lipids as phospholipids and sterols,

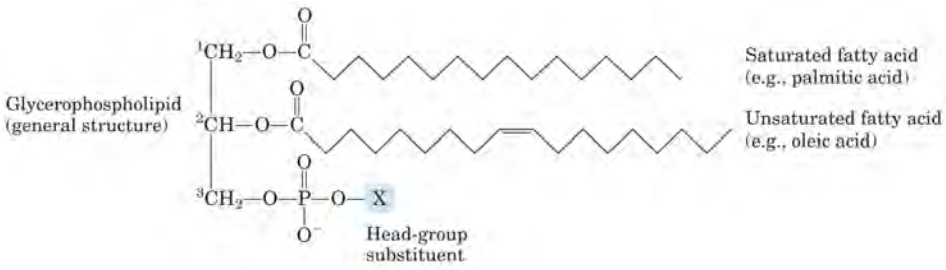

Figure 8: Glycerophospholipids. The common glycerophospholipids are diacylglycerols linked to headgroup alcohols through a phosphodiester bond. Each derivative is named for the headgroup alcohol, with the prefix "phosphatidyl-". Figure and description from [2].

Table 2: Most common phospholipids in biological membranes.
Net charges at pH 7. Adapted from [2, 5].

Phospholipid	Polar Head ("X" in fig. 8)	Charge
Phosphatidic acid (PA)	R-OH	Negative (-1)
Phosphatidyl serine (PS)	R-$OCH_2CHNH_2COO^-$	Negative (-1)
Phosphatidyl glycerol (PG)	R-$OCH_2CHOHCH_2OH$	Negative (-1)
Phosphatidyl inositol (PI)	R-$OHC_6H_5(OH)_5$	Negative (-4)
Cardiolipin (CL)	R-$OCH_2CHOHCH_2$	Negative (-2)
Phosphatidyl choline (PC)	R-$OCH_2CH_2N^+(CH_3)_3$	Zwitterionic (0)
Phosphatidyl ethanolamine (PE)	R-$OCH_2CH_2NH_3^+$	Zwitterionic (0)

consisting of a hydrophobic and a hydrophilic portion, are the major structural elements of biological membranes. According to the hydrophobic effect [45], the hydrophobic moieties of the lipids self-associate, entropically driven by surrounding water, while the hydrophilic headgroups interact with each other as well as with the aqueous environment. As a consequence, biological membranes are formed spontaneously as described in section 1.1.[43] Thirdly, lipids can act as messengers in signal transduction and molecular recognition processes.[43]

The most common lipids in most eukaryotic and prokaryotic membranes are glycerophospholipids, in which two fatty acids are attached via ester linkage to the first and second carbons of glycerol, while at the third carbon a highly polar or charged headgroup is attached through a phosphodiester bond (see figure 8 and table 2).[2, 5] In bacterial membranes, phosphatidylethanolamine (PE) and phosphatidylglycerol (PG) are the major species, while phosphaditylcholine (PC) is the most abundant species in animal cell membranes.[5]

Table 3: Fatty acids commonly found in lipids of biological membranes. Adapted from [5].

Fatty acid	chain length : unsaturation
Lauric	12 : 0
Myristic	14 : 0
Palmitic	16 : 0
Palmitoleic	16 : 1 (9-*cis*)
Stearic	18 : 0
Oleic	18 : 1 (9-*cis*)
Vaccenic	18 : 1 (11-*cis*)
Linoleic	18 : 2 (9-*cis*, 12-*cis*)
γ-Linolenic	18 : 3 (6-*cis*, 9-*cis*, 12-*cis*)
α-Linolenic	18 : 3 (9-*cis*, 12-*cis*, 15-*cis*)
Arachidic	20 : 0
Eicosenoic	20 : 1
Arachidonic	20 : 4 (5-*cis*, 8-*cis*, 11-*cis*, 14-*cis*)
Behenic	22 : 0

The fatty acids of glycerophospholipids vary in length (C14 - C24), branching, and degree of unsaturation. Saturated fatty acid chains are very flexible, since each single bond has complete freedom of rotation. However, the most probable conformation is the fully extended chain. Unsaturated fatty acids have rigid kinks because of the nonrotating nature of double bonds. While the rarely naturally occuring *trans* configuration resembles the extended form of saturated fatty acids, the *cis* double bond produces a kink of nearly 30°.[5, 46] The most frequently occuring saturated fatty acids in natural membranes are palmitic, stearic and miristic, while oleic acid (stearic acid with one double bond in *cis* configuration; 18:1 (9-*cis*)) is the most abundant unsaturated fatty acid.[5] A non-conclusive enumeration of fatty acids commonly found in lipids of biological membranes can be found in table 3.

Next to the common glycerophospholipids there are other groups of phospholipids as galactolipids (predominant in plant cells), sphingolipids (no glycerol moiety), sterols (e. g. cholesterol) and membrane lipids unique in archaea.[2] Most of the archaea live in ecological niches with extreme conditions as high temperatures, low pH or high ionic strength to name a few.[2] These environments require extreme adaptations in the membrane lipid composition. Thus, archaeal membranes have membrane lipids containing long-chain (C32) branched hydrocarbons linked at each end to glycerol via ether bond. The ether linkage is much more stable to hydrolysis at low pH and high temperature compared to the ester bonds found in lipids of bacteria and eukaryotes.[2, 5, 47] These archaeal lipids called glycerol dialkyl glycerol tetraethers are twice the length of phospholipids or sphingolipids, thus spanning the

entire width of the membrane.[2, 5, 47] Additionally, the stereoconfiguration of the glycerol moiety of archaeal lipids is not the same as in bacterial and eukaryotic lipids. While in the other domains the central carbon of glycerol is in the S configuration, in archaea it is in the R configuration.[2, 5]

1.4 Detergents.

Detergents are micelle-forming surfactants which constitute a major tool in the investigation of biological membranes, even more important in the investigation of MPs.[48]

Detergents are amphiphilic molecules which consist of a polar hydrophilic or an ionic head group facilitatiing interaction with aequous environment, and of an unpolar, lipophilic tail (see figure 9 on the following page). This hydrophilic tail is able to interact with hydrophobic regions of a MP. Thus, detergents are able to replace and mimic the natural lipid environment of MPs.

One key feature of detergents is their ability to form micelles. Micelles are aggregates of single detergent molecules, where all the hydrophilic headgroups are facing outwards towards the aequous environment, while the hydrophobic tails are facing inwards, thus being shielded from the afore mentioned aequous environment satisfying the hydrophobic effect. The size of the micelles is characteristic for each detergent. Another characteristic for each detergent is the lowest concentration at which this detergent still can form micelles, called critical micellar concentration (CMC). A short selection of different detergents can be found in table 4 on the next page. Besides being characteristical for each detergent, the CMC is dependent on further parameters as temperature, ionic strength, pH, presence of bi- or trivalent cations or organic solvents. MPs can be introduced as hydrophobic molecules into such micelles and therefore can be solubilized in a non-natural environment. Often, their biological activity is conserved when solubilized by detergents. [49]

1.5 Model Membrane Systems.

In their natural environment, MPs are embedded in a mosaic lipid bilayer. This bilayer is a complex, heterogeneous and dynamic environment even in the simplest organisms. Therefore, many standard biophysical techniques to determine structure and function of MPs – such as NMR, X-ray crystallography, circular dichroism, ligand-binding studies, classical kinetic characterization, or the identification of

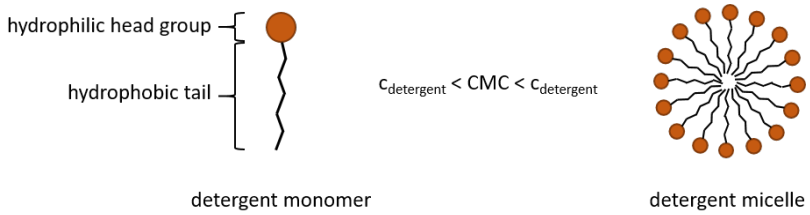

Figure 9: Detergent micelles. Left: Detergent molecule monomer with hydrophilic headgroup and hydrophobic tail. Right: Detergent micelle. In a micelle, the hydrophilic head groups are exposed towards the outer aequous environment, while the hydrophobic tails are facing towards the center of the micelle and are thus shielded from the aequous environment. If the concentration of the detergent is below its CMC, detergent molecules are present as monomers, whereas micelles are formed above CMC.

Table 4: A selection of detergents.
n: aggregation number for formation of micelles; M: mass; CMC: critical micellar concentration; DDM: n-dodecyl β-D-maltoside; LMNG: lauryl maltose neopentyl glycol; OGNG: octyl glucose neopentyl glycol; CHAPS: 3-[(3-Cholamidopropyl)dimethylammonio]-1-propanesulfonate; Zwittergent 3-12: *n*-dodecyl-*N*,*N*-dimethyl-3-ammonio-1-propanesulfonate. n.a.: not available to my knowledge. [1]: estimated by SEC-LS experiments, suggesting the dissociation of the largest LMNG complexes upon sample dilution on the column.[50] [2]: introduced by [51]. Table adapted from [49] and supplemented as indicated.

Detergent	**M of monomer [Da]**	**n**	**M of micelle [kDa]**	**CMC [mM]**	**type of detergent**
Sodium dodecyl sulfate (SDS)	288	60-100	> 18	8	ionic
Sodium deoxycholate	416	10	4	4 (in 50 mM NaCl)	ionic
Sodium cholate	431	2-5 [52]	0.9-2.2	9.5-14 [53, 54]	ionic
Triton X-100	∼ 628	140	90	0.2	non-ionic
Tween 80	∼ 1310	58	76	0.02	non-ionic
DDM	511	141	72	0.17	non-ionic
Octylglucoside (OG)	292	30-100	8	15	non-ionic
LMNG	1005	63-620 [50]	67-76 [1]	0.01 [55] / 0.04 [50]	non-ionic
OGNG [2]	567	n.a.	n.a.	1.02 [55] / 1.13 [56]	non-ionic
CHAPS	615	4-14	6	4	zwitterionic
Zwittergent 3-12	335	10	3	3.6	zwitterionic

structure-function relationships – are limited.[57] Assigning effects observed in whole cells to the mechanism of action, its kinetics or to the specificity of one specified MP is all but impossible due to the complexity of the natural environment of MPs. When investigating on transport MPs as e. g. solute carriers (SLCs) [58], a way to defy these difficulties is to exploit substrate specificity in transport assays, where transporter-specific labeled substrates are taken up into cells. Different studies for example investigated on the uptake of the transporter-selective substrate α-methylaminoisobutyric acid (MeAIB) [59] by the sodium-coupled neutral amino acid transporter 2 (SNAT2; SLC38A2) by using radioactively labeled MeAIB.[59–61] This approach however is not applicable when studying enzymes transporting substrates as e. g. protons, since many different proton transporting systems are present in cells.

As a consequence, a *bottom-up* approach is often chosen, in which purified components are assembled to produce more advanced supramolecular structures, and MPs are investigated in isolation, providing important information on their mechanism. However, investigating MPs in isolation is not trivial at all. Many factors are complicating this undertaking, including the notorious difficulty in achieving sufficient expression of the MP in heterologous systems. After successful expression, MPs require extraction from their native environment to be purified afterwards. The mentioned extraction, which is a considerable bottle neck requiring much empirical investigation for each MP, is also called solubilization and is typically carried out by detergents. Once in isolation solubilized by detergents or mixed micelles, MPs display increased flexibility and are usually less stable than in their native environment. Further, since MPs naturally exist and function within membranes, which are highly regulated specific environments, a wide variety of MPs can only execute their correct natural function and retain their activity in a membrane. Therefore, isolated and purified MPs require re-insertion into a lipid bilayer environment [62], illustrating the principles of a *bottom-up* approach. Since the functional activities of MPs can be modulated by the structure of the surrounding lipid molecules in the membrane [63, 64], the composition of the lipid bilayer can affect the inter- or intra-molecular interactions between the lipid bilayer and MPs.[65, 66] Crystal structures of MPs often include phospholipid molecules. These phospholipids are presumed to be positioned in the crystals as they are in native membranes. Many thereof are laying on the MP surface, where their head groups are interacting with polar amino acid residues at the inner and outer membrane-water interfaces and their side chains are associated with nonpolar residues. Such lipids, termed annular lipids, are required for activity

of most MPs.[67] They form a bilayer shell (annulus) around the MP, while being orientated roughly as expected for phospholipids in a bilayer.[2]

The process of re-insertion of a MP into an artificial model membrane system is called reconstitution. Further information on the reconstitution process can be found in section 1.6.

Depending on the MP of interest and the type of mechanistic information to be investigated, MPs can be reconstituted into various model systems, which can be divided into two categories, symmetric or compartmental.

1.5.1 Symmetric Reconstitution Systems.

Symmetric, non-compartment model membrane systems offer the advantage of the complete accessibility of both faces of a MP.[62] Two such symmetric systems are briefly introduced here.

Nanodiscs.

Nanodiscs were described by Bayburt, Grinkova, *et al.* [68] as a symmetric model membrane system where an integral MP is reconstituted into phospholipids in the presence of a class of proteins derived from apolipoprotein A1 (ApoA1) lacking a globular N-terminal domain present in its native form. Native ApoA1 is the major polypeptide of human plasma high density lipoprotein (HDL), which is transporting triglycerides and cholesteryl esters in plasma in the form of a hydrophobic core surrounded by a surface monolayer of polar phospholipids encircled by ApoA1.[69] The derived class of amphipatic helical proteins lacking the globular N-terminal domain is termed "membrane scaffold proteins" (MSP).[70] Composed of a discoidal phospholipid bilayer encircled by a belt of two molecules of MSP [62, 70], nanodiscs typically are 8 to 16 nm in diameter.[70] Since there are differently sized MSPs, the size of nanodiscs is not only determined by the stoichiometry of the lipids used in the self-assembly process, but also by the length of the used MSP.[70] Hence, reconstitution of a MP into nanodiscs involves specific parameters such as the stoichiometric ratio of MSP and lipids to the MP of interest and the size of the MSP. The ratios need to be empirically optimized for each MP of interest. If the ratios are not optimal, the MP might get destabilized and the size range of the nanodiscs formed will be rather broad.[62] The reason for the potentially broad size range is, that native ApoA1 does not produce monodisperse HDL particle sizes [71, 72], and by changing the lipid to ApoA1 stoichiometry it is possible that the size of reconstituted HDLs varies with broad size distributions.[73, 74] However, using engineered MSP proteins instead of

ApoA1, a high yield of monodisperse lipoprotein particles (nanodiscs) can be obtained if the optimal lipid to protein stoichiometry is used.[73, 75, 76] MPs reconstituted into nanodiscs are stable because of strong interactions between the acyl chains of lipids and the hydrophobic residues of the MSP.[62]

Nanodiscs can be prepared following two different strategies. In the first strategy, detergent extracted MPs are first chromatographically purified and subsequently added to a mixture of MSP and lipids at an appropriate ratio. In the second strategy, MSP and lipids are first added to the ensemble of all detergent-solubilized MPs of a cell and the target MP within nanodiscs is only then purified by chromatography. The two strategies for the assembly process of nanodiscs including reconstitution of MPs is illustrated in more detail in figure 10 on the following page.

Advantages of Nanodiscs are their stability, the ability of precisely manipulating the nanodisc composition, and the presence of a full length lipid bilayer arrangement.[62] Compared to liposomes, the protein to lipid ratio is high. Possibly due to a loss of lateral pressure, many proteins lose activity in detergent solution.[77, 78] The required lateral pressure however can be provided by nanodiscs. Due to the monodispersity of nanodisc size, these are often the model membrane system of choice for spectroscopic studies of target proteins, at least when using small MSPs. Larger MSPs however tend to generate large nanodiscs that may not be compatible with spectroscopical techniques due to scattering.[62, 79] Nanodiscs have their limitations as well, e. g. that – similar to the use of detergent micelles and liposomes – the procedure for reconstitution requires the use of detergents. Further, the α-helical structure of MSP can interfere with EPR- and NMR-based assays. Last but not least, unlike to liposomes, the lack of compartmentalization makes vectorial transport measurements on MPs in nanodiscs impossible.[62] Nanodiscs have been used to study a variety of MPs, including cytochrome P450s (CYPs) [80–86], NADPH-cytochrome P450 reductase (CPR) [87, 88], bR [89, 90], G protein-coupled receptors (GPCRs) [91] and bacterial chemoreceptors [92].[93]

Styrene Maleic Acid Lipid Particles.

Styrene Maleic Acid Lipid Particles (SMALPs), also known as Lipodisq particles or native nanodiscs, were first introduced by Knowles *et al.* [94] for the purification of bacteriorhodopsin and the lipid A palmitoyltransferase PagP [95]. In contrast to other methods requiring extraction of MPs from the membranes of the expression system with potentially destabilizing detergents (see section 1.1) and subsequent reconstitution into a model membrane system (see section 1.6), the use of styrene

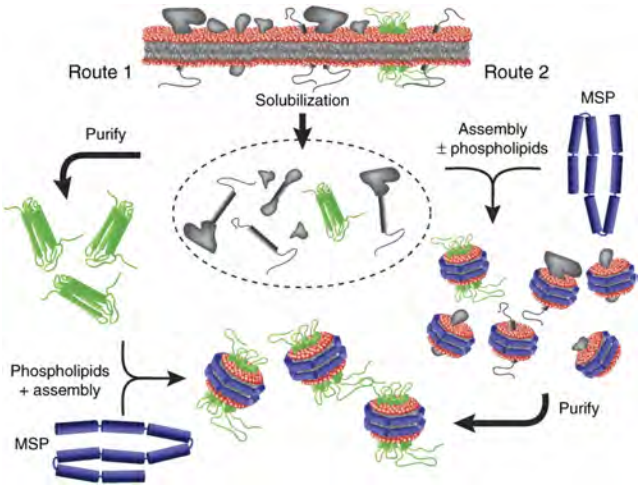

Figure 10: Nanodisc assembly. The standard method for self-assembling a MP into a nanodisc is shown in route 1 (left): After detergent solubilization and purification, the target MP (green) is mixed with the membrane scaffold protein (MSP, blue) and lipids at the correct stoichiometry, followed by detergent removal though incubation with hydrophobic beads. Often, however, the MP is not stable in detergent for the extended times needed for purification. Alternatively (route 2, right), the starting membrane or tissue can be directly solubilized with excess lipid and scaffold protein and rapid detergent removal, resulting in placement of the target MP (green), together with other MPs (gray) in the tissue, into the nanodisc. Subsequent purification, often with an affinity tag, is performed, and the target is stabilized in the nanodisc environment. This latter route can also be used to generate a soluble MP library that faithfully represents the MPs in the starting tissue. Figure and description from [70]

maleic acid (SMA) enables detergent-free isolation of MPs. Hence, importantly, the detergent-free method of MP purification is partially retaining the natural lipid environment, especially the MP's annular lipids introduced earlier, resulting in maintenance of protein function.[96] Since hydrophobic (styrene) and hydrophilic (maleic acid) moieties are alternating, SMA is amphipatic and thus capable of inserting into biological membranes, resulting in the extraction of small discs of lipid bilayer comparable to nanodiscs (see figure 11A). These discs encircled by polymer, typically containing an integral MP, are called SMA lipid particles (SMALPs). Because such SMALPs are water-soluble, if the encapsulated MP is suitably tagged, they can be purified by standard affinity chromatography.[96]

However, there are some limitations to the use of SMALPs, the first of which is the relatively narrow pH optimum (pH 7 - 8); at values below, the polymer precipitates out of solution and therefore, the MP with it. Additionally, SMALPs are sensitive to divalent cations.[62] ZipA, a membrane tether involved in cell division in *E. coli*,

was purified with and reconstituded in different types of SMAs and shown to be susceptible to Mg^{2+} and to precipitate at or above concentrations between 1 and 4 mM, depending on the type of SMA used.[97] *E. coli* outer-membrane phospholipase A (OmpLA) [98] in SMALPs was shown to precipitate in presence of 2 mM Ca^{2+}.[99]

Despite of these limitations, MP extraction by SMA was applied in numerous studies. Combined with negative stain electron microscopy (EM) for example, MP extraction by SMA provides an efficient and rapid approach for studying the structures of MPs in their native lipid environments.[96] Postis *et al.* [96] reported the use of an SMA co-polymer for extraction and purification of the *E. coli* multidrug transporter AcrB [100] followed by structural investigation by negative stain EM (see figure 11B). Further, Smirnova, Sjöstrand, *et al.* [101] exploited the advantage that the use of SMA enables detergent-free isolation of MPs by extracting cytochrome *c* oxidase (C*c*O) in its native lipid environment from mitochondria of *Saccharomyces cerevisiae*. However, they reported that interactions of the SMA co-polymer with C*c*O reversibly strongly inhibits the O_2-reduction activity of the enzyme by interfering with the cytochrome *c* binding to the C*c*O.[101] Later, they developed further their method by incorporating C*c*O, previously isolated with native lipids from *S. cerevisiae* mitochondria using SMALPs, into liposomes without the use of any detergent. Eventually, reconstituted C*c*O was reported to be active in the prepared proteoliposomes.[102] For further information about SMALPs, consider Dörr *et al.* [103].

1.5.2 Compartment-based Reconstitution Systems.

To investigate the transport activity of MPs, a two-compartment system is required. The most common system consists of liposomes, representing the membrane model system of choice for the functional investigation for a wide range of MPs including ion channels, receptors, enzymes and transporters. There exist also other systems as e. g. polymersomes, which are self-assembled vesicles made from amphiphilic (di-)block copolymers, first introduced by Discher, Won, *et al.* [105]. While these synthetic (di-)block copolymers have amphiphilicity similar to lipids, they are much larger in molecular weight, resulting in polymersome membranes being thicker (5 - 50 nm) compared to liposomal membranes (3 - 5 nm) or membranes of eukaryotic cells (8 - 10 nm).[106, 107] While liposomes are closer mimics to cell membranes but rather difficult in handling, polymersomes are thougher, more malleable and more stable vesicles.[107] This leads to the conclusion that polymersomes may be more important in synthetic biology, whereas liposomes are preferred for functional investigations on

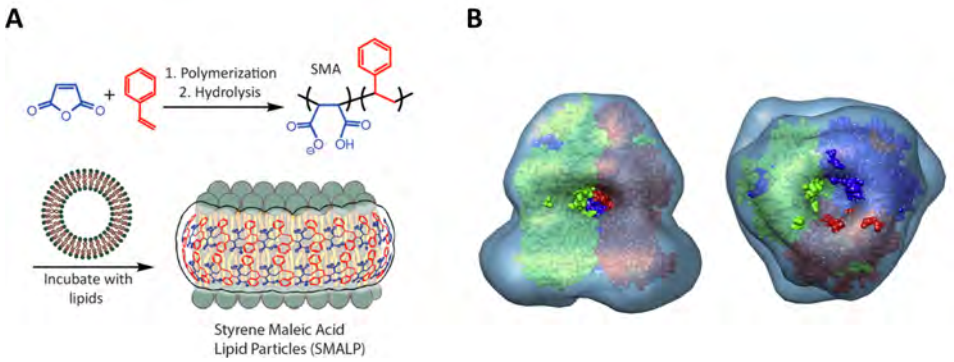

Figure 11: SMALPs. (A) Synthesis and structure of styrene maleic acid (SMA) and formation of SMALPs. Note how the alternating moieties are positioned in SMALPs. The styrene moieties (red) are shielding the lipid's hydrophobic tails, while the maleic acid moieties (blue) are directed towards the aequous surrounding. Figure adapted from [104]. (B) AcrB reconstitution in SMALPs. Fitting of the AcrB crystal structure (PDB: 1IWG; [100]) into the electron density obtained by negative stain EM of the AcrB reconstitution in SMALPs. Left: side view; right: top view. Extra density can be seen surrounding the transmembrane domain of the AcrB structure, which is accounted for by the SMA/phospholipid envelope. Figure and description adapted from [96].

MPs. Consequently, in the following the focus is exclusively laid on liposomes. For further information about polymersomes however, consider the reviews by Discher & Ahmed [106] and Rideau *et al.* [107].

Liposomes - SUVs, LUVs & GUVs.

Liposomes are self-closed lipid bilayer vesicles [62], which enclose an aqueous inner compartment (lumen) and separate it by the lipid bilayer from the surrounding aequous environment (see figure 12 on the next page). The use of liposomes in science is not limited to the investigation on MPs – on the contrary, liposomes are an important tool for clinical applications. Liposomes are the first nano drug delivery systems successfully applied in clinical treatments.[108] Depending on their solubility, drugs can be encapsulated in different manners into liposomes for drug delivery. While hydrophilic drugs are entrapped in the aqueous cavity, hydrophobic drugs have affinity to the phospholipid bilayer. The first liposome-based nanodrug approved by the U.S. Food and Drug Administration (FDA) was Doxil®. It was successfully introduced to the american market in 1995 for the treatment of patients with ovarian cancer and AIDS-related Kaposi's sarcoma after the failure of or intolerance to systemic chemotherapy.[108, 109] A recent overview of liposomal formulations in clinical use was published by Bulbake *et al.* [108].

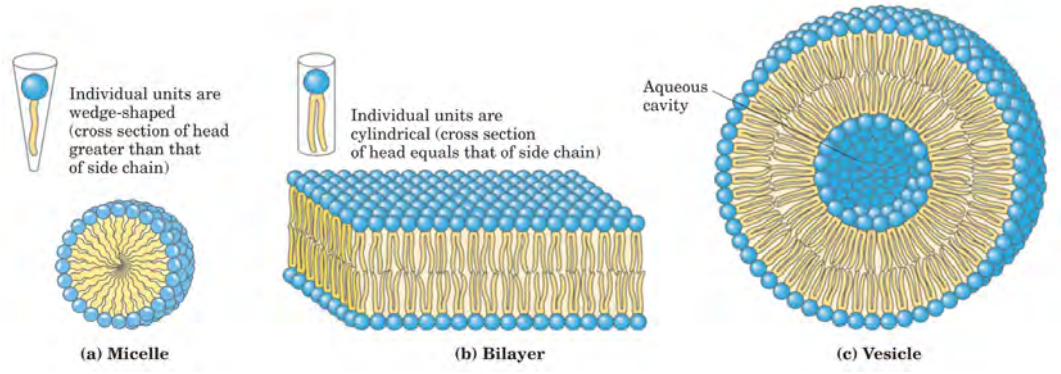

Figure 12: Amphipathic lipid aggregates that form in aequous solutions. (A) In micelles, the hydrophobic chains of the fatty acids are sequestered at the core of the sphere. There is virtually no water in the hydrophobic interior. (B) In an open bilayer, all acyl side chains except those at the edges of the sheet are protected from interaction with water. (C) When a two-dimensional bilayer folds on itself, it forms a closed bilayer, a three-dimensional hollow vesicle (liposome) enclosing an aqueous cavity (lumen). Figure and description from [2]

Liposomes are subclassified according to their size as illustrated in figure 13. Liposomes with a diameter smaller than 100 nm are termed small unilamellar vesicles (SUVs), while liposomes with a diameter between 100 and 800 nm are called large unilamellar vesicles (LUVs). Liposomes even bigger than LUVs with diameters larger than 0.8 µm are named giant unilamellar vesicles (GUVs).[24] Besides several drawbacks (e. g. stability, difficulty to reconstitute MPs), GUVs have an enormous advantage over smaller liposomes. As they are similar in size as cells, GUVs can be monitored and resolved by light microscopy. Therefore, Biner, Schick, Müller, *et al.* [110] have developed a technique to reconstitute MPs into GUVs, where the MPs are delivered to the GUVs' membranes by charge-mediated fusion of smaller liposomes to GUVs.[24, 110]

SUVs and LUVs are most commonly made by first mixing the desired composition of lipids from stock solutions in organic solvent. The ability to generate very specific, defined lipid mixtures is an important advantage of liposomes. The lipid mixture in organic solvent is then dried under vacuum to form a lipid film on the bottom of a round bottom flask. The dried lipid film is dispersed in aqueous buffer by vortexing under 1 atm N_2, until the lipids are fully resuspended and (multilamellar) liposomes are formed spontaneously. The composition of the aqueous solution in the lumen of the liposomes can be composed and defined very specifically according to the application's needs. Multilamellar liposomes having higher lipid contents

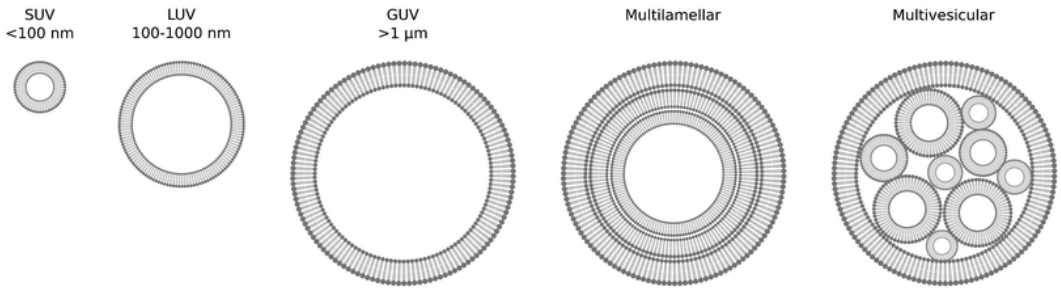

Figure 13: The common vesicle size and lamellarity classification system. Small unilamellar vesicles (SUV) are less than 100 nm in diameter; large unilamellar vesicles (LUV) are between 100 and 1000 nm (or 800 nm, depending on literature source; [24]) and giant unilamellar vesicles (GUV) are larger than 1 µm (or larger than 800 nm). Multilamellar vesicles have many membrane layers, while multivesicular vesicles encapsulate smaller vesicles. Figure not to scale. Figure from [111].

are capable of encapsulating higher amounts of hydrophobic molecules compared to unilamellar liposomes, rendering them interesting for delivery of hydrophobic drugs. For investigations on MPs however, unilamellar liposomes are preferred because of their reduced complexity. In order to break possible multilamellarity of the formed liposomes, the suspension then undergoes several rounds of freeze/thawing in liquid nitrogen and a heat block. Finally, the vesicles are extruded through a filter with the desired pore size to generate homogeneously sized unilamellar vesicles.[62]

To reconstitute MPs into the liposomal membrane, a variety of techniques is used, some of which are discussed in section 1.6.

1.5.3 Further Reconstitution Systems.

In addition to the afore introduced membrane model systems, there are some special model systems as supported planar lipid bilayers, tethered bilayer lipid membranes, peptidiscs, or amphipols, to name a few.

Supported planar lipid bilayers are planar lipid bilayers placed on a solid support. They are simplest prepared by fusion of SUVs on solid supports such as SiO_2, glass or modified gold surfaces by van der Waals, electrostatic, hydration and steric forces.[65]

Tethered bilayer lipid membranes are similar to supported planar lipid bilayers, but the lipids facing the solid support are partially chemically anchored to the solid substrate (e. g. gold: used for electrochemical measurements and surface plasmon spectroscopy).[112] Tethered bilayer lipid membranes are conveniant for characterization of molecular properties of integral MPs, such as topology and interdomain interaction, by atomic force microscopy (AFM).[113] While in primal

tethered bilayer lipid membranes lipids are anchored to a solid support, in a recent approach a detergent solubilized MP was immobilized on the planar solid support. Then, detergent-destabilized liposomes were added to fill the space inbetween the immobilized substrates. After detergent removal a supported planar lipid bilayer was generated with reconstituted anchored MPs applicable for AFM.[114]

Recently presented peptidiscs use a short amphipathic bi-helical peptide (NSP_r), multiple copies of which wrap around to shield the membrane-exposed part of the target MP. In contrast to nanodiscs, requiring MSP scaffold proteins and precise amounts of appropriate lipids, no additional lipids are necessary during peptidisc reconstitution, except for those lipids having co-purified with the MP, i. e. annular lipids.[115, 116]

Amphipols are a family of synthetic short amphipathic polymers carrying a large number of hydrophobic chains. Therefore, amphipols are able to associate with the transmembrane surface of MPs by multiple contact points.[117] Amphipols have been used as an environment to fold both β-barrel and α-helical integral membrane proteins to their active form in the absence of detergent.[118] Further, also more complex G protein-coupled receptors (GPCRs) were successfully folded *in vitro* using amphipols.[119] Amphipols are more extensively reviewed in [120–123].

1.6 Reconstitution of MPs into Liposomes.

As explained in section 1.5, most MPs need to be reconstituted into a model membrane system to be investigated. Here, the focus is exclusively laid on reconstitution in liposomes as model membrane system.

In order to obtain an overview on different techniques to reconstitute MPs into liposomes, including the use of organic solvents, mechanical means, or detergents, see figure 14 on the following page. Further, I recommend the reading of Rigaud, Pitard, *et al.* [124], which is a hallmark review on MP reconstitution techniques; alternatively consider Etemadi [125]. For more recent reviews regarding this topic consider [57, 62, 65, 126].

To begin with, I would like to quote Skrzypek *et al.* [62], giving a perfect classification of the reconstitution techniques:

> *This process, known as reconstitution, may be considered by some as an art-form.*

This quotation has its origin in the fact that the detergent-mediated reconstitution of integral MPs into liposomes constitutes a difficult task requiring optimization for

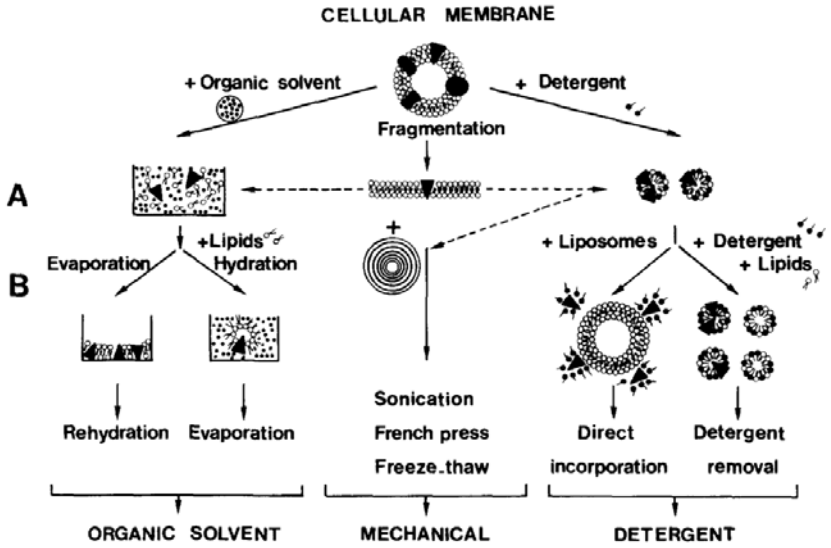

Figure 14: Schematic representation of different strategies for the functional reassembly of MPs into liposomes. Starting from purified cellular membranes of eukaryotic or procaryotic cells, MPs can be isolated either in a mixed micelle with detergent, dissolved in an organic solvent or in an aqueous environment as aggregates or membrane fragments (A). Once isolated and purified, these membrane proteins are supplemented with an excess of phospholipids and can be reconstituted into liposomes following three main strategies (B): organic solvent-mediated reconstitutions (reverse-phase evaporation, rehydration of lipid-protein films); mechanical means (sonication, French press, freeze-thaw); detergent-mediated reconstitutions (detergent removal, dilution or direct incorporation). Figure and description from [124].

each and every single MP of interest. This optimization is inevitable, however certain leads can be given as discussed below. The art of re-insertion of MPs into membrane structures has been initiated almost five decades ago in the laboratory of Efraim Racker at Cornell University.[6] According to Eytan [6], the first enzymes which were functionally reconstituted were a mitochondrial proton-translocating ATPase [127], a proton translocating cytochrome *c* oxidase [128] and a Ca^{2+}+Mg^{2+}-P-ATPase from skeletal sarcoplasmic reticulum [129].

In the following, the focus is laid on detergent-mediated reconstitution of MPs into liposomes.

1.6.1 Detergent-mediated Reconstitution into Liposomes.

Generally, the process of detergent-mediated reconstitution of MPs in liposomes can be divided into two main steps. First, a detergent-solubilized, purified MP is

mixed with lipids. Second, the detergent is removed from the mixture, leading to the incorporation of the MP into liposomes.

In the first step, the lipids can be added to the solubilized MP either as mixed detergent-lipid micelles or as preformed, detergent-destabilized vesicles. When the lipids are introduced as mixed detergent-lipid micelles, the purified membrane protein comicellizes in an excess of phospholipids and appropriate detergent, leading to a solution of lipid-detergent micelles and ternary complexes of lipids, detergents and MPs.[5, 126] Upon detergent removal from these micellar solutions, closed lipid bilayers are progressively formed, in which such ternary complexes eventually incorporate by participating in the membrane formation process.[126] It was also proposed that detergent removal results in the in the separate dissociation of lipid-detergent micelles and ternary complexes, and the MP must insert into preformed detergent-doped bilayers.[126]

Knol, Veenhoff, *et al.* [130] however studied reconstitution of the purified lactose transport protein (LacS) of *Streptococcus thermophilus* systematically and reported reconstitution of LacS being most successful and highly reproducible when LacS was reconstituted into preformed, detergent-destabilized liposomes. The highest transport activities of LacS were obtained when it was reconstituted with low amounts of detergent at the onset of liposome solubilization.[130]

1.6.2 Reconstitution into Preformed, Partially Detergent-solubilized Liposomes.

The Other Way Round: Solubilization of Liposomes.
To pave the way towards understanding detergend-mediated reconstitution of MPs into preformed liposomes, reflections on solubilization of liposomes by detergent have to be considered. Because of their geometry, most phospholipid molecules are curvophobic, thus having a spontaneous tendency to form (flat) bilayers. Most detergent molecules on the opposite are curphophilic, forcing them to aggregate into more or less spherical micelles.[48] This difference in geometry is the main reason why detergents destabilize and thus solubilize (liposomal) membranes (see figure 15). Rigaud, Pitard, *et al.* [124] describe the process of liposome solubilization by detergent as a "three-stage model", where the behaviour of liposomes in the presence of increasing concentrations of detergent is explained. In stage I, an increase in the total detergent concentration increases both the concentration of monomeric detergent and the fraction of detergent in the liposomes, but no micelles are formed. In stage

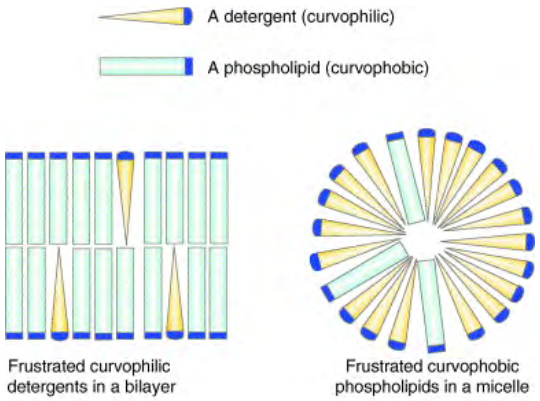

Figure 15: Curvophobic and curvophilic molecules. Because of their geometry most phospholipid molecules have a spontaneous tendency to form flat bilayers. They can be said to be 'curvophobic', which is in opposition to most detergent molecules, the geometry of which forces them to aggregate into more or less spherical micelles and are, thus, said to be 'curvophilic' (compare also to figure 12 on page 23). A curvophilic detergent will experience some degree of structural strain, that is, it will be 'frustrated' when incorporated into a flat bilayer and, conversely, a curvophobic phospholipid will be 'frustrated' when making part of a micelle. Figure and description from [48].

II, liposome solubilization occurs with the appearance of co-existing populations of mixed micelles. In this stage, the molar fraction of detergent in the liposomes plateaus at its saturation level. The micelles however contain a different, but also constant molar fraction of detergent. In stage III finally, the lipids are totally solubilized and only mixed lipid-detergent micelles exist.[124]

For a more recent review focusing on biophysical aspects of the mechanism of detergent solubilization of lipid bilayers consider Lichtenberg, Ahyayauch, *et al.* [131]. Different aspects of reconstitution of MPs into preformed, partially detergent-solubilized liposomes have been reviewed by Rigaud & Levy [126], and more recently further investigated by Crouch *et al.* [132].

Transfer to Detergent-mediated Reconstitution into Preformed Liposomes.

Reconstitution of MPs into preformed, partially detergent-solubilized liposomes (see figure 16) builds on the idea that reconstitution is the reverse process of the afore described membrane solubilization.[5] An important point for this kind of reconstitution in the three-stage model is the early onset of phase II, i. e. close to the onset of solubilization, where the liposomes are partially, and only partially, solubilized. A strategy to optimize reconstitution of MPs into preformed, partially

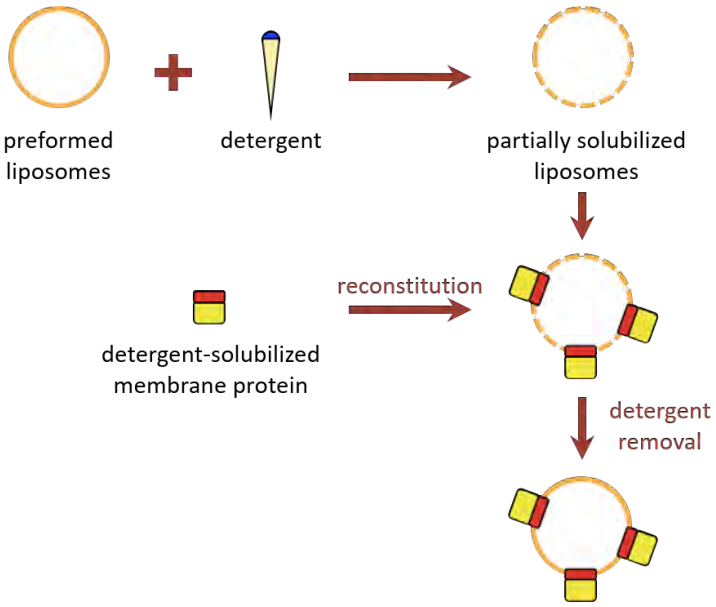

Figure 16: Reconstitution of MPs into preformed, partially detergent-solubilized liposomes. After formation of the liposomes (SUVs or LUVs), an appropriate amount of detergent is added in order to partially solubilize the liposomes, and purified, detergent-solubilized MP is added. After incubation, the detergent is removed, thereby integrating MPs into the vesicular membrane, forming tight and stable proteoliposomes.

detergent-solubilized liposomes was introduced by Rigaud, Pitard, *et al.* [124] as illustrated in figure 17 on the next page.

Detergent Removal – A Critical Point in Reconstitution.

After incubation of detergent-solubilized MPs with preformed, partially detergent-solubilized liposomes, the detergent has to be removed to form tightly closed proteoliposomes. Detergent removal can be achieved by various methods based on the the CMC of the detergent used. Methods for detergent removal are dilution, dialysis, adsorption to polystyrene beads (also known as biobeads) or gel filtration, i. e. size exclusion chromatography (SEC). While gel filtration, dialysis and dilution techniques work best for detergents with a high CMC forming rather small micelles, adsorption with biobeads is more effective for detergents with a low CMC, consequently forming large micelles, such as DDM or Triton X-100.[62, 124]

Additionally, another approach has been described more recently, using cyclodextrins for the selective extraction of detergents from mixed detergent-lipid-protein micelles for the preparation of proteoliposomes. Several types of cyclodextrins exist, which differ in size and thus in affinity for different detergents.[133] Cyclodextrins are

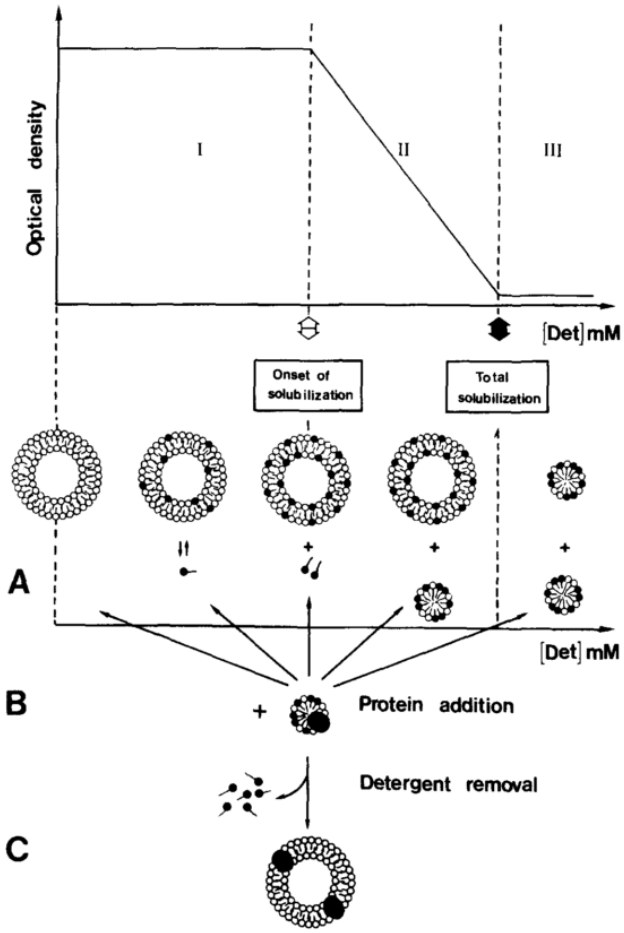

Figure 17: Schematic representation of the strategy for MP reconstitution. The standard procedure for reconstituting MPs is carried out in three different steps: (A) Stepwise solubilization of preformed liposomes (the solubization process can be qualitatively analyzed through turbidimetry). I, II, III correspond to the three stages of the solubilization process described in section 1.6. White and black arrows correspond to the onset and total solubilization, respectively. (B) Protein addition at each step of the lamellar to micellar transition. (C) Detergent removal. Figure and description from [124].

cyclic oligosaccharides consisting of (α-1,4)-linked D-glucopyranose units produced from starch bioconversion (see figure 18). The best known cyclodextrins usually referred to as α-, β-, and γ-cyclodextrins are composed of six, seven and eight glucose units, respectively.[134] Cyclodextrins are able to form host-guest inclusion complexes with detergent molecules. Inclusion complex formation and stability tightly depend on the adaptability of the internal cavity of the cyclodextrin to the dimension of the detergent molecule to be enclosed.[134] OG for example has been shown to form

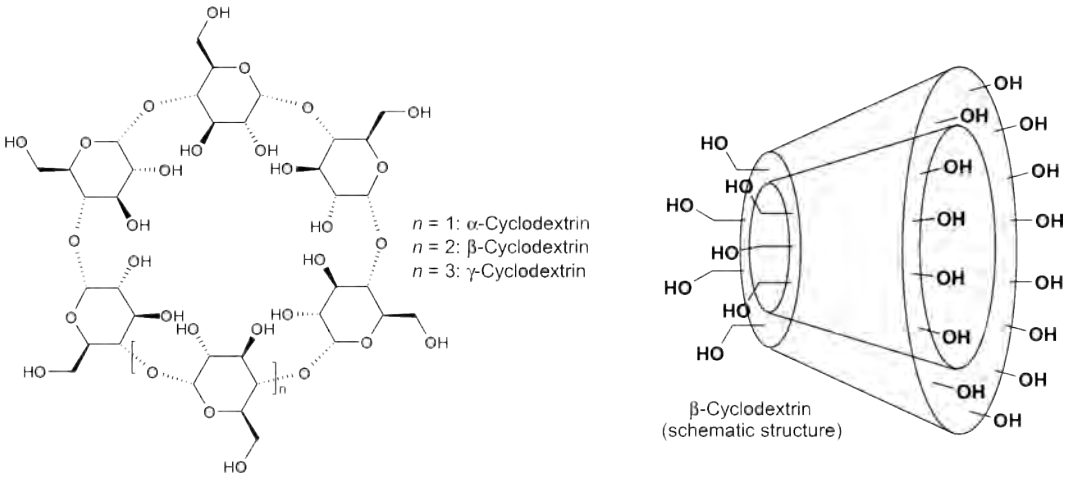

Figure 18: Structures of natural cyclodextrins. α-, β- and γ-cyclodextrin comprise of six, seven and eight (α-1,4)-linked D-glucopyranose units, respectively (left). In a schematic representation (right) β-cyclodextrin has a truncated cone-like structure with primary and secondary hydroxyl groups. During the nanoencapsulation process, hydration water molecules inside the cyclodextrin cavity are replaced by a hydrophobic guest molecule. Figure and description from [135].

1:1 complexes with α-cyclodextrin, provided with the smallest cavity (4.9 Å internal diameter and 7.9 Å depth), with an association constant of K_a close to 2×10^3 M^{-1}, being the highest found among the reported values for amphiphilic analogues of OG.[134] Thus, the uptake of OG by α-cyclodextrin efficiently decreases the number of free surfactant molecules.[134] While OG is efficiently bound by α-cyclodextrin, DDM interacts with α-cyclodextrin only with low affinity ($K_a < 10^3$ M^{-1}). DDM instead binds with a very high affinity ($K_a \geq 10^4$ M^{-1}) to β-cyclodextrin [133] having a cavity bigger than the one of α-cyclodextrin, which is rather too small for DDM. Deduced from a comparison of the molecular shapes of DDM and OG, and from the non-existence of reports of binding OG with β-cyclodextrin to my knowledge, the cavity of the latter however seems to be too big to bind OG with high affinity.

Due to the recently risen public awareness of viral infections I would also like to mention that, only very recently, Jones *et al.* [136] reported that cyclodextrins can exhibit a broad-spectrum virucidal effect against viruses depending on heparan sulfate proteoglycans for attachment to the host's cell surface.[136, 137] For this purpose, they modified cyclodextrins with mercaptoundecane sulfonic acids to mimic heparan sulfates and provide the key nontoxic virucidal action. This resulted in biocompatible macromolecules proven to be active with a broad-spectrum virucidal, irreversible mechanism of action.[136]

The exact mechanism of reconstitution by detergent removal is not fully understood, and the current opinion has not drifted far from that of Rigaud, Pitard, *et al.* [124].[5, 62] However, when the detergent concentration is reaching a critical level during its removal, solubilized MPs cannot be stabilized in detergent-containing micelles anymore. At this point, MPs either precipitate or spontaneously integrate into the phospholipid membrane.[62, 65]

The efficiency of the reconstitution process depends on various factors as e. g. the MP of interest itself, the type of detergent used, the initial detergent concentration, the composition of the lipid membrane, the ionic conditions, or importantly the method and rate of detergent removal.[62] Different methods of detergent removal are listed in table 5 on the following page.

If detergent molecules are more readily removed from partially solubilized liposomes than from the MPs, the liposomes will stabilize without the insertion of MPs. If the detergent is removed from the MP's hydrophobic surfaces at a point beyond MP insertion this will obviously lead to protein denaturation and/or aggregation. These processes are important particularly when MPs are reconstituted via rapid detergent removal.[5] Additionally, according to Knol [5], fast removal of the detergent may decrease the MP's functional activity in proteoliposomes. Decreased transport activity of LacS (*S. thermophilus*) was reported, if purified LacS was reconstituted into liposomes by high initial concentrations of polystyrene beads.[5]

Advantages of Reconstitution into Preformed, Detergent-destabilized Liposomes.

Reconstitution of MPs into detergent-destabilized, preformed liposomes has several advantages over reconstitution techniques from soluble mixtures of detergent, lipid and MP. According to Knol [5], these advantages are:

1. better control over the incorporation of MP into lipid bilayers. The number of MPs per vesicle for example is tunable based on consideration of the size of the liposomes and the lipid to MP ratio. The occupancy statistics of MPs reconstituted in homogeneous liposomes can in theory be described by the Poisson distribution. In reality however, liposomes are heterogeneous, thereby altering the statistics of occupancy.[153];

2. MPs face lower detergent concentrations for a shorter period of time;

3. losses of MPs (aggregation) and lipids are generally low;

Table 5: Methods of detergent removal. Adapted from [62].

Method	Method Description	Advantages	Disadvantages	References
Dilution	Detergent-free dilution buffer is added to lower the detergent concentration. Proteoliposomes form when [detergent] < CMC.	• detergent removal rate controllable, • Proteoliposome formation may be monitored.	• cannot remove all detergent, • heterogeneous and dilute samples	[138, 139]
Gel filtration	Separates monomer and mixed micelles from proteoliposomes based on the difference in size. Elution in a detergent-free buffer.	• fast, simple, efficient and reproducible	• dilute sample, • may lose lipids in the resin	[140–143]
Dialysis	The lipid/detergent/protein mix is dialysed against detergent-free buffer in a dialysis bag.	• gentle process suitable for labile or unstable molecules in liposomes, • inexpensive and simple	• no control over detergent removal rate, • poor reproducibility and long time scale	[142, 144–146]
Adsorption to polystyrene beads	A physical adsorption method. The hydrophobic detergent tails bind to the hydrophobic surface of the beads. Polystyrene beads are removed by filtration, centrifugation or gravity.	• fast (minutes to hours), • control of detergent removal rate	• minor loss of lipids	[124, 147–151]
Cyclodextrins	Selective extraction of detergents from mixed detergent-lipid-protein micelles. Based on much higher affinity of inclusion compounds of cyclodextrin type for detergents in comparison with bilayer-forming lipids.	• fast, simple and efficient, • generally applicable, independent of CMC, • nearly quantitative recovery of MP in proteoliposomes, • low ratio lipid to protein tolerated	• liposome integrity may be affected by lipid composition and type	[133, 152]

4. easier to achieve membrane reconstitution with a (more) uniform orientation of the MPs.[5] In the cases of H^+-F-ATPase, Ca^{2+}-P-ATPase and other MPs [154, 155], a more uniform orientation of the MPs in the reconstituted liposomal bilayer has been observed when the MPs were reconstituted into preformed, partially detergent-solubilized liposomes.[5, 6]

Disadvantages of Reconstitution into Preformed, Detergent-destabilized Liposomes.

Addition of MPs in detergent micelles to preformed liposomes of defined size may alter the size of the latter [62], hence may requiring an additional step of size homogenization by extrusion through a filter with defined pore size. An additional limitation with big impact on functional investigations of MPs reconstituted in proteoliposomes concerns the orientation of the reconstituted MP in the liposomal membrane. This issue is addressed in section 1.7 below.

1.7 The Orientation Problem.

1.7.1 Orientation of MPs in Nature.

The selective and asymmetric, i. e. orientated, insertion of MPs into membranes has been an evolutionarily ancient problem solved by the earliest life forms.[156] In eukaryotes for example, MPs synthesized on cytosolic ribosomes can, amongst others, be targeted to the endoplasmatic reticulum (ER). Insertion into the ER membrane can generally occur following two different main pathways, either co-translationally or post-translationally. While in the co-translational pathway all of the steps from initial protein recognition to final insertion into the membrane occur during protein synthesis, targeting and insertion via post-translational pathways occur after complete MP synthesis (see figure 19).[156]

In prokaryotic cells, MPs are inserted co-translationally into lipid bilayers.[157] In bacteria, the final location and topography of MPs delivered either to the cytoplasmic or outer membrane depends on targeting sequences, hydrophobic domains, or covalently-linked lipids.[158] It is known that upon exiting from the ribosome, the nascent polypeptide chains of MPs enter the translocon [159], a protein complex providing a channel allowing the polypeptide to insert into the lipid bilayer, with their N-terminus ahead.[160] Regarding topology, it is generally accepted that a major determinant is the distribution of positively charged arginine and lysine amino acids

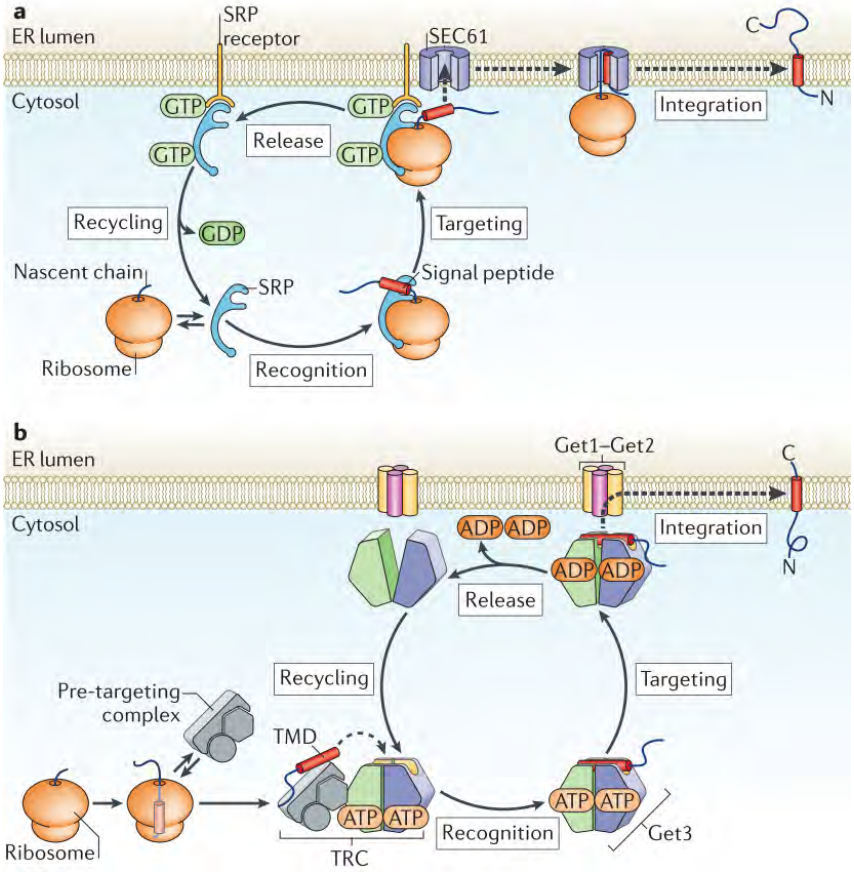

Figure 19: Membrane protein biosynthesis in eukaryotes. (A) In the co-translational pathway for the insertion of endoplasmic reticulum (ER) MPs, signal recognition particle (SRP) recognizes the hydrophobic signal peptide of the nascent chain as it emerges from a translating ribosome. The ribosome-nascent chain-SRP complex is targeted to the membrane by a GTP-dependent interaction with the SRP receptor, resulting in the release of the signal peptide and docking of the ribosome-nascent chain complex to the SEC61 translocon. Translation then resumes, and the nascent polypeptide is inserted into the membrane bilayer. After GTP hydrolysis, SRP is recycled to the cytosol. (B) In the post-translational pathway for the insertion of tail-anchored (TA) ER MPs, a soluble pre-targeting complex captures the hydrophobic transmembrane domain (TMD) of the TA substrate after it emerges from the ribosomal exit tunnel. After loading onto Get3 (TRC40 in mammals), the TA substrate is targeted to the ER membrane by interaction with the Get1-Get2 receptor complex. After ATP has been hydrolysed, the TA substrate is released for insertion into the bilayer. ATP binding recycles Get3 (or TRC40) back to the cytosol. N: amino terminus. Figure and description from [156].

in the loops between transmembrane helices of MPs [160], even though there are additional factors involved as the Sec and YidC translocases [161]. According to the "positive-inside" rule [162] the hydrophilic face of the MP with the most positively charged residues is invariably cytoplasmic.[160, 162] If the distribution of positive charges is similar between both hydrophilic faces, the MP is topologically frustrated, adopting a mixture of the two possible orientations, i. e. a dual topology.[160, 163] An example therefor is EmrE [164], a multidrug transporter located in the inner membrane of *E. coli*. EmrE is functional as a dimer with its monomers arranged in antiparallel orientation having opposite topology, hence being a rare example of a MP adopting dual topology *in vivo*.[160, 164] Recently, it has been discussed controversially whether monomers of EmrE attain their dual topology through reversible topological inversion (flip flop) in the membrane [157], presumably assisted by oligomeric translocons [160], until being trapped in a fixed orientation by dimerization (see figure 20, right pathway). Alternatively, membrane-inserted monomers attain were proposed to attain their final orientations independently of dimerization [165, 166] (see figure 20, left pathway), thus suggesting that flip flopping is an unlikely event *in vivo*.[160] However, Fluman *et al.* [166] eventually reported the initially inserted orientation remaining stable and not being dynamic, at least with respect to the orientation of the entire protein. Their findings suggest that MPs are correctly orientated already during or immediately after synthesis, as they are inserted into the membrane.[166] To summarize, how nascent polypeptide chains of MPs insert into the membrane and fold to eventually attain their final structure and orientation is still sort of an enigma.[160]

1.7.2 Orientation of MPs in Liposomes.

To insert MPs into biological membranes, nature makes use of a set of factors as e. g. chaperones, translocons, assembly factors or signal recognition particles [156], thereby determining the orientation of the inserted MP. Common reconstitution systems however are designed to be very simplistic, most often only containing the liposomal membrane and a number of molecules of the MP of choice. Consequently during liposome reconstitution, none of these helping factors are present. Even though reconstitution of MPs into liposomes may remind us somewhat of the post-translational pathway for MP insertion in eukaryotes, because of the lack of helping factors, reconstitution into synthetic systems as preformed liposomes remains a challenge to be solved in a completely different approach compared to nature.

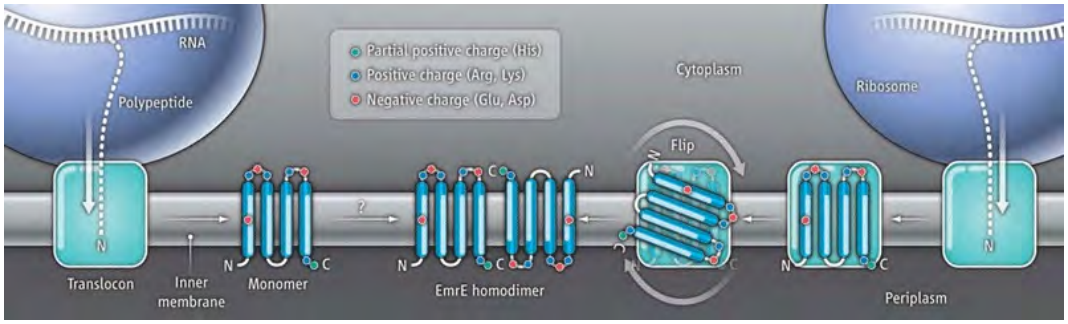

Figure 20: A special example for biosynthesis in bacteria: EmrE biosynthesis. The multidrug transporter EmrE (*E. coli*) is a homodimer consisting of two monomers with opposite topologies (middle). During synthesis, the nascent polypeptide chain exits the ribosome and enters the translocon; once released into the membrane, EmrE probably cannot change its topology (left). However, EmrE could potentially flip in the membrane while associated with the translocon (right), perhaps either while the translocon is still associated with the ribosome or after dissociation. The topology of EmrE is determined predominantly by the positively charged residues. Figure and description from [160].

The orientation of reconstituted MPs seems to be unique for each protein and specific set of reconstitution techniques, hence difficult to predict and influence.[62] Each MP appears to reconstitute into liposomes in a characteristic orientation ratio. Some MPs show only a slight or no preference for one orientation; examples therefor are aa_3 C*c*O (*R. sphaeroides*) [167] or bacteriorhodopsin [168], to name a few. Further, e. g. 80 % of reconstituted Ca^{2+}-P-ATPase from rabbit sarcoplasmic reticulum were reported to be facing outwards [147], while 70 % of the human large-conductance calcium- and voltage-activated potassium channel (BK) were orientated inside-out [140]. A few MPs however seem to insert essentially unidirectionally, as e. g. F_1F_0 ATP (*E. coli*; [169]), or LacS [130].[170]

In the previous discussion of MP reconstitution in section 1.6, the aspect of orientation of the inserted MP in the liposomal membrane was neglected. Orientation of the inserted MP however strongly affects functional studies of these MPs! If a MP exhibiting vectorial function is present in two populations differing in orientation in liposomes, no net conclusion can be drawn on the efficiency and the functionality of that MP.

If a MP transporting a substrate vectorially across the liposomal membrane is reconstituted in two opposite orientations approximately evenly distributed, net transport of the substrate across the membrane would be close to zero, at least if both enzyme populations are activated by the driving force. If one of the two orientation

populations is predominant, but not exclusively present, the minor population reduces the net result, making conclusive statements about the MP's efficiency impossible.

In some cases, the problem of not unidirectionally reconstituted MPs in proteoliposomes can be circumvented by imposing unidirectional function either by blocking one orientation population from interacting with the substrate, or by restricting the location of the respective substrate (e. g. aa_3 C*c*O; discussed below).[6] In the case of Na^+/K^+-P-ATPase for example, which catalyzes ATP hydrolysis accompanied by sodium extrusion and potassium uptake into cells, activity can be selectively inhibited by the plant-derived toxic substance ouabain and by vanadate ions. Ouabain interacts with a site located on the exterior, while vanadate ions interact with sites located on the interior.[6, 171] This allows for selectively blocking one of the two orientation populations of the reconstituted ATPase, resulting in unidirectional function despite of symmetric orientation of the reconstituted enzyme.

Orientation of MPs in Coreconstitution Systems.

This described effect can have even worse consequences when investigating coupled activity of two or more MPs depending on each other's function. When coreconstituting a purified terminal oxidase with a purified ATP synthase to build a minimal respiratory chain in liposomes (figure 21) for example, the efficiency of ATP generation by the synthase is expected to be strongly affected by the orientation of the oxidase. The two enzymes are functionally coupled via proton translocation. Upon addition of reducing equivalents, the terminal oxidase creates and maintains a *pmf* energizing synthesis of ATP by the F_1F_0 ATP synthase under steady state conditions.[170] In other words, the rotational motive force of the F_1F_0 ATP synthase is driven by the transmembrane electrochemical proton gradient generated by the terminal oxidase.

von Ballmoos, Biner, *et al.* [170] reported methodology allowing coreconstitution of purified ATP synthases from *E. coli* and spinach chloroplasts with the purified quinol bo_3 oxidase from *E. coli* and purified C*c*O from *R. sphaeroides*.

As already briefly mentioned above, F_1F_0 ATP synthase of *E. coli* was shown to automatically and reproducibly orientate unidirectionally when reconstituted into preformed, partially detergent-solubilized liposomes.[169] The reason therefor are the size (∼379 kDa [36]) and hydrophilicity of the F_1 part of the ATP synthase, thus preventing the F_1 part to pass the liposomal membrane. Wiedenmann *et al.* [169] reported >97 % of the F_1 moieties facing outwards upon reconstitution of the synthase. Consequently, protons need to be imported to the proteoliposomal lumen

by the terminal oxidase to create an electrochemical gradient being positive and acidic on the inside to fuel ATP synthesis by the reconstituted ATP synthase.[170]

C*c*Os however were shown to reconstitute mainly (60 - 80 %) with the soluble domain of subunit II carrying the cytochrome *c* binding site facing the outside of proteoliposomes.[167] C*c*Os with this orientation pump protons to the outside of the liposomes. Since C*c*O's substrate cytochrome *c* is membrane-impermeable, this problem could be circumvented by providing soluble cytochrome *c* and electrons only on the inside of the liposomes, hence only activating the population of C*c*Os in the desired orientation. In other words, the problem of not unidirectionally orientated reconstitution of C*c*O in proteoliposomes may be circumvented by imposing unidirectional function by the location of the respective substrate.[6]

In the case of membrane-permeable substrates as ubiquinol for the bo_3 oxidase however, both populations are inevitably activated, hence being expected to compete with each other.[170] Using single enzyme experiments, it was reported that reconstituted bo_3 oxidase was present in both orientations in proteoliposomes; about 72 to 77 % of active vesicles were shown to pump protons out of the liposomes.[25, 172] Consequently, if the majority of enzymes is not orientated to facilitate proton import, increasing amounts of oxidase enzymes per proteoliposome should theoretically be decreasing the relative number of proteoliposomes with a net proton influx. von Ballmoos, Biner, *et al.* [170] however reported this to not be the case, hence implying different explanations: *a)* their reconstitution method yields majorly bo_3 oxidase reconstituted in the desired orientation, *b)* differential binding kinetics of ubiquinone Q_1 to the quinone binding site of the two enzyme orientation populations may produce kinetic assymmetries in enzyme turnover and thus proton transport, or *c)* localized proton transfer along the membrane surface may lead to rapid lateral distribution of pumped protons along the inner surface of the liposome [173], hence leading to significant local acidification and thus local pH gradients.[170] During my thesis writing however, Sabina Deutschmann, a PhD candidate in our lab, observed a shift of the average bo_3 oxidase orientation ratio towards the desired, inwardly pumping orientation when coreconstituting the oxidase with F_1F_0 ATP synthase of *E. coli* (unpublished).

The example of investigations on coreconstitution of bo_3 oxidase and F_1F_0 ATP synthase and measurements of their coupled activity illustrates well the problem of orientation in MP reconstitution. In short, a homogeneous distribution, including unidirectional orientation, of enzymes in the proteoliposomes is a prerequisite for the determination of the coupling efficiency between the coreconstituted enzymes.[174]

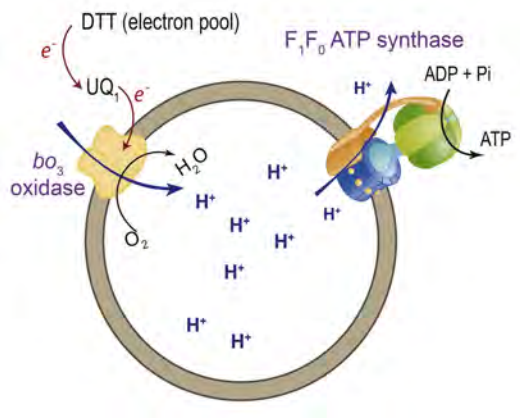

Figure 21: Respiratory-driven ATP synthesis. Cartoon showing proteoliposomes containing coreconstituted ATP synthase and bo_3 oxidase, both from *E. coli*. The electron donor (DTT) and electron mediator (ubiquinol Q_1) are also indicated. Shown is the proton flux during ATP synthesis with correctly orientated enzymes. Figure and description from [170].

Consequently, an optimal method to unidirectionally reconstitute MPs should not only provide unidirectionality of the reconstituted MP, but should also allow to chose and predefine the orientation of the inserted MP.

Different Approaches to Influence Orientation of MPs in Liposomes.

Since the orientation problem is of eminent importance, it has been addressed in many different approaches so far.

Dehydration/rehydration method. Nomura *et al.* [175] reported unidirectional reconstitution of the bacterial mechanosensitive channel of small conductance (MscS) by the dehydration/rehydration method, which involves first creating small unilamellar vesicles using sonication, then mixing these with purified detergent-solubilized channel protein and then sequentially dehydrating (on glass slide; 4 h, desiccator, 4 °C) and rehydrating (in Petri dish under humid conditions; overnight, 4 °C) the sample as described by Delcour *et al.* [176] and Hase *et al.* [177]. While this method seemed to be promising for the reconstitution of some channels, it provides no solid control over orientation. A major drawback of this method is that it might not be applicable to large and complex multi-subunit MPs as e. g. the enzymes of oxidative phosphorylation, being very sensitive towards dehydration. Further, this method does not provide the possibility to actively chose one of the two possible orientation populations.

Exploiting calculations of enzyme mechanism stoichiometries. Verkhovskaya *et al.* [178] reported a technique of enzyme reconstitution for which they claim that it yields essentially unidirectionally orientated bo_3 oxidase vesicles, which allow for measuring proton export exclusively. The reconstitution method is based on a method described by Rigaud, Pitard, *et al.* [124], where lipids were resuspended in buffer containing detergent and mixed with purified bo_3 oxidase, followed by *de novo* formation of liposomes during biobead-mediated detergent removal. However, the reconstitution method is neither containing any attempt to actively influence orientation of bo_3 oxidase, nor are Verkhovskaya *et al.* [178] providing any biochemical proof for the claimed unidirectionality of reconstituted bo_3 oxidase. Their statements concerning MP orientation were based on results of proton pumping experiments, which were compared to theoretical calculations describing the mechanism and stoichiometries of proton translocation by bo_3 oxidase. Even though the results of the proton pumping experiments were admittedly close to the predictions made by calculations, there is no solid biochemical proof of unidirectional orientation.

Preformed, partially detergent-solubilized liposomes. It is generally admitted that a more uniform orientation can be obtained when the MPs are reconstituted into preformed, partially detergent-solubilized liposomes compared to *de novo* formation of proteoliposomes by detergent removal from ternary phospholipid-detergent-protein micelles.[5, 6, 154, 155, 179] It was suggested that, when incorporating a MP into preformed liposomes, the most hydrophilic domain will be least efficient in crossing the bilayer, and the protein will insert with its more hydrophobic side first.[5, 154] As mentioned in section 1.6.2, in the cases of H^+-F-ATPase, Ca^{2+}-P-ATPase and other MPs [154, 155], a more uniform orientation of the MPs in the reconstituted liposomal bilayer has been observed when the MPs were reconstituted into preformed, partially detergent-solubilized liposomes.[5, 6] All their data indicate that the hydrophobic portion of MPs incorporate first in liposomal membranes, however it is notable that orientation was never 100 % unidirectional. This may point out to either leakiness of proteoliposomes or some other potential insertion mechanism of MPs in the liposomal membrane.

However, the suggestion of the more hydrophobic side of the MP entering the lipid bilayer first was further supported by unidirectional reconstitution of purified LacS (*S. thermophilus*), containing a large hydrophilic domain, into detergent-destabilized liposomes. A purified single-cysteine mutant of LacS with the single cysteine located in a putative cytoplasmic loop (LacS C320A/S384C) was reconstituted into liposomes

titrated with a low concentration (1.8 mM) of Triton X-100 and the accessibility of the cysteine for a membrane-impermeable probe was tested. The labeling of reconstituted LacS (C320A/S384C) was complete when the probe was present on the outside. No enhancement of rate or extent of labeling were observed when making the inside of the proteoliposomes accessible to the probe, hence suggesting that LacS was indeed reconstituted unidirectionally with the large hydrophilic domain on the outside.[130]

Detergents & detergent concentrations. As already briefly mentioned above, to optimize reconstitution of LacS and to influence its orientation in liposomes, Knol, Veenhoff, *et al.* [130] tested various detergents and detergent concentrations (OG, 0.8 - 2.0 %; DDM, 0.1 - 1.0 %; $C_{12}E_8$, 0.5 - 8.0 %; Triton X-100, 0.1 - 2.0 %).

This work was continued as reported in Knol, Sjollema, *et al.* [180], focusing on the two nonionic detergents Triton X-100 and DDM. To do so, the strategy introduced by Rigaud, Pitard, *et al.* [124] described in section 1.6.2 was applied, involving stepwise solubilization of preformed liposomes and MP incorporation at different stages of liposome solubilization.[180] Thereby it was observed that Triton X-100 and DDM affect the structure of liposomes in a completely different manner. While preformed liposomes treated with Triton X-100 were observed by cryo-TEM to maintain their bilayer structure far beyond the onset of solubilization, with DDM vesicular structures were already disrupted at the onset of solubilization. DDM-treated lipsomes formed open bilayer structures, further being converted to long threadlike micelles at higher DDM-to-lipid ratios (figure 22).[180] After removal of the respective detergent by biobeads, LacS-mediated lactose transport activity was assessed with a lactose counterflow assay in proteoliposomes using [^{14}C]-radiolabeled lactose. It was observed to be maximal when LacS was inserted into preformed liposomes titrated with Triton X-100. Further, orientation of LacS in proteoliposomes was determined by treating proteoliposomes on the outside with antibodies specifically recognizing the hydrophilic IIA domain of LacS. It was thereby concluded that Triton X-100 (1.8 - 4 mM, $\sim$0.1 - 0.3 %) allowed LacS to be reconstituted with the hydrophilic surface exposed to the outside of the proteoliposomes, whereas reconstitution using DDM (4 - 8 mM, $\sim$0.2 - 0.4 %) led to random incorporation.[180]

Even though LacS was eventually reconstituted unidirectionally, hitherto existing drawbacks yet stay the same; this method does not provide the possibility to actively chose between the two possible orientation populations. Additionally, this method is very characteristic for the used model protein LacS and would require elaborate optimization for each further MP of interest.

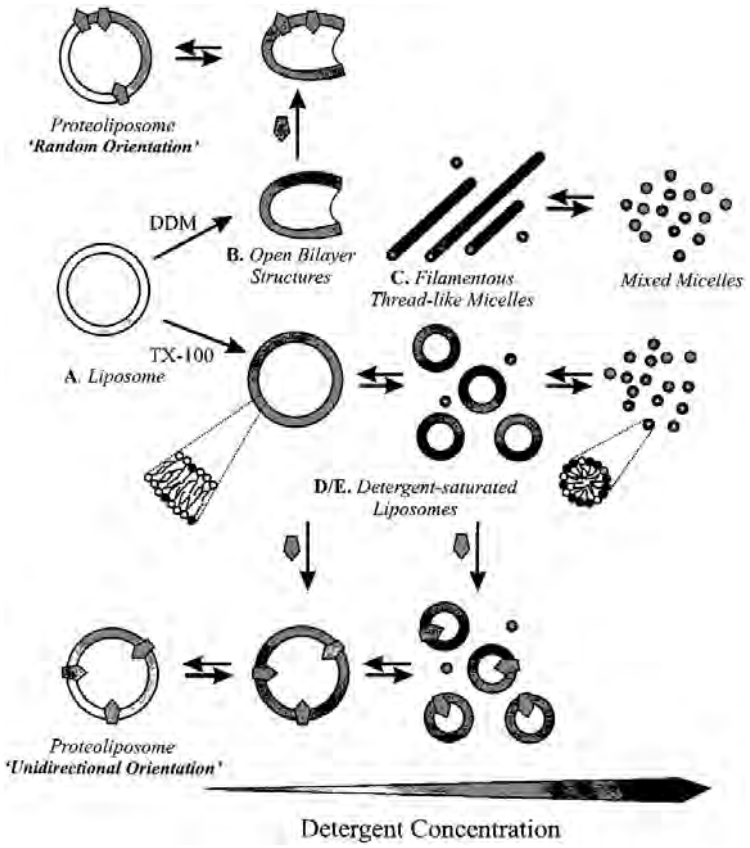

Figure 22: Model for MP reconstitution mediated by DDM or Triton X-100. A - E correspond to structures Knol, Sjollema, *et al.* [180] observed by cryo-TEM. LacS is represented by pentagons. TX-100: Triton X-100. Figure and description from [180].

Rate of detergent removal. It has been stated, that the rate of detergent removal during reconstitution does not only influence reconstitution as discussed in section 1.6, but that it may also have an impact on orientation.[5] Investigating the cholate-mediated reconstitution of H^+-F-ATPase showed that the insertion of the MP after detergent removal by dialysis (slow) is unidirectional, whereas cholate removal by dilution (fast) leads to a random orientation.[5, 6] In these studies however, the MPs were not reconstituted into preformed, partially detergent-solubilized liposomes, but the liposomes were formed *de novo* in the presence of the solubilized MPs. Hence, if the detergent is removed slowly, the formation of closed vesicles can apparently precede the (unidirectional) membrane insertion. Contrarily, if the detergent is removed rapidly, bilayer formation and insertion of the MP occur simultaneously, leading to a symmetric orientation distribution of the MP.[5] Similar results were reported by de Lima Santos *et al.* [181], who determined the orientation of Na^+/K^+-P-ATPase in proteoliposomes.

Lipid composition, pH, ionic strength, membrane curvature. In order to more actively influence orientation of MPs during reconstitution into liposomes, numerous investigations on various parameters have been carried out. Insertion and orientation of MPs are expected to be primarily determined by their interactions with the membrane.[182] For example, it was reported that orientation of bacteriorhodopsin (bR) in proteoliposomes was depending on several factors, including lipid composition of the liposomes, pH value, ionic strength and membrane curvature. The most effective determinant was observed to be the lipid type, modulating insertion and orientation of bR in membranes by changing membrane surface charge and membrane fluidity. pH value and ionic strength were shown to play secondary roles by tuning the nature of electrostatic interactions, while membrane curvature was found to have only minor effects on orientation of bR.[182]

Composition & surface charge of lipid bilayer. Besides studying further reconstitution parameters such as pH, presence of low concentrations of divalent cations or lipid tail saturation levels, Tunuguntla *et al.* [183] varied the composition and surface charge of lipid bilayers. The basis for this approach was constituted by Happe *et al.* [184], who stated that the surface charge of liposomes may play an important role in determining the orientation assumed by MPs (in their case bacteriorhodopsin) in the reconstituted vesicles. By introducing charged lipids into the liposomal membrane Tunuguntla *et al.* [183] could exploit the characteristic of proteorhodopsin (pR) that its structure has an asymmetric charge density, i. e. the C-terminus of pR has an

overall positive charge because of an abundance of positively charged residues, while the N-terminus contains a number of negatively charged residues. Through the use of either positively (DOTAP) or negatively (POPG) charged lipids in liposomes based on DOPC or DOPC, the N- or the C-terminus of pR, located on opposite sides of the enzyme, could be attracted towards the liposomal membrane, respectively (compare to figure 4 on page 7). By accordingly modifying the surface charge of liposomes they were hence able to chose either of the two possible orientations and incorporate pR unidirectionally in liposomal membranes in the desired orientation. The use of liposomes consisting exclusively of DOPC however indicated that charge-neutral surfaces do not induce significant vectorial pR orientation.[183] Orientation of reconstituted pR was assessed by various assays, as proteolytic digestion from the outside of the proteoliposomes followed by SDS-PAGE analysis, surface potential measurements, an immunolabeling assay exploiting an HSV epitope on the C-terminal end of pR, and by monitoring vectorial proton pumping of reconstituted pR using the membrane-impermeable and pH-sensitive fluorophore 5,6-carboxyfluorescein.[183]

Further, lipids of different fatty acid chain saturation levels were tested by comparing negatively charged or charge-neutral liposomes either based on POPC or DOPC. Negatively charged POPG-doped POPC liposomes were compared to negatively charged DOPG-doped DOPC liposomes; and charge neutral liposomes of pure POPC were compared to charge neutral liposomes of pure DOPC. Their results indicated that MP insertion is directed by the polar headgroup charges and not by lipid tail saturation.[183]

The approach described by Tunuguntla *et al.* [183] provides a higher degree of active control over orientation of a reconstituted MP compared to previously described approaches. Nevertheless, this approach is very specific for the MP used in their study.

Bead-supported approaches. A bead-supported approach to unidirectionally reconstitute MPs was published by Schadauer *et al.* [185], and further applied as reported in Geiss *et al.* [186]. In this approach, commercially available silica nanoparticles functionalized with nickel nitrilotriacetic acid (Ni-NTA) were used for the orientated encapsulation of MPs into liposomes as illustrated in figure 23 on page 47. As a proof of concept, the cytochrome *c* oxidase (C*c*O) from *Paracoccus denitrificans* was used. The silica nanoparticles used have a diameter of around 25 nm, hence allowing formation of proteoSUVs.[185] According to the authors, their system is relatively simple in application. First, detergent-solubilized His-tagged C*c*O was immobilized

on Ni-NTA-functionalized nanoparticles to yield proteobeads. Subsequently, the proteobeads were mixed with resuspended lipids and the mixture was dialyzed to remove the detergent, hence forming proteo-lipobeads *de novo*. The membrane of these proteo-lipobeads was reported to form a sealing lipid bilayer acting as ion barrier for potassium and protons.[185] With a final size of about 50 nm, their developed proteo-lipobeads are suited for UV-Vis studies, particularly of multiredox center proteins, and fluorescence spectroscopy studies, because the effects of light scattering are negligible.[185]

However, this approach has some drawbacks. Firstly and most obvious, there is no way to remove the encapsulated nanoparticle at the end of the reconstitution process. The encapsulated nanoparticles also increase the weight of the vesicles. Further, silica surfaces immersed in water (or aequous buffers) are known to acquire negative charge density, primarily through the dissociation of terminal silanol groups.[187] Thus, silica nanoparticles may possibly interact with substrates of the immobilized MP thus falsifying results of functional studies. Further, the activity of reconstituted C*c*O was reportedly drastically reduced when embedded in proteo-lipobeads. The authors held the immobilization of C*c*O on the proteobeads responsible for this decrease in activity and tried to sell it as an advantage "for kinetic studies on MPs that are too fast to be followed by kinetic methods usually applied to live cells".[185] In their publication, a method to actually determine the orientation of C*c*O reconstituted in proteo-lipobeads is missing. Last but not least, when measuring enzyme kinetics of C*c*O in proteo-lipobeads, C*c*O's substrate cytochrome *c* was applied only to the outside of the proteo-lipobeads.[185] Cytochrome *c* however is unable to cross the liposomal membrane. Hence, in this setup cytochrome *c* only reduces C*c*Os orientated with their cytochrome *c* binding site accessible from the outside of the proteoliposomes. Potentially oppositely orientated oxidases however are not reduced due to the lack of cytochrome *c* in the lumen. Consequently, it is not possible to draw any conclusions on C*c*O orientation based on such functional measurements.

A similar approach has been reported by Zheng, Lee, *et al.* [188]. They describe a *b*ead-*s*upported *u*nilamellar *m*embrane (bSUM) system facilitating unidirectional insertion of the voltage-dependent K^+ channel (K_VAP) from the hyperthermophilic archaebacterium *Aeropyrum pernix* [189, 190] into LUVs and GUVs. It was demonstrated that Ni-NTA-functionalized silica beads were able to retain a high density of His-tagged channel molecules, which then acted as "membrane organization centers" during bilayer reconstitution, allowing the formation of continuous, tight unilamellar bilayers on the surface of individual beads (see figure 24). bSUMs were prepared

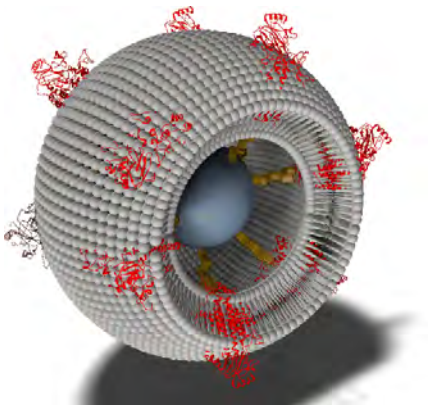

Figure 23: Schematic of a proteo-lipobead. MPs such as cytochrome *c* oxidase (marked in red) are attached to a Ni-NTA-modified central particle (marked in dark gray) via His-tag technology. Phospholipid molecules (marked in light gray) are inserted in-between the proteins to form a freely suspended lipid bilayer membrane. Figure and description from [185].

similarly to the proteo-lipobeads described above. After mixing the protein-bound beads with lipids in detergent, the detergent was stepwise removed using biobeads to reconstitute the bilayer membrane around the surface-anchored channels.[188] Using silica beads of different sizes (0.2 - 20 µm) the size of bSUMs was reported to be tunable, hence allowing generation of proteoLUVs and -GUVs. Unilamellarity of bSUMs was confirmed by cryoEM.[188] According to the authors, selective attachment of the MPs to the surfaces of the beads in detergent yielded "relatively uniform orientation" of the inserted MPs.[188] As in the approach using proteo-lipobeads described above, a method to determine the orientation of K_VAP reconstituted in bSUMs is missing. Regarding this topic, the authors just stated stated that their "cryoEM is still not able to recognize the orientation of the channels" and that "new assays will need to be developed".[188]

bSUMs have drawbacks similar to those of proteo-lipobeads, such as not being able to get rid of the encapsulated silica beads, increased weight of the vesicles and potential interactions of the silica beads with substrates of the MPs in functional studies. Further, the beads can interfere with the liposomal membrane, thereby may leading to ruptures.

Pfleger *et al.* [13] reported an approach, where the beads assisting unidirectional reconstitution are not located in the liposomal lumen. Detergent-solubilized C-terminally His-tagged proteorhodopsin is initially bound to Ni-NTA-coated silicate particles with a diameter of 0.2 µm. Subsequently, pR bound to these beads was

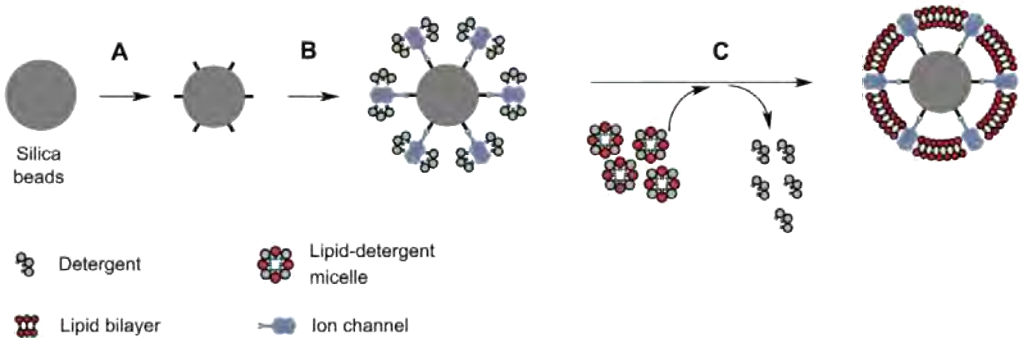

Figure 24: Chemical principles behind the formation of bSUMs. (A) Surface functionalization through chemical oxidization and bioconjugation. (B) Binding of transmembrane proteins via active ligands on the surface of the beads. (C) Reconstitution of a lipid bilayer around the anchored MPs on the beads. Figure and description from [188].

reconstituted into preformed, detergent destabilized liposomes in the presence of pyranine, followed by detergent removal using biobeads. The size of the silicate beads is thereby intended to enforce a net C_{out}-N_{in} orientation of pR. Compared to the bead-supported approaches described above, it is an elegant feature that the silicate beads were removed after reconstitution by addition of imidazole and subsequent centrifugation. Residual pyranine was removed by dialysis, resulting in a system with unidirectionally orientated pR in proteoliposomes with encapsulated pyranine. By monitoring proton pumping of pR by pyranine a net C_{out}-N_{in} orientation was confirmed.[13] Further, as already mentioned in section 1.2.1, by monitoring proton pumping of net C_{out}-N_{in}-orientated pR at different pHs (pH 6 and pH 8.5), pH-dependent bidirectionality of pR-mediated proton transport was confirmed (see also 4D). Importantly, Pfleger *et al.* [13] do not claim 100 % unidirectional C_{out}-N_{in} orientation of pR, but "net" (i. e. >50 %) C_{out}-N_{in} orientation. This is owed to pyranine-mediated monitoring of proton pumping, not allowing to draw quantitative conclusions on the direction of proton pumping, but rather relative statements.

Orientated MPs in tethered bilayers – a strategy applicable to liposomes? There are approaches applying the idea of exploiting the His-tag for orientation of MPs in tethered bilayers for atomic force microscopy, as e. g. described by Bronder *et al.* [113], Sumino *et al.* [114] or Friedrich, Robertson, *et al.* [191]. In these studies, detergent-destabilized liposomes were used to fill spaces between MPs and lipids anchored on a solid support, finally forming a tethered bilayer (see section 1.5.3).

It can be speculated that this method may be adopted for unidirectional reconstitution of MPs into liposomes. After immobilizing the detergent-solubilized MP of interest on a planar solid support, detergent-destabilized liposomes could be added to reconstitute around the immobilized MPs followed by removal of the detergent. Disconnecting the reconstituted MPs from their solid support would lead to release of reconstituted proteoliposomes to the bulk for collection. However, a three-dimensional liposome approaching a two-dimensional surface containing immobilized MPs would not allow for delivery of a substantial number of MPs per proteoliposome for spacial reasons. This would be a clear disadvantage of this putative approach, especially if the liposomes shall be used for functional studies requiring multiple copies of the MP per liposome.

Fusion domains. Ritzmann *et al.* [192] reported that large soluble units as fusion domains can guide the orientated insertion of proteorhodopsin into liposomes. By genetic engineering they added GFP to the C-terminus (pR-GFP) or mCherry to the N-terminus (mCherry-pR) of pR as fusion domains, respectively. On one hand, overexpressed pR-GFP and mCherry-pR in *E. coli* were first shown to both pump protons in the same direction from the cytosol to the periplasm, regardless of the C- or N-terminal fusions, respectively.[192] As discussed in section 1.7.1, it is known that upon exiting from the ribosome, nascent polypeptide chains of MPs in bacteria enter the translocon with their N-terminus ahead.[160] Therefore, it is expected that in *E. coli* the C-terminal GFP of pR-GFP is located in the cytosol, while N-terminal mCherry of mCherry-pR is located in the periplasm. This leads to the same N_{out}-C_{in} orientation of pR for both constructs, hence proton pumping in the same direction in the *E. coli* inner membrane, thereby confirming the expectations. On the other hand, they demonstrated that the two fusion proteins were reconstituted in opposite directions in liposomes, hence leading to oppositely directed proton transport across the liposomal membrane.[192] This met the earlier described expectations of MPs inserting with their more hydrophobic side first [5, 154], while bulky, hydrophilic domains will be least efficient in crossing the lipid bilayer.

In order to reconstitute pR-GFP or mCherry-pR, liposomes were first destabilized by 0.75 % OG, followed by extrusion through a filter with a pore diameter of 200 nm. After extrusion, 0.5 mM $CaCl_2$ was added, and the liposomes were briefly incubated. Then, the MP was added to the preformed liposomes to a final lipid to protein ratio of 11.5 (w/w), resulting in approximately 80 MPs per proteoliposome when assuming a liposome diameter of 100 nm and a molar lipid to protein ratio of ∼1000. By

addition of the MP, total concentration of OG increased to 0.8 %. The reconstitution mixture was subsequently incubated for 3 h and detergent was eventually removed by dialysis.[192]

Orientation and functionality of of overexpressed pR-GFP and mCherry-pR in *E. coli* as well as pR-GFP and mCherry-pR reconstituted in liposomes were assessed by a photo-activity assay in proteoliposomes by monitoring the pH in unbuffered extracellular solution using a micro pH-electrode. Further, orientation of the fusion proteins reconstituted in liposomes was assessed by proteolytic digestion from the outside of the liposomes followed by SDS-PAGE and analysis of in-gel fluorescence of GFP and mCherry.

Despite of the success to reconstitute pR unidirectionally in a predefined orientation, their method has several drawbacks. First, the fusion domain might interfere with the functionality of pR. Their method however does not provide any possibility to remove the fusion domain from reconstituted pR prior to functional measurements. Introducing protease cleavage sites between pR and the fusion domains could be a solution to this problem. In the DNA sequence of pR-GFP provided in the supplementary information of Ritzmann *et al.* [192], a HRV 3C as well as a TEV cleavage site between pR and GFP are included, potentially enabling removal of the fusion domain. The DNA sequence of mCherry-pR however did not contain any protease cleavage site.

Second, while introducing fusion domains to termini of single-subunit MPs as pR is rather straight forward and likely to not affect successful expression and correct folding of the fusion protein, this might be more difficult for more complex multi-subunit MPs. Operons of multi-subunit proteins consist of multiple structural genes, which may overlap, hence introduction of fusion domains at termini can be difficult. Further, folding and assembly of multi-subunit MPs may potentially be disturbed by artificially introduced fusion domains in the size range of GFP or mCherry, depending on the location of the respective modified terminus in the quarternary structure of the MP. Therefore, applying the reported method to multi-subunit MPs as bo_3 oxidase might be rather difficult. Additionally, it has to be considered that the application of the reported method to larger multi-subunit MPs might require an increase in the size of the fusion domain to still influence orientation of the reconstituted MP in liposomes; this however remains speculation. Therefore, it would be advantageous if the large soluble unit guiding orientated insertion would not be introduced as a fusion domain, but rather be attached to the MP after the latter's expression and purification, but before reconstitution.

Last but not least, as mentioned in section 1.2.1, pR shows bidirectional transport. The net transport direction is strongly depending on the surrounding pH. Reconstituted wild type pR exports protons at pH 6, while it imports protons at pH 8.5.[13] Our own measurements showed that the reversal point is in the range of pH 7.2 to 7.6 (see section 4.3.5). Interestingly, Ritzmann *et al.* [192] set the measurement pH at pH 7.4, which is very close to the inflection point. However, the reported method allows to unidirectionally reconstitute pR in a predefined orientation, and the underlying idea is very stimulating.

Determining the Orientation of MPs in Liposomes.

In the most common approach to determine orientation of MPs reconstituted in liposomes, the outside of the proteoliposomes is subjected to proteolytic digestion. Membrane impermeability for proteins prevents proteases to enter the proteoliposomes, resulting in partial proteolytic digest only of domains of the reconstituted MPs accessible from the outside of the proteoliposomes. The resulting proteolytic cleavage pattern can eventually be analyzed by SDS-PAGE, western blotting, or mass spectrometry.

Other approaches rely on properties of the reconstituted MPs. Orientation of reconstituted aa_3 C*c*O from *R. sphaeroides* for example can be determined by an assay in which C*c*O is first reduced by cytochrome *c*, only able to reduce these C*c*Os in which the cytochrome *c*-binding site faces the outside, followed by reduction with dithionite, reducing also the inwardly-facing population. Using this method, Näsvik Öjemyr *et al.* [167] reported the orientation of reconstituted aa_3 C*c*O to be 70 - 80 % with the cytochrome *c*-binding site toward the outside, independently of the lipid composition of the proteoliposomes.[167]

Some approaches are further depending on the functionality of the reconstituted MP. Orientation of proton transporting enzymes for example can be assessed by monitoring the direction of proton transport using the pH-sensor pyranine (see section 3.4). This method however only allows qualitative statements on MP orientation, i. e. determination of the net proton pumping direction.

A novel method to determine orientation of MPs in proteoliposomes based on fluorescence quenching of labeled MPs, independent of the MP's functionality, is currently being developed in our lab as discussed in section 4.4.

Unidirectional Reconstitution of MPs in a Predefined Orientation – An Ongoing Daunting Feat.

Following the discussions above, it has obviously been and still is a daunting challenge to control the orientation of MPs in proteoliposomes. Many attempts have been made to reconstitute MPs unidirectionally in a predefined orientation into liposomes, but none of them is generally applicable. There is currently lacking a method to reconstitute each and every MP of interest in liposomes in exactly the one predefined orientation required for the desired downstream application.

2 Aims of the Thesis.

The von Ballmoos research group is especially interested in coreconstitution of a complete respiratory chain in liposomes in order to investigate on consecutive processes thereof. As discussed in section 1.7, this requires unidirectional orientation of each of the participating MPs in a predefined orientation to allow the enzymes of oxidative phosphorylation to generate a *pmf* ($\Delta\,\mathrm{pH} + \Delta\,\psi$) which can be used by the ATP synthase to drive ATP synthesis.

However, there is currently lacking a generally applicable method to unidirectionally reconstitute integral MPs in a predefined orientation into liposomes.

In the cases of enzymes with membrane-impermeable substrates this problem can be circumvented. If a membrane-impermeable substrate is added to the outside of proteoliposomes, only the fraction of MPs with the substrate binding site orientated towards the outside (e. g. ATP with ATP synthase, cytochrome *c* with cytochrome *c* oxidase) is activated.[170]

In the case however of using the membrane-soluble substrate ubiquinol with the cytochrome bo_3 ubiquinol oxidase, substrate availability cannot be used to discriminatingly activate one of the two orientation populations of the enzyme, since binding of the substrate happens in the membrane. Thus, both inwardly and outwardly orientated oxidases have access to the substrate and are activated. Consequently, protons are pumped across the membrane in both opposite directions, leading to a competition between the two orientation populations of the bo_3 oxidase.[170]

As discussed in section 1.7.2, the F_1F_0 ATP synthase of *E. coli* automatically reconstitutes unidirectionally into preformed, partially solubilized liposomes with its F_1 part on the outside of the vesicles. The reason for this behaviour are the size and the hydrophilicity of the F_1 part, preventing it to pass the liposomal membrane. Hence, such reconstituted ATP synthase has to export protons from the proteoliposomes to drive ATP synthesis.

We would like to provide the required proton gradient by coreconstitution of the synthase with the bo_3 oxidase. Because of the above discussed problematic of the membrane-solubility of the bo_3 oxidase's substrate ubiquinol, this requires the bo_3 oxidase to be unidirectionally reconstituted to exclusively facilitate proton import into the proteoliposomes. Therefore, the principal aim of my thesis was to develop a method to unidirectionally reconstitute the bo_3 oxidase in the predefined, desired orientation.

As discussed in sections 1.6 and 1.7, according to Knol [5], one has a better control over the incorporation of the MP into the bilayer if reconstituting into preformed, partially detergent-solubilized liposomes. It has further been observed that a more uniform orientation is obtained by reconstitution of MPs into such preformed liposomes [5, 6]. Therefore, the challenge of unidirectional reconstitution of bo_3 oxidase was faced exclusively for the reconstitution into such preformed, partially detergent-solubilized liposomes.

To pursue the aim of my thesis, the automatically unidirectionally reconstituting ATP synthase was used as a role model. The bo_3 oxidase was modified by attachment of large soluble units (LSUs) mimicking the properties of the F_1 part of the synthase, which is guiding its unidirectional insertion into the liposomal membrane. In order to create an approach which ideally would be applicable not only to the bo_3 oxidase, but to any MP of choice, we intended to use the frequently used His-tag for the attachment of the LSUs to the MP.

Implementation of the approach exploiting the His-tag for the attachment of the LSUs however turned out to be less straight forward than expected. Therefore, several different approaches (more specific vs. more generally applicable) were designed and tested. A potential final method needs to fulfill a list of requirements such as that it must not interfere with the function of the MP; or that it is generally applicable to every MP of choice, ideally with the possibility to chose and predefine either of the two orientations possible. It should further be elegant and not too expensive in application.

Unidirectionally reconstitution of the bo_3 oxidase however proved to be more difficult than expected. Therefore, proteorhodopsin (pR) was further chosen as a model MP to develop approaches for unidirectional reconstitution. pR has the advantages that it can be expressed with reasonable yields in *E. coli*, and that it consists of only one subunit, hence being less susceptible to genetic modifications than the bo_3 oxidase.

3 Methods.

If not stated otherwise, chemicals were purchased from Sigma-Aldrich (Merck, Germany). Detergent concentrations are always stated as % (w/v).

3.1 Expression & Purification of Proteins.

All plasmids are listed in table 6 on the next page.

Cytochrome *bo₃* ubiquinol oxidase

All variants of *bo₃* oxidase were expressed with plasmids based on pETcyo, containing the sequences for *bo₃* oxidase subunits I-IV, with a His-tag at the C-terminus of subunit II, in *E. coli* C43 Δcyo [197] in LB medium containing 200 µg ml^{-1} ampicillin. Additionally, 1 mM $MgSO_4$, 1 mM $MgCl_2$ and 100 µM $CuSO_4$ were added. After growing the bacteria at 37 °C until reaching OD_{600} of 0.5 using a standard shaker system, protein expression was induced by addition of 1 mM IPTG and continued for 5 h at the same temperature. Subsequently, cells were harvested by centrifugation and broken by MAXIMATOR (High Pressure Homogenizer Type HPL6, MAXIMATOR Schweiz AG, Switzerland) in the presence of DNase I, protease inhibitors PMSF and Pefabloc, and lysozyme in 50 mM HEPES pH 8.0, 100 mM NaCl. Membranes were isolated by ultracentrifugation (200 000 x g, 1 h, 4 °C) followed by solubilization using 2 % DDM in the presence of the afore mentioned protease inhibitors in the same buffer. Unsolubilized membranes were removed by ultracentrifugation (200 000 x g, 0.5 h, 4 °C), and the supernatant containing solubilized His-tagged *bo₃* oxidase was applied to Ni-NTA affinity chromatography in 50 mM K_2HPO_4 pH 8.3, 0.1 % DDM. Bound protein was washed with 10 column volumes (CV) of the same buffer additionally containing 10 mM imidazole and eventually eluted with 3 CV of the same buffer additionally containing 250 mM imidazole. Finally, the eluate was concentrated using centrifugal filters (Amicon Ultra, Merck, Germany) with 100 kDa molecular weight cut-off (MWCO) and imidazole was removed either by repeated steps of diluting and concentrating using the same centrifugal filters or by SEC using CentriPure P10/P25/P50 desalting columns (Zetadex-25, emp Biotech, Germany).

Proteorhodopsin.

All variants of pR were expressed in *E. coli* C43(DE3) in TB medium containing 50 µg ml^{-1} kanamycin. After growing the bacteria at 37 °C until reaching OD_{600} of 0.6 when using a standard shaker system, or until reaching OD_{600} of 1.9 when using

Table 6: Plasmid collection.
Concentrations of antibiotics for expression: Amp: $100\,\mu g\,ml^{-1}$; Kan: $50\,\mu g\,ml^{-1}$.

Protein	**Plasmid**	**Antibiotic Resistance**	***E. coli* Expression System**	**Location of His-tag**	**Further Characteristics**
bo$_3$ oxidase	pETcyo-II	Amp^r	C43 Δcyo	C-terminus of subunit II	[193]
bo$_3$-Avi	pETcyo-II-AviTagCSubI	Amp^r	C43 Δcyo	C-terminus of subunit II	AviTag (GLNDIFEAQKIEWWHE) with preceding GS linker at C-terminus of subunit I; subunits I & III overlapping; based on pETcyo-II [193]
bo$_3$-Spy	pETcyo-II-SpyTagCSubI	Amp^r	C43 Δcyo	C-terminus of subunit II	SpyTag (AHIVMVDAYKPTK) at C-terminus of subunit I; subunits I & III not overlapping; based on pETcyo-II [193]
pR-NHis	pET27b(+)-pR-NHis	Kan^r	C43(DE3)	N-terminus	Plasmid designed by C. von Ballmoos, synthesized by Genscript Biotech (USA)
pR-CHis	pET27b(+)-pR-C-TEV-His	Kan^r	C43(DE3)	C-terminus	TEV cleavage site N-terminal of His-tag; plasmid designed by C. von Ballmoos, synthesized by Genscript Biotech (USA)
pR-CSpy	pET27b(+)-pR-CHis-CSpy	Kan^r	C43(DE3)	C-terminus	SpyTag at C-terminus of pR, but N-terminal of His-tag
pR-NSpy	pET27b(+)-pR-CHis-NSpy	Kan^r	C43(DE3)	C-terminus	SpyTag at N-terminus
pR-CSpy-sCys	pET27b(+)-pR-CSpy-sCys	Kan^r	C43(DE3)	C-terminus	SpyTag at C-terminus, but N-terminal of His-tag; Cys residues replaced by Ala; single Cys near C-terminus, N-terminal of SpyTag
pR-NSpy-sCys	pET27b(+)-pR-NSpy-sCys	Kan^r	C43(DE3)	C-terminus	SpyTag at N-terminus; Cys residues replaced by Ala; single Cys near C-terminus, N-terminal of His-tag
BirA	pET28a-BirA (w400-2)	Kan^r	BL21 pLysS	C-terminus	Addgene plasmid 26624, gift from Eric Campeau
SC-ELP-GFP	pQE80L-SpyCatcher-ELP-GFP	Amp^r	C43(DE3)	N-terminus	Addgene plasmid 69835, [194], gift from Viviana Gradinaru; TEV site C-terminal from His-tag
SC-MBP	pMBP-SpyCatcher	Amp^r	C43(DE3)	C-terminus	Addgene plasmid 79053, [195], gift from James Bowie; vector backbone: pDEST14; SC C-terminal from MBP, TEV site inbetween
SC-MBPx	pET21-MBPx-SpyCatcher	Amp^r	C43(DE3)	N-terminus	Addgene plasmid 72327, [196], gift from Mark Howarth; thrombin site C-terminal from His-tag
SC-MBP-3xFLAG	pMBP-SC-3xFLAG	Amp^r	BL21 pLysS	C-terminal from MBP, but N-terminal from SC	based on pMBP-SpyCatcher; 3xFLAG-tag N-terminal
SC-MBPx-3xFLAG	pET21-MBPx-SC-3xFLAG	Amp^r	BL21 pLysS	N-terminus	based on pET21 MBPx-SpyCatcher; 3xFLAG-tag C-terminal from His-tag, but N-terminal from MBPx-SC

a LEX-48 bioreactor system (epiphyte3, Canada), protein expression was induced by addition of 2 mM IPTG and 10 mg L^{-1} all-trans-retinal and continued for 16 h at 20 °C or 27 °C, respectively. Cells were harvested by centrifugation and broken by MAXIMATOR (High Pressure Homogenizer Type HPL6, MAXIMATOR Schweiz AG, Switzerland) in the presence of DNase I, protease inhibitors PMSF and Pefabloc, and lysozyme in 50 mM MOPS pH 7.0, 300 mM NaCl. Membranes were isolated by ultracentrifugation (200 000 x g, 1 h, 4 °C) followed by solubilization using 1.5 % DDM in the presence of the afore mentioned protease inhibitors in the same buffer. Unsolubilized membranes were then removed by ultracentrifugation (200 000 x g, 0.5 h, 4 °C) and solubilized His-tagged pR was purified via Ni-NTA affinity chromatography in 50 mM MOPS pH 7.0, 300 mM NaCl with decreasing concentrations of DDM until a final concentration of 0.05 % DDM. Bound protein was washed with 10 CV of buffer containing 5 mM imidazole and eluted with 6 CV of buffer containing 250 mM imidazole and the final concentration of DDM. Finally, the eluate was concentrated using centrifugal filters (Amicon Ultra, Merck, Germany) with 100 kDa MWCO and imidazole was removed either by repeated steps of diluting and concentrating using the same centrifugal filters or by SEC using CentriPure P10/P25/P50 desalting columns (Zetadex-25, emp Biotech, Germany).

SpyCatcher-containing LSUs.

Plasmids of some basic SpyCatcher-containing constructs are made available via Addgene (USA) (pQE80L-SpyCatcher-ELP-GFP; pMBP-SpyCatcher; pET21-MBPx-SpyCatcher), while others (pMBP-SC-3xFLAG, pET21-MBPx-SC-3xFLAG) were genetically engineered using standard molecular biology techniques on their respective available bases in our lab.

All SpyCatcher-containing LSUs were expressed either in *E. coli* C43(DE3) (SC-ELP-GFP, SC-MBP, SC-MBPx) or in *E. coli* BL21 pLysS (SC-MBP-3xFLAG, SC-MBPx-3xFLAG) in LB medium containing the respective antibiotic for selection. After growing the bacteria at 37 °C until reaching OD_{600} of 0.6 using a standard shaker system, protein expression was induced by addition of 2 mM IPTG and continued for 16 h at 27 °C. Subsequently, cells were harvested by centrifugation and broken by MAXIMATOR (High Pressure Homogenizer Type HPL6, MAXIMATOR Schweiz AG, Switzerland) in the presence of DNase I, protease inhibitors PMSF and Pefabloc, and lysozyme in TBS (Tris-buffered saline; 20 mM Tris-HCl pH 7.4, 150 mM NaCl). Unbroken cells and debris were removed by centrifugation (8000 x g, 20 min, 4 °C) and soluble His-tagged LSU was purified via Ni-NTA affinity chromatography in TBS.

The eluate was concentrated using centrifugal filters (Amicon Ultra, Merck, Germany) with suitable MWCO depending on the size of the LSU. Imidazole was removed either by dialysis against three times 2 L TBS for 16 h at 4 °C (SC-ELP-GFP), by repeated steps of diluting and concentrating the sample using respective centrifugal filters (SC-MBPx, SC-MBPx-3xFLAG), by SEC using CentriPure P50 desalting columns (Zetadex-25, emp Biotech, Germany), or by dialyzing against three times 2 L of 50 mM HEPES pH 7.0, 20 mM NaCl (low salt; SC-MBP, SC-MBP-3xFLAG). SC-MBP and SC-MBP-3xFLAG were further subjected to anion exchange chromatography using a Mono Q anion exchange chromatography column (GE Healthcare, UK).

Biotin Ligase BirA.

The *E. coli* biotin ligase BirA was expressed with plasmid pET28a-BirA (w400-2) (Addgene plasmid 26624, gift from Eric Campeau) in *E. coli* BL21 (DE3) pLysS in LB medium containing and 0.75 % glucose. After growing the bacteria at 37 °C until reaching OD_{600} of 0.5 using a standard shaker system, protein expression was induced by 0.5 mM IPTG and continued for 16 h at 25 °C. Cells were harvested by centrifugation and broken by MAXIMATOR (High Pressure Homogenizer Type HPL6, MAXIMATOR Schweiz AG, Switzerland) in the presence of DNase I, protease inhibitors PMSF and Pefabloc, and lysozyme in 25 mM Tris-HCl pH 8.0, 200 mM NaCl, 1 % Triton X-100. Unbroken cells and debris were removed by centrifugation (8000 x g, 20 min, 4 °C) and soluble His-tagged BirA was purified via Ni-NTA affinity chromatography in the same buffer. The eluate was concentrated using centrifugal filters (Amicon Ultra, Merck, Germany) with 10 kDa MWCO and imidazole was removed by SEC using CentriPure P10 desalting columns (Zetadex-25, emp Biotech, Germany), where the buffer was exchanged to 50 mM HEPES pH 8.0, 200 mM KCl.

3.2 Preparation of Liposomes.

Liposomes used throughout this thesis were always prepared in the same way, only differing in the composition of the liposome buffer and the liposome size. These two parameters are always stated in the figure legends of the according results.

Lecithin (90 %, soybean; Alfa Aesar by ThermoFisher Scientific, USA) (10 mg ml^{-1}) was resuspended in liposome buffer by vortexing for 30 min at room temperature under 1 atm N_2. Multilamellarity was broken by seven consecutive cycles of freezing in liquid nitrogen followed by thawing at 29.4 °C using a heat block. Directly before use, the size of the liposomes was adjusted by extrusion through a polycarbonate membrane (Whatman, UK) with a pore size of either 100 or 200 nm.

3.3 Membrane Protein Reconstitution.

bo$_3$ oxidase (*E. coli*) and F_1F_0 ATP synthase (*E. coli*) were typically either reconstituted individually or coreconstituted into liposomes as described by von Ballmoos, Biner, *et al.* [170]. Briefly, to a liposome suspension (250 or 480 µl, depending on downstream application) was added 0.4 % cholate (from a 20 % stock solution) to partially solubilize the vesicles. If needed for the chosen downstream application, at this point, pyranine (trisodium 8-hydroxypyrene-1,3,6-trisulfonate) (3 mM) was added as well. Typically either 25 µl 20 µM *bo*$_3$ oxidase or 2 µl 40 µM ATP synthase or both MPs was / were then added from stock solutions and the mixture was incubated for 30 min at 25 °C with occasional flicking. For detergent removal (and removal of residual pyranine), the mixture was applied to prepacked CentriPure P10 desalting columns (Zetadex-25, emp Biotech, Germany) equilibrated with a buffer suitable for the desired downstream application. After the mixture entered the column resin completely, the volume difference of the mixture to the maximal application volume was added in buffer, before the liposomes were collected with a final addition of 1.2 to 1.5 ml buffer. If needed, proteoliposomes were diluted and concentrated by ultracentrifugation (229 600 x g, 1 h, 4 °C).

Reconstitution of pR is described in detail in section 4.3.7 on page 108. Briefly, after 1 % OG was added to DDM-solubilized pR, DDM was removed from the mixture and bound selectively by using a 3-fold excess of heptakis(2,6-di-*O*-methyl)-β-cyclodextrin (β-cd) and incubated for 30 min. Subsequently, pR was reconstituted into purified liposomes using a total concentration of 0.75 % OG for partial solubilization. If required for the desired downstream application, pyranine (3 mM) was added during this step as well. The mixture was incubated for 45 min at 25 °C with occasional gentle mixing and thereafter, OG and soluble β-cd-DDM complexes (and external pyranine) were removed using a CentriPure PF10 desalting column (Zetadex-50, emp Biotech, Germany). Finally, proteoliposomes were washed by dilution and collected by ultracentrifugation (229 600 x g, 1 h, 4 °C) and thus separated from potentially last residual soluble β-cd-DDM complexes.

3.4 Functional Assays.

Proton Uptake Measurements with ACMA.

Proton uptake monitored by ACMA (9-amino-6-chloro-2-methoxyacridine) was measured as described by von Ballmoos, Biner, *et al.* [170] with some minor changes. Briefly, 40 to 60 µl of proteoliposomes were diluted into 1.5 ml of buffer HMK (10 mM

HEPES pH 7.4, 2 mM $MgCl_2$, 100 mM KCl, 10 mM KNO_3), and mixed with 2 µM ACMA until a stable baseline was obtained. Proton pumping was then initiated by addition of 2 mM DTT and 20 µM ubiquinol Q_1 or 15 µM ubiquinol Q_2 for the *bo*$_3$ oxidase or by addition of 0.33 mM ATP for the ATP synthase in order to start ATP hydrolysis. After the reaction had reached an equilibrium, the proton gradient was dissipated by addition of 30 mM NH_4Cl. Changes in ACMA fluorescence were monitored using 410 nm and 480 nm as excitation and emission wavelengths, respectively. (slits: 5 nm).

Transmembrane Proton Pumping Detected with Pyranine.

Proton pumping across liposomal membranes (import and export) was measured using the membrane-impermeable pH-sensitive fluorophore pyranine (trisodium 8-hydroxypyrene-1,3,6-trisulfonate or 8-hydroxypyrene-1,3,6-trisulfonic acid, HPTS), which was entrapped in the proteoliposomal lumen during MP reconstitution as described above. Changes in internal pH in vesicles can be assessed by the pyranine fluorescence ratio (F406/F460) of emission at 510 nm by alternating excitation wavelengths at 406 nm and 460 nm.

To measure proton pumping by *bo*$_3$ oxidase or ATP synthase, 10 - 60 µl proteoliposomes were diluted in measurement buffer (2 mM MOPS pH 7.3, 25 mM K_2SO_4; same as liposome buffer) containing 2 mM DTT and 0.1 µM valinomycin. After a stable baseline was obtained, proton pumping was initiated by addition of 50 µM ubiquinol Q_1 or Q_2 for the *bo*$_3$ oxidase or by addition of 0.33 mM sodium ATP for the ATP synthase to start ATP hydrolysis. After the reaction had reached an equilibrium, the proton gradient was dissipated by addition of 0.7 µM nigericin, a ionophore acting as an antiporter of H^+ and K^+.

To measure proton pumping by pR, 40 - 100 µl proteoliposomes were diluted in measurement buffer (0.5 mM MOPS pH 6.5, 25 mM K_2SO_4; same as liposome buffer). After a stable baseline was obtained, proton pumping was initiated by illumination of the sample using a Led Lenser P5 (140 lm; LedLenser, Germany).

Coupled Enzyme Activity – ATP Synthesis.

Coupled enzyme activity of coreconstituted *bo*$_3$ oxidase and ATP synthase was measured by measuring ATP synthesis by the synthase facilitated by a proton gradient set up by the oxidase as described by von Ballmoos, Biner, *et al.* [170]. In some experiments, instead of using 20 µM ubiquinol Q_1, 30 µM ubiquinol Q_2 were used to start proton pumping by *bo*$_3$ oxidase.

Results of coupled enzyme activity measurements were normalized to specific activity of *bo₃* in the respective proteoliposomes assessed by oxygen consumption measurements using an Oxygraph+ (Hansatech Instruments, UK). To 1 ml measurement buffer (50 mM K_2HPO_4 pH 8.3, 0.1 % DDM) 50 µl proteoliposomes were added and the mixture was incubated for 15 min at 25 °C to solubilize the proteoliposomes. The mixture was then transferred to the Oxygraph+, 2 mM DTT were added and after a stable baseline was obtained, O_2 consumption by *bo₃* oxidase was initiated by addition of 25 µM ubiquinol Q_1 or Q_2.

3.5 Methods Specific for the AviTag System.

Biotinylation of Avi-tagged *bo₃* Oxidase by BirA.

Avi-tagged *bo₃* oxidase was essentially enzymatically biotinylated as described by Fairhead *et al.* [198] yielding *bo₃*-Avi-biot. Briefly, to Avi-tagged *bo₃* oxidase in 50 mM K_2HPO_4 pH 8.3, 0.1 % DDM, 5 mM $MgCl_2$, 2 mM ATP, 1 µM BirA and 150 µM D-biotin were added. The mixture was incubated (1 h, 30 °C) with gentle mixing, before the same amounts of BirA and fresh biotin were added and the mixture was incubated for another hour. Finally, biotinylated *bo₃* oxidase was purified by SEC using a Superose 6 Increase 10/300 GL column (GE Healthcare, UK) in 50 mM K_2HPO_4 pH 8.3, 0.1 % DDM.

Modifying the Large Soluble Unit.

To bind streptavidin (SA) (IBA Life Sciences, Germany) or SA-containing large soluble units (LSUs) to *bo₃*-Avi-biot, a 2- to 10-fold excess thereof was incubated with *bo₃*-Avi-biot for 2 h at 20 °C with gentle mixing. The resulting product was purified by SEC (Superdex 200 Increase 10/300 GL (GE Healthcare, UK), in PBS pH 7.4, 0.05 % DDM).

To increase the size of SA-based LSUs, an excess of the size-increasing moiety (e. g. biotinylated BSA, ThermoFisher Scientific; biotinylated methoxypolyethylene glycols, mPEG-biot, Creative PEGWorks; biotinylated dextrans, Fina Biosolutions) was incubated with SA (free or already bound to *bo₃*-Avi-biot) for 2 h at 20 °C with gentle mixing. The resulting product was purified by SEC as above.

SA was labeled with a 10-fold excess of 5/6-carboxyfluorescein NHS-ester for 1 h at 25 °C with gentle mixing. Excess NHS-activated dye was quenched using Tris-HCl and removed by SEC using CentriPure P10 desalting columns (Zetadex-50, emp Biotech, Germany).

3.6 Methods Specific for the SpyTag-SpyCatcher System.

Coupling of Spy-tagged MPs to SC-LSUs.

To couple pR-Spy or bo_3-Spy to SpyCatcher-containing LSUs, two slightly different methods were used depending on their downstream application.

Either, a 3- to 10-fold excess of SC-LSU was simply incubated with the Spy-tagged MP for 1 h at 25 °C. MBP-containing constructs were purified by SEC (Superdex 200 Increase 10/300 GL; GE Healthcare, UK), or by MBP affinity chromatography (MBP-Trap HP; GE Healthcare, UK).

Or, SC-LSUs containing a 3xFLAG-tag (SC-MBP-3xFLAG, SC-MBPx-3xFLAG) were first immobilized on ANTI-FLAG M2 Affinity Gel by incubation for 2 h at 25 °C with gentle mixing in TBS. Excess free SC-LSU-3xFLAG was washed away, TBS was exchanged for buffer containing detergent (20 mM HEPES pH 7.0, 150 mM NaCl, 0.05 % DDM), and a 2- to 5-fold excess of Spy-tagged MP was added to the immobilized LSU and coupled by incubation for 16 h at 10 °C with gentle mixing. After unbound Spy-tagged MP was washed off with 20 CV of buffer, immobilized protein constructs were released from the affinity resin by competition with a 3xFLAG-peptide (2.5 mg ml^{-1}; APExBIO, USA). The final product was concentrated using centrifugal filters (Amicon Ultra, Merck, Germany) with 100 kDa MWCO.

SC-LSUs without 3xFLAG-tag (SC-MBP, SC-MBPx) were immobilized to amylose resin (New England Biolabs, USA) according to the manufacturer's instructions and Spy-tagged MP was coupled to the immobilized LSU as described above. After washing with 20 CV of buffer, immobilized protein constructs were released from amylose resin by competition with 10 mM maltose and the resulting construct was concentrated as described.

Assessment of pR-Spy-SC-LSU by Limited Proteolysis and Western Blot.

Protease treatment of the outside of proteoliposomes reconstituted with pR-C/NSpy-SC-MBP-3xFLAG with the protease thermolysin (Promega, USA) was carried out according to the latter's manufacturer's instructions. Briefly, proteoliposomes were resuspended in thermolysin digestion buffer (50 mM Tris-HCl pH 8.0, 0.5 mM $CaCl_2$) containing thermolysin (thermolysin/MP ratio: 1:20) for 14 h at 37 °C with gentle mixing. After stopping proteolysis by addition of 0.5 % formic acid, the proteoliposomes were disrupted by addition of 1.4 % cholate and subjected to SDS-PAGE followed by western blotting. MBP was probed using an anti-MBP anti-

body (Anti-Maltose Binding Protein antibody [R29.6], ab65, Abcam, UK; secondary antibody: IRDye 680RD Donkey anti-Mouse IgG Secondary Antibody, Licor, USA).

3.7 Synthesis of trisNTA.

In general, I followed the syntheses of trisNTA published by Huang, Park, *et al.* [199] and Huang, Hwang, *et al.* [200]. The synthesis consisted of five main steps with one or two selective final deprotection steps as shown in figure 64 on page 139. Below, a more detailed synthesis protocol is given; dedicated NMR and MS spectra can be found in the supplementary information (section 7).

*Compound **2**.* To a suspension of H-Lys(Z)-OtBu.HCl (5.0 g, 13.4 mmol; *compound **1***, Bachem) in DMF (100 ml) were added tert-butyl bromoacetate (8.0 ml, 54.0 mmol) and diisopropylethylamine (DIPEA) (11.5 ml, 67.6 mmol) under N_2, and the reaction mixture was stirred for 16 h at 55 °C. After the volatiles were evaporated under reduced pressure at 60 °C, the slurry residue was extracted three times (3 x 200 ml) with hexane-ethyl acetate (3:1) and dried over sodium sulfate. Combined extracts were subsequently concentrated and purified by high performance flash chromatography (HPFC) with an elution gradient (25 - 40 % ethyl acetate in hexane). Yield: 91.8 % with respect to (wrt) **1** (H-Lys(Z)-OtBu.HCl). TLC: $R_f = 0.42$ in hexane-ethyl acetate (3:1). ^{1}H-NMR: see supplementary figure S1 on page 199.

*Compound **3**.* To a solution of **2** (2 g, 3.54 mmol) in chloroform (15 ml) were added trifluoracetic acid (TFA) (6 ml) and triisopropylsilane (TIPS) (0.3 ml, 1.46 mmol) and the reaction mixture was then stirred at 25 °C and monitored by TLC for 3 h. Since the reaction has not come to completion yet, stirring was continued for 15 h, before methanol (3 ml) and water (1.5 ml) were added to the mixture. Thereafter, volatiles were evaporated under reduced pressure and the residue was dried azeotropically with toluene and triturated with anhydrous ether. Eventually, white precipitate was collected and dried over high vacuum. Yield: 57 % wrt **2**. TLC: $R_f = 0.03$ in chloroform-methanol-water (65:25:4). ^{1}H-NMR: see supplementary figure S2 on page 200. MS: see supplementary figure S3 on page 201.

*Compound **5**.* To a suspension of H-Orn(Z)-OtBu.HCl (5.0 g, 13.93 mmol; *Compound **4***, Bachem) in DMF (100 ml) were added tert-butyl bromoacetate (8.3 ml, 56.1 mmol) and diisopropylethylamine (DIPEA) (12.0 ml, 70.3 mmol) under N_2, and the reaction mixture was stirred for 16 h at 55 °C. After the volatiles were evaporated under reduced pressure at 60 °C, the slurry residue was extracted three times (3 x 200 ml) with hexane-ethyl acetate (3:1) and dried over sodium sulfate. Combined

extracts were subsequently concentrated and purified by HPFC with an elution gradient (25 - 40 % ethyl acetate in hexane). Yield: 97.5 % wrt **4** (H-Orn(Z)-OtBu). TLC: $R_f = 0.44$ in hexane-ethyl acetate (3:1).^{1}H-NMR: see supplementary figure S4 on page 202.

*Compound **6**.* This step was optimized by adaptation to Felpin *et al.* [201]. To a stirred solution of **5** (3.5 g, 6.3 mmol) in methanol (8.0 ml) were added a mixture of charcoal (C) (191.7 mg) and $Pd(OAc)_2$ (1.5 mol %, 21.3 mg), with a ratio of $Pd(OAc)_2$/C of 10:90 (wt:wt), in tetrahydrofuran (THF) (750 µl). The resulting mixture was vigorously stirred at 25 °C for 12 h under 1 atm of H_2. Then, Pd/C was filtered off over celite, the filtrate was concentrated under reduced pressure and purified by HPFC (10 - 20 % methanol in chloroform). Yield: 91.4 % wrt **5**. TLC: $R_f = 0.48$ in chloroform-methanol (6:1). Free primary amine was detected by staining with ninhydrin. ^{1}H-NMR: see supplementary figure S5 on page 203. MS: see supplementary figure S6 on page 204.

*Compound **7**.* To a solution of **3** (1.15 g, 2.9 mmol) in anhydrous dichloromethane (DCM) (58 ml) were added *N*-hydroxysuccinimide (NHS) (2.07 g, 18.0 mmol), 4,4-dimethylaminopyridine (DMAP) (0.5 g) and dicyclohexylcarbodiimide (DCC) (3.68 g, 17.88 mmol). The reaction was kept at 25 °C for 5 h. Reaction progress was monitored by TLC. While **3** is not fully soluble in DCM at start, solubility increases during the reaction. Additionally, the reaction produces dicyclohexylurea (DCU), which is not soluble; its appearance is an indication for the reaction. Then, a solution of **6** (4.3 g, 10.3 mmol) and anhydrous DIPEA (1.4 ml) in anhydrous DCM (25 ml) was added. After 24 h reaction at 25 °C, the reaction mixture was filtered to remove DCU and the filtrate was evaporated to dryness under reduced pressure. The residue was purified by HPFC (0 - 4 % methanol in chloroform). Yield: 3.28 g, 71.0 % wrt **3**. TLC: $R_f = 0.70$ in chloroform-methanol (9:1). ^{1}H-NMR: see supplementary figure S7 on page 205. MS: see supplementary figure S8 on page 206.

*Compound **8**.* To a stirred solution of **7** (1.5 g, 0.95 mmol) in methanol (16 ml) were added a mixture of charcoal (C) (28.8 mg) and $Pd(OAc)_2$ (1.5 mol %, 3.2 mg), with a ratio of $Pd(OAc)_2$/C of 10:90 (wt:wt), in THF (100 µl). Additionally, according to Mandal *et al.* [202], addition of triethylsilane (Et_3SiH) to palladium-charcoal-catalyzed deprotection of benzyl carbamates suggests that Et_3SiH/Pd/C behaves as a hydrogenation reagent through in situ generation of H_2, hence fueling and speeding up the deprotection reaction, making the application of 1 atm H_2 redundant. We replaced Et_3SiH in this system with TIPS (9.45 mmol, ∼2 ml; 10-fold wrt **7**). The reaction was carried out under N_2 and vigorously stirred for 17 h at 30 °C. Then,

Pd/C was filtered off over celite, the filtrate was washed twice by repeated evaporation with methanol and eventually evaporated to dryness under reduced pressure and high vacuum. Since TIPS was hard to remove, the crude product was then purified by HPFC (9 % methanol in chloroform). Yield: 78.6 % wrt **7**. TLC: $R_f = 0.35$ in chloroform-methanol (9:1). ^{1}H-NMR: see supplementary figure S9 on page 207. MS: see supplementary figure S10 on page 208.

*Compound **9**.* To a solution of **8** (356.1 mg, 0.244 mmol) in chloroform (10 ml) were added TIPS (0.77 ml, 3.76 mmol) and TFA (3.45 ml). After 3 h reaction at 25 °C, the volatiles were evaporated under reduced pressure and the residue was precipitated from diethyl ether (10 ml) at −20 °C. The precipitate was subsequently dissolved in methanol, evaporated, and precipitated from cold ether again. The solid was then collected and dried over high vacuum. Yield: 305.9 mg, 63.3 % wrt **8** when considering **9** to be present as TFA-salt. ^{1}H-NMR: see supplementary figure S11 on page 209. MS: see supplementary figure S12 on page 210.

According to Silverman *et al.* [203] and Fujii *et al.* [204], **9** can also be directly obtained from **7** by unselective deprotection. For this purpose, to a solution of **7** (100 mg, 0.06 mmol) in THF (1 ml), pure TFA (500 µl) and thioanisole (0.64 mmol, 80 µl) were added. The mixture was stirred for 3.5 h at 25 °C before addition of TIPS (25 µl, 0.12 mmol). After the reaction was continued for 18 h with vigorous stirring, methanol (0.6 ml) and deionized water (0.3 ml) were added and the volatiles were evaporated under reduced pressure. The residue was dried azeotropically with toluene and triturated with anhydrous ether at −20 °C. Yield: 43.7 % wrt to **7**.

3.8 Methods Specific for the trisNTA System.

Synthesis of LysNTA- and trisNTA-PEG$_4$-biotin.
To a solution of EZ-Link NHS-PEG$_4$-Biotin (ThermoFisher Scientific, USA) (2 mg, 3.4 µmol) in aequous buffer ($NaHCO_3$ pH 8.0) (250 µl), a 3-fold excess of trisNTA (**9**) (9.7 mg, 10.2 µmol) or lysineNTA (LysNTA, N_α,N_α-bis(carboxymethyl)-L-lysine hydrate) was added. After incubation for 16 h at 25 °C with gentle mixing, the mixture was dried using a speedvac. trisNTA-biotin was analyzed by MS (supplementary figure S14 on page 211).

Testing the Two Functionalities of trisNTA.

trisNTA-biotin was immobilized on streptavidin-coated 96-well plates (Pierce Streptavidin Coated High Capacity Plates, Clear, 8-Well Strip; ThermoFisher Scientific, USA) according to the latter's manufacturer's instructions in TBST-BSA (25 mM

Tris-HCl pH 7.2, 150 mM NaCl, 0.1 % bovine serum albumin (BSA), 0.05 % Tween-20). trisNTA-biotin, as well as commercially available Biotin-X-NTA (N_ε-(N-(+)-Biotinyl-6-aminohexanoyl)-N_α,N_α-bis(carboxymethyl)-L-lysine) and LysNTA-PEG_4-biotin were immobilized for comparison. Hexahistidine-tagged and fluorescently labeled (tetramethylrhodamine, TMR; λ_{ex}: 557 nm, λ_{em}: 585 nm) peptide AKAGEH_6AE, with TMR on its N-terminus (GenScript, USA) (1 nmol ml^{-1}, 100 µl) was added to immobilized NTA-biotin variants after the latter had previously been treated with either 100 mM $NiSO_4$ or 100 mM EDTA in buffer for 10 min and washed with buffer (3 x 200 µl). The peptide was incubated in the wells for 30 min at 25 °C and unbound peptide was thereafter washed away with buffer (3 x 200 µl). TMR-fluorescence was read out while the wells contained 100 µl buffer.

trisNTA (**9**) was coupled to NHS-activated agarose beads (NHS-activated agarose, G-Biosciences, USA) according to the latter's manufacturer's instructions. Immobilized trisNTA was treated with Ni^{2+} or EDTA as described above in buffer (20 mM sodium phosphate pH 7.4, 500 mM NaCl, 20 mM imidazole) and the same His-tagged peptide (5 nmol per condition) was applied in the same buffer. After washing away unbound peptide with 12 x 1 CV of the same buffer, bound peptide was eluted from the trisNTA-beads by 4 x 1 CV of the same buffer containing 500 mM and TMR fluorescence of the eluate was measured.

trisNTA (**9**) and LysNTA were immobilized by EDC-mediated coupling (see figure 68 on page 143) on metallic magnetic beads with biocompatible surface chemistry PEG-brushes with carboxy-functionality (TurboBeads PEG-Carboxy, TurboBeads, Switzerland) according to the latter's manufacturer's instructions. After washing of NTA-functionalized magnetic beads with 10 CV 100 mM EDTA, NTA was loaded with Ni^{2+} by incubation (10 min, 25 °C) with 2 CV 100 mM $NiSO_4$, or kept free of Ni^{2+}. Unbound Ni^{2+} was repeatedly washed away with buffer (3 x 10 CV; 20 mM sodium phosphate pH 7.4, 500 mM NaCl, 20 mM imidazole) and hexahistidine-tagged, TMR-labeled peptide (1 nmol ml^{-1}) introduced above was bound (30 min, 25 °C). Unbound peptide was washed away with buffer (3 x 2 CV) and bound peptide was eluted by 3 x 1 CV buffer containing imidazole (500 mM) (5 min, 25 °C). Collected elution fractions were transferred to a 96-well plate (Corning 96 Well Black Polystyrene Microplate, flat bottom, clear) and fluorescence was measured in a plate reader (Infinite M1000, Tecan, Switzerland). Dose-response curves were recorded by adaptation of the imidazole concentration for peptide elution (50 - 500 mM imidazole).

Coupling trisNTA to Different LSUs.

trisNTA (**9**) was coupled to NHS-coated silica beads (NHS-coated sicastar beads, micromod Partikeltechnologie GmbH, Germany) according to the latter's manufacturer's instructions (in 50 mM HEPES pH 7.5) or to the NHS-activated agarose beads introduced above as described. After trisNTA was loaded with Ni^{2+} by incubation (10 min, 25 °C) with $NiSO_4$ (100 mM), excess Ni^{2+} was washed away with buffer, and DDM (0.05 %) and His-tagged MP were added and incubated (30 min, 25 °C). After incubation, residual free MP was washed away with buffer containing DDM (0.05 %) by repeated steps of dilution and centrifugation, before bound MP was either eluted (10 min, 25 °C) using buffer containing DDM (0.05 %) and EDTA (50 mM) and detected by UV-Vis, or the construct was reconstituted into liposomes.

trisNTA (**9**) and LysNTA were coupled to mono-carboxy-functionalized dextrans of different sizes (70, 250, 500, 2000 kDa; Fina Biosolutions, USA) by EDC-mediated coupling. To a solution of dextran (14.2 nmol) in 50 mM MES buffer pH 5.5 (50 µl), EDC from a freshly prepared stock solution (10 mg ml^{-1}) in buffer (50 µl) and freshly prepared NHS (10 mg ml^{-1}) in buffer (50 µl) were added. The mixture was incubated for 30 min at 25 °C with gentle mixing, before excess EDC and NHS were removed using a PD-MiniTrap G-25 desalting column (spin protocol, according to manufacturer's instructions; GE Healthcare, UK). To the eluate, a 10-fold excess of trisNTA or LysNTA (143 nmol) wrt dextran was added and the mixture was incubated for 45 min at 25 °C with gentle mixing. NTA was loaded by addition of $NiSO_4$ (1 mM) and further incubation for 20 min at the same temperature, before excess Ni^{2+} and trisNTA or LysNTA were removed by a PD-MiniTrap G-25 desalting column. The synthesized tris-/LysNTA-dextrans were tested by binding the His-tagged, TMR-labeled peptide introduced earlier via Ni^{2+} as described before. Unbound peptide was removed using a PD-MiniTrap G-25 desalting column (GE Healthcare, UK), and TMR fluorescence was measured.

Coupling of trisNTA (**9**) to a 40 kDa-dextran functionalized with 10 amino groups (DEX40k10; Fina Biosolutions, USA) and for comparison to the previously introduced mono-carboxy-functionalized dextrans was done by click chemistry (see figure 71 on page 148). trisNTA was therefor coupled to methyltetrazine-*sulfo*-NHS-ester (tet) (ClickChemistryTools, USA) according to the manufacturer's instructions (in PBS pH 7.4), while DEX40k10 was linked to TCO-PEG_4-NHS ester (TCO) (ClickChemistryTools, USA) according to the manufacturer's instructions (in PBS pH 7.4). After coupling (1 h, 25 °C, gentle mixing) a 20-fold excess of the respective click chemistry reagent to DEX40k10 or trisNTA, respectively, the reaction was quenched by addition

of Tris-HCl (50 mM) (5 min, 25 °C) and excess click chemistry reagent was removed by SEC using PD MiniTrap G-25 desalting columns (in PBS pH 7.4). The two newly synthesized click chemistry partners trisNTA-tet and DEX40k10-TCO were mixed in a 1:1 ratio in PBS pH 7.4 and incubated for 1 h at 25 °C. The synthesized trisNTA-click-DEX variants were tested as described above. Modification: unbound peptide was removed by SEC using Z-50 CentriPure MINI Spin Columns (CentriPure MINI Spin Column Desalt Z-50, emp Biotech, Germany).

Analogously, trisNTA-tet was coupled to the TCO-functionalized fluorophore Cy5-TCO (Cy5 TCO, ClickChemistryTools, USA).

trisNTA (**9**) and LysNTA were coupled to NHS-activated PEGs of different sizes (2, 5, 10, 20 kDa; Nanocs, USA) (see figure 30 on page 82). To a solution of PEG-NHS (50 nmol) in "Buffer NHS" (part of NHS-activated agarose; G-Biosciences, USA) (100 µl) was added trisNTA or LysNTA (2.5 µmol; 50-fold excess wrt PEG-NHS) and the mixture was incubated for 1 h at 25 °C with gentle mixing. Afterwards, the reaction was quenched using ethanolamine (0.1 µmol; 4-fold excess wrt PEG-NHS) for 15 min at the same temperature. Finally, excess ethanolamine and unreacted NTA-variant were removed by SEC using PD-MiniTrap G-25 desalting columns (in PBS pH 7.4). trisNTA-PEG or LysNTA-PEG were loaded with Ni^{2+} (30-fold excess; incubation at 25 °C for 10 min; free Ni^{2+} removed by PD-MiniTrap G-25 desalting columns) and His-tagged pR was bound to it in 20 mM HEPES pH 7.4, 300 mM NaCl, 0.04 % DDM, as described above. The constructs were then subjected to SEC using a Superdex 200 Increase 5/150 GL (GE Healthcare, UK) column in the same buffer.

3.9 Synthesis of trisNTA-Spy.

The paragraphs concerning the synthesis of trisNTA-Spy are based on a protocol written by Dr. Sacha Javor, who supervised and guided me during the synthesis of trisNTA-Spy.

Materials & Methods.

Analytical RP-HPLC was performed with an Ultimate 3000 Rapid Separation LC System (DAD-3000 RS diode array detector) using an Acclaim RSLC 120 C18 column (2.2 µm, pore size 120 Å, 3.0 x 50 mm, flow rate 1.2 ml min^{-1}) from Dionex (USA). Compounds were detected by UV absorption at 214 nm. Data recording and processing was performed with Thermo Scientific Xcalibur version 4.1.31.9 (ThermoFisher Scientific, USA). For all RP-HPLC, HPLC-grade acetonitrile (ACN)

and Milli-Q deionized water were used. The elution solutions were: A: H_2O with 0.05 % trifluoracetic acid (TFA); B: H_2O/ACN (10:90) with 0.1 % formic acid (FA).

Preparative RP-HPLC was performed either with a Waters Prep 150 LC system using a Dr. Maisch HPLC GmbH (Germany) Reprospher Column (C18-DE, 5 µm, 100 x 30 mm, pore size 100 Å, flow rate 40 ml min^{-1}). Compounds were detected by UV absorption at 214 nm using a Waters (USA) 486 Tunable Absorbance detector. For all RP-HPLC, HPLC-grade ACN and Milli-Q deionized water was used. The elution solutions were: A: H_2O with 0.1 % TFA; B: H_2O/ACN (10:90) with 0.1 % TFA.

MS spectra were recorded on a Thermo Scientific LTQ OrbitrapXL (ThermoFisher Scientific, USA) by the mass spectrometry service of the Department of Chemistry and Biochemistry at the university of Bern.

^{1}H- and ^{13}C-NMR spectra were measured on a Bruker (USA) Avance 300 spectrometer (at 300 MHz and 75 MHz, respectively) or on a Bruker Avance II 400 spectrometer (at 400 MHz and 101 MHz, respectively). ^{1}H and ^{13}C chemical shifts are given in ppm (δ) relative to the solvent proton impurity signals, and resonance multiplicities are reported as s (singlet), d (doublet), t (triplet), q (quartet), p (pentet), and m (multiplet); br = broad peak.

Peptide Synthesis.

Peptides were synthesized manually using the following general procedure. The synthesis was performed using a TentaGel S Ram resin (loading: 0.25 mmol g^{-1}) in a 10 ml polypropylene syringe fitted with a polypropylene frit, a Teflon stopcock and a stopper. The resin was swollen in DCM (5 ml, 10 min). After removal of DCM, the Fmoc-protecting group of the resin was removed by using a solution of 20 % piperidine in NMP. Stirring of the reaction mixture at any given step was performed by attaching the closed syringes to a rotating axis. The completion of the reaction was checked by using the TNBS test. Removal of the Fmoc-protecting group was performed by using a solution of 20 % piperidine in NMP (5 ml, 2 x 10 min). After filtration, the resin was washed with NMP (3 x 4 ml), MeOH (3 x 4 ml) and DCM (3 x 4 ml). Coupling of amino acids was performed by using Fmoc-protected amino acids (3 eq.), Oxyma (3 eq.) and DIC (3 eq.) in NMP (5 ml). The resin was stirred for 1 h before it was washed with NMP, MeOH and DCM (3 x 4 ml each).

Peptide Cleavage.

TFA cleavage and global deprotection were performed by adding a solution of TFA/TIS/DODT/H_2O(95:2:2:1, v/v/v/v, 20 ml g^{-1} resin) to the resin for 5 h. The

peptide was precipitated with *t*-BuOMe, dissolved in H_2O/MeCN with 0.1 % TFA and subsequently purified by preparative RP-HPLC.

Syntheses of trisNTA-Spy Variants.

Dedicated NMR and MS spectra can be found in the supplementary information (section 7).

*Compound **10***. **8** (0.10 g, 0.069 mmol) in dry CH_3CN (0.69 ml) was added to chloracetic anhydride (ClAc) (18 mg, 0.10 mmol, 1.5 eq.) and diisopropylethylamine (DIPEA) (36 µl, 27 mg, 0.21 mmol, 3 eq.) in dry CH_3CN (0.69 ml) at 0 °C and stirred at RT for 2 h. The solvents were evaporated, and the residue purified by silica gel flash chromatography (DCM:MeOH, 0 to 5 % MeOH) to yield **10** as a white sticky solid (57.9 mg, 55.1 %). ^{1}H-NMR (see figure S16 on page 212) (300 MHz, $CDCl_3$) δ 4.03 (s, 2H), 3.58 - 3.11 (m, 28H), 1.81 - 1.49 (m, 18H), 1.48 - 1.37 (m, 81H). HRMS (NSI+) (see figure S17 on page 213 and figure S18 on page 214): $C_{75}H_{134}ClN_8O_{22}$ $[M+H]^+$ calc./found 1533.9296/1533.9313 Da.

*Compound **11***. **10** (58 mg, 0.038 mmol) was stirred in CH_3Cl/TFA (2:1) (6.0 ml) for 5 h. The solvents were evaporated, and the residue was purified by RP-HPLC and obtained in the form of TFA salt as a white solid (19.0 mg, 33.9 %). ^{1}H-NMR (see figure S19 on page 215) (300 MHz, D_2O) δ 4.17 - 3.66 (m, 22H), 3.26 (m, 8H), 2.06 - 1.64 (m, 14H), 1.62 - 1.50 (m, 2H), 1.41 - 1.26 (m, 2H). HRMS (NSI+) (see figure S20 on page 216 and figure S21 on page 217): $C_{39}H_{62}ClN_8O_{22}$ $[M+H]^+$ calc./found 1029.3662/1029.3673 Da.

*Peptide **SpyC***. AHIVMVDAYKPTKC-NH_2. Peptide **SpyC** was synthesized using 100 mg of resin (0.25 mmol g^{-1}) and obtained in the form of TFA salt as a fluffy white solid after RP-HPLC purification (12.7 mg, 6.3 µmol, 25 %). HRMS (NSI+) (see figure S22 on page 218 and figure S23 on page 219): $C_{70}H_{116}N_{19}O_{18}S_2$ $[M+H]^+$ calc./found 1574.8182/1574.8185 Da.

*Peptide **SpyGSGSC***. AHIVMVDAYKPTKGSGSC-NH_2. Peptide **SpyGSGSC** was synthesized using 100 mg of resin (0.25 mmol g^{-1}) and obtained in the form of TFA salt as a fluffy white solid after RP-HPLC purification (4.5 mg, 1.9 µmol, 7.8 %). HRMS (NSI+) (see figure S24 on page 220 and figure S25 on page 221): $C_{80}H_{133}N_{23}O_{24}S_2$ $[M+2H]^{2+}$ calc./found 931.9671/931.9622 Da.

*Peptide conjugate **SpyC-trisNTA***. AHIVMVDAYKPTKC(trisNTA)-NH_2. Peptide **SpyC** (4.8 mg, 2.4 µmol) (5.0 mg ml^{-1}) in ammonium bicarbonate buffer (50 mM, pH 8.0) and TCEP (1.0 mM) and **11** (7.4 mg, 5.0 µmol, 2.1 eq.) in CH_3CN/H_2O (3:1) (1.6 ml) were stirred for 16 h and the solvents were evaporated. **SpyC-trisNTA** was

obtained in the form of TFA salt as a fluffy white solid after RP-HPLC purification (3.2 mg, 0.92 µmol, 38 %). HRMS (NSI+) (see figure S26 on page 222 and figure S27 on page 223): $C_{109}H_{175}N_{27}O_{40}S_2$ [M] calc./found 2566.1931/2566.1979 Da.

Peptide conjugate ***SpyGSGSC-trisNTA***. AHIVMVDAYKPTKGSGSC(trisNTA)-NH_2. Peptide **SpyGSGSC** (4.5 mg, 1.9 µmol) (5.0 mg ml^{-1}) in ammonium bicarbonate buffer (50 mM, pH 8.0) and TCEP (1.0 mM) and **11** (6.1 mg, 4.1 µmol, 2.2 eq.) in CH_3CN/H_2O(3:1) (1.4 ml) were stirred for 16 h and the solvents were evaporated. **SpyGSGSC-trisNTA** was obtained in the form of TFA salt as a fluffy white solid after RP-HPLC purification (2.6 mg, 0.69 µmol, 36 %). HRMS (NSI+) (see figure S28 on page 224 and figure S29 on page 225): $C_{119}H_{191}N_{31}O_{46}S_2$ [M] calc./found 2854.3001/2854.3045 Da.

3.10 Methods Specific for the trisNTA-Spy System.

Coupling of trisNTA-SpyC to SC-ELP-GFP.
The His-tag of SC-ELP-GFP (SEG) was cleaved off by TEV protease (New England Biolabs, USA) according to the manufacturer's instructions. Afterwards, the cleavage product was purified by reverse immobilized metal affinity chormatography (IMAC) in 50 mM MOPS pH 7.0, 150 mM NaCl.

trisNTA-SpyC was coupled to SEG (w/o His-tag) by addition of a 3-fold excess of trisNTA-SpyC (32.26 nmol; added from 1 mM stock solution prepared in 20 % ethanol in water containing 9.6 mM NaOH, 208 µl) to a solution of SC-ELP-GFP (w/o His-tag) (10.75 nmol) in 50 mM MOPS pH 7.0, 150 mM NaCl. The mixture was incubated for 3 h at 25 °C with gentle mixing. trisNTA was then loaded with Ni^{2+} by addition of a 10-fold excess of $NiSO_4$ (32.3 µl of a 10 mM stock solution) and incubation for 10 min at the same temperature with gentle mixing. Finally, excess Ni^{2+} and trisNTA-SpyC were removed by SEC using PD-MiniTrap G-25 desalting columns (GE Healthcare, UK) (in 50 mM MOPS pH 7.0, 150 mM NaCl), resulting in 315.5 µl 34 µM trisNTA-SpyC-SEG.

Complexing of trisNTA-SpyC-SEG via Ni^{2+} to His-tagged MPs.

trisNTA-SpyC-SEG was either bound to different solubilized His-tagged MPs in 20 mM HEPES pH 7.0, 150 mM NaCl, 0.05 % DDM or it was used to probe His-tagged ATP synthase (location His-tag: subunit β) reconstituted in proteoliposomes (binding of trisNTA (-SpyC-SEG) to His-tagged MP via Ni^{2+} as described earlier). If needed, the construct was pulled down by immunoprecipitation using GFP-Trap

agarose affinity resin (gta-20; ChromoTek, Germany). After extensive washing, His-tagged and thus bound MP was eluted from trisNTA-SpyC-SEG-resin by incubation with EDTA (100 mM) for 30 min at 25 °C in buffer. If trisNTA-SpyC-SEG was used to probe reconstituted His-tagged ATP synthase, unbound trisNTA-SpyC-SEG was washed away by dilution and collection of the probed proteoliposomes by ultracentrifugation (229 600 x g, 1 h, 4 °C). Subsequently, GFP fluorescence was measured and/or trisNTA-SpyC-SEG was released from reconstituted ATP synthase by EDTA (50 mM) or histidine (100 mM).

3.11 TCEP-based Orientation Determination Assay.

To assess orientation of reconstituted pR-N/CSpy-SC-MBPx-3xFLAG, the LSU SC-MBPx-3xFLAG was first unspecifically labeled with DY-647P1-NHS (Dyomics GmbH, Germany) ester according to the manufacturer's instructions, and then coupled to pR-N/CSpy (see section 3.6). pR-N/CSpy-SC-MBPx-3xFLAG-DY-647P1 was then reconstituted into liposomes as described earlier in this thesis (see section 3.3). 40 - 100 µl proteoliposomes were then diluted in 1.4 ml measurement buffer (250 mM Tris-HCl pH 8.5), and DY-647P1-fluorescence (672 nm) was measured by excitation at 580 nm (slits: 5 nm / 10 nm). After a stable baseline was obtained, fluorophore molecules accessible from the outside of the proteoliposomes were quenched by addition of tris(2-carboxyethyl)phosphine (TCEP) (14.3 mM). After quenching was completed, proteoliposomes were solubilized by addition of 0.6 % DDM, thus enabling quenching of previously inaccessible fluorophore molecules and hence leading to maximal quenching of DY-647P1. Orientation was determined by calculating the ratio of fluorophore quenched by TCEP from the outside versus fluorophore quenched by TCEP in total after solubilization of the proteoliposomes.

4 Results & Discussion.

4.1 General Idea & Strategy.

As described in section 1.7, it was shown that the F_1F_0 ATP synthase of *E. coli* (structure: see figure 7 on page 11) is unidirectionally orientated with the F_1 headpiece on the outside when reconstituted into preformed, partially detergent-solubilized liposomes.[169] The reason for this behaviour is quickly found. The F_1 part of the ATP synthase is very large and hydrophilic. Therefore, it is unable to cross the hydrophobic part of the liposomes' lipid bilayer during the reconstitution process, forcing the ATP synthase to reconstitute unidirectionally. This observation promoted our idea to adopt this strategy in order to influence the orientation of other MPs. As shown in figure 25, the strategy derived thereof was to couple a large soluble unit (LSU) mimicking the F_1 part of the F_1F_0 ATP synthase to the MP of choice at a specific site in order to force the unidirectional insertion of the MP into the liposomal membrane. After reconstitution, the LSU ideally would be removed from the reconstituted MPs to avoid any interference with the latter's function.

To test this hypothesis, four suitable main ingredients have to be found and combined, which are:

- a model integral MP,
- appropriate reconstitution conditions,
- an LSU,
- an appropriate hetero-bifunctional linker system to connect the LSU and the MP.

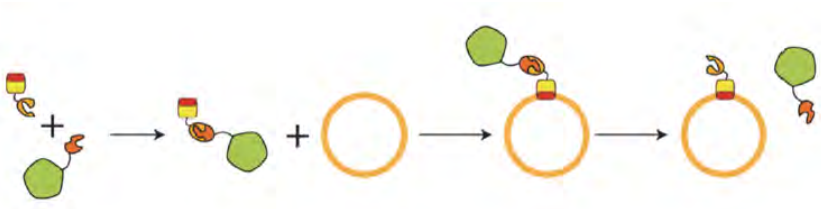

Figure 25: General strategy. The (multisubunit) MP (red & yellow) is first coupled via its linker (light orange) to the large soluble unit (LSU; green; mimicking the F_1 part of the ATPase) via the latter's linker counterpart (dark orange). The coupling product is then reconstituted into preformed, partially solubilized liposomes. Because of its size and hydrophilicity, the LSU is unable to cross the hydrophobic part of the lipid bilayer, thus forcing the MP to reconstitute unidirectionally into the liposomes. After subsequent detergent removal, the LSU ideally is removed to avoid any interference with the MP's function. Figure adapted from C. von Ballmoos.

In each of the approaches described in the following sections, one of the MPs introduced before (cytochrome bo_3 ubiquinol oxidase, see section 1.2.2; or proteorhodopsin, see section 1.2.1) was used. As explained in section 1.6, conditions for functional reconstitution have to be found for each individual MP of interest. Even though these are known for these two MPs, some optimization had to be done, which will be described in the according results' sections.

Regarding the choice of appropriate LSUs, a wide spectrum of chemical and biochemical moieties would be applicable, as long as the moiety is large (kDa to MDa) and hydrophilic. Additionally, potential LSUs should be straightforward to couple to the linker system of choice. For the nature of possible LSUs, soluble proteins as well as commercially available options as polyethylene glycol (PEG) chains of variable length, (mono- or multifunctionalized) dextrans or ficolls, beads of any kind or even DNA were considered.

The linker has to be hetero-bifunctional in order *a)* to be coupled to the LSU and *b)* to connect the LSU with the linker counterpart on the MP. Potential strategies to link LSUs to the MPs of interest can be more specific or generally applicable. More specific systems may involve introduction of more extensive genetic modifications into MPs such as large soluble fusion domains as e. g. GFP to guide directed insertion into the liposomal membrane (see section 1.7.2). Further, rather specific systems may rely on the insertion of short peptide tags enabling attachment of LSUs instead of large fusion domains directly acting as LSUs. Examples for such peptide tags are the AviTag and the SpyTag discussed below. However, in order to minimize the extent of genetic modifications in the MPs of interest, also a more commonly used, generally applied tag should be considered. His-tags are commonly used for affinity purification of (membrane) proteins, hence His-tags are often readily available, thus representing the most elegant approach. Instead of inserting a second tag, the position of the His-tag could be adjusted to the side of the MP eventually desired to face the outside of the proteoliposomes after reconstitution. To link the His-tagged MP to LSU's, Ni-NTA-based linkers could be used, especially trisNTA as discussed below, eventually allowing dissociation of the LSU from the unidirectionally reconstituted MP under mild conditions. An additional advantage of a His-tag-based system would presumably be uncomplicated adaptation and application to further MPs of choice with little effort.

The most straightforward system that might be considered would involve the use of monoclonal antibodies as LSUs. In such a system, the two ingredients LSU and linker system would be combined to one ingredient. Therefore, either commercially available

antibodies against properly placed, commonly used affinity tags (e. g. anti-His-tag, anti-Strep-tag, or anti-FLAG-tag) could be used, or antibodies against epitopes specific for the surface structure of the side of the MP of interest which is eventually desired to face the outside of the proteoliposomes. However, the amounts of antibody needed for this approach has to be considered. Typically, around 25 µl of a 20 µM stock solution of MPs as bo_3 oxidase or pR are reconstituted for functional experiments. Applying a MP to antibody ratio of 1:1 for the immunoreaction and assuming the size of the antibody to be ∼27 kDa (e. g. Anti-6X His tag mouse monoclonal antibody [HIS.H8]; ab18184, Abcam, UK), one reconstitution would require ∼14 µg of antibody. Antibodies however are commonly sold in units of 100 µg (€520 for the exemplar, 13.03.2020). Hence, only ∼7 reconstitutions could be performed with 100 µg of antibody. Combined with the fact that rather tens of milligrams of antibody would be required in the course of investigating on such an antibody-based system, this would lead to unaffordable costs. If antibodies against more MP-specific epitopes would be used, in most cases, they would have to be raised on our own for each MP to be unidirectionally reconstituted. Consequently, antibody-based approaches for unidirectional reconstitution of MPs are not practicable. Therefore, more general, less costly systems had to be developed.

In the following, four approaches to achieve unidirectional reconstitution of MPs into liposomes are described, each one based on an own linker system combined with different LSUs. The different approaches are not introduced in chronological order. At the beginning of my PhD, after the general strategy manifested above was established, we were aiming for the most elegant method, using trisNTA introduced in section 4.5. Therefore, trisNTA was synthesized and characterized, and then it was tried to apply it to His-tagged MPs for orientation. We further concentrated on bo_3 oxidase as a model protein, because it was in the focus of other projects in our group. Nevertheless, we then rather unexpectedly faced many problems, especially regarding coupling of trisNTA to potential LSUs. These problems made us put this most elegant method aside for a while and look for alternative approaches, which might be more straightforward to establish than the trisNTA-based method in combination with the bo_3 oxidase. Since we were especially interested in unidirectional insertion of MPs allowing the generation of a (positive inside) *pmf*, we held on to the bo_3 oxidase in the next approach.

The first of these alternative approaches was the AviTag system described in section 4.2, which is based on a genetically introduced AviTag. The AviTag is a peptide tag consisting of 15 amino acids which can be specifically enzymatically biotinylated.

Subsequently, streptavidin-based LSUs can be bound to Avi-tagged, biotinylated MPs. Using the AviTag method, we still focused on the bo_3 oxidase. After facing several problems connected to the composition of LSUs, it was decided to look out for a second alternative approach. Enhancing the size of the streptavidin-based LSUs with biotinylated building blocks (as e. g. biotinylated bovine serum albumin (BSA), PEG moieties or dextrans) turned out to to be less straightforward than expected. Further, purification after each step of MP modification (biotinylation, binding of streptavidin, increasing the size of streptavidin-based LSU) led to reasonable loss of MP. These pitfalls eventually prevented us from developing further the AviTag system.

In order to test a new approach, it was decided to introduce a new model MP, thereby reducing complexity of the MP by replacing the multi-subunit bo_3 oxidase with the mono-subunit MP proteorhodopsin (pR). Besides reducing complexity of the MP itself, this was especially useful regarding the supply of MP. Because it consists of only one subunit, pR is less susceptible to genetic modifications (as e. g. artificially introduced peptide tags) compared to the multi-subunit bo_3 oxidase. Further, it is expressed in *E. coli* with high yields. Last but not least, unidirectionally reconstituted pR as the bo_3 oxidase allows the generation of a (positive inside) *pmf*, hence representing at least partially an actual alternative to the bo_3 oxidase for the coreconstitution with ATP synthase to form a minimal respiratory chain.

As an alternative to the AviTag system we exploited a system based on the SpyTag-SpyCatcher linker system described in section 4.3. The 13 amino acid peptide tag SpyTag was genetically introduced to the termini of pR, while its larger linker counterpart SpyCatcher was introduced into various solubility enhancer proteins (as e. g. maltose binding protein (MBP) or GFP) intended to act as LSUs. An advantage of this system compared to the previously applied AviTag system is that the bond between SpyTag and SpyCatcher is of covalent nature, hence preventing dissociation of the MP from its LSU. Further, by using SpyCatcher-LSU fusion proteins, complexity of the installation of the LSUs could be reduced. The SpyTag-SpyCatcher system was developed and first successfully applied to pR, before bo_3 oxidase was considered again.

Finally, the most general and most elegant approach based on trisNTA was readopted, however the trisNTA system was modified and combined with the advantages of the SpyTag-SpyCatcher system, resulting in the trisNTA-Spy system described in section 4.6.

Because of these jumps in chronology, it was decided to introduce the approaches to the reader in a non-chronological order, starting with the most basic approach bearing

the most drawbacks (AviTag system), and to develop the idea of our strategy further (SpyTag-SpyCatcher system) and further (trisNTA) up to the most general and most elegant approach based on trisNTA-Spy. The reader therefore may pardon potential conflicts owed to the deviation from the chronological order of the development of the different approaches.

4.2 Approach I – The AviTag System.

4.2.1 Introduction to the AviTag System.

A first interesting linker system is based on the AviTag first described by Beckett *et al.* [205] and refined by Fairhead *et al.* [198]. The AviTag can conveniently be added genetically at the N- or C-terminus or in exposed loops of a target protein.[198] It consists of 15 amino acids with the sequence GLNDIFEAQKIEWHE, containing the recognition sequence for the *E. coli* biotin ligase (BirA). The AviTag was developed from the only natural substrate of BirA in *E. coli* [206, 207], which is the biotin carboxyl carrier protein (BCCP).[198, 207] Hence, BirA is highly specific in covalently attaching biotin (also known as vitamin H or vitamin B_7) to the lysine side chain of the AviTag as shown in figure 26.[198] Since biotin is a small molecule (244.31 Da), in most cases it does not affect the biological activity of biologically active macromolecules, i. e. enzymatic catalysis.[208]

The AviTag has for example been used to study protein-protein interactions using surface plasmon resonance or ELISA assays [209]; to develop a biotin/avidin-bead based multiplex assay to monitor dengue virus seroconversion [210]; or for *in vivo* biotinylation of the luciferase from *Gaussia princeps* as a reporter for *in vivo* imaging of human glioma cells or brain tumor formation in mice [211].

Due to the above described properties, it was decided to introduce an AviTag at the C-terminus of subunit I of the bo_3 oxidase. Once biotinylated, one can take advantage of the tight binding of biotin to avidin or streptavidin (SA). Avidin and

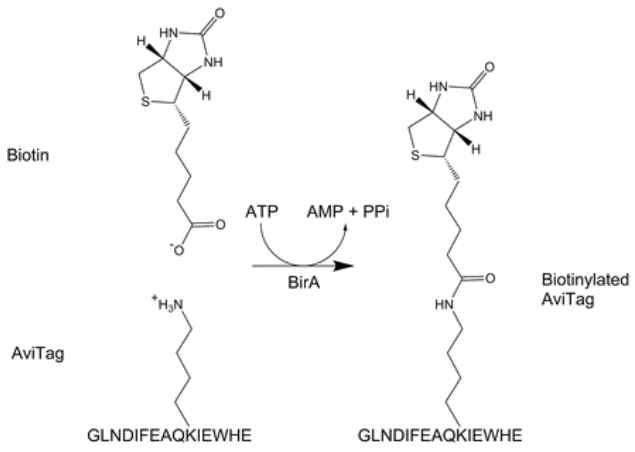

Figure 26: Biotin ligase (BirA) reaction. Enzymatic reaction of BirA, covalently linking free biotin to the lysine residue of the AviTag. Figure adapted from [198].

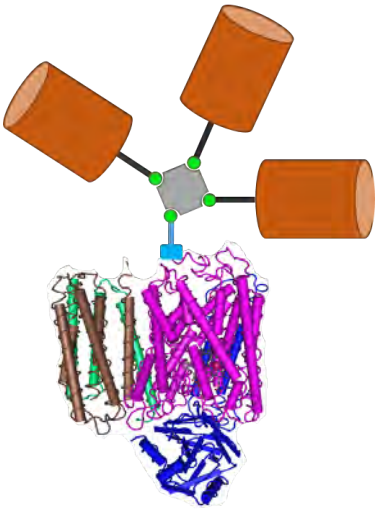

Figure 27: The AviTag system. An AviTag (bright blue) was genetically introduced at the C-terminus of subunit I of the bo_3 oxidase (PDB: 1FFT; [26]). This AviTag is biotinylated (green dot connected to AviTag) at its lysine residue by BirA. To the biotinylated bo_3 oxidase, SA (grey) is bound, acting as a preliminary LSU (60 kDa). The three remaining free biotin binding sites of SA can be used to enlarge the preliminary LSU with biotinylated moieties of variable size and nature (orange, connected to green biotin). Figure not to scale.

SA are functional and structural analogues [212] binding to biotin with extremely high affinity (avidin: dissociation constant K_d $\sim 10^{-15}$ [213]; SA: K_d $\sim 4 \times 10^{-14}$ M [214, 215]), representing one of the strongest non-covalent biological interactions known to date.[198] Avidin was derived from eggs of oviparous vertebrates [212, 216] and avidin activity has been observed in eggs and oviducts of many species of birds and in the egg jelly of frogs [213], while SA was derived from *Streptomyces avidinii* [212].

In solution, SA forms very stable tetramers (M_w of SA tetramer: 60 kDa [208]). Even if multiple times smaller compared to the role model (F_1 part of F_1F_0 ATP synthase, $\sim$379 kDa [36]) SA tetramers constitute already a reasonably-sized preliminary LSU. The advantage of SA tetramers is that they allow the coupling to four molecules of biotin or biotin-bearing molecules.[208] Consequently, if SA is added stoichiometrically to a MP with biotinylated AviTag, one tetramer of SA binds per biotinylated MP, leaving three free binding sites behind. These three remaining binding sites can be deployed to further increase the size of the preliminary LSU as illustrated in figure 27. For this purpose, an excess of any suitable biotinylated hydrophilic moiety can be applied, such as biotinylated proteins, biotinylated PEGs, or biotinylated dextrans, to name a few.

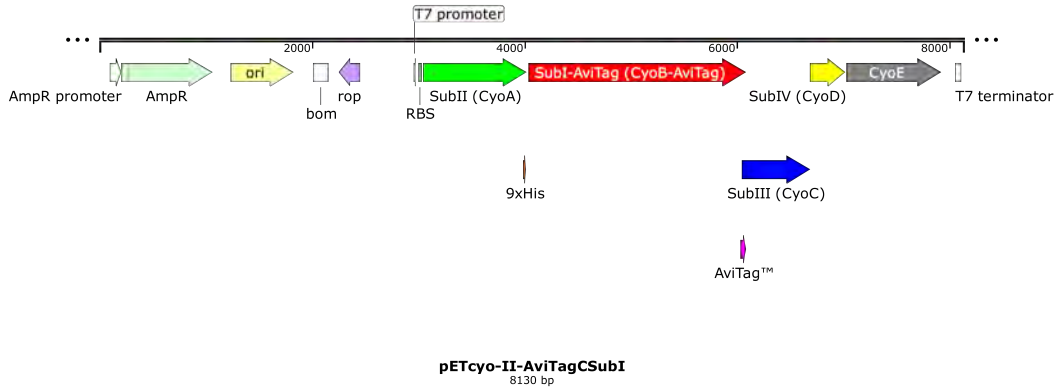

Figure 28: Plasmid map of *bo*$_3$-AviTag. The AviTag (purple) was genetically introduced at the C-terminus of subunit I (red). Since the sequences for subunit I and III are overlapping on the plasmid, the insertion of the AviTag at the C-terminus of subunit I also prolongs subunit III (blue) at its N-terminus. Due to the readily present frame shift between subunits I and III, the first three amino acids of subunit III (MAT) were replaced by the 13 amino acids sequence MIFSKHRKLNGMS. A His_9-tag (orange) was already present in the precursor plasmid pETcyo-II, located at the C-terminus of subunit II (green). Subunit IV (yellow) and CyoE (gray) remain as encoded in pETcyo-II.

4.2.2 Cloning, Expression and Purification of *bo*$_3$ Oxidase with AviTag.

The AviTag with a preceding GS-linker was genetically introduced at the C-terminus of subunit I (CyoB) of the *bo*$_3$ oxidase using standard molecular biology techniques. The plasmid map of the construct can be found in figure 28. The construct was cloned, expressed in *E. coli* C43(DE3) Δcyo, and purified by Ni-NTA affinity chromatography by our former lab technician Sandra Schär. In the following, the *bo*$_3$ oxidase with the AviTag at subunit I will be referred to as *bo*$_3$-Avi.

4.2.3 Biotinylation of *bo*$_3$-Avi.

The AviTag on subunit I of *bo*$_3$-Avi was biotinylated as described by Fairhead *et al.* [198] and subsequently separated from non-biotinylated *bo*$_3$-Avi using SoftLink SoftRelease Avidin Resin. The efficiency of the biotinylation process was assessed by probing for biotin on a western blot (figure 29) using IRDye streptavidin. While lane 1 of the western blot shows *bo*$_3$-Avi which was not biotinylated by BirA, lane 2 shows BirA-biotinylated *bo*$_3$-Avi. The observation that *bo*$_3$-Avi is found biotinylated without addition of BirA suggests biotinylation to occur endogeneously during protein expression in *E. coli*. As controls, in each of the lanes 3 to 7 one of the ingredients for the biotinylation process by BirA has been omitted. In lane 3 no signal can be

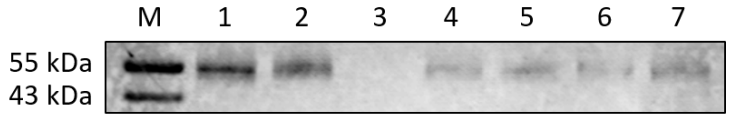

Figure 29: Western blot assessing biotinylation of *bo₃*-Avi. 1: *bo₃*-Avi only; 2: *bo₃*-Avi biotinylated by BirA; 3: biotinylation reaction without *bo₃*-Avi; 4: biotinylation reaction without BirA; 5: biotinylation reaction without biotin; 6: biotinylation reaction without ATP; 7: biotinylation reaction without $MgCl_2$; M: marker. Probing for biotin using IRDye Streptavidin (Licor). Subunit I of the *bo₃* oxidase has a molecular mass of 74 kDa, however its apparent mass in SDS-PAGE is 55 kDa [27] (see section 1.2.2).

detected as *bo₃*-Avi has not been added to the sample. In lanes 4 to 7, either BirA, biotin, ATP or $MgCl_2$ have been left out during the biotinylation process, respectively. In these four conditions *bo₃*-Avi was still biotinylated, demonstrating the extent of endogeneous biotinylation during expression of *bo₃*-Avi in *E. coli*.

4.2.4 Attaching Streptavidin to Biotinylated *bo₃*-Avi.

In order to monitor binding of SA to *bo₃*-Avi, SA was unspecifically labeled with NHS-activated fluorescein (NHS ester reaction scheme: see figure 30 on the following page). According to the manufacturer's information, the SA used had a molecular weight per subunit of 13.3 kDa, hence a molecular weight of 53.3 kDa per functional SA tetramer. Humbert *et al.* [217] showed that in SDS-PAGE (under denaturing conditions and at room temperature), SA is mainly detected as a tetramer. Therefore, we expected to detect the used SA in SDS-PAGE at ∼53 kDa. The observed (apparent) mass however (see lane 4 in figure 31A) was about 15 kDa higher than expected. The reason therefor remains unclear, especially since the purchased lyophilized SA was dissolved and analyzed by SDS-PAGE without any further modifications of the original product. As shown in lane 2 of figure 31A, SA binds efficiently to *bo₃*-Avi which was biotinylated by BirA, causing a shift of fluorescein-labeled SA towards higher mass. Subunit I of the *bo₃* oxidase has a molecular weight of 74 kDa. Hence, SA bound to subunit I of *bo₃*-Avi was expected to have a molecular weight of 127.3 kDa. The observed mass was slightly higher than 116 kDa (limit of the marker protein ladder used by S. Schär, preventing more accurate statements). The assembly of bands of higher molecular weight might be aggregates where one moiety of SA binds more than one entity of biotinylated *bo₃*-Avi. 83 % of SA were bound to the biotinylated AviTag in subunit I of *bo₃*-Avi, leaving 17 % of SA unbound (lane 2). In the condition where *bo₃*-Avi was not biotinylated by BirA (lane 4), only 11 % of the SA were bound to *bo₃*-Avi and

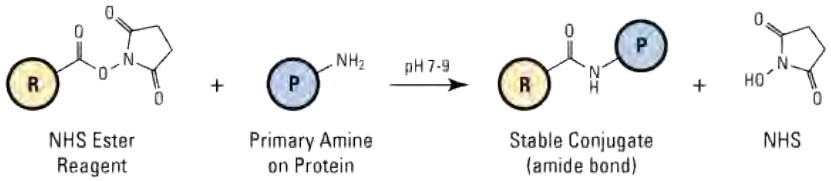

Figure 30: NHS ester reaction scheme for chemical conjugation to a primary amine. R represents a labeling reagent or one end of a crosslinker having the N-hydroxysuccinimide (NHS) ester reactive group (present case: fluorescein); P represents a protein or other molecule that contains the target functional group, i. e. primary amine (present case: SA). Figure from ThermoFisher Scientific.

89 % were present unbound. These results might also be an indicator for the levels of endogeneous biotinylation of the AviTag during the expression of *bo$_3$*-Avi in *E. coli* (see section 4.2.3). As expected, in the control lanes 1 and 3 no fluorescein signal could be detected, since there was no fluorescein-labeled SA in these samples.

These results were reproducible as shown in figure 32 on the next page, where the binding of *bo$_3$*-Avi to fluorescein-labeled SA was compared to binding to unlabeled SA (ratio *bo$_3$*-Avi to SA: 1:1). In lane 4, hardly any fluorescein-labeled SA is freely present (between 43 and 55 kDa), since most of it is bound to the biotinylated *bo$_3$*-Avi, causing a shift to higher mass. Consequently, less free biotinylated *bo$_3$*-Avi subunit I is present at approximately 55 kDa. The expected mass of the coupling product consisting of biotinylated *bo$_3$*-Avi subunit I and SA is approximately 110 kDa, considering the apparent mass of subunit I. The three fainter bands of apparent masses bigger than 130 kDa in lane 4 might be aggregates where one moiety of SA binds more than one entity of biotinylated *bo$_3$*-Avi. Formation of such aggregates might be prevented by using an excess of SA over biotinylated *bo$_3$*-Avi instead of a *bo$_3$*-Avi to SA ratio of 1:1. Comparing the silver stains of lanes 2 and 4, as expected, no significant difference can be found and the above described effects are exactly the same. Consequently, labeling of SA with NHS-activated fluorescein does not impair binding of SA to biotinylated *bo$_3$*-Avi subunit I.

In summary, SA could be bound to biotinylated *bo$_3$*-Avi as intended to and illustrated in figure 27 on page 79. This construct will be referred to in the following as *bo$_3$*-Avi-biot-SA.

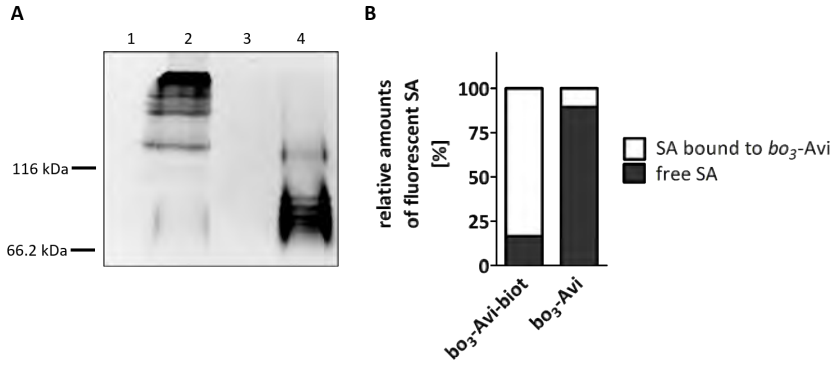

Figure 31: Binding of SA to biotinylated *bo₃*-Avi. (A) SDS-PAGE analysis of fluorescein-labeled SA bound to *bo₃*-Avi, detection of fluorescein fluorescence. 1: *bo₃*-Avi biotinylated by BirA; 2: *bo₃*-Avi biotinylated by BirA with bound SA; 3: *bo₃*-Avi, non-biotinylated; 4: *bo₃*-Avi, non-biotinylated, mixed with SA. Since the marker is non-fluorescent it was added manually by superimposition of this image with the same gel stained by silver. SDS-PAGE by Sandra Schär. (B) Readout of in-gel fluorescein fluorescence from (A). White: SA bound to *bo₃*-Avi; black: free SA.

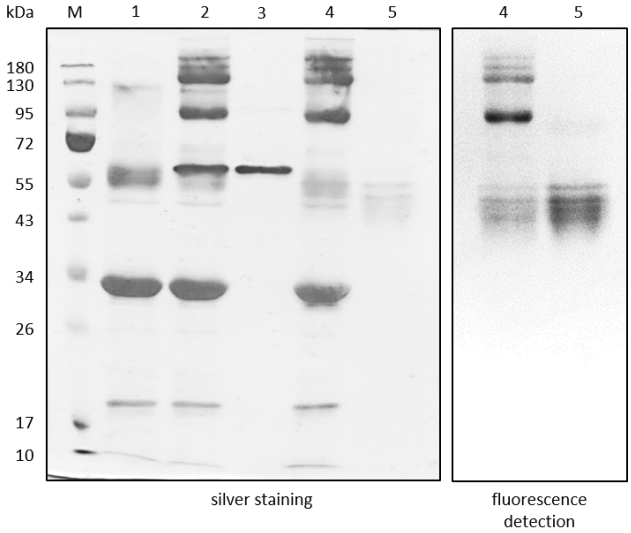

Figure 32: Reproducible binding of SA to biotinylated *bo₃*-Avi subunit I and effect of fluorescein labeling on SA. Left: Silver staining; right: In-gel fluorescein fluorescence detection of lanes 4 and 5. 1: *bo₃*-Avi biotinylated by BirA (sizes of subunits according to [27]. Subunit I: 74 kDa, apparent mass in SDS-PAGE: 55 kDa[27]; subunit II: 33 kDa; subunit III: 12 kDa; subunit IV: 12 kDa); 2: biotinylated *bo₃*-Avi + SA (ratio 1:1); 3: SA; 4: biotinylated *bo₃*-Avi + fluorescein-labeled SA (ratio 1:1); 5: fluorescein-labeled SA; M: marker. SDS-PAGE by Sandra Schär.

4.2.5 Increasing the Size of the LSU by Binding Different Biotinylated Moieties to Streptavidin.

With its size of 53.3 kDa, SA acts already as a preliminary LSU in terms of our strategy illustrated in section 4.1. Further, the advantage was taken of having the possibility to enlarge this preliminary LSU by exploiting the three remaining free biotin binding sites of SA as illustrated in figure 27 on page 79.

To enlarge the size of the preliminary LSU, several different biotinylated moieties were tested. Biotinylated bovine serum albumin (BSA; 66.5 kDa) for example is soluble and would definitely fulfill the demand of enlargement of the LSU, especially when bound three times to SA. However, no mono-biotinylated BSA was commercially available. Mono-biotinylated BSA may potentially be produced by labeling the only non-oxidized cysteine (Cys-34) of BSA [218] with maleimide-activated biotin. The use of poly-biotinylated BSA (labeling: unspecific with sulfo-NHS-biotin) was shown by SDS-PAGE analysis to lead to formation of aggregates consisting of multiple bo_3-Avi oxidases bound to one molecule of biotinylated BSA via SA (not shown).

Next, the focus was laid on dextrans, which are branched glucans, i. e. branched polysaccharides of glucose molecules (see figure 33 on the following page). Dextrans are highly soluble in water and are commercially available with sizes of up to 1 MDa. However, these dextrans had several drawbacks too. Using poly-biotinylated dextrans led to similar problems regarding aggregation as described above for poly-biotinylated BSA. Finally, we found a company claiming that their dextrans were mono-functionalized. Nevertheless, SA bound to such supposedly mono-functionalized dextrans was shown by SDS-PAGE analysis to cause the same problem of formation of very large aggregates as with poly-biotinylated dextrans (not shown). After asking further questions to the provider of the supposedly mono-functionalized dextrans regarding the way of introduction of the mono-functionality into the dextrans, no satisfying answers were received. Therefore, it had to be assumed that mono-functionalization of the provided dextrans was based on statistics, but it could not be attested.

In a third approach, biotinylated methoxypolyethylene glycols (mPEG-biot) of variable sizes (2 - 30 kDa) were tested. Compared to BSA and dextrans used before, only one biotin moiety was present per mPEG-biot. To test binding of mPEG-biot to previously described bo_3-Avi-biot-SA (see section 4.2.4), the latter was purified by SEC (Superdex 200 Increase 10/300 GL), incubated with an excess of 5 kDa-mPEG-biot and purified by SEC again. Reported stability of the interaction between

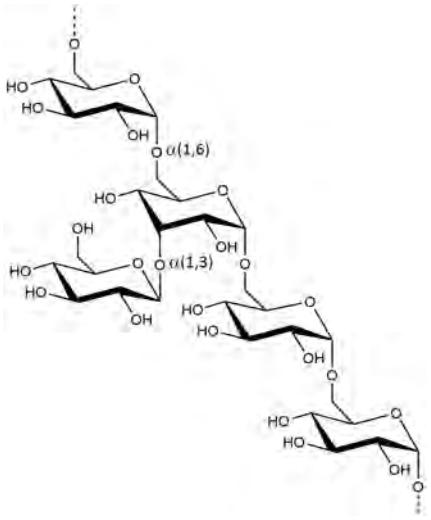

Figure 33: Structure of dextrans. Dextrans are branched glucans, i. e. branched polysaccharides of glucose. The predominant linkage is of the $\alpha(1,6)$ type.

biotinylated substrates and SA under denaturing conditions in SDS-PAGE [217] allowed to analyze the resulting protein-PEG construct *bo3*-Avi-biot-SA-$(PEG5k)_3$ by SDS-PAGE (see figure 34 on the next page). By addition of three units of 5 kDa-mPEG-biotin to subunit I of *bo3*-Avi-biot-SA (110 kDa, see section 4.2.4), the molecular weight increases to 125 kDa for subunit I of *bo3*-Avi-biot-SA-$(PEG5k)_3$ as confirmed by SDS-PAGE analysis. This demonstrates that the complete construct of the AviTag system according to figure 27 can be set up if using mono-functionalized PEGs. The assembly of such *bo3*-Avi-biot-SA-$(PEG)_3$ constructs was shown to work independently of the size of mPEG-biotins. However, the yields were quite low. It has therefore to be speculated that during purification by SEC substantial amounts of *bo3*-Avi-biot-SA-$(PEG5k)_3$ might had dissociated, despite of the very strong (but still non-covalent; see section 4.2.1) binding of biotin to SA. Holmberg *et al.* [219] reported that the streptavidin-biotin interaction can reversibly and efficiently be broken in nonionic aqueous solutions by a brief exposure to high temperature (70 °C). This may indicate that high pressure during SEC possibly results in dissociation of the streptavidin-biotin interaction as well; this however remains speculation.

A different approach would be to produce first the complete LSU, i. e. SA-$(PEG)_3$, leaving one biotin binding site of SA unoccupied. In fact, this would be an even more elegant approach as the coupling of *bo3*-Avi to the complete, preformed LSU could be performed in a single step. We tested this idea by adding a 4-fold excess of 30 kDa-mPEG-biotin to SA. The expected result was that after incubation, a mixture

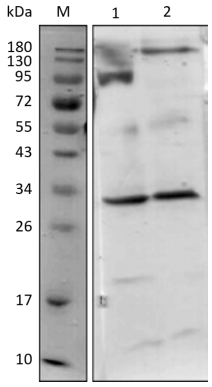

Figure 34: Binding of mPEG-biotin to *bo₃*-Avi-biot-SA. 1: SEC-purified *bo₃*-Avi-biot-SA; 2: *bo₃*-Avi-biot-SA-$(PEG5k)_3$; M: marker. In both lanes 1 and 2, *bo₃* oxidase subunit II can be easily detected at correct height (apparent mass of 31 kDa), while subunits III (apparent mass of 20 kDa) and IV (apparent mass of 11 kDa) are just faintly detectable, but present. As expected, free subunit I (apparent mass of 55 kDa) can hardly be detected. In lane 1, subunit I is bound to SA, resulting in a mass of approximately 110 kDa, as described in section 4.2.4. In lane 2, this band is shifted towards higher molecular weight, since three units of 5 kDa-mPEG-biotin have to be added to the mass of *bo₃*-Avi-biot-SA, resulting in an approximate mass of 125 kDa for subunit I of *bo₃*-Avi-biot-SA-$(PEG5k)_3$. Silver staining. SDS-PAGE by Sandra Schär.

of SAs with one, two, three or four PEG moieties was present. This expectation was confirmed by SEC (Superose 6 Increase 10/300 GL) followed by SDS-PAGE analysis as shown in figure 35 on the following page. In the mixture, SA (53.3 kDa) was found to be bound to two, three or four moieties of 30 kDa-mPEG-biotin, resulting in molecular weights of 113.3 kDa (SA-$(PEG30k)_2$, peaks and lanes 3 and 4), 143.3 kDa (SA-$(PEG30k)_3$, peak and lane 2) or 173.3 kDa (SA-$(PEG30k)_4$, peak and lane 1), respectively. Application of a 4-fold excess of 30 kDa-mPEG-biotin over SA resulted in a predominance of LSUs consisting of three or four units of 30 kDa-mPEG-biotin bound to SA (peaks 1 and 2). In lane 1 of the SDS-PAGE, the single band visible appears at higher molecular weight than expected. According to Zheng, Ma, *et al.* [220], the migration properties of PEGylated proteins can be very different from that of protein of same molecular weight because of complex interactions between PEG chains (either free or coupled to protein) and SDS micelles, between PEG chains and protein, and consequently also between the PEGylated protein and SDS micelles. These interactions may explain migration of SA-$(PEG30k)_4$ at higher molecular weight than expected.

bo₃-Avi-biot was subsequently incubated with SEC-purified SA-$(PEG30k)_3$. The expected coupling product *bo₃*-Avi-SA$(PEG30k)_3$ was attempted to be purify by

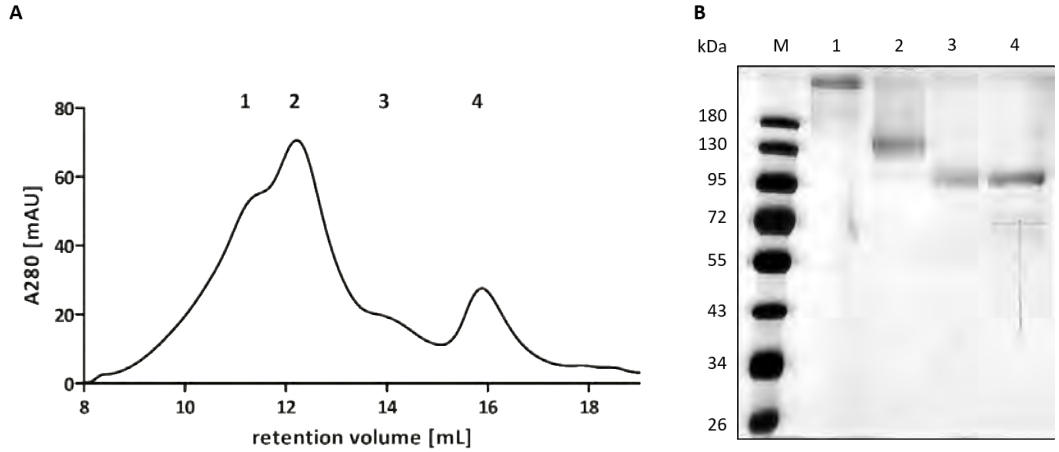

Figure 35: Analysis of LSU consisting of SA and mPEG-biotin. (A) Size exclusion chromatogram of a mixture of SA with a 4-fold excess of 30 kDa-mPEG-biotin. Column: Superose 6 Increase 10/300 GL. Four peaks (1 to 4) can be detected. A fraction of each of these peaks was analyzed by SDS-PAGE. (B) SDS-PAGE analysis of peaks 1 to 4 of the SEC in (A). Lanes 1 to 4: peaks 1 to 4; M: marker. Silver staining.

SEC. The obtained yields however were not reasonable, not allowing performance of a single functional assay. Therefore, we returned to the approach where SA was first bound to *bo*$_3$-Avi-biot and subsequently saturated with biotinylated PEGs.

4.2.6 Functional Experiments with *bo*$_3$-Avi-biot-SA-(PEG)$_3$.

At the time when this approach was developed, to my knowledge there existed no method to physically determine the orientation of reconstituted *bo*$_3$ oxidase independent of functional studies, apart from limited enzymatic proteolysis from the outside of the proteoliposomes followed by analysis of the digestion pattern by SDS-PAGE and western blotting. Since this approach is rather time-consuming, it was decided to assess orientation by functional experiments.

As described in section 1.2.2, in essence the *bo*$_3$ oxidase reduces O_2 to water accompanied by pumping protons across the membrane. Functionality can therefore be assessed by monitoring oxygen consumption. However, monitoring oxygen consumption does not allow to draw any conclusions concerning the orientation of the oxidase in the liposomal membrane. Alternatively, functionality of the *bo*$_3$ oxidase can be assessed by monitoring proton pumping across the liposomal membrane. Proton transport in either direction across the liposomal membrane leads to changes of the pH in the liposomal lumen and consequently to a Δ pH across the membrane. As discussed

in section 1.7.2, the membrane-permeable substrate of the *bo₃* oxidase, ubiquinol Q_1, inevitably activates both orientation populations of reconstituted oxidase, which are consequently expected to compete with eachother. Therefore, it is expected that variation of the ratio between inwardly and outwardly pumping *bo₃* oxidase results in differences of the observed net proton pumping across the membrane.

Proton Uptake Measurements with ACMA.

ACMA (9-amino-6-chloro-2-methoxyacridine) is a fluorescent dye which can be adsorbed at membranes. Its fluorescence is quenched by imposing transmembrane Δ pHs (acidic-inside only), artificially induced by proton uptake, approaching saturation when Δ pH is equal to or bigger than 2.[221] The principle of the ACMA proton pumping assay with *bo₃* oxidase is illustrated in figure 36 on the next page. ACMA is expected to be quenched at higher extent, the higher the ratio of inwardly pumping *bo₃* oxidases to totally present *bo₃* oxidases. Due to ACMA getting quenched by acidic-inside Δ pHs only, no ACMA quench would theoretically be expected for vesicles in which the population of inwardly pumping *bo₃* oxidases is smaller than 50 %. Because ACMA fluorescence is not influenced by basic-inside proton gradients, and since the variation of the orientation ratio of inwardly pumping to total proton pumping *bo₃* oxidases within a liposome population is expected to vary following a poisson distribution, ACMA quenching can be observed although the average of inwardly pumping oxidases over the whole population of liposomes is smaller than 50 %. This is different compared to the use of the pH-sensor pyranine, which enables to monitor net proton influx and efflux (discussed below).

As discussed in section 1.7.2, reconstitution of *bo₃* oxidase into liposomes was reported to result in vesicles in which 72 - 77 % of the inserted oxidases were orientated to export protons out of the proteoliposomes. This leads to the expectation that proton pumping by conventionally reconstituted *bo₃* oxidase does lead to only little or no ACMA quenching. However, the higher the share of *bo₃* oxidases reconstituted in the desired orientation (i. e. importing protons into the proteoliposomes), the higher the expected extent of ACMA quenching.

In a first experiment, *bo₃*-Avi was modified with two LSUs differing in the size of mPEG-biotin (5 and 30 kDa) bound to SA, and inserted via detergent-mediated reconstitution (0.4 % cholate, detergent removal by SEC) into the membranes of preformed, partially solubilized liposomes. Proton pumping of the reconstituted *bo₃* oxidase was measured via ACMA fluorescence. While no ACMA quench could be measured with reconstituted *bo₃*-Avi-biot (net proton export, not shown), the addition

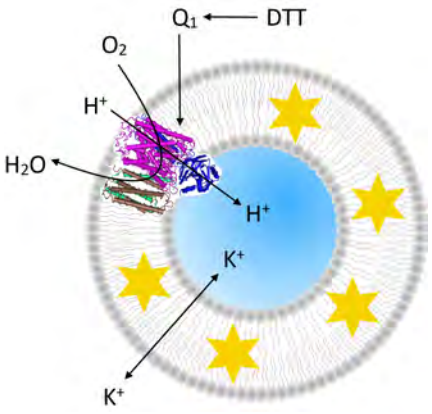

Figure 36: Principle of the ACMA proton pumping assay with *bo*$_3$ oxidase. Ubiquinone Q_1 reduced by dithiothreitol (DTT) to ubiquinol Q_1H_2 serves as electron donor for the *bo*$_3$ oxidase. The electrons are first transferred from Q_1H_2 to heme *b* and subsequently to the catalytic site of the *bo*$_3$ oxidase consisting of heme *o*$_3$ and Cu_B (see section 1.2.2 on page 7). The released free energy is conserved by pumping protons across the membrane, thus generating a Δ pH what consequently quenches ACMA (yellow stars) fluorescence. The electrical gradient $\Delta\psi$ is abolished by valinomycin-mediated shuttling of potassium ions across the membrane.

of the preliminary LSU consisting of SA led to a small quench as shown in figure 37A (green trace). When the LSU was enlarged by binding of mPEG-biotin to SA prior to reconstitution, the ACMA quench was significantly increased. Additionally, a dependance of this increase in ACMA quench on the size of the mPEG-biotin used could be shown. Consequently, reconstitution of *bo*$_3$-Avi-biot-SA-$(PEG)_3$ using 30 kDa-mPEG-biotin (black trace) led to a bigger ACMA quench compared to when a 5 kDa-mPEG-biotin was used (blue trace). While increasing the preliminary LSU with mPEG-biotin of 5 kDa resulted in 1.8-fold higher ACMA quench, increasing the preliminary LSU with mPEG-biotin of 30 kDa led to a 4.4-fold increase of the observed ACMA quench. These results were reproducible and perfectly met the expectations.

A drawback of the ACMA assay is that no absolute statement regarding the orientation ratio can be made. Since the output of the ACMA assay is of relative nature only, providing no absolute, quantitative results, it only allows the conclusion that orientation of the *bo*$_3$ oxidase can be influenced to a certain extent, and that the size of the LSU plays an important role. It is not possible to deduce whether total unidirectionality was achieved.

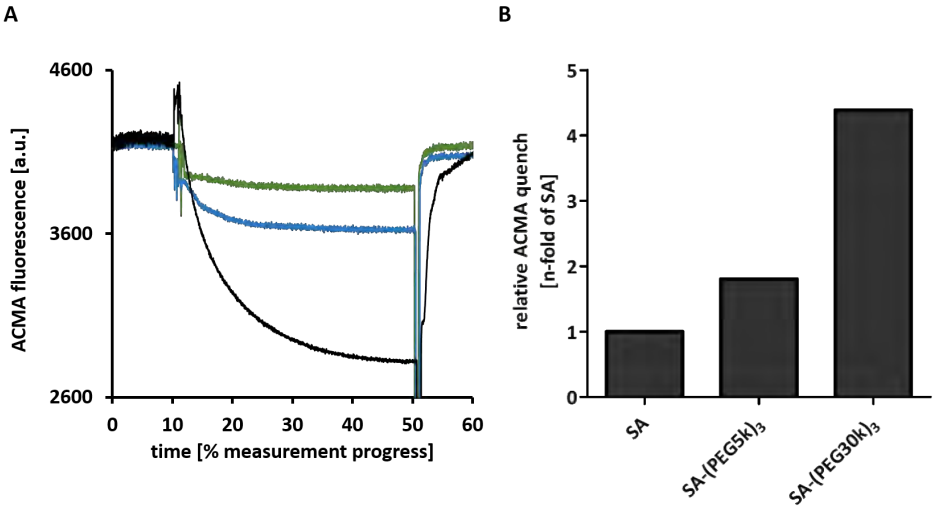

Figure 37: ACMA quenching assay with *bo*$_3$-Avi-biot-SA-(PEG)$_3$. (A) Raw data. Green: *bo*$_3$-Avi-biot-SA; blue: *bo*$_3$-Avi-biot-SA-(PEG5k)$_3$; black: *bo*$_3$-Avi-biot-SA-(PEG30k)$_3$. First, to the proteoliposomes in buffer HMK (10 mM HEPES pH 7.4, 2 mM $MgCl_2$, 100 mM KCl, 10 mM KNO_3), 50 µM ubiquinone Q_1, 1.5 µM ACMA and 70 nM valinomycin were provided. Proton pumping was started by addition of 2 mM DTT at 10 % time. When ACMA fluorescence was stable again, at 50 % time the built-up proton gradient was dissipated by addition of 30 mM NH_4Cl. In all conditions, after additions of DTT and NH_4Cl, mixing artefacts are visible. Assay measured by Sandra Schär. (B) Readout of ACMA quench from (A) as n-fold of condition "SA". Liposomes: 10 mg ml^{-1} 90 % lecithin, soybean; 100 nm; in 20 mM HEPES pH 7.5, 100 mM KCl.

Nevertheless, this experiment indicated that our strategy to unidirectionally reconstitute the *bo*$_3$ oxidase by attaching LSUs using the AviTag system is promising.

In the previous experiment, reconstitution was mediated by cholate and detergent removal was carried out by SEC, a method for reconstitution of the *bo*$_3$ oxidase developed in our lab. However, other groups have used a second method for detergent removal (see also section 1.6) [172, 178, 222], i. e. polystyrene beads (SM-2 Bio-Beads) to adsorb detergent molecules. We wanted to see if the promising results from figure 37 could be confirmed using this alternative method for detergent removal.

For this purpose, *bo*$_3$ oxidase attached to differently sized LSUs was reconstituted with cholate and the detergent was subsequently removed either by SEC (CentriPure P10 desalting columns) as before, or by SM-2 Bio-Beads. Proton import into the proteoliposomes was eventually measured using the ACMA quenching assay as shown in figure 38. For both reconstitution methods, the previous findings could be confirmed. Indepent of the method of detergent removal, orientation of reconstituted *bo*$_3$ oxidase

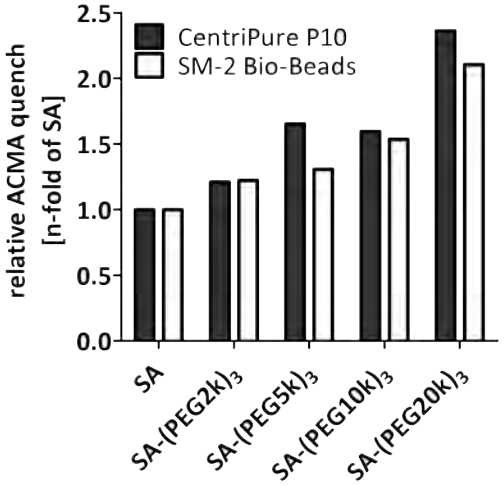

Figure 38: Testing two different reconstitution methods using the ACMA quenching assay with *bo*$_3$-Avi-biot-SA-(PEG)$_3$. Five LSUs of different size have been bound to *bo*$_3$-Avi-biot: -SA, -SA-(PEG2k)$_3$, -SA-(PEG5k)$_3$, -SA-(PEG10k)$_3$, -SA-(PEG20k)$_3$. Measurements carried out as described in the legend of figure 37. Results as n-fold of condition "SA". Black: detergent removal by CentriPure P10 desalting columns; white: detergent removal by adsorption to polystyrene beads (SM-2 Bio-Beads, Bio-Rad). Liposomes: 10 mg ml^{-1} 90 % lecithin, soybean; 100 nm; in 20 mM HEPES pH 7.5, 100 mM KCl. Assay measured by Sandra Schär.

can be influenced to a certain extent, and the size of the LSU plays an important role. With increasing size of the LSU, the ACMA quench and hence the fraction of inwardly pumping oxidases increases. Additionally, these results may be interpreted as a trend that fast detergent removal by SEC (CentriPure P10 desalting columns) leads to a higher degree of unidirectionality of reconstituted *bo*$_3$ oxidase than slow detergent removal by adsorption to polystyrene beads. This might seem to be contradictory to studies [5, 6, 181] discussed in section 1.7.2, reporting fast detergent removal (dilution) to lead to random insertion of MPs into the liposomal membrane, while slow removal of the detergent (dialysis) leads to unidirectional insertion. In contrast to our results presented here, in these studies the MPs however were not reconstituted into preformed, partially detergent-solubilized liposomes, but the liposomes were formed *de novo* in the presence of the solubilized MPs. Therefore, our results do not conflict these previous studies.

Proton Pumping – Pyranine Assay.

A second assay to monitor pumping of protons across the liposomal membrane is based on the hydrophilic and membrane-impermeable, pH-sensitive fluorescent dye 8-hydroxypyrene-1,3,6-trisulfonic acid (HPTS), better known as pyranine. Because pyranine contains three negatively charged sulfonate groups it cannot readily diffuse through the phospholipid bilayer. Therefore, it can be entrapped into the liposomal lumen in order to be used as a sensitive reporter of internal pH variations associated with proton pumping.[223]

Pyranine is usually entrapped in the liposomal lumen and measures the actual pH in the liposome. Further, recording standard curves describing the dependency of pyranine fluorescence on the pH allows pyranine fluorescence to be quantified.[169] Pyranine can be excited at two different excitation maxima ($\lambda_{ex\ 1}$: 405 nm and $\lambda_{ex\ 2}$: 450 nm), with one single emission maximum for both excitation maxima (λ_{em}: 510 nm). Pyranine can therefore be used as a ratiometric fluorescent pH indicator, making it one of the most advantageous available probes for pH measurements in liposomes.[224] The measurement output is the ratio F405/F450 of fluorescence emission intensities at 510 nm at excitation wavelengths of 405 nm and 450 nm, respectively. If the pH in the liposomal lumen increases, i. e. protons are pumped out of the liposome, the ratio F405/F450 decreases, and vice versa. Therefore, pyranine allows determination of the direction of proton translocation across liposomal membranes, making it indispensable for assessing the orientation of any proton pumping MP in liposomes, especially of the *bo₃* oxidase.

bo₃ oxidase-mediated proton pumping was monitored by measuring fluorescence of pyranine entrapped in the liposomal lumen, and started by addition of DTT to reduce ubiquinone Q_1. The electrical gradient $\Delta\psi$ was abolished by addition of valinomycin, which shuttles potassium ions across the membrane. Pyranine-mediated monitoring of proton pumping was performed using weakly buffered systems (e. g. 0.5 mM MOPS).

To test the AviTag system with the pyranine assay, *bo₃*-Avi, *bo₃*-Avi-biot and *bo₃*-Avi-biot-SA(PEG20k)$_3$ were reconstituted into preformed, partially detergent-solubilized liposomes in presence of pyranine (see figure 39 on page 94). While a net majority of *bo₃*-Avi-biot transports protons out of the liposomes upon reduction of ubiquinone Q_1 by DTT (figure 39A), average directionality of proton pumping changed with *bo₃*-Avi-biot-SA-(PEG20k)$_3$ (figure 39B), even if the changes in the pyranine fluorescence ratio were admittedly small. As a control for an outwardly pumping system, *bo₃*-Avi was reconstituted into liposomes (figure 39C), known to net

pump protons out of liposomes. Since *bo₃*-Avi and *bo₃*-Avi-biot differ in one molecule of biotin only, no difference in orientation and thus proton pumping direction is expected. However, proton pumping by *bo₃*-Avi resulted in a much bigger pyranine quench compared to figure 39A. The difference in the extent between the pyranine quenches in figures 39A and 39C is due to a loss of *bo₃* oxidase activity, caused by the elaborate production process of *bo₃*-Avi-biot-SA-$(PEG20k)_3$ from *bo₃*-Avi, including biotinylation of *bo₃*-Avi for 1 h at 30 °C, several periods of incubation at room temperature as well as two SEC purification steps. Further, oxygen consumption activity of the corresponding variants of *bo₃* oxidase has been assessed by monitoring O_2 consumption of the pure enzymes solubilized in detergent using an Oxygraph+. As a control for a system pumping protons exclusively into liposomes, purified F_1F_0 ATP synthase from *E. coli* was used, known to orientate unidirectionally with its F_1 head piece on the outside of the liposomes (figure 39D). By addition of ATP to the outside of the proteoliposomes, the ATP synthase starts hydrolyzing ATP, and due to the membrane-impermeability of ATP exclusively pumps protons inwardly, as previously reported by Wiedenmann *et al.* [169].

These results can be interpreted as a tendency into the right direction, but they must not be over-interpreted neither. With the AviTag system it might be possible to influence orientation of *bo₃* oxidase during reconstitution at least to a certain extent. The experiments were repeated several times, but unfortunately, the differences observed in figures 39A and 39B could only be seen in the minority of experiments, whereas in the majority, no proton pumping could be observed at all. This possibly indicates an orientation ratio of 50 % inwardly and 50 % outwardly pumping *bo₃* oxidases. Another possible explanation could be a low reconstitution efficiency, i. e. that the perfect conditions for the reconstitution of the *bo₃* oxidase coupled to its LSU have not been found yet. Additionally, the production of *bo₃*-Avi-biot-SA-$(PEG)_3$ involved many steps, during which activity of the *bo₃* oxidase is partially lost as discussed above, accompanied by substantial losses of protein, making the procedure unsuitable for general application.

Measuring Coupled Activity – ATP Synthesis Assay.

Encouraged of the results of the ACMA proton pumping assay, and not discouraged by the outcome of the pyranine assay, coupled activity of *bo₃* oxidase and F_1F_0 ATP synthase was measured exactly as described by von Ballmoos, Biner, *et al.* [170] (see figure 21 on page 40). Briefly, the *bo₃* oxidase is coreconstituted with the ATP synthase and reduction of the oxidase generates a proton gradient across the

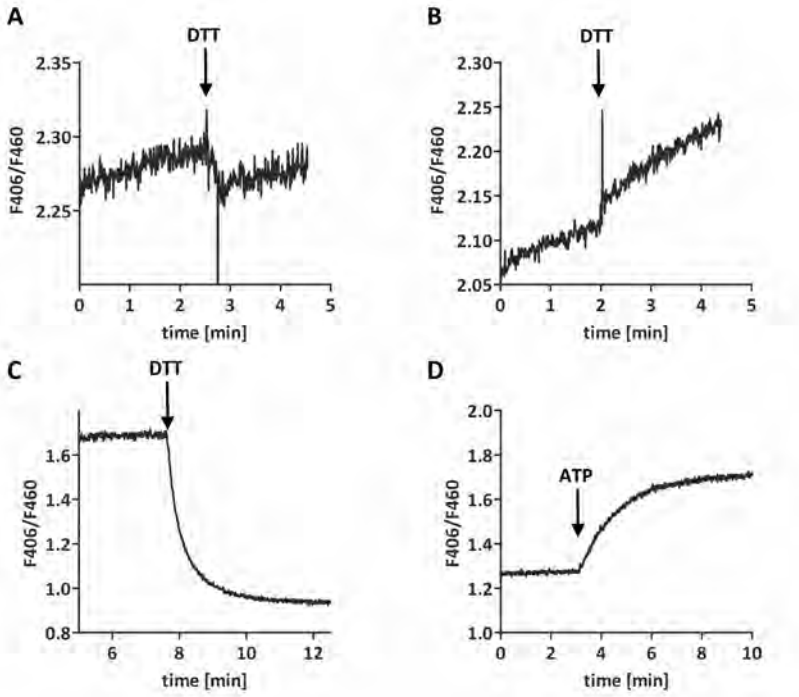

Figure 39: Proton pumping monitored by pyranine. (A) bo_3-Avi-biot; (B) bo_3-Avi-biot-SA-(PEG20k)$_3$; (C) bo_3-Avi; (D) ATP hydrolysis by F_1F_0-ATP synthase. While in (A) after starting the reaction by addition of DTT protons are net pumped out of the proteoliposomes by not unidirectionally orientated bo_3 oxidase, in (B) protons are net pumped inwardly. (C) and (D) represent controls for protons being pumped out of liposomes or inwardly, respectively. (A) and (B) measured by Sandra Schär. Liposomes: 10 mg ml^{-1} 90 % lecithin, soybean; 200 nm; in 2 mM MOPS pH 7.3, 25 mM K_2SO_4. Measurement buffer: same as liposome buffer.

membrane, which can then be used by the ATP synthase to produce ATP from ADP and organic phosphate. Due to unidirectional orientation of the ATP synthase (see section 1.7), the efficiency of the coupled activity just depends on the orientation of the *bo*$_3$ oxidase and not additionally on the one of the ATP synthase, and all the ATP produced is found on the outside of the liposome and none inside. According to von Ballmoos, Biner, *et al.* [170], ATP synthesis and thus coupled enzyme activity can be assessed by measuring luminescence as illustrated in figure 40, using the luciferin/luciferase system originally reported by de Wet *et al.* [225] (for a review on this system see [226]). The luciferase first catalyzes binding of D-luciferin to the α-phosphate of ATP-Mg^{2+}, forming PP_i-Mg^{2+} and luciferyl-AMP. The latter is subsequently oxidized by O_2 to form AMP, CO_2 and oxyluciferin in an excited state emitting a photon while returning to the ground state.[227]

In a first experiment (figure 41A), coupled enzyme activity of purified *E. coli* F_1F_0 ATP synthase coreconstituted with either *bo*$_3$ oxidase wild type (wt), *bo*$_3$-Avi-biot-SA, or *bo*$_3$-Avi-biot-SA-(PEG30k)$_3$ is measured. This experiment showed a 1.8-fold increase in ATP synthesis if the *bo*$_3$ oxidase was modified with the preliminary LSU SA compared to *bo*$_3$ wt. ATP synthesis rate was further increased to 5.5-fold compared to *bo*$_3$ wt by enlarging the preliminary LSU to SA-(PEG30k)$_3$. These results indicated a dependency of coupled enzyme activity, hence of orientation of the *bo*$_3$ oxidase, on the size of the LSU.

To investigate on this indication, the first experiment was expanded by the use of additional differently sized LSUs (figure 41B). The results showed on one hand that increasing the preliminary LSU SA to SA-(PEG2k)$_3$ did not have any effect on coupled enzyme activity. On the other hand it was observed that using SA-(PEG5k)$_3$, SA-(PEG10k)$_3$, and SA-(PEG20k)$_3$ each led to an increase of the ATP synthesis rate. These results not only confirmed the findings in figure 41A, but also the results of the previously assessed proton pumping of *bo*$_3$ oxidase measured by the ACMA assay. Consequently, increasing size of the LSU leads to more unidirectionally reconstituted *bo*$_3$ oxidase.

To start *bo*$_3$ oxidase-mediated proton pumping in the experiments shown in figures 41A and 41B, 50 µM ubiquinol Q_1 were used. We however then wondered whether the observed differences in coupled enzyme activity are even higher at different concentrations of ubiquinol Q_1. Therefore, ubiquinol Q_1 was titrated in a dose-response experiment to proteoliposomes coreconstituted with the ATP synthase and either *bo*$_3$ wt, *bo*$_3$-Avi-biot-SA, or *bo*$_3$-Avi-biot-SA-(PEG30k)$_3$ (figure 41C). At ~50 µM ubiquinol Q_1 the ATP synthesis rate starts to plateau for all three variants of

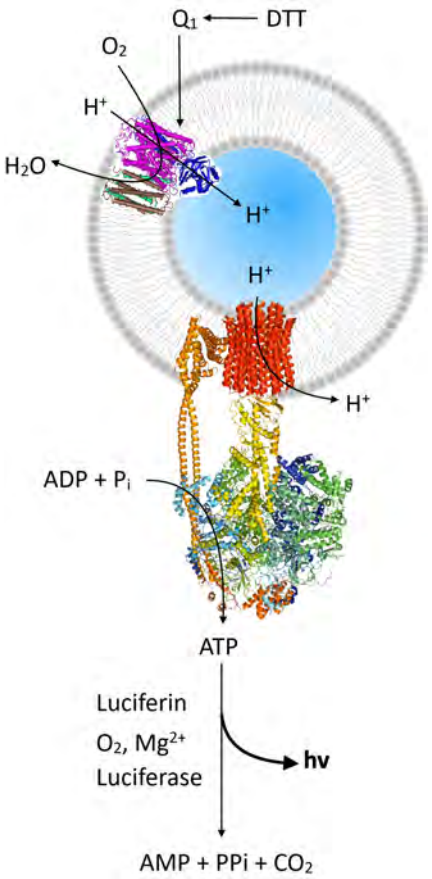

Figure 40: Luciferin/luciferase-based assay to monitor respiratory-driven ATP synthesis. In addition to the elements already shown in figure 21, the principle of the luciferin/luciferase assay to monitor ATP synthesis by luminescence is shown. ATP produced by the ATP synthase, using the proton gradient provided by the bo_3 oxidase, is consumed by luciferase from the firefly *Photinus pyralis* to oxidize D-luciferin in the presence of O_2 and Mg^{2+}, producing light emission.[225, 228] Figure adapted from [229].

bo₃ oxidase. However, the relative differences in coupled enzyme activity between the three variants did not vary significantly at different concentrations of ubiquinol Q_1. Further, these results showed that the K_m of the coupled activity stayed constant, i. e. the variation in size of the LSUs did not change the catalytic activity of this coupled enzyme system.

Analogously to the experiments where proton pumping of *bo₃* oxidase was monitored by ACMA quenching, we also compared two reconstitution methods either using SEC (CentriPure P10 desalting columns) or SM-2 Bio-Beads for detergent removal with ATP synthesis measurements (figure 41D). Our results show that the modification of *bo₃* oxidase with the LSU SA-$(PEG20k)_3$ leads to higher ATP synthesis rates for both reconstitution methods. This effect is more pronounced if SEC is used for detergent removal, confirming the results of the previous ACMA-mediated measurements of proton pumping by *bo₃* oxidase.

4.2.7 Conclusions to the AviTag System.

Reconstitution of *bo₃* wt was reported to result in vesicles with 72 - 77 % of the inserted oxidases orientated to export protons out of the proteoliposomes.[25, 172] Using the AviTag system however, orientation of reconstituted and coreconstituted *bo₃* oxidase can be influenced. *bo₃*-Avi-biot was modified with LSUs consisting of SA-$(PEG)_3$ with biotinylated PEG moieties of varying sizes and reconstituted into preformed, partially detergent solubilized liposomes. By pyranine- and especially ACMA-mediated assessment of proton pumping of such variants of *bo₃*-Avi-biot-SA-$(PEG)_3$ we showed that the fraction of inserted oxidases orientated to export protons out of the liposomes was decreased to be <50 %, and vice versa, the population of oxidases pumping protons in the desired direction, i. e. importing protons into the proteoliposomes, was increased from 23 - 28 % to >50 %. Further, it was observed that this effect depends on the size of the LSU. The bigger the LSU, the more the orientation of reconstituted *bo₃* oxidase was shifted towards the desired direction. Measuring coupled activity of ATP synthase coreconstituted with LSU-modified *bo₃* oxidase confirmed these effects. Attachment of LSUs on *bo₃*-Avi-biot resulted in higher ATP synthesis rates, increasing with the size of the LSU.

A mutual drawback of the applied functional assays is that they do all just allow to draw relative conclusions on the orientation of *bo₃* oxidase. Therefore it would be advantageous to have at hand a biochemical method to physically determine orientation of reconstituted *bo₃* oxidase, independent of its functionality, and not

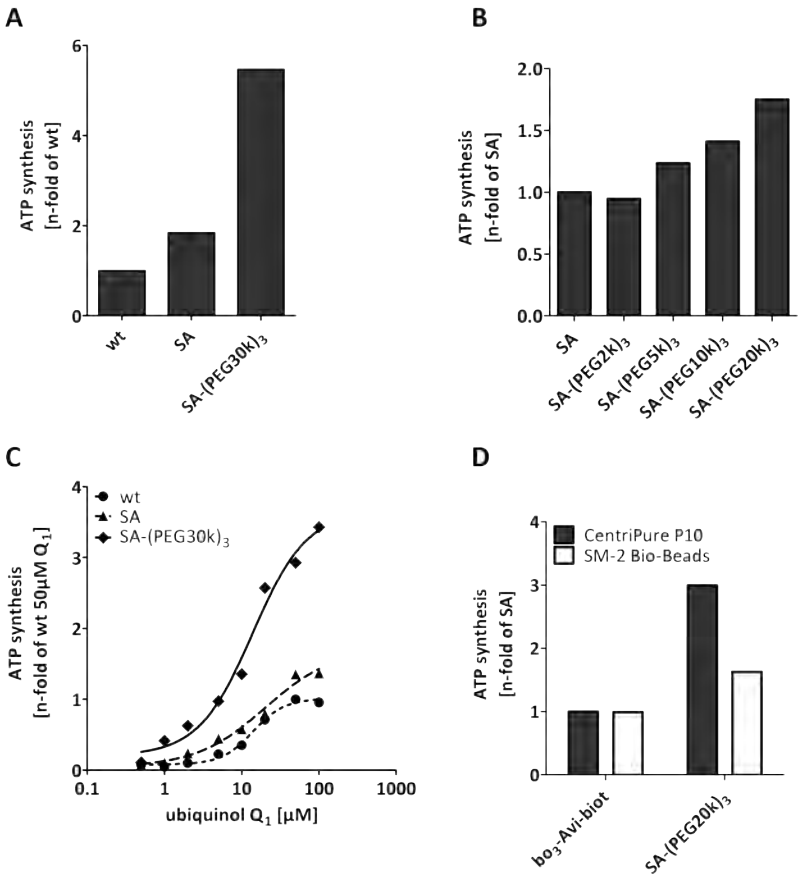

Figure 41: Coupled activity of *bo₃*-Avi-biot-SA-(PEG)$_3$ and ATP synthase. Continuous respiratory-driven ATP synthesis, i. e. coupled activity of the coreconstituted *bo₃* oxidase and and ATP synthase was monitored by measuring luminescence using the luciferin/luciferase system detecting newly synthesized ATP as described in figure 40 on page 96. The measured ATP synthesis rates were normalized to specific activity of *bo₃* oxidase assessed by oxygen consumption measurements. The same amount of ATP synthase from the same batch of purification was used for each experiment. wt: wild type *bo₃* oxidase; SA: *bo₃*-Avi-biot-SA. (A) Endpoint measurements of coupled activity with 50 µM ubiquinol Q_1. Compare to (B). (B) *bo₃*-Avi-biot was coupled to LSUs of different sizes and subsequently coreconstituted with the ATP synthase using CentriPure P10 desalting columns for detergent removal. (C) Dose-response experiment investigating the dependency of the coupled activity on the input of ubiquinol Q_1. (D) Two different reconstitution methods (detergent removal either by CentriPure P10, black; or by SM-2 Bio-Beads, white) were compared using *bo₃*-Avi-biot without any LSU and *bo₃*-Avi-biot enlarged by the LSU SA-(PEG20k)$_3$. Data for (B) and (D), where CentriPure P10 columns were used, were produced by Sandra Schär in two biologically distinct experiments, however, preparation of the LSUs and the reconstitution method were identical. Liposomes: 10 mg ml^{-1} 90 % lecithin, soybean; 200 nm; in 20 mM HEPES pH 7.5, 100 mM KCl, 2.5 mM $MgCl_2$, 25 g L^{-1} sucrose. Measurement buffer: 20 mM Tris-phosphate pH 7.4, 5 mM $MgCl_2$, 4 mM DTT, 80 µM ADP.

based on proteolytic cleavage. Because migration properties of PEGylated proteins can be very different from that of proteins of same molecular weight (see section 4.2.5) [220], proteolytic cleavage from the outside of the proteoliposomes followed by analysis of the digestion pattern by SDS-PAGE or western blotting was no valid option to determine orientation in the present case. In the meantime however, such an assay was developed in our lab by Lukas Rimle (see section 4.4). A future student might revisit the AviTag system to measure the output with this method.

During the development of the AviTag system, unexpected pitfalls occured, and too many steps had to be introduced which were not planned initially. The LSU could not be completely built prior to its attachment to *bo*$_3$-Avi-biot, but it had to be built "on" the enzyme by first binding SA to *bo*$_3$-Avi-biot with subsequent saturation of the remaining biotin binding sites of SA with biotinylated PEGs. Required SEC purification after each step of modification of the *bo*$_3$ oxidase (biotinylation, binding of streptavidin, increasing the size of streptavidin-based LSU) led to reasonable loss of protein, thus to very low yields of the final constructs of *bo*$_3$-Avi-biot-SA-$(PEG)_3$. On top of low yields, activity of *bo*$_3$ oxidase was partially lost during this procedure. To investigate on the reason for the loss of activity, thermal stability of the *bo*$_3$ oxidase was assessed. *bo*$_3$ oxidase wt incubated at different temperatures (4 - 30 °C) for more than 5 h however did not show any decrease in the oxidase's oxygen consumption activity (see supplementary figure S30 on page 226). Consequently, incubation periods of *bo*$_3$ Avi-biot during assembly of *bo*$_3$-Avi-biot-SA-$(PEG)_3$ could be ruled out as reason for the partial loss of activity. Another explanation might be that repeated SEC-mediated purification of *bo*$_3$ oxidase derivatives possibly leads to a loss of remaining associated annular lipids. Annular lipids however are essential to maintain full functionality of most MPs.[67] These pitfalls eventually prevented us from developing further the AviTag system.

4.3 Approach II – The SpyTag-SpyCatcher System.

4.3.1 Introduction to the SpyTag-SpyCatcher System.

Due to the drawbacks of approach I using the AviTag, including complicated manufacturing and low yields of the final *bo₃*-LSU construct, and loss of *bo₃* oxidase activity, a new linker system was needed. Such a new linker system should ideally provide covalent binding of the MP to the LSU to prevent dissociation during potential purification steps and during reconstitution, nevertheless offer the possibility to remove the LSU from the MP after reconstitution. Additionally, the assembly of the LSU should be less complicated as in the first approach, and the new linker system should allow quick coupling of the LSU to the MP. Given these requirements, the most promising candidate found was the SpyTag-SpyCatcher system (figure 42) rather recently developed and described by Zakeri *et al.* [230] and later refined by Li, Fierer, *et al.* [231].

Briefly, the SpyTag and its linker counterpart SpyCatcher were generated by splitting the CnaB2 domain from the fibronectin-binding protein FbaB from *Streptococcus pyogenes*, with its provenience also explaining its name (*Spy*).[231, 232] The CnaB2 domain was split into a 13-residue peptide called SpyTag with the sequence AHIVMVDAYKPTK and the 116 residue complementary domain SpyCatcher. SpyTag and SpyCatcher are able to spontaneously form an isopeptide bond under a range of temperatures (at least 4 - 37 °C), pH values (5 - 8), buffers (no specific anion or cation required) and even in the presence of non-ionic detergents.[232] The linking system works best if the tags are fused to the N- or C-terminus of the proteins of interest thereby reacting to high yield with a half-time of just over 1 minute (rate constant: $1.4 \times 10^3\ M^{-1}s^{-1}$) under optimal conditions.[232] For a review on recent applications of the SpyTag-SpyCatcher technology, the reader is directed to Keeble *et al.* [233] and the connected online database "SpyBank" (https://www.bioch.ox.ac.uk/howarth/info.htm).

The SpyTag-SpyCatcher system meets the requirement to provide covalent linkage. Additionally, no special conditions nor adjuvants are needed for coupling, hence the system being compatible with a broad spectrum of applications. Furthermore, with 13 residues only, the SpyTag is still small enough to most probably not interfering with expression and folding of very complex integral MPs. It was decided to introduce the SpyTag to the MPs of interest and its bigger counterpart SpyCatcher to LSUs, hence implying soluble proteins as LSUs instead of the PEG moieties used in the AviTag system.

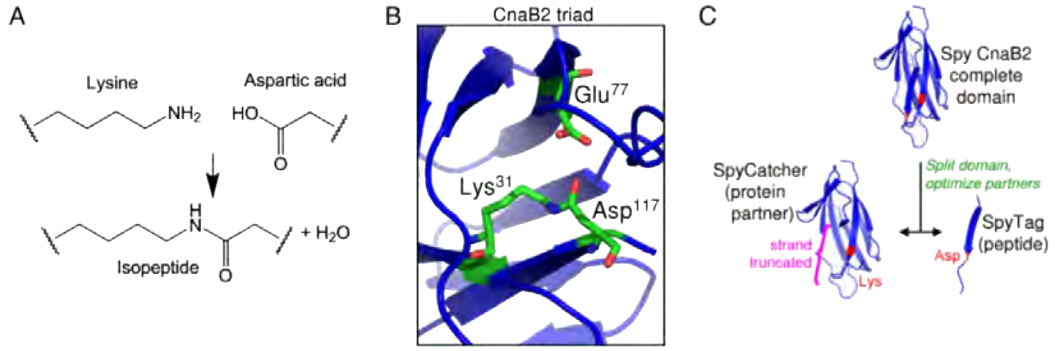

Figure 42: Spontaneous intermolecular amide bond formation by SpyTag. (A) Amide bond formation between Lys and Asp side chains. (B) Key residues for amide bond formation in CnaB2 shown in stick format, based on PDB: 2X5P (C) Cartoon of SpyTag construction. *S. pyogenes (Spy)* CnaB2 was dissected into a large N-terminal fragment (SpyCatcher, left) and a small C-terminal fragment (SpyTag, right). Reactive residues are highlighted in red. Figure adapted from [230].

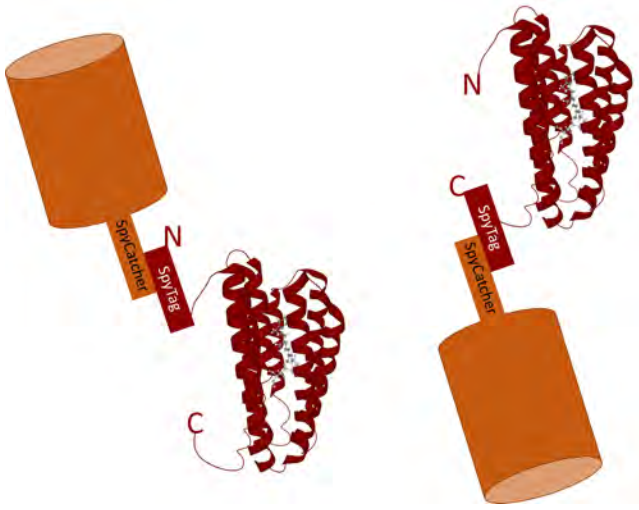

Figure 43: The SpyTag-SpyCatcher system applied to pR. A SpyTag was genetically introduced either at the N- or the C-terminus of pR (PDB: 2L6X; [20]). Via its SpyTag, pR (red) can be covalently linked to the SpyCatcher of an LSU of variable size (orange), hence generating a stable coupling product. Figure not to scale.

Table 7: A selection of solubility enhancer tags.
For an extended list consider [234]. aa: amino acids.

Tag	Protein	Size (aa)	Organism	References
MBP	Maltose-binding protein	396	*E. coli*	[237, 240, 241]
NusA	N-utilization substance	495	*E. coli*	[242]
Trx	Thioredoxin	109	*E. coli*	[243]
ArsC	Stress-responsive arsenate reductase	141	*E. coli*	[244]
GST	Glutathione-*S*-transferase	211	*Schistosoma japonicum*	[245]
SUMO	Small ubiquitin modified	∼100	*Homo sapiens*	[246, 247]
Fh8	*F. hepatica* 8-kDa antigen	69	*Fasciola hepatica*	[248, 249]
SET	Solubility-enhancer peptide sequences	<20	Synthetic	[250]

4.3.2 Finding a Suitable LSU.

Along with the SpyTag-SpyCatcher system, LSUs consisting of soluble fusion proteins with SpyCatcher are most convenient. Importantly, protein fusions to be used as LSUs need to be hydrophilic and of reasonable size (tens of kDa).

Often, fusion tags are used to improve protein production yields, folding and solubility in *E. coli* expression systems.[234] Typical examples for such solubility enhancers can be found in table 7; for a review see [234]. One of the most common solubility enhancer tags is maltose-binding protein (MBP). MBP is a large (43 kDa, highly soluble periplasmic protein encoded by the *malE* gene of *E. coli*, and it has a native affinity property to function as a purification tag.[234–237] MBP plays an important role in the translocation of maltose and maltodextrins as it has a natural protein binding site used to interact with other proteins involved in maltose signaling and chemotaxis.[234, 238] It has a large hydrophobic cleft close to the protein binding site undergoing conformational changes upon maltose binding.[234, 237] It is well documented that MBP fusions increase expression levels, assist folding and increase solubility of heterologous recombinant proteins.[235] Further, MBP can be used for affinity chromatography with amylose resins, completely orthogonal to Ni-NTA affinity chromatography. Binding to amylose resins however is highly dependent on the nature of the passenger protein, possibly blocking or reducing MBP's interaction with amylose.[239] Another possibility for an LSU might be the usage of a GFP fusion, where GFP can additionally be used as a reporter.

Conveniently, plasmids of fusions of MBP or GFP with SpyCatcher for expression in *E. coli* were deposited by researchers in the Addgene database (see also table 6 on page 56). Especially, MBP-SpyCatcher has been extensively used by the Howarth group to create synthetic protein constructs.[196, 230, 251] Thus, SpyCatcher-ELP-

GFP (SEG; 49.9 kDa; Addgene 69835; [194]), SpyCatcher-MBP (SC-MBP; 55.8 kDa; Addgene 79053; [195]) as well as a fusion to a tandem high affinity version of MBP (MBPx), SpyCatcher-MBPx (SC-MBPx; 95.9 kDa; Addgene 72327; [196]) were ordered, expressed and purified as described by the respective providers of the plasmids (SDS-PAGE analyses: see supplementary figure S31A).

To avoid reconstitution of a mixture of MP-LSU and free MP, it is essential that after coupling of the LSU to the MP no free MP is present anymore. Therefore, our strategy requires purification of the coupling product to remove unbound MP, either after coupling, or by immobilization of the LSU prior to coupling. Because of its affinity towards amylose resins, MBP provides a possibility for immobilization, hence for co-purification of uncoupled MBP-containing LSUs with MP-LSU. Co-purification of uncoupled LSU is not expected to disturb planned downstream functional experiments. Other than reported by Veggiani *et al.* [196] however, first tests revealed, that in our hands, SC-MBP and SC-MBPx were only poorly bound to amylose resin (see also section 4.3.11). This might be a serious disadvantage when a coupling product as e. g. pR-SpyTag-SC-MBP is to be purified from its reaction mixture. Therefore, SC-MBP and SC-MBPx were modified using standard molecular biology techniques by introducing a 3xFLAG-tag (a FLAG-tag [252, 253] used in three-tandem [254]) at the particular N-terminus, leading to the two new constructs SC-MBP-3xFLAG (58.7 kDa) and SC-MBPx-3xFLAG (99.1 kDa) (figure 44). These two constructs were expressed and purified the same way as their precursors described above (SDS-PAGE analyses: see supplementary figures S31B and S31C).

4.3.3 Cloning, Expression and Purification of pR with SpyTag.

As a first model, the single-subunit MP pR (see section 1.2.1) was used as a proof of principle, before advancing to bo_3 oxidase, consisting of multiple subunits thus being of higher complexity.

A SpyTag was genetically introduced into pR containing a C-terminal His-tag either at the N- or the C-terminus, resulting in pR-NSpy or pR-CSpy, respectively (30.2 kDa; see figure 45 on page 105). The two plasmids were transformed in *E. coli* C43(DE3) and grown at 37 °C. When cell density reached $OD_{600} = 0.6$, protein expression was induced by addition of IPTG and all-trans-retinal, the ligand for pR's retinal biding site, was added. After cell growth, membranes were prepared by ultracentrifugation and solubilized with DDM as a detergent. Finally, pR was purified

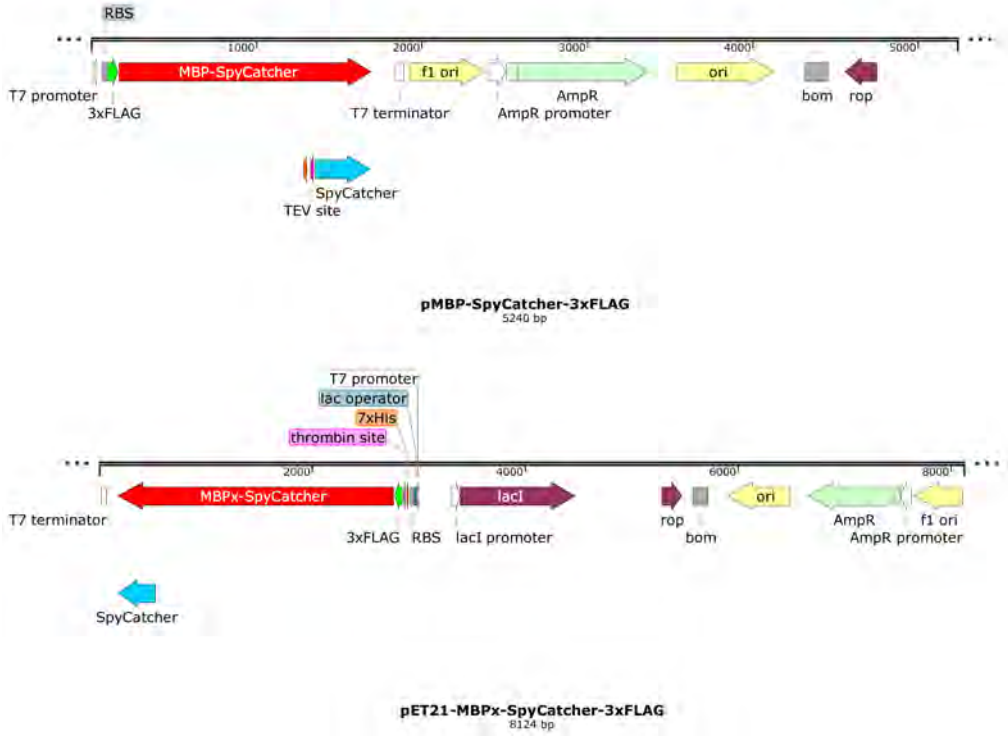

Figure 44: Plasmid maps of SC-MBP-3xFLAG and SC-MBPx-3xFLAG. A 3xFLAG-tag (green) was genetically introduced at the N-terminus of SC-MBP (red, top) or SC-MBPx (red, bottom). Blue: SpyCatcher; orange: His-tag; purple: protease cleavage sites.

from the solubilization supernatant by Ni-NTA affinity chromatography utilizing the His-tag.

4.3.4 Coupling of pR-SpyTag to SC-MBP-3xFLAG.

For coupling to pR-NSpy or pR-CSpy, SC-MBP-3xFLAG was first immobilized on anti-FLAG M2 affinity gel, and excess unbound protein was washed away. Then, a 2- to 5-fold excess of pR-Spy was added as coupling partner. After incubation for 2 h or overnight, at 25 °C or 10 °C, respectively, remaining unbound pR-Spy was washed away and the coupling product pR-N/CSpy-SC-MBP-3xFLAG was eluted from the resin by using a 3xFLAG-peptide (2.5 mg ml^{-1}). The eluate was subsequently concentrated using centrifugal filters (MWCO: 100 kDa) and subjected to SDS-PAGE analysis (figure 46). In lanes 1, 2, and 4, the coupling partners SC-MBP-3xFLAG, pR-CSpy, and pR-NSpy, respectively, were loaded. In lanes 3 and 5, the eluates from the coupling reaction, pR-CSpy-SC-MBP-3xFLAG and pR-NSpy-SC-MBP-3xFLAG, are

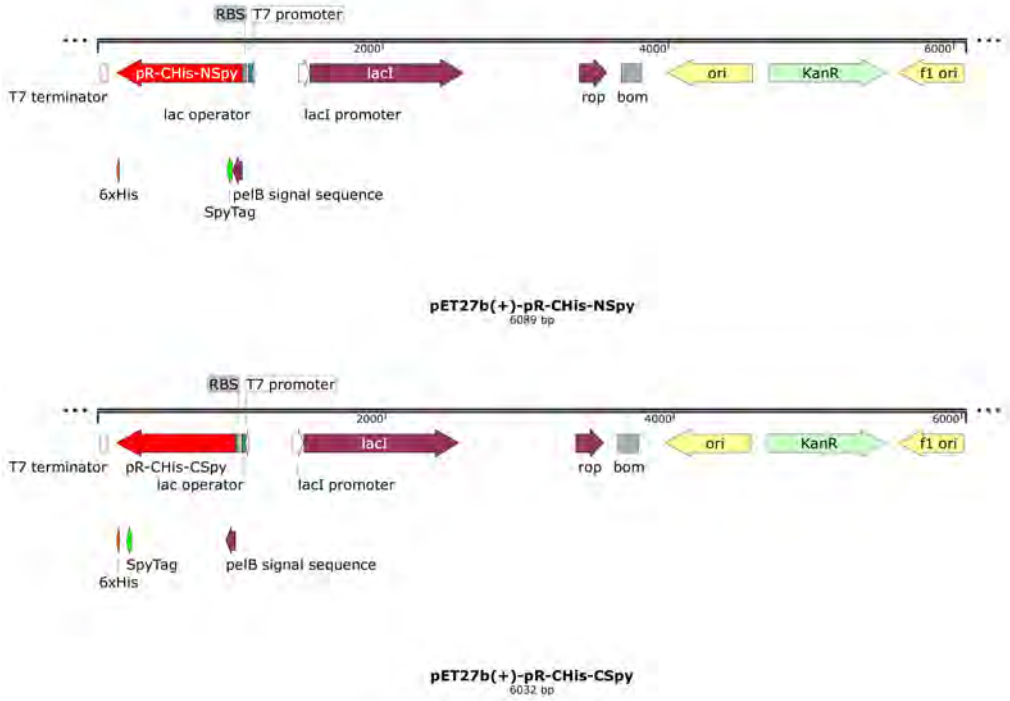

Figure 45: Plasmid maps of pR-SpyTag. The SpyTag (dark green) was genetically introduced to the N-terminus (top) or C-terminus (bottom) of pR, resulting in pR-NSpy or pR-CSpy, respectively (red). In both constructs, a His-tag was introduced at the C-terminus.

shown, respectively. The main band in both lanes is the respective coupling product with a molecular weight of 88.9 kDa. In both lanes, unbound SC-MBP-3xFLAG (58.7 kDa) is detected. This met our expectations as SC-MBP-3xFLAG was added in a 1- to 5-fold excess and it is co-purified with the coupling product. Uncoupled SC-MBP-3xFLAG is not expected to disturb downstream functional measurements and was therefore not removed. The band running around 26 kDa in lanes 3 and 5 is free pR-N/CSpy (30.2 kDa), the occurence of which can be avoided by more extensive washing before elution of the coupling product. The yields of the coupling reaction were estimated from SDS-PAGE analysis to be in the range of 80 - 85 % as previously reported for other SpyTag-SpyCatcher coupling products by Zakeri *et al.* [230]. It can thereby be concluded that this procedure to couple the LSU SC-MBP-3xFLAG to pR-N/CSpy works as intended.

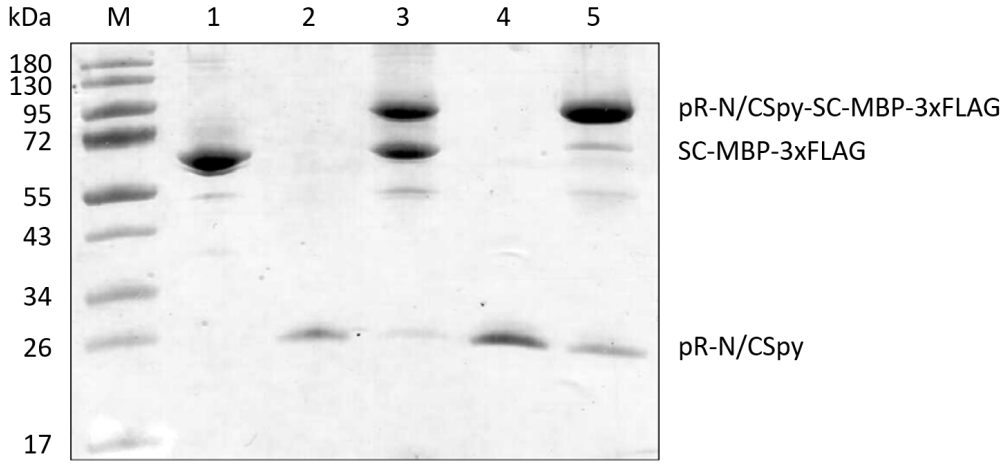

Figure 46: SDS-PAGE analysis of pR-N/CSpy-SC-MBP-3xFLAG. 1: SC-MBP-3xFLAG; 2: pR-CSpy; 3: pR-CSpy-SC-MBP-3xFLAG; 4: pR-NSpy; 5:pR-NSpy-SC-MBP-3xFLAG; M: marker. Coomassie staining.

4.3.5 How to Measure Proton Pumping of pR Using Pyranine.

We aimed to determine the orientation of reconstituted pR in the proteoliposomal membrane based on the direction of pR-mediated proton pumping. Therefore, proton pumping by pR was to be monitored by the pyranine assay introduced in section 4.2.6. In advance however, optimal conditions for pyranine-based proton pumping measurements with pR had to be found.

For this purpose, a standard curve showing the pH dependency of the pyranine fluorescence ratio F406/F460 was recorded (figure 47A). pR was reconstituted into preformed, detergent-destabilized liposomes ($10\,\mathrm{mg\,ml^{-1}}$, 90 % lecithin, soybean) in the presence of pyranine using cholate (0.4 %) as detergent. After reconstitution, cholate and external pyranine were removed by SEC (CentriPure P10 desalting columns). These proteoliposomes were then equilibrated overnight in buffer with different pHs, and the pyranine fluorescence ratio F406/F460 was measured. As expected (compare to [224]), it could be shown that F406/F460 decreased by increasing the pH. The same proteoliposomes were subsequently illuminated to drive pR-mediated proton pumping across the membrane until an equilibrium was reached. Proton efflux from proteoliposomes reconstituted with pR was observed at pHs ≤ 7.2, while protons were imported into vesicles at pHs ≥ 7.2 (figure 47B), indicating a turning point between pH 7.2 and pH 7.6. The direction of proton pumping by pR is hence strongly dependent on the pH as expected (see section 1.2.1; compare to [19]). The results in

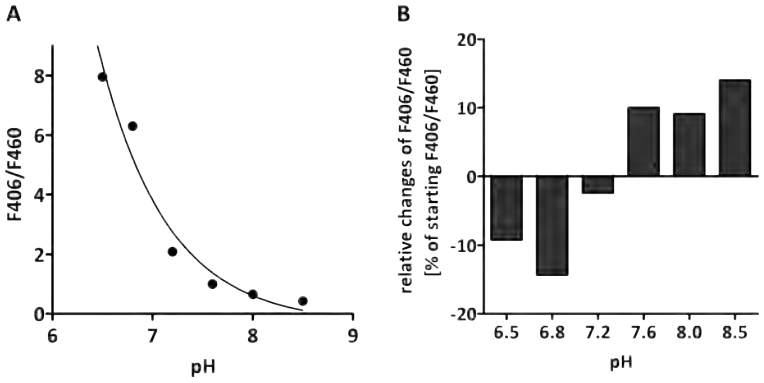

Figure 47: pH dependency of pyranine and pR. Proteoliposomes containing pR-NSpy (w/o LSU) were equilibrated overnight at different pHs before measuring proton pumping by pyranine. (A) pH dependency of the pyranine fluorescence ratio F406/F460 at the start of each measurement of (B). Fitting curve: one phase decay, R^2: 0.9627, GraphPad Prism. (B) Relative changes in F406/F460, resulting from proton pumping of reconstituted pR-NSpy at different pH values upon illumination. Changes assessed between F406/F460 at start of measurements and F406/F460 after an equilibrium was reached upon illumination. Liposomes: 10 mg ml^{-1} 90 % lecithin, soybean; 200 nm; in 0.5 mM MOPS pH 6.5 - 8.5, 25 mM K_2SO_4. Measuring buffer: same as liposome buffer.

figure 47B suggest that pyranine-mediated monitoring of proton pumping of pR is optimally performed at a pH around 6.5. On one hand, at either pH 6.5 or pH 8.5 protons are exclusively pumped in one direction by pR. On the other hand, at pH 6.5 the ratio F406/F460 is higher than at any higher pH, making it easier to detect smaller changes in F406/F460 than at any higher pH. Therefore, all following measurements of pR orientation were conducted at pH 6.5 exclusively.

4.3.6 A First Attempt to Unidirectionally Reconstitute pR-N/CSpy-SC-MBP-3xFLAG.

In a first attempt to influence orientation of pR-N/CSpy, the two pR variants pR-N/CSpy were coupled to the LSU SC-MBP-3xFLAG as described in section 4.3.4. Each of the two pR variants with or without LSU-modification were then reconstituted into preformed, detergent-destabilized liposomes in the presence of pyranine, using the standard reconstitution method of our lab. Cholate (0.4 %) was used as detergent for liposome destabilization and the detergent as well as external pyranine were removed after reconstitution by SEC using CentriPure P10 desalting columns (Zetadex-25, exclusion size 5 kDa). Proton pumping of the four conditions

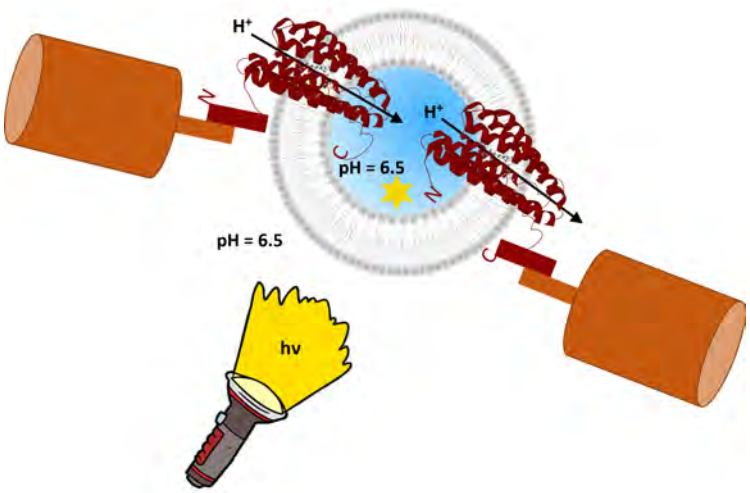

Figure 48: Principle of the pyranine proton pumping assay with pR-N/CSpy-SC-LSU. During reconstitution of pR (with or without LSU), the pH sensor pyranine (yellow star) is entrapped into the proteoliposomes. The starting pH for the measurements was equally 6.5 inside and outside of the proteoliposomes. Proton pumping by pR was facilitated by illumination and resulting pH changes in the lumen were detected by pyranine.

pR-N/CSpy and pR-N/CSpy-SC-MBP-3xFLAG was assessed by pyranine at pH 6.5 as illustrated in figure 48. Each of the four conditions however showed proton efflux from the proteoliposomes upon illumination, no differences in the direction of proton pumping was observed (traces comparable to figure 49C; not shown).

Since we had faith in the SpyTag-SpyCatcher-based strategy to influence orientation of pR, these results suggested to optimize the reconstitution method.

4.3.7 A Novel Method to Reconstitute pR into Liposomes.

Different methods for reconstitution of pR into liposomes are reported in literature. Pfleger *et al.* [13] for example reported efficient reconstitution of pR using DDM to solubilize their liposomes for reconstitution. This protocol cannot be used for two reasons. First, the liposomes were fully solubilized for reconstitution, being incompatible with the general idea of my project to exploit destabilization of preformed liposomes. Second, Knol [5] described unfavourable effects of DDM on solubilization of lipid bilayers, leading to pores in the liposomal bilayer and thus more or less random orientation of his MP of interest (LacS; see section 1.7) in proteoliposomes.

According to Knol [5], reconstitution of bacteriorhodopsin from *Halobacterium salinarium*, sharing a 30 % sequence identity with pR, was reported to efficiently reconstitute using octylglucoside (OG) to partially solubilize preformed liposomes followed by detergent removal with SM-2 Bio-Beads. Therefore, a similar protocol was tested for reconstitution of pR. However, since using SEC to remove the detergent has the advantage over the use of SM-2 Bio-Beads that the procedure is much less time-consuming, it was desirable to hold on to the use of SEC. Hence, instead of SM-2 Bio-Beads, OG was removed after reconstitution by SEC using CentriPure PF10 desalting columns (Zetadex-50). These columns have an exclusion size of $\geq$25 kDa, which should be sufficiently large to efficiently remove OG micelles (mass of micelle: 8 kDa; see table 4 on page 16) during the chromatography. Reconstitution of pR-N/CSpy and pR-N/CSpy-SC-MBP-3xFLAG however led to the exact same results as described for our cholate-based standard reconstitution method. Pyranine-mediated monitoring of proton pumping of the four conditions at pH 6.5 each showed proton efflux from the proteoliposomes upon illumination (traces comparable to figure 49C; not shown).

A third, very time consuming and elaborate protocol was proposed recently by Goers *et al.* [255]. Liposomes were produced by rehydration of a lipid film in aequous buffer containing OG, thus obviously being solubilized at their formation. After addition of the pR-GFP fusion protein, the mixture was incubated for 30 - 60 min, and the detergent was removed in a rather unusual combination of three techniques. First, the samples were dialyzed using a 15 kDa MWCO dialysis tubing for 48 h against buffer containing SM-2 Bio-Beads to ensure a constant dialysis gradient, representing a second technique. Third, after dialysis was complete and the samples were extruded through a 200 nm membrane, the proteoliposomes were passed through a SEC (G-25 MiniTrap). In total, the procedure spreads over three days (72 h), which is unusually long and might affect integrity and function of the proteoliposomes.

As mentioned in section 4.3.3, we isolated and purified pR-N/CSpy using DDM (0.05 % final concentration). Due to unfavourable effects of DDM on solubilization of lipid bilayers [5] however, the use of DDM for reconstitution should be avoided. Possibly, our first attempt to unidirectionally reconstitute pR-N/CSpy-SC-MBP-3xFLAG by OG-mediated reconstitution failed, because DDM was disturbing reconstitution. This left us basically two possibilities. Either we had to express and purify the two pR variants again using 1 % OG instead of DDM. Alternatively, we could try to circumvent this effort by using the available pR variants, but replacing DDM with

OG prior to reconstitution. By deciding for the latter option, we developed a novel method to reconstitute pR-N/CSpy which was purified in DDM.

As discussed in section 1.6.2, DDM present in the MP solution can efficiently be removed by the use of β-cd and exchanged with OG. To replace DDM with OG, first, 1 % OG was added to the pR variant to be reconstituted (pR-N/CSpy with or without LSU). Residual DDM was then removed from the mixture and bound selectively by using a 3-fold excess of heptakis(2,6-di-*O*-methyl)-β-cyclodextrin (β-cd) over DDM during an incubation of 30 min. After incubation with β-cd, pR was reconstituted into preformed liposomes (10 mg ml^{-1} 90 % lecithin, soybean; 200 nm) using 0.75 % OG (total concentration) for partial solubilization. If needed for downstream functional assays, pyranine was introduced during this step. The mixture was incubated for 45 min at 25 °C with gentle mixing before the suspension was passed over a CentriPure PF10 desalting column to remove OG, complexes of β-cd and DDM (β-cd-DDM), and free β-cd (and external pyranine). Finally, since the integrity of the proteoliposomes might be affected by the presence of possibly residual cyclodextrins [256], the proteoliposomes were washed by dilution and collected by ultracentrifugation, thereby eliminating possibly remaining free β-cd and β-cd-DDM. The entire procedure lasts approximately 2.5 h, thus being rapid compared to other methods as e. g. using polystyrene beads for detergent removal.

4.3.8 Unidirectional Reconstitution of pR-N/CSpy-SC-MBP-3xFLAG!

Using the new reconstitution method described in section 4.3.7, it was observed that both, pR-CSpy (figure 49C) and pR-NSpy (figure 49D) reconstituted without LSU at pH 6.5, they led to a decrease of the pyranine fluorescence ratio upon illumination, indicating that protons were net transported out of the proteoliposomes. The SpyTag on either terminus of pR does not influence orientation. Reconstituted pR-CSpy bound to the LSU SC-MBP-3xFLAG (figure 49A) pumps protons outwardly as well. pR-NSpy-SC-MBP-3xFLAG (figure 49B) on the contrary clearly shows an increase of the fluorescence ratio and thus net proton import into the proteoliposomes.

These experiments were performed repeatedly, exhibiting a 100 % reproducibility of the results. These results demonstrate that our strategy of attaching LSUs via SpyCatcher to Spy-tagged MPs can indeed be used to guide unidirectional reconstitution of pR in in either of the two orientation directions in a predefined manner.

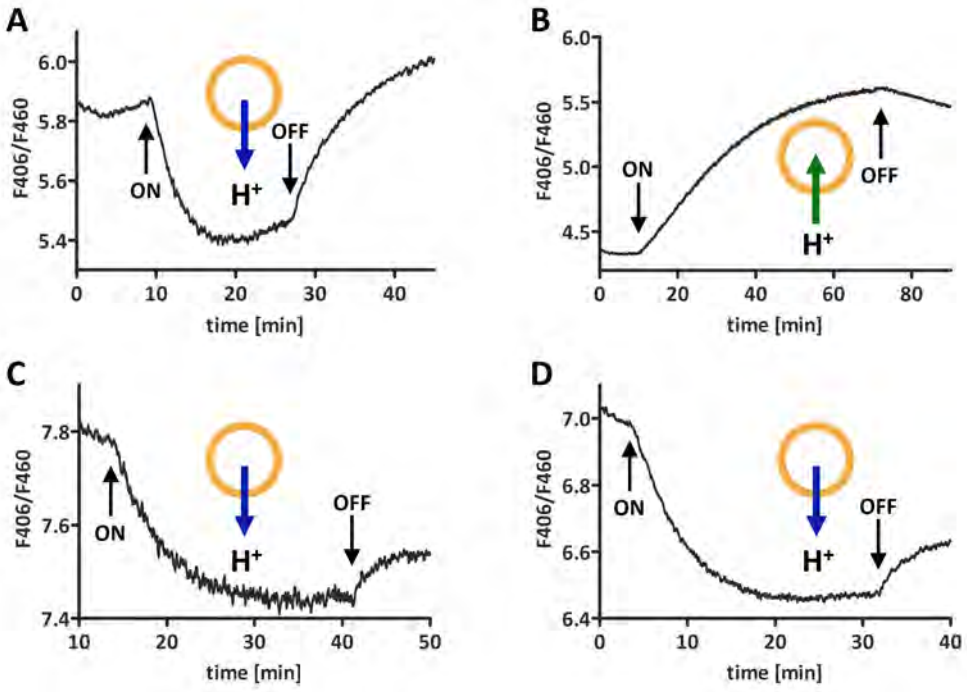

Figure 49: Representative results of pyranine-monitored proton pumping of modified pR. (A) pR-CSpy-SC-MBP-3xFLAG. (B) pR-NSpy-SC-MBP-3xFLAG. (C) Control: pR-CSpy w/o LSU. (D) Control: pR-NSpy w/o LSU. Illumination was turned on or off at the indicated time points. The net proton pumping direction derived from each graph is illustrated in each panel (blue: H^+ efflux; green: H^+ influx). Liposomes: 10 mg ml^{-1} 90 % lecithin, soybean; 200 nm; in 0.5 mM MOPS pH 6.5, 25 mM K_2SO_4. Measuring buffer: same as liposome buffer.

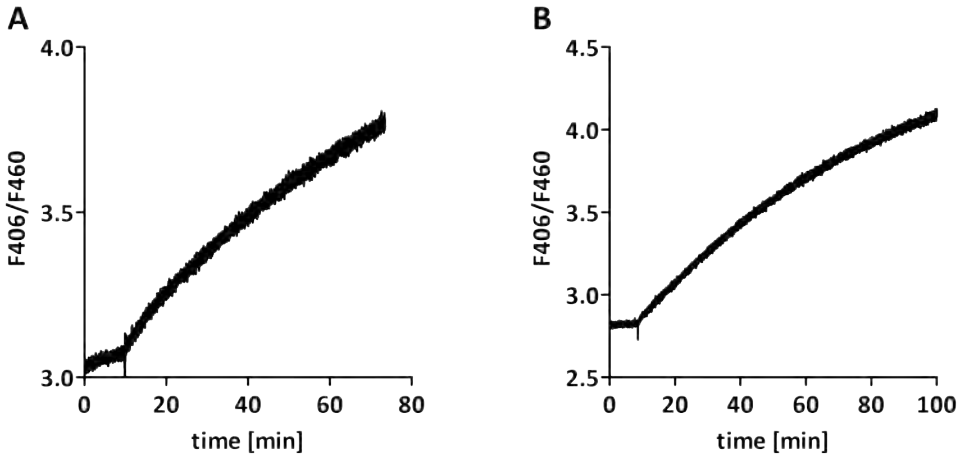

Figure 50: Effect of freeze/thaw cycles on pR orientation. Pyranine was entrapped into the proteoliposomes after reconstitution was completed by three freeze/thaw steps. (A) pR-CSpy-SC-MBP-3xFLAG. (B) pR-NSpy-SC-MBP-3xFLAG. Illumination was turned on at 10 min. Liposomes: 10 mg ml^{-1} 90 % lecithin, soybean; 200 nm; in 0.5 mM MOPS pH 6.5, 25 mM K_2SO_4. Measuring buffer: same as liposome buffer.

As mentioned in section 4.3.7, pyranine was entrapped into the preformed, partially solubilized liposomes during reconstitution of pR. Another commonly used possibility to encapsulate pyranine is to add it to afore reconstituted liposomes and perform three freeze/thaw cycles. Interestingly, this procedure resulted in proton influx into the proteoliposomes for both, pR-CSpy-SC-MBP-3xFLAG and pR-NSpy-SC-MBP-3xFLAG (figure 50), indicating that freeze/thaw cycles manipulate orientation of reconstituted pR. A possible explanation for these results may be given from Pick [257], suggesting that during the rapid freezing process, the organization of the membrane is broken up by water molecules crystallizing on the membrane interface. During thawing, a reassembly is taking place [124], apparently providing the MPs a chance to change orientation in the membrane. Thus, the freeze/thaw method is prone to strong randomization of the MP's orientation.[10] Even though encapsulation of pyranine via freeze/thaw cycles seems to be a convenient and efficient method, it is not suitable for our experiments, in which processes affecting orientation by randomization should be avoided.

4.3.9 Confirming Unidirectional Reconstitution of pR-N/CSpy-SC-MBP-3xFLAG.

We wanted confirm the effect of orientation observed with the functional assay with a second method independent from pR's functionality.

Similar to the approaches of [183, 258, 259], we deployed limited proteolysis to determine the orientation of reconstituted pR in proteoliposomes. The liposomal membrane shields the hydrophobic core of incorporated MPs, leaving only hydrophilic residues forming loop regions exposed to the solution.[183] In our setup, also the LSUs are expected to remain exposed to the solution. Addition of proteases to the outside of the proteoliposomes leads to proteolytic digestion of loop regions and LSUs exposed to the extravesicular solution. It is generally accepted that loop regions, and hence also LSUs, exposed to the lumen of the liposomes however will not be digested because of the protease's membrane-impermeability (even though there is no confirmation that inwardly orientated LSUs are unaffected by the protease treatment). This allows quantification the ratio of inwardly orientated LSU to total LSU by probing the LSU in western blot analysis of protease-treated and -untreated proteoliposomes, respectively.

For this purpose, liposomes reconstituted with pR-C/NSpy-SC-MBP-3xFLAG (88.9 kDa; compare to figure 46) were treated with the metalloprotease thermolysin from *Bacillus thermoproteolyticus* (cleavage N-terminally from Leu, Phe, Val, Ile, Ala, Met) to digest outwardly orientated SC-MBP-3xFLAG, and subsequently subjected to SDS-PAGE analysis followed by western blotting and probing for the LSU with an anti-MBP antibody.

According to the results previously obtained by function-based orientation determination (section 4.3.8), it was expected that virtually all of the MBP-containing LSU SC-MBP-3xFLAG should be located on the outside of the proteoliposomal membrane, and almost none in the lumen.

As expected, proteolytic digest by thermolysin on the outside of the proteoliposomes led to depletion of MBP in comparison to not protease-treated proteoliposomes as shown in figure 51. Only 6 % and 25 % of the MBP-containing LSUs of reconstituted pR-CSpy-SC-MBP-3xFLAG and pR-NSpy-SC-MBP-3xFLAG were detected after thermolysin treatment, respectively. These results, in addition to the results of the functional assay, suggest unidirectional reconstitution of pR in proteoliposomes guided by our SpyTag-SpyCatcher system.

Figure 51: Limited proteolysis of pR-LSU. Proteoliposomes reconstituted with pR-C/NSpy-SC-MBP-3xFLAG or pR-C/NSpy w/o LSU before and after proteolytic cleavage at the outside with thermolysin. (A) After SDS-PAGE analysis and western blotting, the blots were probed with an anti-MBP antibody (Anti-Maltose Binding Protein antibody [R29.6], Abcam; secondary antibody: IRDye 680RD Donkey anti-Mouse IgG Secondary Antibody, Licor). 1/5: pR-CSpy-SC-MBP-3xFLAG; 2/6: pR-NSpy-SC-MBP-3xFLAG; 3/7: pR-CSpy w/o LSU; 4/8: pR-NSpy w/o LSU. Samples 1-4 were treated with thermolysin, samples 5-8 were not treated with any protease. M: marker. Liposomes: 10 mg ml^{-1} 90 % lecithin, soybean; 200 nm; in 0.5 mM MOPS pH 6.5, 25 mM K_2SO_4. (B) Relative abundances of MBP detected in (A). Integrated densities of bands from (A) were measured with ImageJ. Thermolysin-treated samples were normalized to respective non-protease treated samples.

Other LSUs of different sizes mentioned in section 4.3.2 (SC-MBPx-3xFLAG or SC-ELP-GFP) have not been tested yet for orientating pR with the SpyTag-SpyCatcher system due to the approaching end of the PhD thesis; however, they will be tested by a co-worker. Such experiments are expected to give valuable insights on the dependence of orientation on the size of the LSU.

Further investigations on this topic however would profit from a physical assay to measure orientation of pR, independently of pR's function, and less time-consuming than western blotting. Such an assay is currently being developed in our lab by Lukas Rimle. Although his assay was still in development, we used it to confirm our observations on unidirectional reconstitution of pR-N/CSpy-SC-MBPx-3xFLAG as shown in section 4.4.

4.3.10 Cloning, Expression and Purification of *bo*$_3$ Oxidase with SpyTag.

A method to guide unidirectional reconstitution of pR into liposomes was successfully introduced. This was veryfied in a functional assay as well as by limited proteolysis. The developed method should be applicable to larger, more complex MPs, however

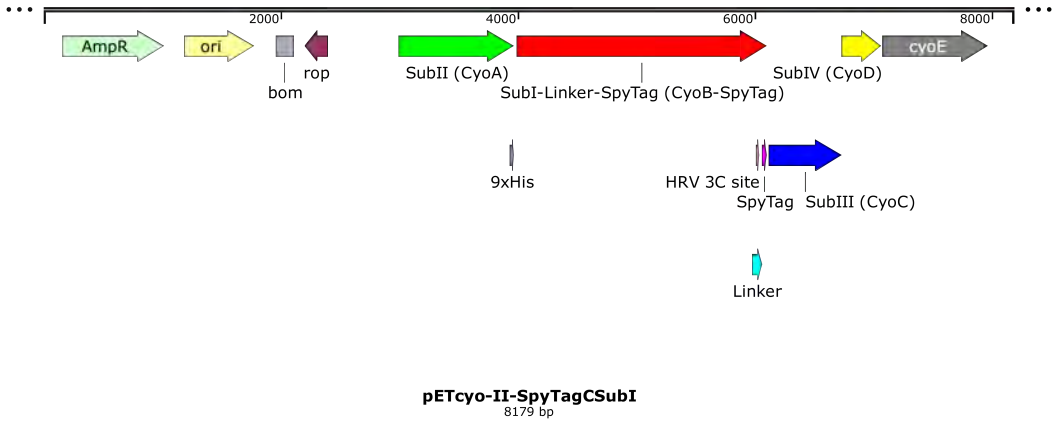

Figure 52: Plasmid map of *bo*$_3$-SpyTag. The SpyTag (purple) was genetically introduced to the C-terminus of subunit I (red) after a short linker (turquoise). Compared to the *bo*$_3$-AviTag construct (see figure 28 on page 80), subunits I and III were genetically separated by a linker such that their sequences do not overlap anymore. A His_9-tag (violet) was introduced at the C-terminus of subunit II (green). Subunits III, IV and CyoE remain as in *bo*$_3$ oxidase wild type.

minor adjustments (e. g. in size of the LSU or in reconstitution method) may be required. These positive results inspired us to adapt this system to *bo*$_3$ oxidase as well.

In contrast to pR, *bo*$_3$ oxidase is a multi-subunit MP, which is organized in one operon. Consequently, genetic introduction of a SpyTag is less straightforward. We analyzed the structure and decided to introduce the SpyTag genetically to the C-terminus of subunit I (CyoB). In *bo*$_3$-Avi, the AviTag was also introduced to the C-terminus of subunit I. Because the sequences of subunit I and III are overlapping (including a frame shift), the insertion results in a prolongation of subunit III at its N-terminus (see figure 28 on page 80). In the present case of Spy-tagged *bo*$_3$ oxidase, subunits I and III were genetically separated (figure 52). 3' to the coding sequence of subunit I, a 19 bp spacer sequence precedes the 5' start of the coding sequence of subunit III. This spacer sequence on one hand retains the frame shift between the coding sequences of subunits I and III, and on the other hand disjoines the overlap of these two subunits. The construct was cloned using standard molecular biology techniques, expressed in *E. coli* C43(DE3) Δcyo and purified by Ni-NTA affinity chromatography by our former lab technician Sandra Schär. In the following, the *bo*$_3$ oxidase with the SpyTag at subunit I will be referred to as *bo*$_3$-Spy.

4.3.11 Coupling of *bo₃*-Spy to SC-LSU.

Some of the following experiments were partly performed in parallel to the experiments with pR-Spy. Working with both MPs at the same time however may lead to some chronological inconsistencies by describing these approaches separately.

To test coupling of *bo₃*-Spy to LSUs containing SpyCatcher, *bo₃*-Spy was coupled in buffer (100 mM MES, 100 mM MOPS, pH 6.5, 0.1 % DDM) to a 3-fold excess of SC-MBP or SC-MBPx (see section 4.3.2) and subsequently subjected to SDS-PAGE analysis (figure 53).

Purified *bo₃*-Spy, SC-MBP, and SC-MBPx are shown in lanes 1 to 3, while the reaction after 2 h with *bo₃*-Spy and SC-MBP and SC-MBPx are shown in lanes 4 and 5, respectively. In both reactions, a new band for the coupled product appeared, indicating that the reaction was successful. The new bands correspond to *bo₃*-subI-Spy (SubI: 74 kDa, apparent mass in SDS-PAGE: 55 kDa; [27]) coupled to SC-MBP (55.8 kDa) and SC-MBPx (95.9 kDa), resulting in total masses of 129.8 kDa and 169.9 kDa, respectively.

Interestingly considering the 3-fold excess of SC-MBP or SC-MBPx, unbound *bo₃*-subI-Spy was still present in both reactions. This indicates two possible explanations. First, DDM present in the reaction mixture possibly interferes with with the coupling reaction. Second, even though accessibility of the SpyTag is supposedly provided because of its localization at the exposed C-terminus of *bo₃* oxidase subunit I, coupling to the LSUs might be impaired due to sterical hindrance. These explanations however both remain speculation.

Incomplete coupling of *bo₃*-Spy to the LSUs induces the necessity to remove unlabeled *bo₃*-Spy from *bo₃*-Spy-SC-LSU to ensure that no unlabeled *bo₃*-Spy will be reconstituted in downstream functional measurements of *bo₃* oxidase activity.

In order to get rid of unlabeled *bo₃*-Spy and to improve purity of *bo₃*-Spy-SC-LSU, *bo₃*-Spy was mixed with a 3-fold excess of SC-MBPx and analyzed by SEC (Superderdex 200 Increase 10/300 GL) in comparison to SEC analysis of purified *bo₃*-Spy and SC-MBPx (figure 54A). Since the performed SEC would not allow to separate *bo₃*-Spy-SC-MBPx from unlabeled *bo₃*-Spy, the reaction mixture was subjected to MBP affinity purification using an amylose resin (figure 54B). The eluate was analyzed by SDS-PAGE and compared to *bo₃*-Spy and SC-MBPx (figure 55). Lanes 1 and 2 show purified *bo₃*-Spy and SC-MBPx, respectively. As shown in lane 3, the coupling product between SC-MBPx and subunit I of *bo₃*-Spy was indeed formed and is detected at slightly higher apparent mass than the expected mass of 169.9 kDa.

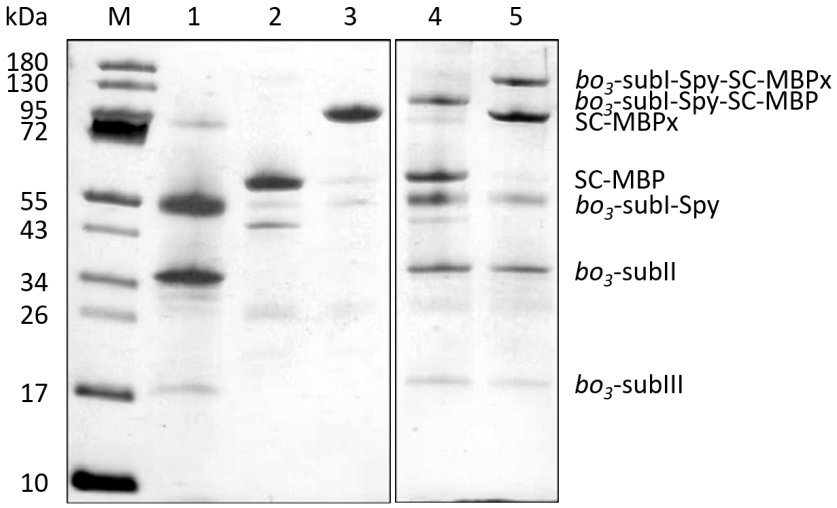

Figure 53: SDS-PAGE analysis of *bo₃*-Spy coupled to SC-MBP or SC-MBPx. 1: *bo₃*-Spy; 2: SC-MBP; 3: SC-MBPx; 4: *bo₃*-Spy-SC-MBP; 5: *bo₃*-Spy-SC-MBPx; M: marker. Silver staining.

Further, no free subunit I of *bo₃*-Spy was detected, but neither were subunits II, III and IV, thus either indicating low yields or loss of subunits II - IV.

Consequently, another protocol for coupling and purification was tested, adapted from Veggiani *et al.* [196], where SC-MBPx was immobilized on amylose resin for coupling to *bo₃*-Spy. This experiment was performed chronologically prior to the same experiment using pR described in section 4.3.2, signifying that 3xFLAG-tagged LSUs were not yet at hand.

First, SC-MBPx was immobilized on amylose resin by incubation at 25 °C for 1.5 h. After unbound SC-MBPx was washed away, and a 5-fold excess of *bo₃*-Spy was added. After incubation at 25 °C for 1 h followed by extensive washing to remove excess free *bo₃*-Spy, immobilized protein was eluted from the amylose resin by 50 mM D-maltose and subjected to SDS-PAGE analysis (figure 56).

Lanes 1 and 2 show purified SC-MBPx and *bo₃*-Spy, respectively. As shown in lane 3, the coupling product *bo₃*-subI-Spy-SC-MBPx was formed and is detected at correct mass (169.9 kDa). Interestingly, free SC-MBPx was detected (95.9 kDa), indicating that, despite of a 5-fold excess of *bo₃*-Spy added, coupling to immobilized SC-MBPx was not complete. Further, free *bo₃*-Spy subunit I was detected, indicating the possibility of strong, unspecific interactions of *bo₃*-Spy with the amylose resin. However, since the contamination was minor, it was not followed further; especially

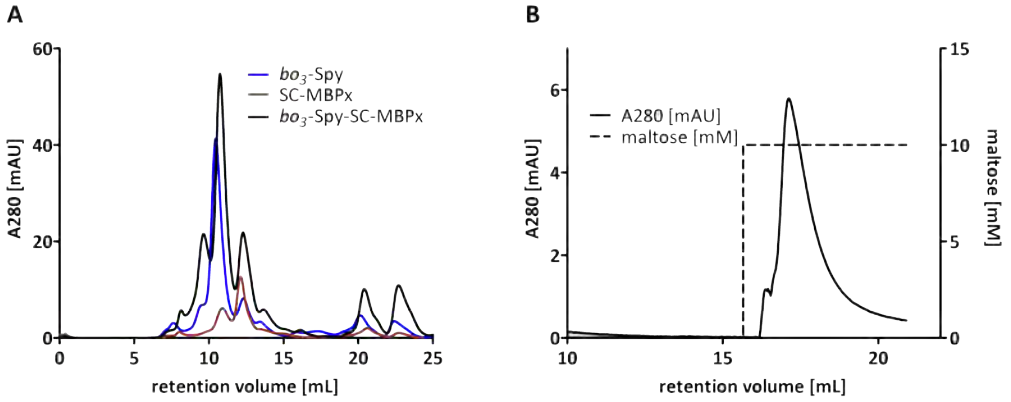

Figure 54: Purification of *bo₃*-Spy-SC-MBPx. (A) Purification of bo_3-Spy-SC-MBPx (black) by SEC using a Superdex 200 Increase 10/300 GL column in 50 mM K_2HPO_4 pH 8.3, 0.05 % DDM. Chromatograms of bo_3-Spy (blue) and SC-MBPx (red) are shown for comparison. (B) MBP affinity chromatography using an MBP-Trap HP column in 50 mM K_2HPO_4 pH 8.3, 1 mM EDTA, 0.05 % DDM for purification of bo_3-Spy-SC-MBPx. After extensive washing, bound MBP-containing proteins were eluted using 10 mM D-maltose. Eluted protein was subjected to SDS-PAGE analysis.

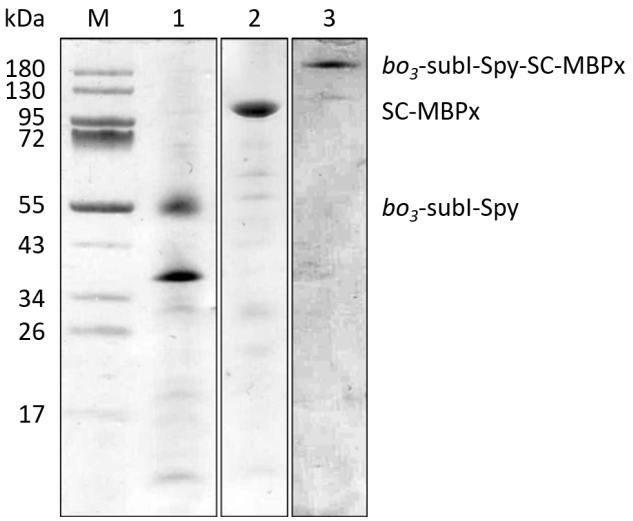

Figure 55: SDS-PAGE analysis of *bo₃*-Spy-SC-MBPx purified by SEC followed by MBP affinity chromatography. 1: bo_3-Spy; 2: SC-MBPx; 3: purified bo_3-Spy-SC-MBPx, contrast increased for reasons of detectability; M: marker. Coomassie staining. Side note: According to Rumbley *et al.* [28] it is normal, that subunit II of bo_3 oxidase as shown in lane 1 appears as a double band, namely as a native, uncleaved and a cleaved form.

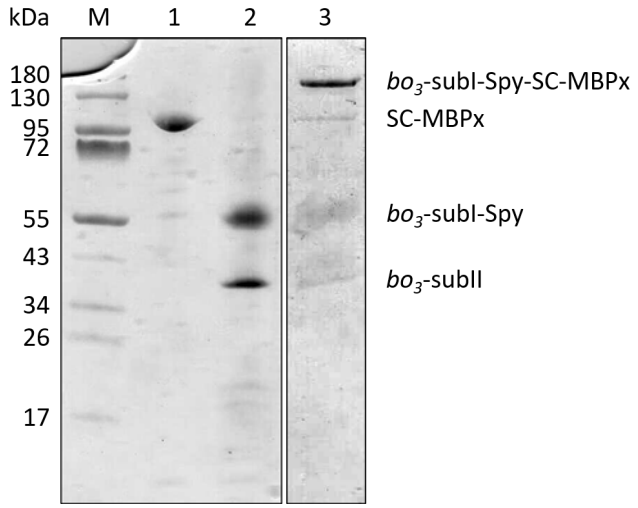

Figure 56: SDS-PAGE analysis of *bo*$_3$-Spy-SC-MBPx coupled on amylose resin. 1: SC-MBPx; 2: *bo*$_3$-Spy; 3: purified *bo*$_3$-Spy-SC-MBPx; M: marker. Coomassie staining.

also because soon after this experiment the FLAG-tagged version of this LSU (SC-MBPx-3xFLAG) became available, making the amylose-assisted coupling obsolete.

As soon as the LSU SC-MBPx-3xFLAG was available, coupling thereof to *bo*$_3$-Spy was tested. For coupling to *bo*$_3$-Spy, SC-MBPx-3xFLAG was first immobilized on anti-FLAG M2 affinity gel, and excess unbound protein was washed away, before a 2- to 5-fold excess of *bo*$_3$-Spy was added as coupling partner. After incubation for 2 h or overnight, at 25 °C or 10 °C, respectively, remaining unbound *bo*$_3$-Spy was washed away and the coupling product *bo*$_3$-Spy-SC-MBPx-3xFLAG was eluted from the resin by using a 3xFLAG-peptide (2.5 mg ml^{-1}). The eluate was subsequently concentrated using centrifugal filters (MWCO: 100 kDa) and subjected to SDS-PAGE analysis (figure 57).

Lanes 1 and 2 show purified *bo*$_3$-Spy and SC-MBPx-3xFLAG, respectively. The eluate is shown in lane 3, where two main bands are detected, the lower one being identified as excess free SC-MBPx-3xFLAG (99.1 kDa), and the higher one representing the coupling product *bo*$_3$-subI-Spy-SC-MBPx-3xFLAG (173.1 kDa). Subunit II (33 kDa) of the *bo*$_3$-Spy is faintly visible as well. Importantly, no free *bo*$_3$-subI-Spy was detected. This is a prerequisite for downstream functional measurements of *bo*$_3$ oxidase activity, where it must be ensured that no unlabeled *bo*$_3$-Spy will be core-constituted with *bo*$_3$-Spy-SC-MBPx-3xFLAG. The yields of the anti-FLAG affinity gel-assisted coupling reaction were estimated from SDS-PAGE analysis to be around 20 %, hence being exceptionally low compared to application of the same procedure to

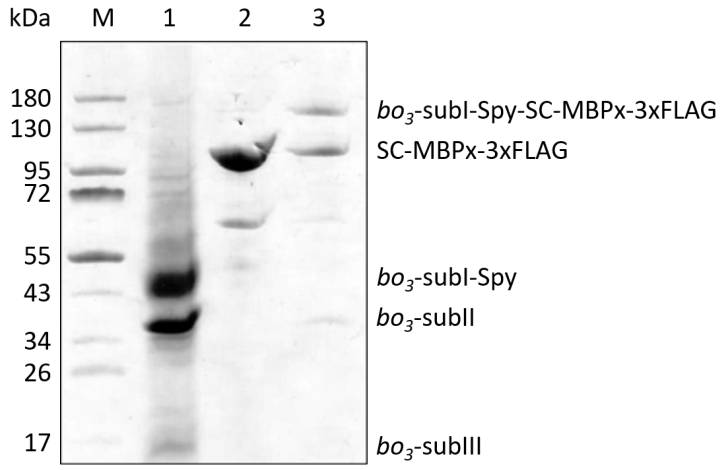

Figure 57: SDS-PAGE analysis of purified *bo₃*-Spy-SC-MBPx-3xFLAG. 1: *bo₃*-Spy; 2: SC-MBPx-3xFLAG; 3: purified *bo₃*-Spy-SC-MBPx-3xFLAG; M: marker. Coomassie staining.

pR-N/CSpy (see section 4.3.4). Despite of the low yields, this procedure for coupling of *bo₃*-Spy to SC-MBPx-3xFLAG was considered successful, hence applied in all further experiments requiring coupling of *bo₃*-Spy to SC-MBPx-3xFLAG.

4.3.12 Functional Experiments with *bo₃*-Spy.

After anti-FLAG affinity gel-assisted coupling of *bo₃*-Spy to SC-MBPx-3xFLAG as LSU, we aimed to see if we can affect the orientation of *bo₃*-Spy during reconstitution. For this purpose we used similar assays as described earlier for the AviTag (ATP synthesis assay, pyranine assay; see section 4.2.6).

Side note: The following sets of experiments concerning reconstitution and orientation of *bo₃*-Spy and *bo₃*-Spy-LSU were performed at the very end of my time in the lab. Therefore, these sets are not concluding. Measurements of coupled activity using the ATP synthesis assay have so far only been deployed to observe first trends, while proton pumping measurements with the pyranine assay have just been used to investigate on optimal reconstitution conditions for *bo₃*-Spy.

Measuring Coupled Activity – ATP Synthesis Assay.

In parallel with the efforts to manufacture *bo₃*-Spy-SC-MBPx-3xFLAG without any free *bo₃*-Spy left, we were eager to observe first trends in coupled enzyme activity using the SpyTag-SpyCatcher system; especially regarding the influence of orientation of *bo₃* oxidase coreconstituted with ATP synthase. Higher amounts of inwardly

pumping *bo*$_3$ oxidase are expected to result in a higher *pmf*, and consequently in higher ATP synthesis rates.

Since purified *bo*$_3$-Spy-SC-MBPx-3xFLAG without residual *bo*$_3$-Spy was not yet at hand at that time, *bo*$_3$-Spy was coupled to a 3-fold excess of SC-MBPx in solution. The reaction mixture was then coreconstituted with purified *E. coli* F_1F_0 (0.4 % cholate, detergent removal by CentriPure P10 desalting column). Coupled enzyme activity was subsequently measured using the ATP synthesis assay as described in section 4.2.6. The measured ATP synthesis rates were normalized to specific activity of *bo*$_3$ oxidase assessed by oxygen consumption measurements. The only difference in the measurement setup was that ubiquinol Q_2 was used to reduce *bo*$_3$ oxidase instead of Q_1. The reason for this change was that there was more Q_2 available because it had been synthesized in our lab. Olivier Biner, a former PhD student in our lab, verified that ubiquinol Q_2 can be used to reduce *bo*$_3$ oxidase at least as efficiently as by using Q_1.

It was observed that *bo*$_3$-Spy-SC-MBPx coreconstituted with the ATP synthase leads to an 1.67 ± 0.05 fold increase in ATP synthesis rate compared to non-orientated *bo*$_3$-Spy is used (for both conditions: $n = 3$) (figure 58A). This is remarkable, since free *bo*$_3$-Spy was not removed from *bo*$_3$-Spy-SC-MBPx prior to coreconstitution.

To test if increasing *pmf* leads to enhanced ATP synthesis rates, we varied the amounts of reconstituted *bo*$_3$-Spy or *bo*$_3$-Spy-SC-MBPx from 3 enzymes *bo*$_3$ oxidase or 23.6 pmol *bo*$_3$ oxidase, to 30 enzymes *bo*$_3$ oxidase per proteoliposome, while the amounts of reconstituted ATP synthase were kept constant (figure 58B). It could be shown that increasing amounts of reconstituted *bo*$_3$ oxidase indeed increase coupled activity, resulting in higher ATP synthesis rates. Further, proteoliposomes in which ATP synthase was coreconstituted with *bo*$_3$-Spy-SC-MBPx showed 1.3- (15 *bo*$_3$ oxidases per proteoliposome) to 2.7-fold (6 *bo*$_3$ oxidases per proteoliposome) higher ATP synthesis rates compared to proteoliposomes containing the respective amount of *bo*$_3$-Spy.

As mentioned in section 1.7.2, about 72 - 77 % of *bo*$_3$ oxidases reconstituted in liposomes were shown to be orientated to facilitate proton efflux from the liposomes.[25, 172] Sabina Deutschmann, a PhD candidate in our lab, however observed that the orientation ratio of the *bo*$_3$ oxidase is shifted if the oxidase is coreconstituted with ATP synthase. Orientation of coreconstituted *bo*$_3$ oxidase shifts to ∼60 % of the oxidases pumping protons into the proteoliposomes (unpublished). Consequently, increasing the number of *bo*$_3$ oxidases per proteoliposome should increase coupled

activity of the ATP synthase, i. e. lead to higher ATP synthesis rates. This theory inspired the following thought experiment.

The *pmf* is the driving force for ATP synthesis by the ATP synthase, hence protons can be considered as a substrate of the synthase. Increasing the number of bo_3 oxidase enzymes importing protons into proteoliposomes leads to a higher *pmf*, consequently the number of bo_3 oxidases reconstituted may be considered a "substitute" substrate for the ATP synthase. This would allow us to analyze ATP synthesis by coupled enzyme activity in dependence on the concentration of the "substitute" substrate, i. e. the number of bo_3 oxidase enzymes per proteoliposome, using Michaelis-Menten kinetics (figure 58C). Comparing analyses of bo_3-Spy and bo_3-Spy-SC-MBPx showed that v_{max} of both conditions was equal. This makes perfectly sense as the number of molecules of ATP synthases per proteoliposome were not varied, i. e. the ATP synthase is the limiting factor of this system if the *pmf* is restored fast enough. The K_m of bo_3-Spy with ∼60 % of the oxidases pumping protons into the proteoliposomes was observed to be ∼19.5 enzymes bo_3 oxidase. Guiding the orientation of bo_3-Spy further towards proton influx by reconstitution of bo_3-Spy-SC-MBPx however resulted in a lower K_m of ∼5.9 enzymes bo_3 oxidase. It has not escaped our notice that consequently, orientation ratios of bo_3 oxidase could potentially be calculated based on such K_m values. However, more experiments with varying, but known and predefined orientation ratios would be required to develop a respective algorithm.

At this point it has to be stressed again that in these experiments bo_3-Spy-SC-MBPx was not purified after coupling, hence presence of free bo_3-Spy is possible, even though a 3-fold excess of SC-MBPx was used for coupling. Thus, it would be very interesting to repeat the experiments using SC-MBPx-3xFLAG, enabling us to coreconstitute the ATP synthase with purified bo_3-Spy-SC-MBPx-3xFLAG, i. e. free of unlabeled bo_3-Spy.

Proton Pumping – Pyranine Assay.

Encouraged by the results of these investigations on coupled enzyme activity, wanted to monitor proton pumping of bo_3-Spy-SC-LSU using the pyranine assay. First tests however revealed no differences in the direction of proton pumping between bo_3-Spy-SC-LSU and unlabeled bo_3-Spy; both constructs led to proton efflux from the proteoliposomes if reconstituted with the standard reconstitution method of our lab (0.4 % cholate as detergent for liposome destabilization in presence of pyranine;

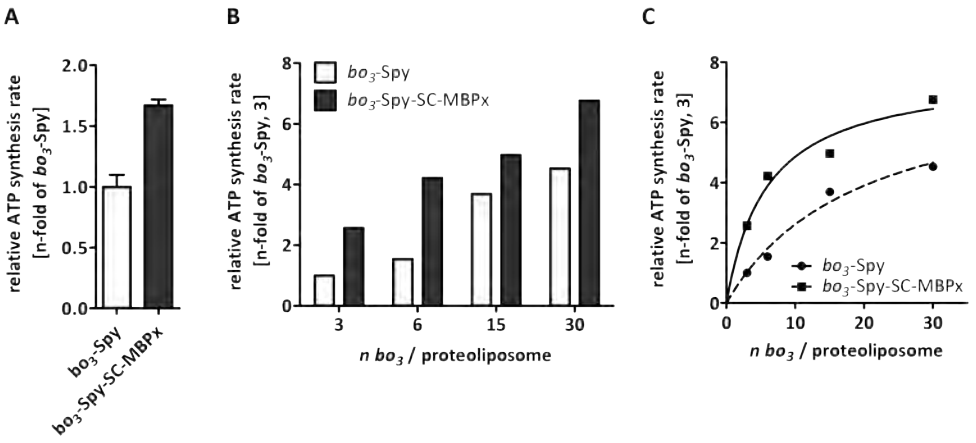

Figure 58: Coupled activity of *bo₃*-Spy-SC-MBPx and ATP synthase. (A) Continuous respiratory-driven ATP synthesis, i. e. coupled activity of coreconstituted *bo₃*-Spy or *bo₃*-Spy-SC-MBPx and ATP synthase, was monitored by measuring luminescence using the luciferin/luciferase system detecting newly synthesized ATP as described in figure 40 on page 96. To reduce *bo₃* oxidase, ubiquinol Q_2 (30 µM) was used. The measured ATP synthesis rates were normalized to specific activity of *bo₃* oxidase assessed by oxygen consumption measurements. The same amount of ATP synthase was used for both experiments. Both conditions were repeatedly measured and average ± sd ($n = 3$) were calculated. (B) While the amounts of used ATP synthase were kept constant, the amounts of *bo₃*-Spy with or without LSU were varied from 3 enzymes *bo₃*-Spy(-SC-MBPx) per proteoliposome or 23.6 pmol *bo₃*-Spy(-SC-MBPx), to 30 enzymes *bo₃*-Spy(-SC-MBPx) per proteoliposome. x-axis: number of *bo₃* oxidase enzymes per proteoliposome; y-axis: relative ATP synthesis rate normalized to the condition 3 enzymes *bo₃*-Spy per proteoliposome. (C) Thought experiment: Data from (B) is analyzed by Michaelis-Menten kinetics using GraphPad Prism. x-axis: number of *bo₃* oxidase enzymes per proteoliposome; y-axis: relative ATP synthesis rate normalized to the condition 3 enzymes *bo₃*-Spy per proteoliposome. *bo₃*-Spy: v_{max}: 7.7-fold of ATP synthesis rate of 3 enzymes *bo₃*-Spy per proteoliposome, K_m: 19.5 molecules *bo₃* oxidase per proteoliposome, R^2: 0.98; *bo₃*-Spy-SC-MBPx: v_{max}: 7.7-fold of ATP synthesis rate of 3 enzymes *bo₃*-Spy per proteoliposome, K_m: 5.9 molecules *bo₃* oxidase per proteoliposome, R^2: 0.94.
Liposomes: 10 mg ml^{-1} 90 % lecithin, soybean; 200 nm; in 20 mM HEPES pH 7.5, 100 mM KCl, 2.5 mM $MgCl_2$, 25 g L^{-1} sucrose. Measurement buffer: 20 mM Tris-phosphate pH 7.4, 5 mM $MgCl_2$, 4 mM DTT, 80 µM ADP. White: *bo₃*-Spy; black: *bo₃*-Spy-SC-MBPx.

SEC (CentriPure P10 desalting columns, Zetadex-25, exclusion size 5 kDa) to remove detergent and external pyranine; not shown).

Consequently, we aimed to optimize the reconstitution process of bo_3 oxidase. As discussed in section 4.3.7, DDM exhibits unfavourable effects on solubilization of lipid bilayers, implying that the use of DDM for reconstitution should be avoided. A method to replace DDM by OG for reconstitution of pR purified in DDM was described earlier in this thesis (section 4.3.7). Since bo_3-Spy was also purified in DDM, we wanted to test if this method was applicable also for DDM-free reconstitution of bo_3-Spy.

According to our procedure, DDM in the bo_3-Spy solution was replaced by 1 % OG using β-cd. Subsequentially, a suitable concentration of OG for reconstitution of bo_3-Spy into preformed liposomes had to be found. The optimal OG concentration was identified by titration of OG in a series of reconstitutions of bo_3-Spy compared in proton pumping activities using the pyranine assay. To remove OG-micelles, excess β-cd and soluble β-cd-DDM complexes after reconstitution, CentriPure PF10 desalting columns with exclusion size of 25 kDa were used.

As shown in figure 59, the concentration of OG used for reconstitution had a significant effect on bo_3-Spy proton pumping activities. Interestingly, spontaneous insertion of bo_3-Spy was observed without OG. Up to 0.3 % OG (different shades of red), no further effect was observed, as proton pumping levels corresponded to that of spontaneous insertion of bo_3-Spy without OG. Increasing the concentration of OG $\geq$0.4 % (different shades of green), robust levels of proton pumping were observed, with the maximal activity at 0.75 % OG (black trace), where 58 % quenching of the pyranine fluorescence ratio were achieved. The concentration of OG was not increased above 0.75 % OG. Knol, Veenhoff, *et al.* [130] followed the state of liposomes by measuring the absorbance at 540 nm during titration of OG. They showed that liposomes are completely solubilized by the detergent at concentrations above 0.75 % OG, while liposomes were only partially solubilized at concentrations $\leq$0.75 %.

To establish an optimal OG concentration for reconstitution it has further to be tested at which detergent concentrations the LSU SC-MBPx-3xFLAG stays on the outside of the proteoliposomes as desired, since encapsulation of the LSU would counteract our approach to influence orientation. Free SC-MBPx-3xFLAG was added to preformed liposomes which were partially solubilized with different concentrations of OG. After mock reconstitution and detergent removal, the liposomes were washed by dilution to a factor of 15 with buffer, collected by ultracentrifugation, and subjected to SDS-PAGE, followed by western blotting, and probing for MBP

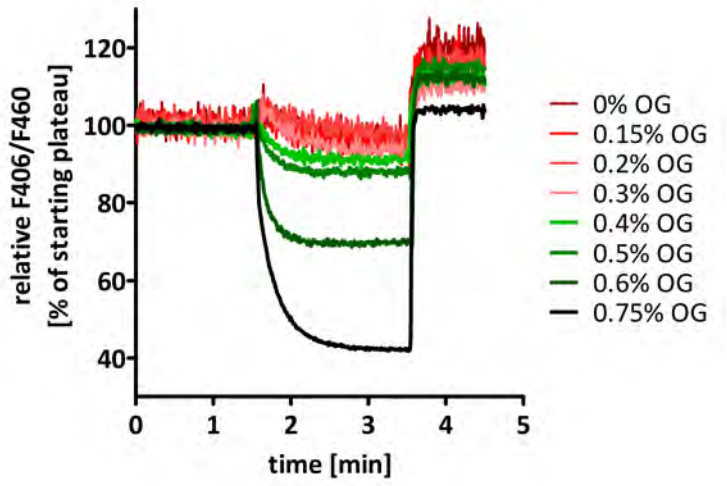

Figure 59: Titration of OG to optimize OG-mediated reconstitution of *bo₃* oxidase. DDM in the protein solution of *bo₃* oxidase was replaced by OG using β-cd as described. Then, OG was titrated for reconstitution of *bo₃*-Spy into liposomal membranes. OG concentrations indicated in the legend correspond to total OG concentration, including the amounts of OG used to replace DDM in the protein solution. After reconstitution, detergent, soluble β-cd-DDM complexes, and external pyranine were removed by CentriPure PF10 desalting columns. Proton pumping was assessed by monitoring the F406/F460 pyranine fluorescence ratio. Liposomes: 10 mg ml^{-1} 90 % lecithin, soybean; 200 nm; in 0.5 mM MOPS pH 6.5, 25 mM K_2SO_4. Measuring buffer: same as liposome buffer.

(figure 60). Surprisingly, SC-MBPx-3xFLAG seemed to be entrapped in the liposomes with whatever concentration of OG was used. SC-MBPx-3xFLAG was also detected if no OG was used and encapsulation hence is impossible. It has to be speculated that SC-MBPx-3xFLAG is present on the outside of the liposomes after one washing step by dilution followed by ultracentrifugation. Therefore, this experiment will be repeated by a co-worker in our lab, who will use more than one washing step to remove SC-MBPx-3xFLAG potentially present on the outside of the liposomes.

As soon as the optimal concentration of OG for reconstitution is found, *bo₃*-Spy-SC-MBPx-3xFLAG and *bo₃*-Spy will be reconstituted into preformed liposomes, and the net direction of proton pumping will eventually be assessed using the pyranine assay.

4.3.13 Conclusions to the SpyTag-SpyCatcher System.

General reflections & advantages. Application of the SpyTag-SpyCatcher system to introduce LSUs guiding unidirectional orientation of MPs is much more user-friendly

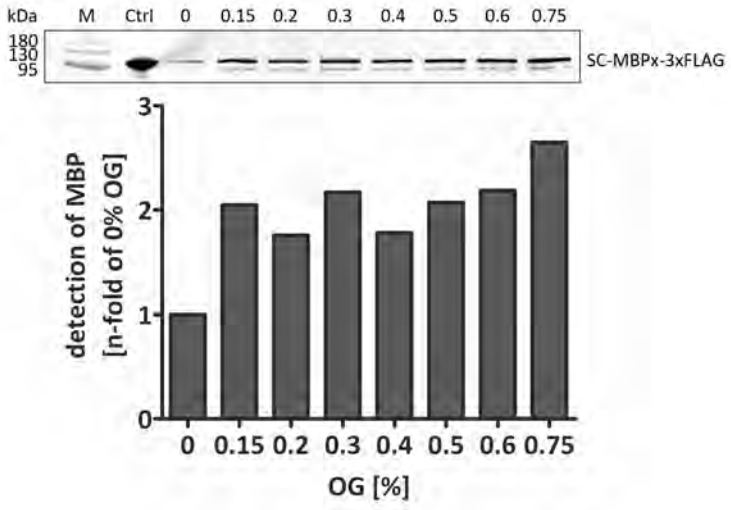

Figure 60: Titration of OG to investigate entrapping of SC-MBPx-3xFLAG into liposomes. SC-MBPx-3xFLAG was added to the liposomes and OG was titrated to imitate reconstitution of bo_3 oxidase into liposomal membranes. OG concentrations indicated on the x-axis correspond to total OG concentration. Detergent was removed by CentriPure PF10 desalting columns after reconstitution. After washing and collection by ultracentrifugation, liposomes were subjected to SDS-PAGE followed by western blotting and probing for MBP using an anti-MBP antibody (Anti-Maltose Binding Protein antibody [R29.6]; secondary antibody: IRDye 680RD Donkey anti-Mouse IgG Secondary Antibody). Bands of MBP in lanes of varying OG concentrations were quantified using ImageJ. Ctrl: pure SC-MBPx-3xFLAG, without liposomes; M: marker. Liposomes: 10 mg ml^{-1} 90 % lecithin, soybean; 200 nm; in 0.5 mM MOPS pH 6.5, 25 mM K_2SO_4.

compared to the AviTag system introduced earlier, and it offers various advantages. We have chosen protein fusions of solubility enhancer proteins with the SpyCatcher as LSUs (SC-LSUs). Compared to the LSUs introduced with the AviTag system (e. g. SA-$(PEG)_3$), SC-LSUs do not require repeated construction and purification steps. Some construction and purification steps to build up the LSUs of the AviTag system had to be performed when the preliminary LSU SA was already attached to the MP. SC-LSUs on the contrary are expressed in *E. coli* and purified to yield the final, complete LSU before coupling to the Spy-tagged MP of interest, thus preventing loss of activity of the latter. Because of the way of production, availability of proteinaceus SC-LSUs is almost limitless. Moreover, the use of soluble protein fusions containing MBP or MBPx as SC-LSUs is advantageous, since it provides the possibility to determine orientation of the reconstituted MP-SC-LSU construct e. g. by limited proteolysis followed by detection with commercially available anti-MBP antibodies, or by fluorescent labeling of the SC-LSU as shown in section 4.4.

Unidirectional reconstitution of pR. Using the SpyTag-SpyCatcher system, it was shown that orientation of pR can be influenced upon reconstitution. As demonstrated by assessing proton pumping across the proteoliposomal membrane monitored by the pH-sensitive fluorophore pyranine, deploying SC-MBP-3xFLAG as SC-LSU combined with a novel reconstitution method led to unidirectional orientation of pR by predefinition in either of the desired directions in the liposomal membrane. These functional results were confirmed by a physical assessment of pR orientation using limited proteolysis followed by western blot analysis. Therewith, it could be shown that the majority of the SC-LSU SC-MBP-3xFLAG was indeed located on the outside of the proteoliposomes, thus proving that pR was orientated as desired.

Proton pumping measurements with reconstituted pR-N/CSpy-SC-MBPx-3xFLAG using the pyranine assay further gave us a hint on effects of freezing and thawing of proteoliposomes. Repeated cycles of freezing and thawing of proteoliposomes appear to randomize orientation of previously reconstituted pR. This conclusion is supported by other studies reporting heterogeneous insertion of the pR-homologue bacteriorhodopsin into liposomes by repeated freezing and thawing combined with sonication.[260–262]

Towards unidirectional reconstitution of bo_3 oxidase. The SpyTag-SpyCatcher system was also applied in order to unidirectionally reconstitute bo_3 oxidase to exclusively import protons into proteoliposomes.

Monitoring of coupled enzyme activity of bo_3 oxidase coreconstituted with ATP synthase resulted in first trends, showing that SC-LSU-guided reconstitution of bo_3 oxidase (bo_3-Spy-SC-MBPx) increased the ATP synthase's driving force *pmf*, hence leading to higher ATP synthesis rates. Further, a model to evaluate coupled enzyme activity of coreconstituted ATP synthase and bo_3 oxidase using Michaelis-Menten kinetics was suggested.

Because the 3xFLAG-tagged version of SC-MBPx was not yet available when these experiments investigating on coupled enzyme activity were performed, bo_3-Spy-SC-MBPx was used which was not purified after coupling. Despite of a 3-fold excess of SC-MBPx used for coupling, bo_3-Spy-SC-MBPx was possibly containing contaminations of unlabeled bo_3-Spy. Consequently, it would be very interesting to repeat these experiments using SC-MBPx-3xFLAG, enabling coreconstitution of the ATP synthase with purified bo_3-Spy-SC-MBPx-3xFLAG, i. e. free of unlabeled bo_3-Spy.

We further wanted to observe differences in proton pumping direction of *bo*$_3$-Spy-SC-LSU and unlabeled *bo*$_3$-Spy using the pyranine assay. First results showing no differences however motivated us to optimize the reconstitution procedure of *bo*$_3$ oxidase. Since DDM is known to exhibit unfavourable effects on solubilization of lipid bilayers as discussed earlier in this thesis, the use of DDM for reconstitution should be avoided; however, all variants of *bo*$_3$ oxidase were purified in DDM. Therefore, we started the optimization of *bo*$_3$ oxidase reconstitution by adapting our β-cd-based method used to replace DDM by OG for reconstitution of pR. We further started investigations on suitable OG concentrations for reconstitution of *bo*$_3$ oxidase.

Drawbacks & outlook. Even though the SpyTag-SpyCatcher system already represents an improvement compared to the AviTag system, it still requires genetic modification to introduce the SpyTag into the MP of interest at a suitable position. Introducing genetic modifications to large, complex multi-subunit MPs as the *bo*$_3$ oxidase is often accompanied by problems with expression and/or misfolding of the fusion protein.

Optimally, the LSU would be detached from the unidirectionally inserted MP directly after reconstitution in order to not impair functional assays, even though we have so far not observed any disturbing effects of the LSUs on activity, neither of pR, nor of *bo*$_3$ oxidase. Anyway, protease cleavage sites were introduced on one hand in pR-N/CSpy and *bo*$_3$-Spy to cleave off the SpyTag and with it the bound SC-LSU, and on the other hand in the SC-LSU constructs to cleave the LSU from SC, enabling cleavage and thus release of the attached LSU prior to functional experiments. Due to limited time, investigations regarding the release of the LSU by exploiting these protease cleavage sites have not been performed to date.

Especially because of the last two discussed drawbacks, a more general method would still be desirable. However, using the SpyTag-SpyCatcher system facilitated unidirectional orientation of reconstituted pR in liposomes and paved the way towards unidirectional reconstitution of *bo*$_3$ oxidase as well.

Last but not least, it has to be concluded that a crucial point on the way towards unidirectional reconstitution of MPs into liposomes in a predefined orientation is comprised of the reconstitution conditions, which have to be optimized for each MP of interest.

4.4 Excursus – A Novel Method to Determine Orientation.

4.4.1 Introduction to the TCEP-based Orientation Determination Assay.

With the exception of the assay using limited proteolysis followed by western blot analysis, the influence of coupled LSUs on MP orientation was always determined with the help of functional assays. Such assays however have a few drawbacks. First, the reconstituted MP must be active. Second, functional assays strongly depend on the nature of the MPs' substrates. Some substrates are membrane-impermeable; addition of such substrates to the outside of proteoliposomes leads to activation only of the fraction of MPs with the substrate binding site orientated towards the outside (e. g. ATP for ATP synthase). Other substrates however are membrane-permeable, hence activating both orientation populations of the MP of interest (e. g. ubiquinols Q_1 and Q_2 for bo_3 oxidase). Therefore, it would be more conveniant to have a robust method to determine orientation quickly, which would be solely based on the physical presence of the MP in proteoliposomes. The known assay based on limited proteolysis followed by SDS-PAGE analysis is not trivial, since it can result in complex cleavage patterns, especially if analyzing orientation of multi-subunit MPs. Even though analysis of limited proteolysis can be simplified by western blotting, it further requires antibodies and is more time-consuming.

Within the framework of the master's thesis of Lukas Rimle in our lab, we have therefore aimed to establish a method to determine orientation of MPs in proteoliposomes independently of MP function, and less time-consuming than the method based on limited proteolysis.

This orientation determination assay is based on findings recently presented by Vaughan *et al.* [263]. They reported that the cyanine dye Cy5 and several of its structural relatives (but not Cy2 or Cy3) are reversibly quenched by the phosphine tris(2-carboxyethyl)phosphine (TCEP). Quenching is mediated by 1,4-addition of the phosphine to the polymethine bridge of Cy5 to form a covalent adduct, and can be reversed either by illumination with UV light or by addition of an excess of the disulfide cystamine (reaction scheme: supplementary figure S32 on page 227).[263] TCEP quenching of cyanines was used as the basis for an internalization assay able to detect whether cargos are outside or inside cells.[263] Because TCEP is membrane-impermeable [264], addition of TCEP to the extracellular medium is selectively quenching dye molecules bound to cargo outside the cell, while dye molecules bound to internalized cargo remain fluorescent.[263]

Further, Huang, Ge, *et al.* [182] described an assay to determine orientation of bacteriorhodopsin in liposomes by quenching the fluorophore 5-carboxytetramethylrhodamine (TAMRA) by free soluble tryptophan zwitterion, which is membrane-impermeable as TCEP. TAMRA-labeled bacteriorhodopsin (4 µM) was reconstituted into liposomes consisting of either POPC, POPG, or DOPC (6 mg ml^{-1}, 100 nm), and external TAMRA fluorescence was quenched with various amounts of tryptophan (0 - 22.5 mM). Interestingly, orientation of bacteriorhodopsin was not directly measured, but calculated using the Stern-Volmer relationship [265], which describes the kinetics of photophysical intermolecular deactivation processes.

Inspired by these two studies, it was decided to combine the features of both these studies and develop a new assay, offering a possibility to discriminate between fluorescently labeled moieties or cargos on the outside and on the inside of liposomes. Since solubility of tryptophan in water (11.4 mg ml^{-1} at 25 °C; PubChem CID: 6305) is significantly lower than solubility of TCEP-HCl (50 mg ml^{-1}; PubChem CID: 57654018), we decided to use the TCEP/Cy5 system.

We aimed to first quench fluorescence of moieties or cargos accessible by TCEP from the outside of liposomes, and subsequently provide access of TCEP also to moieties or cargos on the inside of liposomes. Calculation of the ratio of fluorescence quenching from the outside of the liposomes to total quenching eventually allows to determine orientation.

For this purpose, a MP of interest is genetically engineered such that it does only contain one single cysteine residue at one specific position, which can be specifically labeled with the maleimide of the Cy5-analogue DY-647P1 (DY-647P1 maleimide, M_w: 830.96 g mol^{-1}, λ_{ex}: 653 nm, λ_{em}: 672 nm, ε: 250'000 M^{-1}cm^{-1}). This labeled single cysteine should be located at a position in the MP as distant as possible from the membrane and exposed to the aequous surrounding to ensure free accessibility for reaction with TCEP. Further, it has to be taken care that the newly introduced cysteine residue does not affect MP function. Consequently, we suggest positioning of the single cysteine residue in loops or at termini of the MP which are accessible for the quencher TCEP. After labeling, the MP is purified by SEC to remove excess fluorophore, and the labeled MP is reconstituted into preformed partially detergent-solubilized liposomes. After reconstitution, the collected proteoliposomes are suspended in measuring buffer and total fluorescence is measured. After obtaining a stable fluorescence signal, TCEP (14.3 mM) is added, quenching all the fluorophore accessible from the outside as illustrated in figure 61, hence leading to a reduction in fluorescence signal. Because of the membrane-impermeability of TCEP, fluorescence of fluorophore molecules

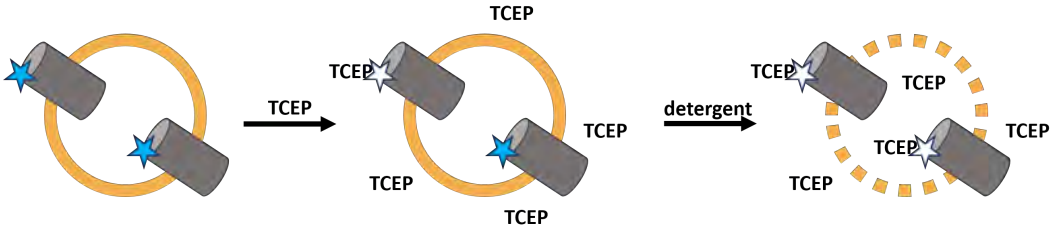

Figure 61: TCEP-based quenching assay to determine orientation of reconstituted MPs. The single-cysteine variant of the MP of interest (gray) is labeled with the maleimide of the fluorophore DY-647P1 (star), which is a structural analogue to Cy5. The labeled MP is reconstituted into liposomes (yellow), and total fluorescence is measured, to which all present fluorophore molecules do contribute (blue stars). Fluorescence of outwardly facing fluorophores is quenched (white stars) by addition of the membrane-impermeable quencher TCEP. At this point, fluorescence of exclusively inwardly facing fluorophores is detected (blue stars). Finally, the proteoliposomes are completely solubilized, hence all fluorophore molecules are accessible for TCEP, leading to maximal quenching of DY-647P1. A ratio of outwardly displayed to total fluorophore present can be calculated, representing the orientation ratio of the two possible orientation populations of the reconstituted MP.

displayed to the liposomal lumen are not quenched. Finally, the proteoliposomes are solubilized by detergent, hence fluorophore molecules initially hidden in the liposomal lumen are getting accessible for TCEP, resulting in maximal quenching. Calculation of the ratio of TCEP-mediated fluorescence quenching from the outside of the proteoliposomes to maximal fluorescence quenching eventually allows to determine orientation of the reconstituted MP.

In his master's thesis Lukas Rimle genetically engineered the bo_3 oxidase to contain only one single cysteine located in the N-terminal region of subunit III (CyoC; A21C). Thereby, he was able to confirm previously published [25, 172] orientation ratios of the bo_3 oxidase (~30 % of bo_3 oxidases orientated in the direction to import protons into proteoliposomes; see section 1.7.1). Similarly, a single cysteine at the same position was also introduced in bo_3-Spy, however this version of bo_3 oxidase has not been tested yet.

4.4.2 Applications of the TCEP-based Orientation Determination Assay.

Application of the developed method using single cysteines introduced at the termini of pR failed (not shown). A possible reason therefor might be that pR is a relatively small MP, consequently fluorophore-labeled single cysteines are located in close proximity of the liposomal membrane, thus restricting accessibility of the fluorophore for TCEP. Addition of detergent in order to solubilize proteoliposomes therefore also

induces changes in the proximate surrounding of the fluorophore molecules, suggesting that fluorophores located in close proximity of the membrane are not suitable for this assay.

Therefore, the TCEP-based orientation determination assay was adapted to the SpyTag-SpyCatcher system developed to unidirectionally orientate pR. Instead of fluorescently labeling pR at a single cysteine, the LSU SC-MBPx-3xFLAG was labeled with the fluorophore DY-647P1.

The biggest advantage of this adaptation of the TCEP-based orientation determination assay is that it does not require any single cysteine variant of pR. Importantly, the LSU SC-MBPx-3xFLAG is hydrophilic, consequently the fluorophore molecules will definitely not be located in proximity of the membrane. Apart from fluorescent labeling of the LSU, no additional efforts are required. The basic idea of the assay as well as its measurement procedure remained exactly the same.

SC-MBPx-3xFLAG was unspecifically labeled with the NHS-ester of DY-647P1 (M_w: 805.91 g mol^{-1}) according to the latter's manufacturer's instructions, and excess fluorophore was removed by SEC (CentriPure P10 desalting column). The DY-647P1-labeled LSU SC-MBPx-3xFLAG was subsequently coupled to pR-N/CSpy (see section 4.3.4), and pR-N/C-Spy-SC-MBPx-3xFLAG-(DY-647P1) was reconstituted into liposomes as described earlier in this thesis (section 4.3.7).

Upon reconstitution of pR-N/CSpy coupled to DY-647P1-labeled SC-MBPx-3xFLAG, the major portion of labeled LSUs is expected be located on the outside of the liposomes (see section 4.3). Therefore, the first TCEP-mediated quenching step right after addition of TCEP to the proteoliposomes should be predominant compared to the second quenching step, where complete solubilization of the proteoliposomes by DDM enables TCEP to quench also fluorophore molecules formerly hidden in the liposomal lumen.

For both of the variants of pR-Spy, nearly unidirectional orientation could be reported as shown in figure 62 on the following page. pR-NSpy-SC-LSU was shown to be reconstituted with ∼81 % of the LSUs on the outside of the proteoliposomes, while pR-CSpy-SC-LSU was observed to be reconstituted with ∼97 % of the LSUs being on the outside.

These results support the results obtained by proteolytic cleavage and western blot analysis (see figure 51 on page 114), showing that the orientation of pR can be guided during reconstitution by the help of LSUs. These two sets of results combined also strongly support the results of the pyranine-based proton pumping assay with pR-Spy (see figure 49 on page 111).

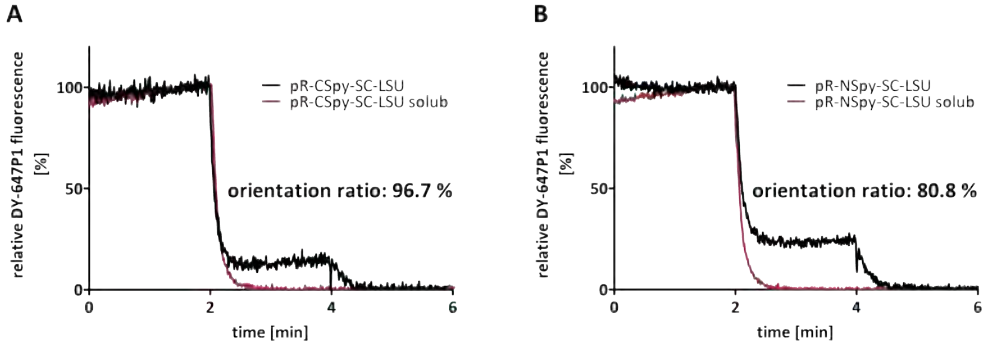

Figure 62: Orientation of pR-N/CSpy using DY-647P1-labeled SC-MBPx-3xFLAG. SC-MBPx-3xFLAG was unspecifically labeled with DY-647P1 NHS-ester, then coupled to pR-N/CSpy, and finally reconstituted into preformed, partially solubilized liposomes as described in section 4.3.7. Two measurements were taken per condition. In the first measurement (black), to the respective pR-Spy-SC-LSU proteoliposomes, TCEP (13.6 mM) was added after 2 min to quench exterior fluorophore. After 4 min, DDM (1.3 %) was added to completely solubilize the proteoliposomes, thus providing TCEP accessibility to inwardly orientated fluorescently labeled LSUs, resulting in maximal fluorescence quenching. The second measurements (red, solub) served as control to see whether maximal quenching was indeed reached at the end of the first measurements. For this purpose, the same proteoliposomes as in the first measurement were completely solubilized at the very beginning of the measurement, making all fluorophore molecules accessible at once for TCEP added after 2 min. (A) pR-CSpy-SC-MBPx-3xFLAG-(DY-647P1). Using pR-CSpy, 96.7 % of the fluorescently labeled LSU were found to be on to be on the outside of the proteoliposomes. (B) pR-NSpy-SC-MBPx-3xFLAG-(DY-647P1). Using pR-NSpy, 80.8 % of the fluorescently labeled LSU were found to be on the outside of the proteoliposomes. At the end of the recording of each measurement, a volume of buffer equal to the volume of the detergent stock addition was added in order to be able to correct the measured orientation ratios for the volume of detergent added. This is the reason why the orientation ratios stated in the graphs at the first look seem to be too high compared to DY-647P1-quenching depicted by the curves. Liposomes: 10 mg ml^{-1} 90 % lecithin, soybean; 200 nm; in 0.5 mM MOPS pH 6.5, 25 mM K_2SO_4. Reconstitution conditions, detergent removal and coupling of the LSU to pR-Spy were identical as for figure 49 on page 111. Measurement buffer: 250 mM Tris-HCl pH 8.5.

As shown in figure 49, reconstituted pR-CSpy-SC-LSU exported protons from the proteoliposomes upon illumination, and proton export plateaued after ∼20 min, while reconstituted pR-NSpy-SC-LSU imported protons, reaching a plateau but after ∼70 min. The results of the TCEP-based orientation determination assay may explain why pR-NSpy-SC-LSU was slower to plateau in proton pumping compared to pR-CSpy-SC-LSU, since pR-CSpy-SC-LSU was shown to be orientated closer to unidirectionality (∼97 %) than pR-NSpy-SC-LSU (∼81 %).

4.5 Approach III – General Approach Using trisNTA.

4.5.1 Introduction to the trisNTA System.

Both approaches using either AviTag or SpyTag-SpyCatcher described in detail in the previous chapters have common drawbacks. They both require extensive genetic modifications. Further, the release of the LSU after reconstitution is not straightforward. It would either require proteolytic cleavage (slow; SpyTag-SpyCatcher system) or dissociation of strong biotin-streptavidin bindings (AviTag system).

Therefore, an idea is to exploit His-tags, which are commonly introduced in many (membrane) proteins, typically on a terminus, to facilitate purification by immobilized metal affinity chromatography (IMAC). His-tags usually consist of six or more consecutive histidine residues. [266] The imidazole rings of histidine residues readily coordinate with divalent transition metal ions such as Ni^{2+} or Co^{2+}, usually immobilized on beads or resins for purification by the chelator nitrilotriacetic acid (NTA).[266] As shown in the inset of figure 63A, two histidine residues are sufficient to bind to nickel-NTA (Ni-NTA) [267], however increasing the number of histidine residues in the His-tag results in higher binding affinity.[267–270] Complexed His-tags can be eluted from Ni-NTA by low pH (4.5 - 6), or by competition with histidine or imidazole. The latter in low concentrations is also used to prevent unspecific binding to Ni-NTA. Earliest works on purification of His-tagged proteins by IMAC showed that His-tags consisting of six histidine residues were successfully used to purify recombinant proteins to 95 % purity in high yield. Importantly, hexahistidine-tags appeared to not interfere with the functions and activities of such tagged proteins.[271–273] Longer His-tags leading to increased affinity however can e. g. be helpful to eliminate persistent contaminants by more stringent washing with imidazole [274] or to purify proteins expressed at low levels [275].

Our idea is to couple a LSU to a His-tag-binding moiety as Ni-NTA to guide unidirectional reconstitution of MPs into liposomes. The only requirement to the MP would be that a His-tag is present on this side of the MP which is desired to be orientated to the outside of the liposomes. After reconstitution, the LSU could be released under mild conditions, e. g. by imidazole.

The interaction between Ni-NTA and the His-tag is very selective and reversible, what makes it an excellent system for protein purification.[200] But exactly this relatively weak affinity (K_d: $\sim$10 µM) [200, 276] is not high enough to attach a LSU to the His-tag of our MP of interest and subsequently purify the complex (e. g. by SEC). Albeit the low affinity, Pfleger *et al.* [13] reported an approach to guide

unidirectional reconstitution of pR assisted by Ni-NTA-coated silicate particles (for more details, see section 1.7.2). Unpublished data from our lab however showed that this seems to be a rather exceptional case, and that this method is not generally applicable, because some MPs became non-functional, and the density of Ni-NTA and consequently His-tagged MP on the silicate particles is too high for reconstitution into liposomes (not shown). The strength of an interaction always depends on the concentrations of the binding partners. Accordingly, stable binding of His-tagged proteins to surfaces densely covered with Ni-NTA has been observed [276–280], while individual His-tag / Ni-NTA complexes in solution are of very low affinity and stability [200, 276, 281–284].

In 2005, Lata, Reichel, *et al.* [276] have found a solution to this problem. A significant increase in binding affinity of Ni-NTA with His-tagged proteins can be achieved through multivalency.[200, 285, 286] Lata, Reichel, *et al.* [276] hence have synthesized a variety of multivalent chelator heads consisting of two, three, or four Ni-NTA moieties (bis-, tris-, tetrakis-NTA), allowing more than just two histidine residues of the His-tag to bind to the chelator simultaneously, thereby increasing affinity. Especially promising for our purposes is trisNTA, a version of which is shown in figure 63B. In trisNTA essentially, three molecules of NTA are combined on a scaffold, hence allowing simultaneous complexing of six sequential histidines of the protein via Ni^{2+} (figure 63A). Compared to monoNTA, the affinity of trisNTA towards a hexahistidine-tag is three orders of magnitude higher, resulting in a K_d of 10 - 40 nM.[200, 276]

We aimed to couple a LSU to trisNTA, which can then be complexed via Ni^{2+} to the suitably placed His-tag in the MP of choice to guide unidirectional reconstitution into liposomes. To prevent potential LSU-mediated impairment of enzyme functionality, the LSU shall be removed from the MP after reconstitution. Removal of the LSU after reconstitution can be facilitated by an exceptional advantage of multivalent interactions. While the affinity of trisNTA for hexahistidine tags is significantly increased compared to monoNTA, the affinity of each single histidine residue for its Ni-NTA moiety stays the same. Dissociation of multivalent interactions as e. g. hexahistidine-tag / trisNTA can thus be accelerated by incubation with monovalent ligands capable of competing for the binding sites.[287] Consequently, fast reversibility of the interaction between trisNTA and His-tags can be achieved under mild conditions using either imidazole, EDTA or histidine, or by lowering the pH.[200, 287]

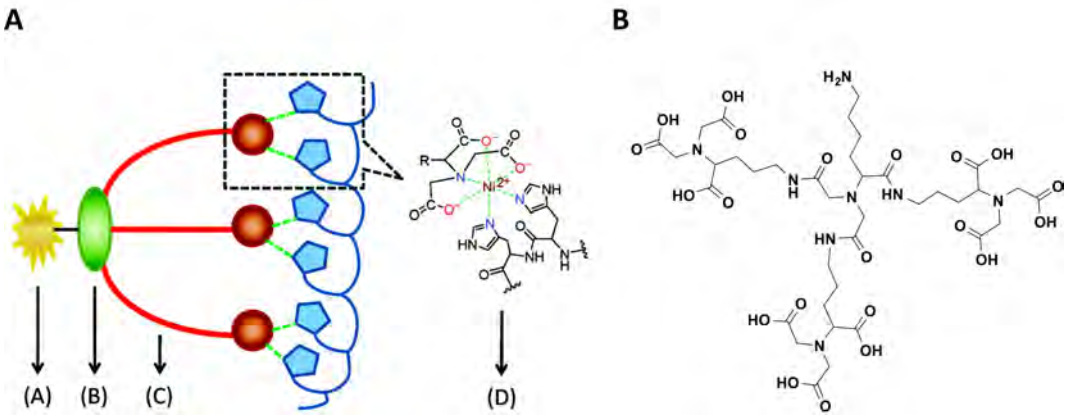

Figure 63: trisNTA – Structure and function. (A) trisNTA-His_6 binding pair. trisNTA is a bifunctional molecule. Three spacers (C) connect the three NTA moieties (D) with the scaffold (B), to which also the second functionality (A) is attached. In our case, the second functionality was a free amine, which was used for coupling trisNTA to the LSU. Figure (A) adapted from [200]. (B) Molecular structure of our trisNTA.

4.5.2 Synthesis of trisNTA.

Multiple variants of trisNTA have been reported, essentially differing in the nature of the scaffold carrying the three NTA moieties, such as cyclic, linear, or dendritic trisNTAs.[288] The different variants of trisNTA have been used in numerous studies for a wide variety of applications. trisNTA has for example been used for *in situ* protein labeling with fluorophores [289], for site-specific orientated attachment of His-tagged proteins on surfaces [290], or to anchor His-tagged proteins to gold nanoparticles for cryo-electron tomography [291], to only name a few. For a recent review highlighting numerous further applications of trisNTA consider Wieneke *et al.* [288]. In summary, trisNTA can be versatilely functionalized, e. g. with fluorophores, quenchers, or gold nanoparticles, and its stoichiometric binding to His-tagged proteins is orthogonal to other protein labeling techniques.[288]

To enable coupling of trisNTA to LSUs in aequous solution, we decided to use a trisNTA functionalized with a primary amine. A variant of such an amino-functionalized trisNTA is commercially available, but 100 µg are e. g. sold for CHF 277.00 by Sigma-Aldrich (tris-NTA amine trifluoroacetate salt solution, Sigma-Aldrich, 14136; 27.01.2020). To establish new constructs and protocols to guide unidirectional reconstitution of MPs however, multiple milligrams of trisNTA were needed; hence purchasing it would have definitively exceeded our budget. It was therefore decided to synthesize a slightly different version from the one sold by Sigma by ourselves.

While the scaffold of commercially available trisNTA is constituted of a more rigid tetraaza cyclam, we synthesized a dendritic version of trisNTA (figure 63B), in which the scaffold consists of a lysine with ornithine spacers as published by Huang, Hwang, *et al.* [200].

In general, I followed the syntheses of trisNTA published by Huang, Park, *et al.* [199] and Huang, Hwang, *et al.* [200], consisting of five main steps as depicted in figure 64.

Briefly, to N^{ε}-benzyloxycarbonyl-L-lysine *tert*-butyl ester (*compound **1***, H-Lys(Z)-OtBu) a 4-fold excess of *tert*-butyl bromoacetate was added to form the first degree dendrimer *compound **2*** via S_N2 reaction, followed by selective deprotection of the three carboxylic acid groups (*compound **3***). In a parallel reaction, *tert*-butyl bromoacetate was also added to N-δ-carbobenzoxy-L-ornithine *tert*-butyl ester (*compound **4***, H-Orn(Z)-OtBu) to form a second degree dendrimer building block (*compound **5***), followed by selective deprotection of the primary amine group to obtain *compound **6***. Then, to the deprotected first degree dendrimer (**3**) three molecules of amine-deprotected second degree dendrimer building block (**6**) were added to form the fully protected second degree dendrimer (*compound **7***). Depending on downstream use, the amine group or the carboxylic acid groups of **7** can be deprotected selectively. Sequential deprotection of the amine group and the carboxylic acid groups (**7** to **9** via **8**), or simultaneous deprotection of these two functionalities (**7** to **9** directly), both eventually yield trisNTA-NH_2 (*compound **9***). The final product as well as all intermediates were successfully identified by NMR and mass spectrometry. In total, ∼1.95 g *tert*-butyl-protected trisNTA-NH_2 (*compound **8***) were synthesized. Dry **8** was stored under Ar atmosphere at −20 °C.

4.5.3 Testing the Two Functionalities of trisNTA.

trisNTA-NH_2 (**9**) is a bifunctional molecule (see figure 63B). On one hand there is a primary amine group which we want to use to couple trisNTA to LSUs, and on the other hand there is the triple NTA-functionality to complex His-tags of proteins via chelated Ni^{2+}. After synthesis of trisNTA-NH_2 (**9**), we first wanted to test these two functionalities.

In a first experiment, the primary amine of fully deprotected trisNTA (**9**) was coupled to PEG_4-biotin via NHS-chemistry (NHS ester reaction scheme: see figure 30 on page 82), yielding trisNTA-biotin (molecular structure: supplementary figure S13 on page 211; M_w: 1424.5 g mol^{-1}; MS: supplementary figure S14). Commercially

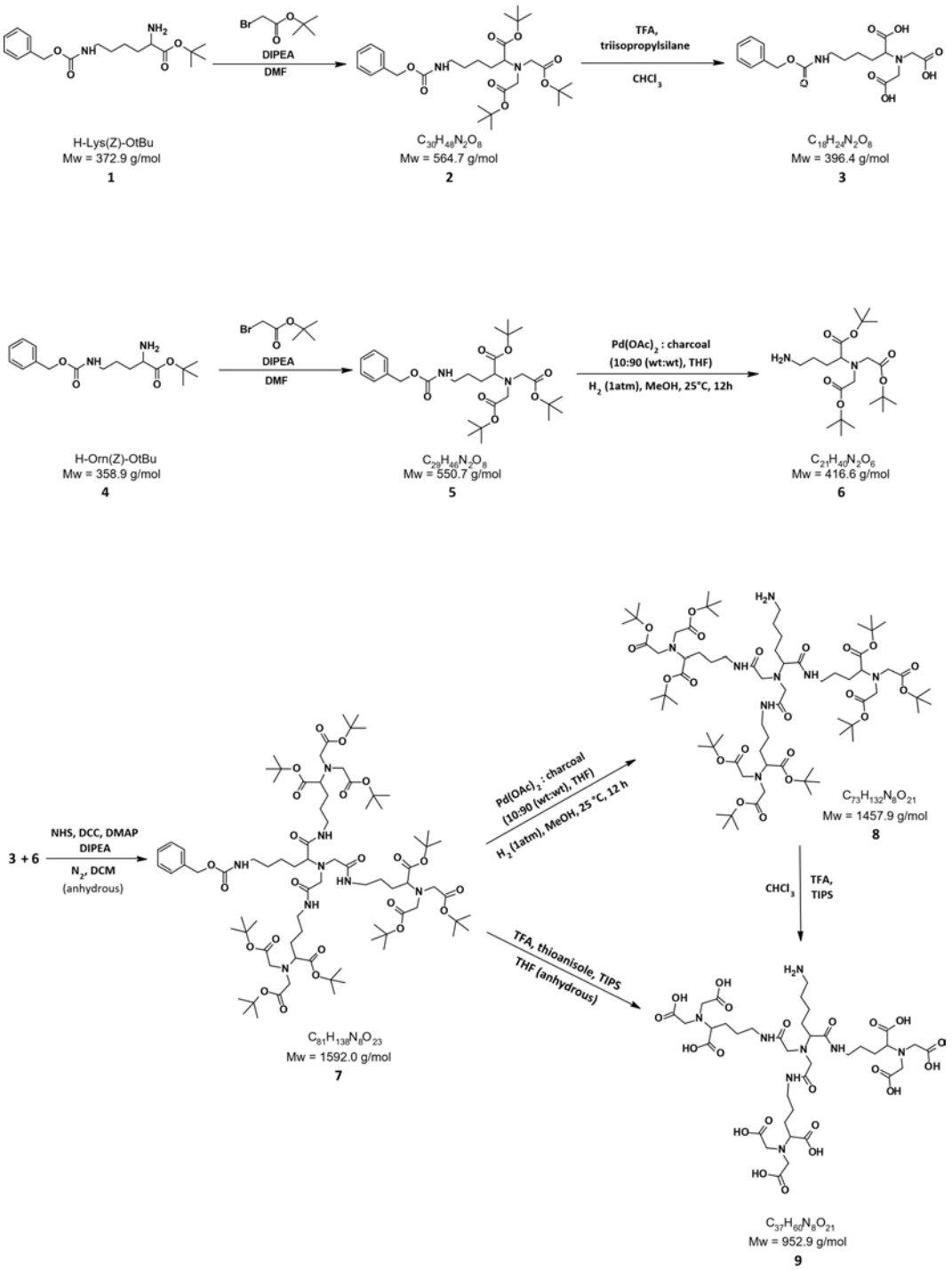

Figure 64: Synthesis scheme of trisNTA. trisNTA was synthesized according to this scheme as described in detail in section 3.7.

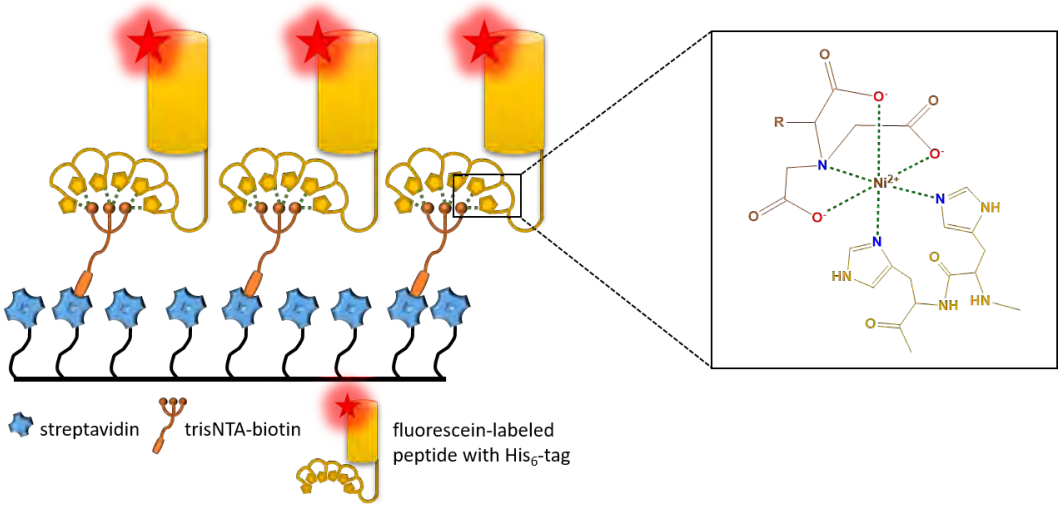

Figure 65: Testing the two functionalities of trisNTA by immobilization of trisNTA-PEG$_4$-biotin in streptavidin-coated wells. trisNTA-PEG$_4$-biotin (orange) was immobilized in streptavidin-coated wells (streptavidin: blue). A fluorescently labeled (red star), hexahistidine-tagged peptide (yellow) was bound to trisNTA via Ni^{2+}.

available lysineNTA (LysNTA; N_α,N_α-bis(carboxymethyl)-L-lysine hydrate; CAS: 941689-36-7) was biotinylated (lysNTA-biotin; molecular structure: supplementary figure S15 on page 211) the same way as trisNTA-biotin.

trisNTA-biotin was subsequentially immobilized in 96-well plates coated with streptavidin as shown in figure 65, as well as LysNTA-biotin and commercially available biotinylated mono-NTA (Biotin-X-NTA; N_ε-(N-(+)-biotinyl-6-aminohexanoyl)-N_α,N_α-bis(carboxymethyl)-L-lysine; CAS: 856661-92-2).

Subsequently, a hexahistidine-tagged and fluorescently labeled (tetramethylrhodamine, TMR) peptide (amino acid sequence: AKAGEH$_6$AE, TMR on N-terminus) was added to the immobilized NTA variants in the presence or absence of Ni^{2+}. In all conditions, the NTA variants were first depleted from divalent cations by extensive washing with EDTA (100 mM). For Ni^{2+}-containing conditions, the NTA variants were subsequently loaded with an excess of Ni^{2+} (100 mM). After loading, residual free Ni^{2+} was removed by washing with buffer. After incubation of the His-tagged peptide for 30 min, unbound peptide was washed away with buffer (3 x 200 µl), and TMR fluorescence was measured in a 96-well plate reader. As shown in figure 66, in the presence of Ni^{2+}, all three variants of immobilized NTA were binding the hexahistidine-tagged peptide as expected, while the absence of Ni^{2+} did not allow binding. Immobilized trisNTA-biotin bound equal amounts of the peptide as the

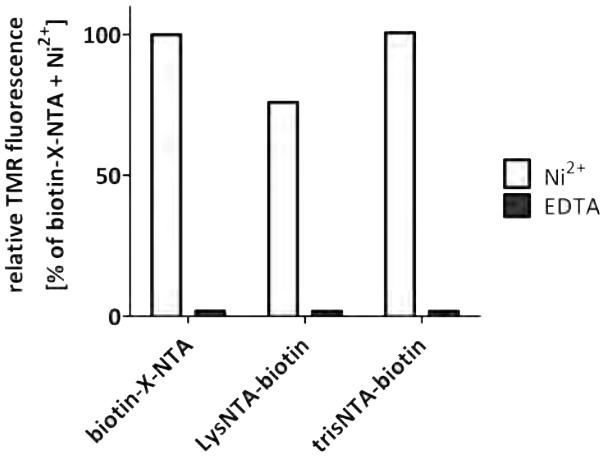

Figure 66: trisNTA-biotin immobilized in streptavidin-coated wells. trisNTA-biotin, and LysNTA-biotin and biotin-X-NTA (positive controls), were immobilized in streptavidin-coated wells as described in figure 65, and loaded with a fluorescently labeled (TMR) hexahistidine-tagged peptide (AKAGEH_6AE, TMR on N-terminus) in the presence (Ni^{2+}, white) or absence (EDTA, black) of Ni^{2+}. After unbound peptide had been washed away, TMR fluorescence was measured.

purchased positive control biotin-X-NTA, while LysNTA-biotin was slightly less efficient. This experiment shows that both functionalities (-NH_2 and NTA) are present, accessible, and fully functional in our trisNTA-NH_2 (**9**).

In a second test experiment, trisNTA-NH_2 (**9**) was immobilized on NHS-activated agarose beads, allowing characterization of trisNTA in column-format. Using these trisNTA-agarose beads we aimed to test the release of His-tagged peptide from trisNTA. Additionally, beads were also treated with ethanolamine as a negative control, where no trisNTA is present. The two agarose bead populations were then either used in the presence or absence of Ni^{2+}. Then, the afore used hexahistidine-tagged, TMR-labeled peptide AKAGEH_6AE was added and incubated for 30 min on the resin. After extensive washing with buffer containing 20 mM imidazole to prevent unspecific binding, the imidazole concentration was increased to 500 mM to elute bound peptide.

As shown in figure 67, of all four conditions, the peptide was efficiently bound only in the presence of Ni^{2+} on agarose beads on which trisNTA was immobilized, and bound peptide was finally eluted using 500 mM imidazole. In the absence of Ni^{2+} (EDTA) or in absence of trisNTA, no binding of the peptide was observed, confirming the findings of the trisNTA-biotin-based assay above. Such trisNTA-agarose beads

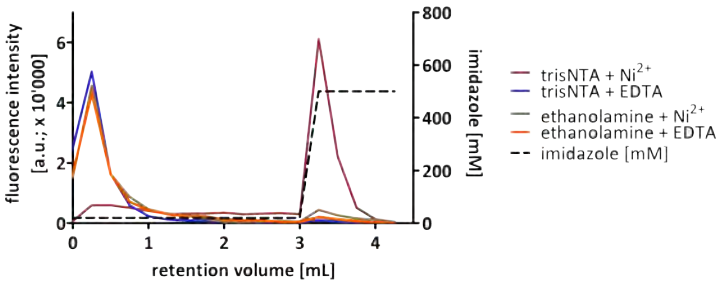

Figure 67: trisNTA immobilized on agarose beads. trisNTA was immobilized on agarose beads and loaded with a fluorescently labeled (TMR) hexahistidine-tagged peptide (AKAGEH_6AE, TMR on N-terminus) in the presence (Ni^{2+}, red) or absence (EDTA, blue) of Ni^{2+}. After unbound peptide had been washed away by 20 mM imidazole, bound peptide was eluted using 500 mM imidazole. Further, ethanolamine-quenched beads without trisNTA were used in presence (brown) or absence (orange) of Ni^{2+} as a control to exclude the possibility of observed peptide binding being a result of unspecific interactions of the peptide with the agarose beads themselves. Black, dashed: imidazole concentration.

could be used for efficient protein affinity purification in rare cases, where commonly used Ni-NTA affinity chromatography was not successful, or in other applications requiring high binding affinity.

Finally, we wanted to test if trisNTA-NH_2 (**9**) could be coupled to LSUs functionalized with carboxylic acid groups in future experiments. For this purpose, trisNTA-NH_2 (**9**) was immobilized on metallic magnetic beads with biocompatible surface chemistry PEG-brushes with carboxy-functionality by EDC-mediated coupling. The molecular structure of EDC (1-ethyl-3-(3-dimethylaminopropyl)carbodiimide HCl) as well as the reaction mechanism of EDC-mediated crosslinking of carboxylic acids to primary amines are illustrated in figure 68 on the next page. Additionally, magnetic beads were also coated with LysNTA for comparison. The two metallic magnetic bead populations were then either used in the presence or absence of Ni^{2+}. Then, the hexahistidine-tagged, TMR-labeled peptide AKAGEH_6AE was added and incubated for 30 min on the resin. After extensive washing with buffer containing 20 mM imidazole to prevent unspecific binding, the imidazole concentration was increased to 500 mM to elute bound peptide.

As shown in figure 69A, of all four conditions, the peptide was efficiently bound only in the presence of Ni^{2+} on metallic magnetic beads on which trisNTA or LysNTA were immobilized, and bound peptide was finally eluted using 500 mM imidazole. In the absence of Ni^{2+} (EDTA) or in absence of tris- or LysNTA, no binding of the peptide was observed, confirming the findings of the agarose bead-based assay above.

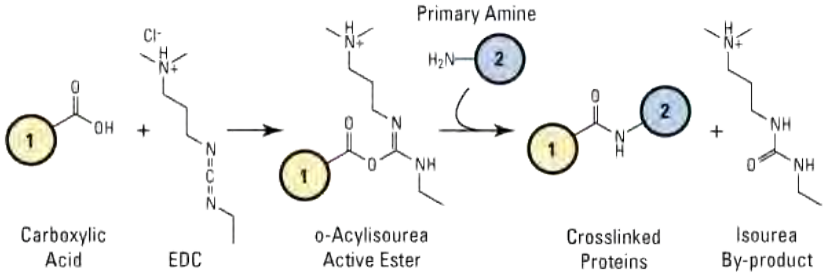

Figure 68: EDC (carbodiimide) crosslinking reaction scheme. Carboxyl-to-amine crosslinking with the popular carbodiimide, 1-ethyl-3-(3-dimethylaminopropyl)carbodiimide HCl (EDC; M_w: 191.7 g mol^{-1}). Molecules 1 and 2 can be peptides, proteins or any chemicals that have respective carboxylate and primary amine groups. When they are peptides or proteins, these molecules are tens-to-thousands of times larger than the crosslinker and conjugation arms diagrammed in the reaction. In the case under consideration, 1 represents the functionalized magnetic beads, while 2 represents trisNTA-NH_2 (**9**). To prevent intramolecular crosslinking of the primary amine and the carboxylic acid groups of trisNTA-NH_2, before addition of trisNTA-NH_2 to the EDC-activated beads, unreacted EDC was removed. Figure from ThermoFisher Scientific.

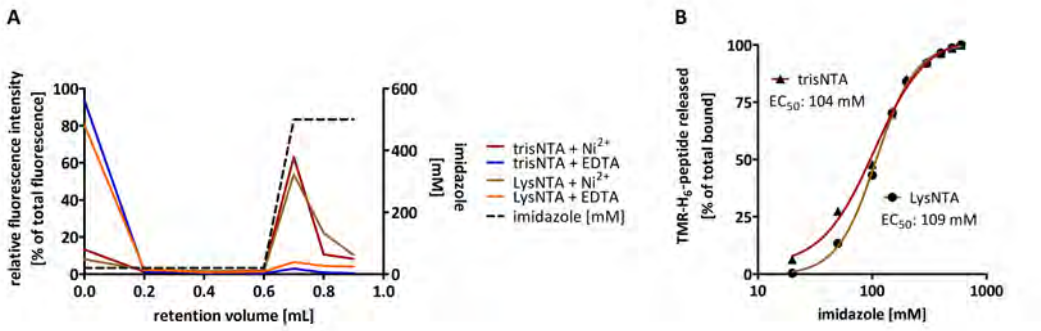

Figure 69: Releasing a hexahistidine-tagged peptide from immobilized trisNTA. (A) trisNTA was immobilized on magnetic beads via EDC-mediated coupling, and loaded with a fluorescently labeled (TMR) hexahistidine-tagged peptide (AKAGEH_6AE, TMR on N-terminus) in the presence (Ni^{2+}, red) or absence (EDTA, blue) of Ni^{2+}. After unbound peptide had been washed away by 20 mM imidazole, bound peptide was eluted using 500 mM imidazole. Further, LysNTA was immobilized on magnetic beads as well and subjected to the same experiment in presence (brown) or absence (orange) of Ni^{2+} for comparison. Black, dashed: imidazole concentration. (B) Dose-response curves describing the release of the hexahistidine-tagged peptide from the immobilized NTA variants by imidazole. Fitting: 4-parametric fit with variable slope, GraphPad Prism. EC_{50} values: trisNTA: 104 mM, LysNTA: 109 mM. Colors as in (A).

In a follow-up experiment, we added increasing amounts of imidazole and monitored the amounts of released peptide in the supernatant. This allowed us to observe the dose-dependent release of the peptide from the trisNTA- and LysNTA-coated metallic magnetic beads (figure 69B). Both resins were eluted with with EC_{50} values of ∼100 mM.

Because of the difference in affinity of trisNTA and mono-NTA towards hexahistidine-tags, on first sight, it might be counterintuitive that the two EC_{50} are identical. However, as illustrated in figure 63A, trisNTA via Ni^{2+} binds to hexahistidine-tags in a trivalent manner, while LysNTA binds monovalently. As discussed in section 4.5.1, dissociation of multivalent interactions (hexahistidine-tag / trisNTA) can be accelerated by diminishing their stability to that of the monovalent interaction (histidine / mono-/LysNTA) by addition of a monovalent ligand (e. g. imidazole) capable of competing for the binding sites.[287] Consequently, hexahistidine tags can be dissociated from trisNTA as efficiently as from mono-/LysNTA, under the same mild conditions by addition of competitors such as imidazole [276], resulting in equal EC_{50} values.

First, these experiments showed that the synthesized trisNTA does successfully bind hexahistidine tags via Ni^{2+}. Second, we were able to couple trisNTA-NH_2 via its primary amine to molecules either having a free or activated (NHS-ester) carboxylic acid. The next step was therefore to find a suitable LSU to be coupled to the primary amine of trisNTA-NH_2.

4.5.4 Attempts to Couple trisNTA to Different LSUs.

As discussed earlier in this thesis, LSUs should be hydrophilic and unable to pass the membrane. To unidirectionally reconstitute the *bo₃* oxidase to exclusively import protons into liposomes, the hydrophilic C-terminal domain of subunit II (∼23 kDa), which in *E. coli* is exposed to the periplasm [292–294], needs to cross the liposomal membrane to eventually be located in the lumen. Therefore, we speculated that potential LSUs to guide orientation of *bo₃* oxidase should have at least the same size (i. e. ≥23 kDa) as the periplasmic domain of subunit II. We tried to couple a wide variety of LSUs to trisNTA; in the following, a selection of such attempts is discussed.

trisNTA-beads.

Pfleger *et al.* [13] used Ni-NTA-coated silicate praticles with a diameter of 200 nm for unidirectional reconstitution of pR into preformed, partially detergent-solubilized liposomes with a diameter of 200 nm. Their size prevents the silicate beads to be

incapsulated in the liposomes, consequently enforcing unidirectional reconstitution of immobilized pR (for more detailed information see section 1.7.2). This inspired us to couple trisNTA to different beads serving as potential LSUs. Considering the size of potential bead candidates, there are generally two options. Either rather small beads in the intended size range of the used LUVs (in our case: 100 nm) are used, or much bigger beads with diameters of up to 30 µm, appearing as flat surfaces from the point of view of the reconstituted LUVs. We followed the strategy of Pfleger *et al.* [13] who have decided for the first option.

Two variants of beads were intended to be used therefor: NHS-activated silica beads as well as the NHS-activated agarose beads described above (figure 67).

First, we coupled our trisNTA-NH_2 to NHS-coated silica beads of a diameter of 300 nm, but this approach was only partially successful. Even though we were able to observe binding of hexahistidine-tagged pR and aa_3 cytochrome c oxidase (aa_3 CcO) from *Rhodobacter sphaeroides* to trisNTA immobilized on those beads, the amounts of protein bound were low (not shown). A reason for this could be that coupling of trisNTA-NH_2 to the NHS-coated silica beads was not as efficient as expected. Further, while Pfleger *et al.* [13] used mono-NTA featuring three carboxylic acid groups, we were trying to couple trisNTA containing nine carboxylic acid groups to the beads. This high number of carboxylic acid groups may lead to electrostatic repulsion from the surface of the silica beads, thus preventing trisNTA-NH_2 from approaching the NHS-functionalized beads and consequently from coupling.

Alternatively, the NHS-activated agarose beads described above were used. As shown in figure 67, coupling of trisNTA to these agarose beads worked and a hexahistidine-tagged peptide was successfully bound and also released thereof. However, when it was tried to reconstitute pR coupled to these trisNTA-agarose beads into preformed, partially detergent-solubilized liposomes we always failed. In each try pR visibly precipitated during detergent removal. This indicated that the MP was not inserted properly into the liposomal bilayer during reconstitution. A possible reason therefor might be that the density of immobilized pR on the trisNTA-agarose beads' surface was too high, allowing only a minority of pR molecules to be inserted into approaching liposomes of a diameter of comparable size to the diameter of the beads for sterical reasons; this however remains speculation.

trisNTA-dextran Variants.

Due to the previously failed attempts, as a next LSU to be tested, more structurally flexible dextrans were used. As described in section 4.2.5, the supposedly mono-

functionalized dextrans were not satisfyingly mono-functional, but we nevertheless gave it a try. Therefore, "mono"-carboxy dextrans of various sizes (70 - 2000 kDa) were coupled via EDC-mediated coupling (reaction mechanism: figure 68) to the primary amine of our trisNTA-NH_2 (**9**). To prevent intramolecular crosslinking of the primary amine and the carboxylic acid groups of trisNTA-NH_2, before addition of trisNTA-NH_2 to the EDC-activated dextrans, unreacted EDC was removed by SEC using PD-MiniTrap G-25 desalting columns. With a 70 kDa mono-carboxy dextran (DEX70k) coupled to trisNTA (trisNTA-DEX70k), the hexahistidine-tagged, TMR-labeled peptide ($\sim$2 kDa) introduced in section 4.5.3 was incubated with trisNTA-DEX70k in the presence of Ni^{2+}, and subsequently subjected to SEC (PD-MiniTrap G-25 desalting column; exclusion size: $\geq$5 kDa) before assessing TMR-fluorescence (figure 70). Attachment of trisNTA-DEX70k via Ni^{2+} leads to an increase in molecular weight of the fluorescently labeled peptide, allowing it to pass through the column. However, only $\sim$24 % of the initially applied peptide were eluted from the SEC column, indicating either loss of binding between the peptide and trisNTA-DEX70k, or low yields of the coupling of trisNTA-NH_2 to DEX70k. Low yields of coupling might be owed to steric hindrance of the coupling by the large bulky dextran. In the absence of either Ni^{2+} (EDTA) or trisNTA-DEX70k (not shown), no fluorescence could be detected after SEC. This experiment enabled us to draw two conclusions. First, trisNTA-NH_2 was successfully coupled to DEX70k, however possibly with low yields. Second, trisNTA-DEX70k was binding the hexahistidine-tagged peptide in the presence of Ni^{2+}, even though binding might be lost during SEC. Repetition of the same experiment using a bigger mono-carboxy dextran of 500 kDa failed repeatedly, supporting the speculation that sterical hindrance might be the reason for low coupling yields of dextrans to trisNTA-NH_2.

Further, the binding of the hexahistidine-tagged peptide via Ni^{2+} to trisNTA-DEX70k was not standing SEC-mediated purification using common columns as Superdex 200 Increase 5/150 GL or Superdex 200 Increase 10/300 GL under pressure ($\leq$3 MPa; not shown), even though the contrary has been reported for the interaction between trisNTA and hexahistidine tags by using Superdex 200 HR 10/30 at lower pressure ($\leq$1.5 MPa).[289, 295]

In order to improve the coupling yield of trisNTA-NH_2 (**9**) and monocarboxy-dextrans, we aimed to use TCO/tetrazine click chemistry.

Click chemistry conjugation reactions are known for their bio-orthogonality, high reaction rates, exquisite specificity, and high yields.[296–298] Using click chemistry reactions, two molecules can be conjugated specifically under aqueous physiological

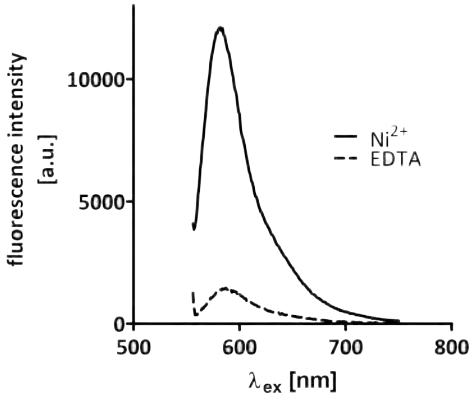

Figure 70: Binding a TMR-labeled, hexahistidine-tagged peptide with trisNTA-DEX70k. The TMR-labeled, hexahistidine-tagged peptide introduced earlier was bound to trisNTA-DEX70k in the presence (continuous trace, Ni^{2+}) or absence (dashed trace, 100 mM EDTA) of Ni^{2+}. Unbound peptide was removed by SEC using a PD-MiniTrap G-25 desalting column followed by release of bound peptide by EDTA and eventually assessing fluorescence of the eluted peptide.

conditions.[299] While the original click chemistry reactions between azide and nitrile groups required copper (Cu(I)), more recent reaction types are free from potentially harmful Cu(I) and thus non-toxic, allowing their application e. g. on cell surfaces or for biomedical applications.[300, 301]

Therefore, the inverse electron-demand Diels-Alder reaction between tetrazine (tet) and trans-cyclooctene (TCO) (reaction scheme: figure 71A) was selected, which has a reaction rate of $k > 10^3\,M^{-1}s^{-1}$.[296, 302–304] trisNTA-NH_2 (**9**) was coupled to methyltetrazine-PEG_4-NHS ester (figure 71B), while the amino-functionalized dextrans intended to act as LSUs were coupled to TCO-PEG_4-NHS ester (figure 71C). This would offer the possibility of setting up a library of different dextrans coupled to TCO, each of which may be clicked to trisNTA-tet, knowing that the final coupling, i. e. the click reaction, would not be the limiting step.

Using the example of the click product trisNTA-tet-TCO-DEX40k10, the drawbacks of this method are illustrated. DEX40k10 is a dextrane of 40 kDa in size with 10 functional amino groups, thus 10 TCO moieties can be coupled to it, consequently leading to 10 click reactions with trisNTA-tet. In other words, per dextran unit, ten hexahistidine-tagged peptides could potentially be bound via Ni^{2+} to trisNTA and eventually to the dextran unit. Using the assay introduced above for investigation of binding of TMR-labeled, hexahistidine-tagged peptide by trisNTA-DEX70k, it

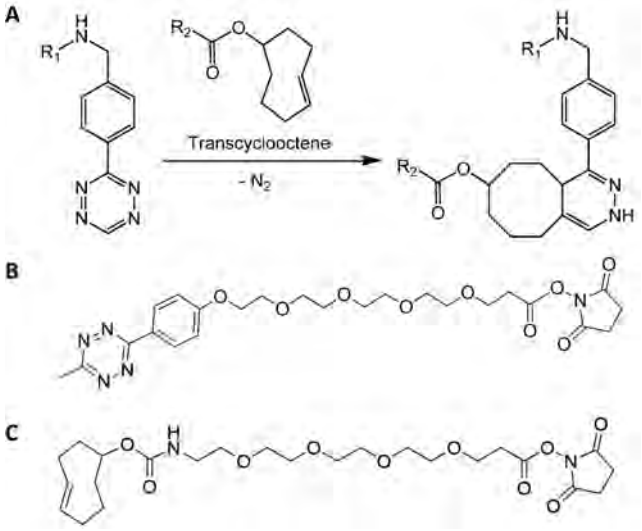

Figure 71: Copper-free click chemistry: tetrazine & TCO. (A) Inverse electron-demand Diels-Alder [4 + 2] cycloaddition click ligation between tetrazine and trans-cyclooctene (TCO) Figure adapted from [304]. (B) methyltetrazine-PEG_4-NHS ester (M_w: 533.53 g mol^{-1}). Figure adapted from Click Chemistry Tools. (C) TCO-PEG_4-NHS ester (M_w: 514.57 g mol^{-1}). Figure adapted from Click Chemistry Tools.

was shown that trisNTA-tet-TCO-DEX40k10 is indeed able to bind His-tags in the presence of Ni^{2+} (figure 72). However, considering the low amounts (∼11 %) of peptide eluted from SEC with respect to the initially applied amounts, it had to be concluded, that coupling of DEX40k10 to TCO, and / or coupling of trisNTA to tet was / were of lower efficiency than expected, consequently also the click reaction resulted in low yields. In the absence of either Ni^{2+} (EDTA) or trisNTA-DEX40k10 (not shown), no fluorescence could be detected after SEC.

Anyway, the list of problems in using dextrans as LSUs, started already in section 4.2.5, was obviously prolonged. Therefore, it was decided to not consider dextrans as possible LSUs anymore, along with the additional decision to not investigate on ficolls as LSUs, for which the same issues have to be expected as observed with dextrans.

An interesting byproduct of these experiments using click chemistry was trisNTA-Cy5, the click product between trisNTA-tet and the fluorescent Cy5-TCO, which was used as a test reaction for monitoring the efficiency of the click reaction between TCO and trisNTA-tet. We suggest that trisNTA-Cy5 can be used as a fluorescent probe for hexahistidine-tagged peptides and proteins in a wide variety of applications as western blotting, or fluorescence microscopy to localize target proteins, to name a few; however, we have not investigated further on trisNTA-Cy5.

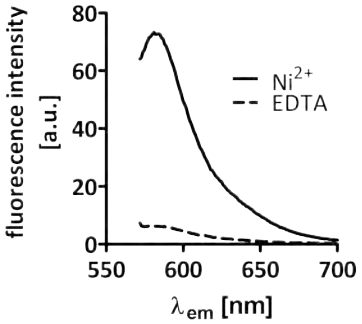

Figure 72: Binding a TMR-labeled, hexahistidine-tagged peptide with trisNTA-tet-TCO-DEX40k10. The TMR-labeled, hexahistidine-tagged peptide introduced earlier was bound to trisNTA-tet-TCO-DEX40k10 in the presence (continuous trace, Ni^{2+}) or absence (dashed trace, 100 mM EDTA) of Ni^{2+}. Unbound peptide was removed by SEC using a Z-50 CentriPure MINI Spin Column.

trisNTA-PEG Variants.

After the unsatisfying results with (mono-)functionalized dextrans, we switched to chemically more defined LSU molecules, namely NHS-activated PEGs. In contrast to dextrans, PEGs are linear and the maximal size available is around 20 - 30 kDa.

An NHS-activated PEG of a size of 20 kDa (PEG20k) was coupled to trisNTA-NH_2 (**9**) (trisNTA-PEG20k). trisNTA-PEG20k in PBS (pH 7.4) was incubated for 10 min with a 30-fold excess of Ni^{2+}, and free Ni^{2+} was removed by SEC (PD-MiniTrap G-25 desalting columns). Ni^{2+}-loaded trisNTA-PEG20k was then complexed to hexahistidine-tagged pR (pR-CHis; see table 6 on page 56) in buffer containing DDM (20 mM HEPES pH 7.4, 300 mM NaCl, 0.04 % DDM) by incubation at 25 °C for 1 h. The mixture was then subjected to SEC analysis using a Superdex 200 Increase 5/150 GL ($\leq$3 MPa) column in the same buffer. Compared to previous experiments, a smaller SEC column of the same column material was used here, but the same flowrate was applied as with the previous column (Superdex 200 Increase 10/300 GL), resulting in approximately the same column pressure according to the manufacturer's instructions.

As illustrated in figure 73 on the next page, it could be shown that trisNTA-PEG20k indeed binds via Ni^{2+} to the His-tag of pR, and thus its pR-containing peak is shifted towards higher molecular weight in SEC compared to free pR. Surprisingly, the complex hexahistidine-tag-Ni^{2+}-trisNTA endured SEC under pressure, in contrast to our previous results, but in agreement with [289, 295].

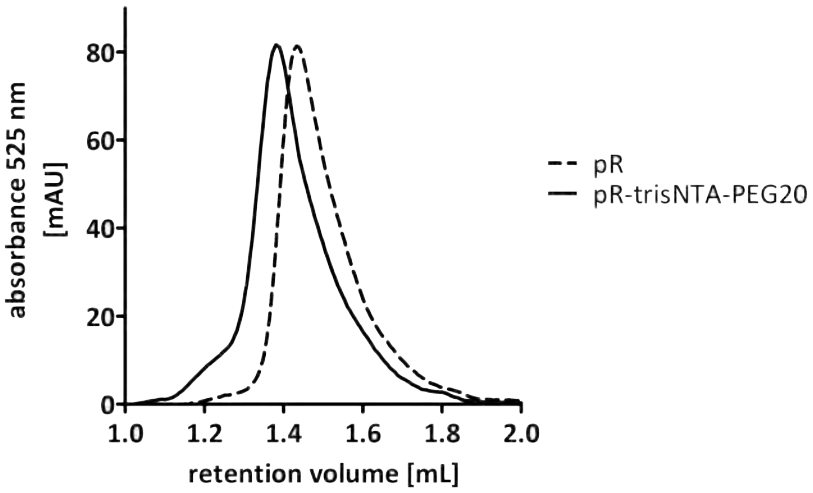

Figure 73: SEC analysis of hexahistidine-tagged pR bound to trisNTA-PEG20k. Hexahistidine-tagged pR was bound to trisNTA-PEG20 via Ni^{2+} and subsequently analyzed by SEC using a Superdex 200 Increase 5/150 GL column. The resulting chromatogram (continuous trace) was compared to a chromatogram where pure pR was analyzed by SEC under the exact same conditions (dashed trace). Buffer: 20 mM HEPES, pH 7.4, 300 mM NaCl, 0.04 % DDM. y-axis: absorbance of pR at 525 nm.

However, any attempts to influence orientation of His-tagged pR labeled with trisNTA-PEG20k failed (not shown)[1], and two reasons are discussed. First, a LSU of 20 kDa might just not be large enough to significantly influence the orientation of pR during reconstitution. Second, these experiments were done prior to the more successful experiments with the SpyTag-SpyCatcher system described earlier in this thesis (see section 4.3). In these later experiments, different reconstitution protocols were used that might have influenced the outcome. The measurements with trisNTA-PEG20k have not been tested with these optimized conditions.

Further, a LSU of 20 kDa will certainly not be sufficiently large to influence orientation of bo_3 oxidase, which has a natural hydrophilic domain of similar size (∼23 kDa) on the C-terminus of subunit II [292–294].

[1] Proton pumping of reconstituted pR-N/CHis and pR-N/CHis-trisNTA-PEG20k measured with pyranine assay. Liposomes: 10 mg ml^{-1} 90 % lecithin, soybean; 100 nm; in 2 mM MOPS pH 7.4, 50 mM K_2SO_4; reconstitution: 0.4 % cholate, in presence of 3 mM pyranine, 30 min; removal of detergent & external pyranine: SEC (CentriPure P10 desalting columns).

trisNTA-biotin-SA-(PEG30k)$_3$.

A next idea was to use a composition of trisNTA-biotin introduced in section 4.5.3 and an LSU consisting of streptavidin-(PEG30k)$_3$ manufactured as described in section 4.2.5. SEC-purified SA-(PEG30k)$_3$ (see figure 35 on page 87) was incubated for 16 h at 20 °C with a 5-fold excess of trisNTA-biotin. Finally, excess free trisNTA-biotin was removed by SEC using a CentriPure P10 desalting column.

The resulting trisNTA-biotin-SA-(PEG30k)$_3$ was incubated with two different pR variants with a His-tag on either the N- or the C-terminus (pR-NHis and pR-CHis) in the presence of Ni^{2+} for 16 h at 20 °C. The mixture was subsequently subjected to SEC analysis (column: Superose 6 Increase 10/300 GL). However, by monitoring absorption of pR at 525 nm, no LSU-induced shift of pR to higher molecular weight was detected (not shown). This allows to draw three different conclusions. First, it is possible that trisNTA-biotin was not successfully bound to SA-(PEG30k)$_3$. Second, if trisNTA-biotin was bound to SA-(PEG30k)$_3$, it possibly failed to complex hexahistidine-tagged pR via Ni^{2+}. Third, if coupling of pR via Ni^{2+} to trisNTA-biotin-SA-(PEG30k)$_3$ was successful, the interaction might has been lost during SEC. The dissociation of trisNTA and hexahistidine-tags has been discussed further above. The same results were obtained by using a different version of trisNTA-biotin, consisting of a trisNTA constituted of a more rigid tetraaza cyclam scaffold (compare to section 4.5.2; aliquot obtained from Oliver Birkholz, research group of Prof. Dr. J. Piehler, University of Osnabrück, Germany).

Nevertheless, the mixtures of pR-NHis or pR-CHis and trisNTA-biotin-SA-(PEG30k)$_3$ were reconstituted into preformed, partially detergent-solubilized liposomes as described in [1] on page 150. However, no changes in orientation were observed by labeling of His-tagged pR with trisNTA-biotin-SA-(PEG30k)$_3$ (not shown). Consequently, no further investigations on trisNTA-biotin-SA-(PEG30k)$_3$ were executed.

4.5.5 Conclusions to the trisNTA System.

A dendritic version of trisNTA was successfully synthesized and thereafter characterized. To verify the bifunctionality of trisNTA-NH_2 it was coupled via its primary amine to NHS-activated coupling partners and by EDC-mediated coupling to partners with carboxy functionality. By specifically binding hexahistidine-tagged peptides and MPs via Ni^{2+}, also the second functionality was verified. Further, the release of a bound hexahistidine-tagged peptide was characterized, showing that the interaction

between our synthesized trisNTA and hexahistidine-tags can be dissociated under mild conditions using imidazole.

Coupling of trisNTA to a variety of potential LSUs as silica or agarose beads, dextrans, or PEGs has been tested. While with some potential LSUs already coupling to trisNTA was an almost insuperable obstacle (silica beads, dextrans), other candidates were coupled successfully to trisNTA, however they either obstructed reconstitution of the bound MP (agarose beads), or did not influence orientation of reconstituted MP (PEGs, trisNTA-biotin-SA-$(PEG30k)_3$).

Synthesis of trisNTA and all trisNTA-related experiments described in this section were carried out in the very beginning of my time in the lab. After encountering the described difficulties in testing potential LSUs, we decided to put the trisNTA system aside for a while. Instead, we focused first on the AviTag system (section 4.2) and later on the SpyTag-SpyCatcher system (section 4.3) to unidirectionally reconstitute bo_3 oxidase and pR. Only after having successfully orientated pR using the covalent Spy-TagSpyCatcher system, we resorted to trisNTA by combining the trisNTA-based approach with the SpyTag-SpyCatcher system, resulting in the trisNTA-Spy approach described in section 4.6.

4.6 Approach IV – General Approach Using trisNTA-Spy.

4.6.1 Introduction to trisNTA-Spy.

On one hand, the SpyTag-SpyCatcher system was successfully applied to unidirectionally reconstitute pR, however it has two major drawbacks (see section 4.3.13). First, it requires genetic modification of the MP of interest to introduce the SpyTag at a suitable position. Second, the interaction between the SpyTag of the MP and the SpyCatcher of the LSU is covalent. While this is advantageous by preventing loss of the LSU until the MP-LSU construct is reconstituted into liposomes, it becomes a disadvantage after reconstitution. There is no possibility to detach the LSU from the MP after reconstitution, except for proteolytic cleavage between the MP and its LSU. The trisNTA system on the other hand would enable mild and quick dissociation of trisNTA-LSUs from the His-tag of reconstituted MPs (see section 4.5.1), but it confronted us with problems in coupling potential LSUs to trisNTA-NH_2 (see section 4.5.5).

Consequently, we aimed to circumvent the disadvantages of both individual approaches by combining them and exploiting their advantages instead. For this purpose, we wanted to synthesize a SpyTag peptide and conjugate it to trisNTA, resulting in a new bifunctional linker molecule (trisNTA-Spy; NTA-functionality, Spy-functionality). As illustrated in figure 74, by this means, trisNTA-Spy could be coupled to LSUs consisting of SpyCatcher fusion proteins (SC-LSUs), and the resulting trisNTA-Spy-SC-LSUs in turn could be complexed via Ni^{2+} to hexahistidine-tagged MPs to guide unidirectional reconstitution. After reconstitution, trisNTA-Spy-SC-LSUs could then be detached from reconstituted MPs under mild conditions using imidazole.

4.6.2 Synthesis of trisNTA-Spy.

We aimed to couple a synthesized SpyTag peptide to the primary amine of trisNTA. For this purpose, we decided to include a cysteine residue at the C-terminus of the SpyTag peptide, which can be coupled to the chloracetic anhydride-activated primary amine of trisNTA after peptide synthesis.

In a first step, two different variants of SpyTag peptides were manually synthesized using Fmoc solid phase peptide synthesis (general steps solid phase peptide synthesis: see figure 75; detailed procedure: see section 3.9). Both peptides consist of the SpyTag and a C-terminal cysteine residue designated as coupling point to trisNTA.

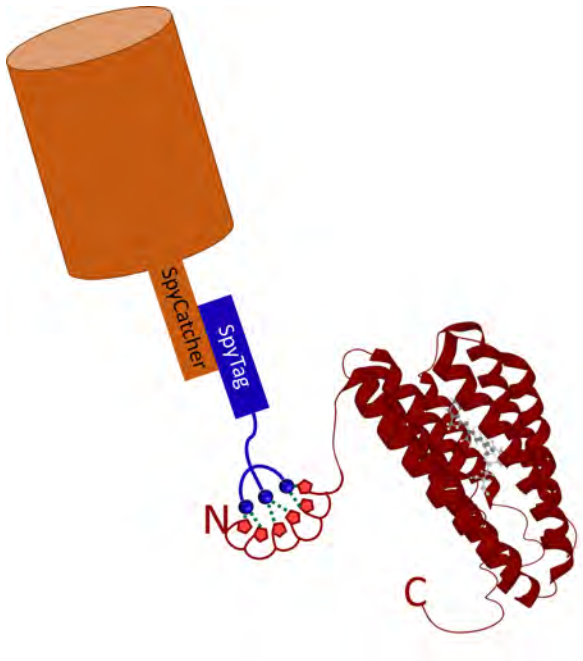

Figure 74: Schematic model of the trisNTA-Spy system. trisNTA attached to a synthetical SpyTag peptide (trisNTA-Spy, blue) can be coupled to any SC-LSU of choice (orange). The construct trisNTA-Spy-SC-LSU can then via Ni^{2+} be complexed to the properly positioned hexahistidine-tag on the MP of interest, here being represented by an N-terminal His-tag on pR (red, based on PDB: 2L6X; [20]). After reconstitution, the LSU can be removed from the MP under mild conditions by dissociation of the binding between trisNTA and the His-tag using imidazole, EDTA, or histidine. Figure not to scale.

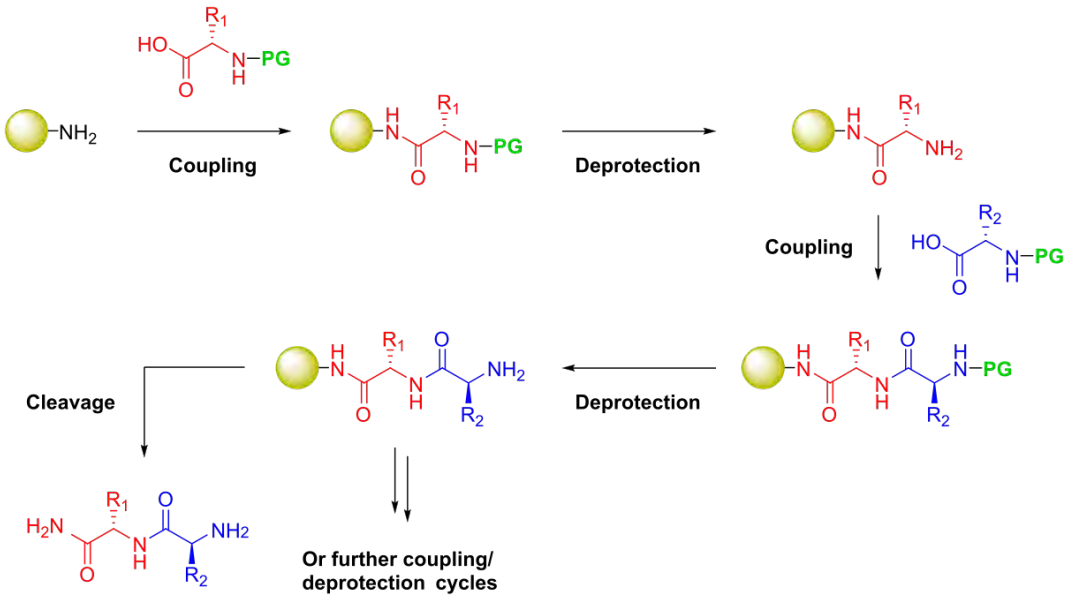

Figure 75: Solid phase peptide synthesis. General steps required to synthesize a peptide on solid phase as described by Merrifield [305]. The amine groups of the amino acids are protected by a protecting group (PG; in our synthesis: Fmoc), allowing for iterative deprotection. Potentially reactive side chain groups are also protected. Figure from: selekt.biotage.com.

One variant additionally contains a GSGS linker between the SpyTag and the C-terminal cysteine, while the other one does not, resulting in the two peptide sequences AHIVMVDAYKPTKC (SpyC, 14 amino acids) and AHIVMVDAYKPTKGSGSC (SpyGSGSC, 18 amino acids), respectively. After removal of Fmoc-protecting groups and cleavage from the solid support resin, the synthesized peptides were purified by preparative RP-HPLC and sequence identity was confirmed by ESI-MS. We thereby obtained 12.7 mg (yield: 25 %) and 4.5 mg (yield: 7.8 %) of the peptides SpyC and SpyGSGSC, respectively.

In a second step, as illustrated in figure 76, *tert*-butyl-protected trisNTA-NH_2 (**8**; compare to figure 64 on page 139) was activated with chloracetic anhydride (ClAc) to yield trisNTA-*t*Bu-ClAc (**10**; yield: 55.1 %), followed by purification by silica gel flash chromatography and analysis by ESI-MS and NMR. Subsequently, the carboxy groups of trisNTA-*t*Bu-ClAc (**10**) were deprotected to yield trisNTA-ClAc (**11**; yield: 33.9 %). Deprotected trisNTA-ClAc (**11**) was coupled to the cysteine residues of the two peptide variants. Finally, the resulting trisNTA-SpyC and trisNTA-SpyGSGSC were purified by RP-HPLC and analyzed ESI-MS, lyophilized and stored under an

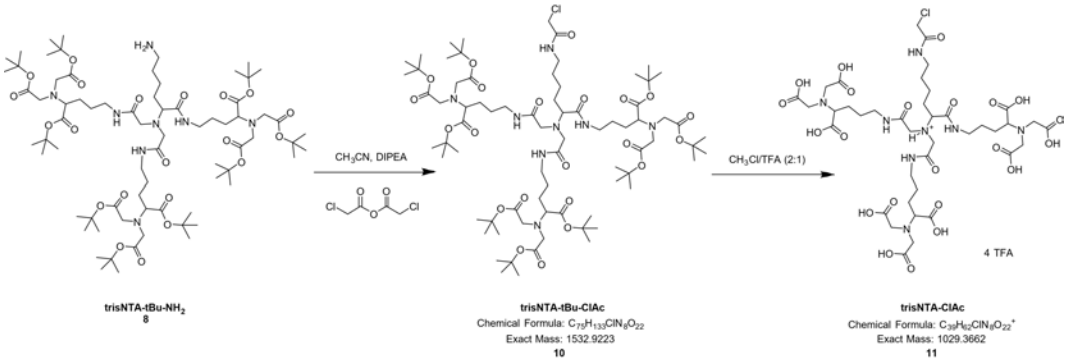

Figure 76: Activation of *t*Bu-trisNTA-NH$_2$ (8) with chloracetic anhydride. *tert*-butyl-protected trisNTA-NH$_2$ (**8**) was activated on its primary amine with chloracetic anhydride (ClAc).

inert atmosphere (Ar) until used in downstream applications (yields: trisNTA-SpyC: 38 %; trisNTA-SpyGSGSC: 36 %).

4.6.3 Functional Characterization of trisNTA-Spy.

trisNTA-Spy is a bifunctional molecule (NTA functionality, Spy functionality) whose two functionalities have to be tested.

In a first experiment, it was aimed to test whether trisNTA-Spy can be coupled to a SC-LSU, and if the coupling product trisNTA-Spy-SC-LSU can be complexed to His-tagged MPs via Ni^{2+}. Additionally, selectivity of trisNTA-Spy was to be tested towards MPs with or without His-tag. As SC-LSU, SC-ELP-GFP (SEG; see section 4.3.2) was chosen, because it can be immunoprecipitated by GFP-trap agarose resin consisting of a GFP nanobody coupled to agarose beads, thereby suggesting the strategy for this experiment. After coupling of trisNTA-Spy to SEG, the resulting trisNTA-Spy-SEG is incubated with different MPs with or without His-tag. Bound MPs can then be co-immunoprecipitated by GFP-trap agarose resin, eluted from trisNTA by incubation with EDTA, and subjected to SDS-PAGE analysis for comparison to remaining protein in the supernatant. However, since all our SC-LSU fusion proteins were purified by Ni-NTA affinity chromatography, the His-tag of SEG has to be removed prior to coupling to trisNTA-Spy to prevent intramolecular complexing.

The His-tag of SEG was cleaved off by TEV protease, before SEG was incubated with a 3-fold excess of trisNTA-SpyC for 3 h at 25 °C in aequous buffer (50 mM MOPS pH 7.0, 150 mM NaCl). trisNTA was subsequently loaded with Ni^{2+} by

incubation with a 10-fold excess of $NiSO_4$ for 10 min, before excess free Ni^{2+} and excess trisNTA-SpyC were removed by SEC (PD-MiniTrap G-25 desalting column). Resulting Ni^{2+}-loaded trisNTA-SpyC-SEG was then incubated with a ∼10-fold excess of different MPs with or without His-tag (pR-NSpy with His-tag; ATP synthase with His-tag; cytochrome bc_1 complex w/o His-tag (*R. sphaeroides*; provided by Roman Mahler); bo_3 oxidase w/o His-tag) in aequous buffer containing detergent (20 mM HEPES pH 7.0, 150 mM NaCl, 0.05 % DDM). Then, bound protein was co-immunoprecipitated by incubation with GFP-Trap agarose affinity resin for 1 h. After centrifugation to pellet the resin, unbound protein in the supernatant was removed and stored for later analysis. After washing with buffer (3 x 17 CV), the resin was incubated for 30 min with EDTA (100 mM) in buffer (2 CV) to elute co-immunoprecipitated protein from immobilized trisNTA-SpyC-SEG. Eluted protein (figure 77B) as well as the previously stored supernatants containing unbound protein (figure 77A) were then subjected to SDS-PAGE analysis.

As shown in figure 77B, only MPs containing a His-tag (lanes 2 & 4) were bound by immobilized trisNTA-SpyC-SEG, while MPs without His-tag (lanes 1 & 3) were not. In lane 2 (pR-NSpy with His-tag), the monomer plus a dimer formation of pR can be found in both, the supernatant and the elution.

These results allow to draw multiple conclusions. First, trisNTA-SpyC was successfully coupled to SEG, thus confirming the SpyTag functionality of trisNTA-SpyC. Second, trisNTA-SpyC-SEG can complex His-tagged MPs via Ni^{2+}, hence confirming the second functionality of trisNTA-SpyC. Third, trisNTA-SpyC is specific for His-tags, since trisNTA-SpyC-SEG did not unspecifically bind to any MPs without His-tag.

An alternative experiment to address these issues would have been to complex trisNTA-SpyC via Ni^{2+} to a hexahistidine-tagged peptide immobilized on agarose bead resin. By subsequent incubation of SEG with the resin, immobilized trisNTA-SpyC-SEG could be formed, and determination of GFP fluorescence of the flowthrough containing unbound SEG would allow to quantify the reaction efficiency of the SpyTag-SpyCatcher coupling. Eventually, binding affinity of trisNTA to hexahistidine tags could be analyzed by elution of trisNTA-SpyC-SEG from the bead-immobilized His-tag with increasing concentrations of imidazole, histidine, or EDTA. However, we did not have any resin with immobilized hexahistidine-tagged peptide at hand, and we especially wanted to monitor binding of trisNTA-SpyC-SEG not to a His-tagged peptide, but to His-tagged MPs, since this was the designation of trisNTA-SpyC-SEG.

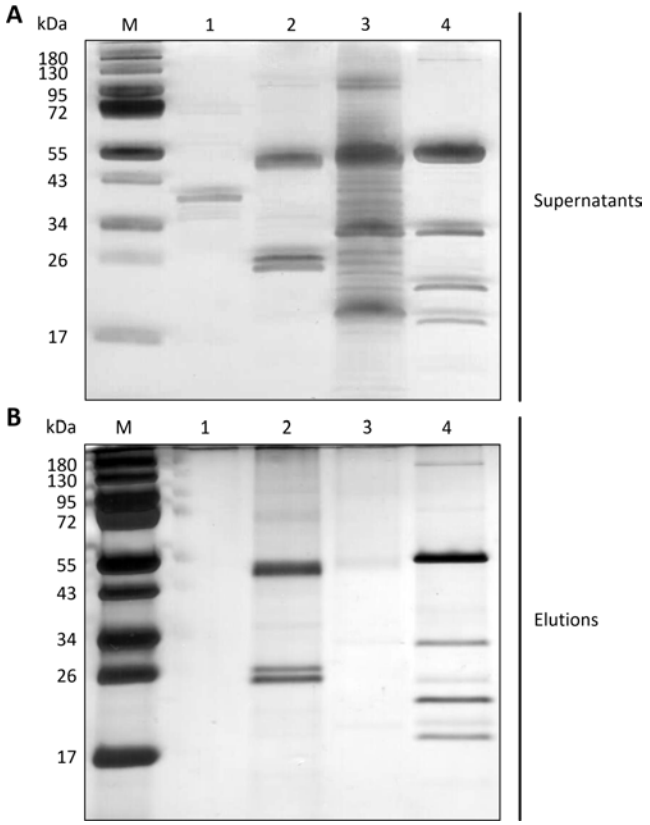

Figure 77: Testing bifunctional trisNTA-Spy in a GFP-co-immunoprecipitation assay. MPs with or without His-tag were presented to trisNTA-SpyC-SC-ELP-GFP immobilized on GFP-trap agarose affinity resin in the presence of Ni^{2+}. Pulled down proteins were released by 100 mM EDTA and analyzed by SDS-PAGE as well as unbound proteins in the supernatant. (A) Unbound protein from supernatant. (B) Eluted fractions. 1: cytochrome bc_1 complex w/o His-tag; 2: pR-NSpy with His-tag; 3: bo_3 oxidase w/o His-tag; 4: ATP synthase with His-tag; M: marker. Buffer: 20 mM HEPES pH 7.0, 150 mM NaCl, 0.05 % DDM.

In a next series of experiments, we wanted to take a step closer to our final aim by moving from solubilized MPs to MPs reconstituted in liposomes. We wanted to find out if trisNTA-SpyC-SEG can be complexed via Ni^{2+} to a MP which is reconstituted in liposomes, representing the final stage of reconstitution. For this purpose, after incubation of proteoliposomes reconstituted with a His-tagged MP with Ni^{2+}-trisNTA-SpyC-SEG, proteoliposomes were separated from unbound LSU by ultracentrifugation, and GFP fluorescence of the proteoliposomes was subsequently measured. We further wanted to show if trisNTA-SpyC-SEG bound to the reconstituted MP can be eluted,

and whether the amount of bound trisNTA-SpyC-SEG corresponded to the amount of reconstituted MP.

First, *E. coli* F_1F_0 ATP synthase – known to orientate unidirectionally with its F_1 part on the outside (see section 1.7) – was reconstituted into liposomes. Its His-tag was located on the β subunit of the F_1 part (see figure 7 on page 11), hence it is known to be accessible from the outside of the proteoliposomes after reconstitution, allowing probing by addition of Ni^{2+}-trisNTA-SpyC-SEG.

Accordingly, trisNTA-SpyC-SEG was loaded with Ni^{2+} by incubation for 10 min with a 10-fold excess of $NiSO_4$, and excess Ni^{2+} was then removed by SEC (PD-MiniTrap G-25 desalting column). A 4-fold excess of Ni^{2+}-trisNTA-SpyC-SEG (with respect to ATP synthase) was subsequently incubated for 20 min with proteoliposomes (0.5 ml; 10 mg ml^{-1} lipids) reconstituted[2] with ATP synthase to complex the His-tag at the outwardly facing F_1 part of the reconstituted ATP synthase. The proteoliposomes were then washed by dilution (7 ml liposome buffer), collected by ultracentrifugation, and GFP fluorescence was assessed.

For further characterization it was tried to release the trisNTA-SpyC-SEG from the His-tag of reconstituted ATP synthase by incubation for 20 min with 2 mM or 50 mM EDTA, or 100 mM histidine. Proteoliposomes without any contact to trisNTA-SpyC-SEG served as negative control.

As shown in figure 78A, trisNTA-SpyC-SEG could indeed be complexed to the exposed His-tag of reconstituted ATP synthase via Ni^{2+}. Importantly, it could be concluded that the interaction between trisNTA, Ni^{2+} and His-tagged MPs is stable enough to undergo ultracentrifugation. Interestingly, trisNTA-SpyC-SEG was only scarcely released by 2 mM EDTA, while trisNTA-SpyC-SEG could be completely eluted by 50 mM EDTA or 100 mM histidine, resulting in GFP fluorescence levels comparable to the negative control.

In a second experiment we aimed to investigate on the efficiency of the binding of the LSU to reconstituted ATP synthase. We wanted to see if Ni^{2+}-trisNTA-SpyC-SEG is complexed to His-tagged ATP synthase proportionally. There are two different possibilities to investigate on this purpose. In the first possibility, an excess of Ni^{2+}-trisNTA-SpyC-SEG is incubated with constant amounts of different proteoliposome populations reconstituted with varying amounts of ATP synthase. In the second possibility, an excess of Ni^{2+}-trisNTA-SpyC-SEG is incubated with variable amounts of one and the same proteoliposome population containing a fixed

[2]Reconstitution of ATP synthase: see figure legend of figure 78 on the next page

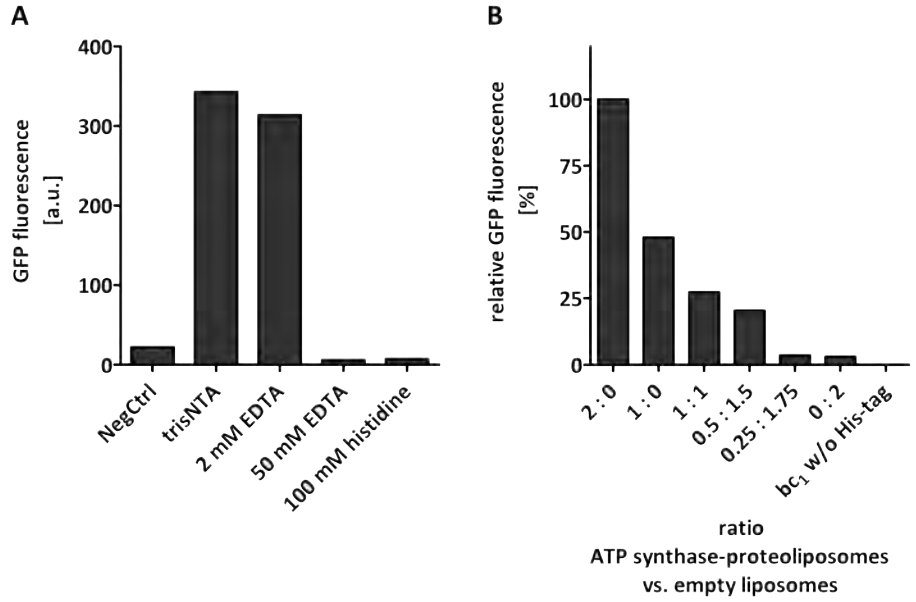

Figure 78: Characterization of trisNTA-SpyC-SC-ELP-GFP. (A) To proteoliposomes reconstituted with *E. coli* F_1F_0 ATP synthase the probe trisNTA-SpyC-SC-ELP-GFP was bound via Ni^{2+} (trisNTA) and eluted using 2 mM or 50 mM EDTA, or 100 mM histidine. As negative control served proteoliposomes which were not treated with the probe (NegCtrl). Liposomes: 10 mg ml^{-1} 90 % lecithin, soybean; 100 nm; in 0.5 mM MOPS pH 6.5, 25 mM K_2SO_4. Reconstitution using 0.4 % cholate and CentriPure P-10 desalting column for detergent removal. (B) Proteoliposomes reconstituted with F_1F_0 ATP synthase were mixed in different ratios with empty liposomes of equal properties in terms of lipid composition, buffer, and size, but without any MP reconstituted. Reconstituted His-tagged ATP synthase was probed using trisNTA-SpyC-SC-ELP-GFP in the presence of Ni^{2+}. Negative control: proteoliposomes reconstituted with cytochrome bc_1 complex w/o His-tag. Liposomes and reconstitution as in (A).

amount of ATP synthase; the difference in proteoliposome concentration between the conditions has to be compensated with empty liposomes. Since the amount of MPs actually reconstituted into preformed partially detergent-solubilized liposomes is not necessarily proportional to the amounts of MP provided for reconstitution, we decided to pursue the second possibility.

A first population of liposomes was reconstituted with the ATP synthase as in the previous experiment, while a second population consisted of empty liposomes, which were identical to the first population in terms of lipid composition, buffer, and size, but without any reconstituted MP. The two liposome populations were mixed in varying ratios and the mixtures were incubated for 20 min with a 4-fold excess

of Ni^{2+}-trisNTA-SpyC-SEG (with respect to the amount of ATP synthase in the liposome mixture containing the highest share of ATP synthase-proteoliposomes). The liposomes were then washed by dilution, collected by ultracentrifugation, and eventually, GFP fluorescence was assessed. Proteoliposomes reconstituted with cytochrome bc_1 complex without His-tag were used as a negative control.

It could be shown that the amount of Ni^{2+}-trisNTA-SpyC-SEG present was directly proportional to the ratio of the two mixed liposome populations, i. e. to the amount of ATP synthase present. Therefore, it was concluded that the LSU trisNTA-SpyC-SEG via Ni^{2+} efficiently binds reconstituted His-tagged MPs, and that this interaction is at least as stable as required to not get lost by ultracentrifugation.

Finally, we wanted to investigate how the activity of the ATP synthase during proton pumping is affected by the presence of trisNTA-SpyC-SEG. To this end, ATP synthase was either first reconstituted into liposomes and then incubated with a 4-fold excess of Ni^{2+}-trisNTA-SpyC-SEG as in the previous experiment, or vice versa, i. e. first incubated with a 4-fold excess of Ni^{2+}-trisNTA-SpyC-SEG and reconstituted into liposomes thereafter. After reconstitution, the proteoliposomes were washed by dilution with buffer without EDTA, and collected by ultracentrifugation. Then, GFP fluorescence was assessed and ATP hydrolysis activity was measured by monitoring proton pumping across the liposomal membrane using the ACMA assay introduced in section 4.2.6. Afterwards, the LSU was released from the His-tag of reconstituted ATP synthase by incubation with 50 mM EDTA for 20 min, and the proteoliposomes were washed by dilution with buffer without EDTA, and collected by ultracentrifugation. Eventually, GFP fluorescence and reverse ATP synthase activity were assessed again. Unlabeled ATP synthase was reconstituted and measured as well.

As shown in figure 79A, ATP hydrolysis was unchanged in each of the conditions 2A to 3B, suggesting that the functionality of the synthase is not affected in presence of the LSU trisNTA-SpyC-SEG. The slightly lower activity of the control (1) is likely due to a deviation in the amount of ATP synthase reconstituted into liposomes. The amount of trisNTA-SpyC-SEG was checked in each condition by measuring GFP fluorescence (figure 79B).

This series of experiments using the ATP synthase shows that the synthesized trisNTA-SpyC works as a bifunctional linker as it was intended to. We demonstrated that Ni^{2+}-trisNTA-SpyC-SEG could efficiently be complexed to reconstituted His-tagged ATP synthase. This interaction was observed to be stable enough to endure ultracentrifugation, or incubation with low amounts of EDTA (2 mM), while incubation with a higher concentration of EDTA (50 mM) resulted in elution of

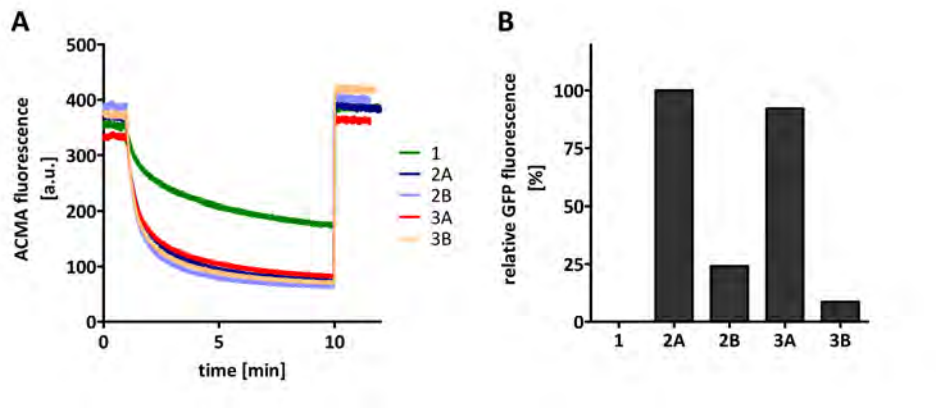

Figure 79: Attachment of an LSU does not impair ATP synthase activity. (A) Inverse ATP synthase activity was assessed by ACMA-mediated monitoring of proton pumping across the liposomal membrane induced by ATP hydrolysis by the *E. coli* F_1F_0 ATP synthase. Proton pumping was started by addition of 0.34 mM ATP to proteoliposomes in buffer HMK (10 mM HEPES pH 7.5, 1 mM $MgCl_2$, 10 mM KNO_3) containing 1.5 µM ACMA, resulting in a quench of ACMA fluorescence. When ACMA fluorescence was stable again, after 10 min, the built-up proton gradient was dissipated by addition of 30 mM NH_4Cl. (B) GFP fluorescence was assessed to control the state of binding of the LSU trisNTA-SpyC-SC-ELP-GFP to the His-tag of the ATP synthase located at the β subunit in the F_1 part. Liposomes: 10 mg ml^{-1} 90 % lecithin, soybean; 100 nm; in 0.5 mM MOPS pH 6.5, 25 mM K_2SO_4. Reconstitution using 0.4 % cholate and SEC (CentriPure P10 desalting column) for detergent removal. 1: unlabeled ATP synthase; 2A: ATP synthase was reconstituted into liposomes first, then incubated with the LSU Ni^{2+}-trisNTA-SpyC-SEG; 2B: 2A, whose LSU was released by incubation with 50 mM EDTA; 3A: ATP synthase was first complexed with the LSU, then the whole complex was reconstituted into liposomes; 3B: 3A, whose LSU was released by incubation with 50 mM EDTA.

Ni^{2+}-trisNTA-SpyC-SEG from reconstituted His-tagged ATP synthase. Eventually, ATP hydrolysis activity of the ATP synthase was shown not to be affected in the presence of Ni^{2+}-trisNTA-SpyC-SEG.

4.6.4 Conclusions to the trisNTA-Spy System.

Two different SpyTag peptides (with or without GSGS-linker between C-terminal cysteine residue and the SpyTag) were synthesized by solid phase peptide synthesis. The purified peptides were coupled to purified chloracetic anhydride-activated trisNTA, resulting in trisNTA-SpyC and trisNTA-SpyGSGSC.

Both functional moieties of trisNTA-SpyC (trisNTA, SpyTag) were successfully tested by showing that trisNTA-SpyC can be coupled to SpyCatcher-ELP-GFP (SEG), and that the resulting trisNTA-SpyC-SEG can be specifically complexed to various

solubilized His-tagged MPs via Ni^{2+}; no unspecific complexing to MPs without His-tag was observed. Further, Ni^{2+}-trisNTA-SpyC-SEG was on one hand successfully complexed to His-tagged ATP synthase which was reconstituted into liposomes beforehand, and on the other hand we were also able to reconstitute His-tagged ATP synthase after complexing the LSU to it. As the amounts of Ni^{2+}-trisNTA-SpyC-SEG complexed to His-tagged ATP synthase were observed to be directly proportional to the amounts of ATP synthase, it can be concluded that binding of the LSU to the His-tagged ATP synthase is efficient. Importantly, the interaction between Ni^{2+}-trisNTA-SpyC-SEG was shown to be strong enough to endure ultracentrifugation and incubation with low concentrations of EDTA (2 mM). trisNTA-SpyC-SEG can be released from His-tagged ATP synthase under mild conditions by using EDTA (50 mM) or histidine (100 mM), or possibly also imidazole as indicated by previous experiments (section 4.5.3). Last but definitely not least, attachment of a trisNTA-Spy-based LSU to a His-tag located in subunit β of the F_1 part of the ATP synthase does not impair the latter's function.

These experiments characterizing trisNTA-Spy have so far only been done using trisNTA-SpyC. It would therefore be very interesting to perform the same experiments using trisNTA-SpyGSGSC, and to compare the two sets of results, aiming to see if the distance between the SpyTag and the C-terminal cysteine coupled to trisNTA influences coupling of trisNTA-Spy to SpyCatcher-LSUs.

While the C-terminal cysteine residue of the peptides SpyC and SpyGSGSC is used for coupling of the peptides trisNTA, the N-terminal alanine residue of both variants of trisNTA-Spy is available for labeling with fluorophores. Preliminary experiments of Sabina Deutschmann, a PhD candidate in our lab, showed, that binding of a SpyCatcher-LSU to either of the peptides, SpyC and SpyGSGSC, was not impaired by an Fmoc-protection group on the N-terminal alanine residue of the peptides. Therefore, we speculate that modification of the N-terminal alanine residue of the Spy-peptides with fluorophores similar in size compared to Fmoc would not disturb coupling between SpyTag and SpyCatcher neither.

To my knowledge, trisNTA-Spy is the first application of the SpyTag as an isolated peptide, beyond its use in protein fusions. Binding of trisNTA-Spy is not limited to the used LSU SpyCatcher-ELP-GFP. The SpyTag peptide of trisNTA-Spy without much doubt enables attachment of trisNTA to a whole library of different SpyCatcher-labeled fusion proteins, opening numerous opportunities for applications of trisNTA-Spy, which are not limited to guiding unidirectional reconstitution of MPs into liposomes. As an example, it has not escaped our notice that trisNTA-SpyC-SEG

could potentially be used as a fluorescent probe for His-tagged (membrane) proteins in a wide variety of applications such as western blotting, fluorescence microscopy, or live-cell imaging, to name a few.

At this exciting point, my time in the laboratory came to an end, preventing me from performing further experiments to adapt the trisNTA-Spy system to be used to guide unidirectional reconstitution of MPs into liposomes. However, the next step for my successor must be to couple trisNTA-Spy to the LSU SC-MBP-3xFLAG, in order to unidirectionally reconstitute proteorhodopsin in a predefined manner, using pR variants with a His-tag either on the N- or the C-terminus. The thereby obtained results may then be compared to the results previously obtained using the SpyTag-SpyCatcher system to unidirectionally reconstitute pR-N/CSpy (see section 4.3.8).

If application of the trisNTA-Spy system successfully leads to a method allowing to unidirectionally reconstitute pR, this method should be applied to His-tagged bo_3 oxidase in order to unidirectionally reconstitute it in the proton-importing orientation. This would eventually pave the way towards coreconstitution of an artificial respiratory chain in liposomes.

5 Conclusions & Outlook.

Twisted paths towards unidirectional orientation. First, the AviTag system was introduced for bo_3 oxidase. An AviTag was genetically introduced at the C-terminus of subunit I, allowing for biotinylation of the oxidase. A preliminary LSU was attached to the biotinylated oxidase by binding of streptavidin (SA). The size of the preliminary LSU was further increased by binding of biotinylated PEG moieties to the remaining three free biotin binding sites of SA. Using the introduced AviTag system, tendencies to orientate bo_3 oxidase in the desired direction could be shown. However, the system was rather laborious and complicated in constitution, requiring completion of the assembly of the LSU while the preliminary LSU SA is already bound to biotinylated bo_3 oxidase. Assembling the LSU on the MP however resulted in partial loss of activity of bo_3 oxidase.

Aiming for a more stable and more simple system, the SpyTag-SpyCatcher system was developed. A SpyTag was genetically introduced at the termini of pR, and SpyCatcher fusion proteins were used as LSUs. This system's advantage is the covalent nature of the linkage between the MP's SpyTag and the LSU's SpyCatcher, enabling coupled constructs to stand a wide variety of thinkable downstream procedures as SEC or ultracentrifugation, to name a few. Using the SpyTag-SpyCatcher system it was shown that pR can be reconstituted unidirectionally into liposomes in a predefined manner. Unidirectionality of reconstituted pR was successfully attested by functional assays as well as by physical means.

Application of the SpyTag-SpyCatcher system to facilitate unidirectional reconstitution of bo_3 oxidase (SpyTag at C-terminus of subunit I) yielded promising trends, however orientation of bo_3 oxidase seems to be much harder to be influenced than orientation of pR. It has to be concluded that a crucial point on the way towards unidirectional reconstitution of MPs into liposomes is comprised of the reconstitution conditions, especially when attempting to influence orientation of complex multi-subunit MPs as the bo_3 oxidase.

It could be demonstrated that the attachment of LSUs using the SpyTag-SpyCatcher system did not impair MP functionality, neither of pR, nor of bo_3 oxidase. Nevertheless, protease cleavage sites had been introduced allowing for detachment of the LSU after reconstitution, however this has not been tested yet.

Spy&Go – A way to improve the SpyTag-SpyCatcher system? In 2019, the Howarth lab (university of Oxford), where the Spy-technology was initially developed,

presented a novel technique named Spy&Go. SpyDock was developed, which in brief is a variant of SpyCatcher able to capture SpyTag-fusions, however without generation of a covalent bond. The affinity of SpyDock for the SpyTag-fusion protein SpyTag-MBP (K_d: $0.75 \pm 0.05\,\mu M$ [306]) was reported to be two orders of magnitude higher than the affinity of Ni-NTA for hexahistidine-tags (K_d: $\sim 10\,\mu M$ [200, 276]). They used Spy&Go for efficient affinity purification of SpyTag-fusions with superior purity than when using Ni-NTA-based metal affinity chromatography. Elution of the SpyTag-fusion from SpyDock was facilitated using 2.5 M imidazole at neutral pH.[306] Hence, it would be very interesting to implement the novel SpyDock entity as a replacement for SpyCatcher. This would allow mild release of the SpyDock-LSU bound to the Spy-tagged MP after reconstitution without the use of any proteases. However, it would have to be investigated whether the interaction between SpyTag and SpyDock would occur and be stable in detergents necessary for MP solubilization, and if it would be stable enough to endure desired downstream applications as e. g. ultracentrifugation for collection of proteoliposomes.

trisNTA – The basis for a generally applicable tool to influence orientation? Attempting to develop more generally applicable procedures for unidirectional reconstitution, without the requirement for any further genetically introduced tags except for a properly positioned His-tag, two systems using trisNTA were introduced. The main advantages of trisNTA-based systems compared to the previous approaches are, that trisNTA-based LSUs can be mildly released from MPs of interest, and that there are no further genetic modifications required but a properly positioned His-tag, which in most MPs is introduced for purification anyway.

A dendritic version of trisNTA was successfully synthesized and characterized. Coupling trisNTA directly to LSUs however turned out to be very difficult. Therefore, two different SpyTag peptides (with and without GSGS-linker between SpyTag sequence and C-terminal cysteine residue) were synthesized by solid phase peptide synthesis and on their C-terminal cysteine residue coupled to chloracetic anhydride-activated trisNTA, resulting in two slightly different versions of trisNTA-Spy. The novel entity trisNTA-Spy combines the advantages of the trisNTA system with those of the SpyTag-SpyCatcher system. trisNTA-Spy can first be coupled to any SpyCatcher-containing member of a SC-LSU library, and subsequently be complexed via Ni^{2+} to the MP's His-tag prior to reconstitution. After reconstitution, the trisNTA-Spy-based LSU can be mildly eluted from reconstituted MPs, thus not impairing functional measurements.

A bright future for trisNTA-Spy. The next steps using the trisNTA-Spy system must be to apply trisNTA-Spy bound to SC-containing LSUs to pR with a His-tag either on the N- or the C-terminus to influence orientation of pR during reconstitution in order to confirm the results obtained with the SpyTag-SpyCatcher system. I am confident that the trisNTA-Spy system will be published soon as a tool kit to mediate unidirectional orientation of MPs. Once successful for His-tagged pR, the focus shall be laid again on orientation of the bo_3 oxidase using the trisNTA-Spy system.

Further considerations regarding the developed methods for unidirectional reconstitution. Most certainly, the attentive reader has already noticed that throughout all the reconstitution experiments described in the underlying thesis, the lipid composition of the liposomes was always the same; liposomes did at most only differ in size (100 / 200 nm) or in the composition of the liposome buffer. We thereby intended to minimize the number of parameters potentially influencing orientation of reconstituted MPs, allowing us to focus exclusively on the developed methods, thus sustaining comparability between those. Nevertheless, it should be taken into account that the reconstitution conditions, including the lipid composition of the liposomal membrane, play a crucial role in MP reconstitution, especially on the way towards unidirectional reconstitution. Consequently, for unidirectional reconstitution of MPs into liposomes, the methods developed in this thesis should be applied in combination with optimized reconstitution conditions for the respective MPs.

In the case of bo_3 oxidase, an additional factor might be influencing reconstitution and orientation. Subunit II (CyoA) of the bo_3 oxidase is posttranslationally processed by proteolytic cleavage to generate the mature form of subunit II with an N-terminus at Cys25.[27] After processing, Cys25 is modified to form glycerylcysteine, to which three palmitic acid residues are attached.[27] According to Ma *et al.* [27], posttranslational processing and subsequent lipidation are not necessary for either the assembly or function of the bo_3 oxidase. Further, since subunit II contains two transmembrane helices, the covalently attached lipid is not necessary for anchoring subunit II to the membrane.[27] However, this lipid anchor might guide reconstitution of bo_3 oxidase into liposomes, thereby possibly influencing orientation of the inserted MP, but this remains speculation. To investigate on a possible effect of this lipidation, orientation of reconstituted wild type enzyme should be compared to orientation of a reconstituted C25A mutant of bo_3 oxidase, which was previously shown to prevent posttranslational processing and consequently is lacking lipidation [27]. If lipidation of Cys25 indeed affects orientation of reconstituted bo_3 oxidase, it would be interesting to apply the

developed methods to influence orientation of MPs (especially SpyTag-SpyCatcher system and trisNTA-Spy system) to the C25A mutant of *bo₃* oxidase.

Since the orientation of *bo₃* oxidase appeared to be particularly difficult to be influenced, it should be considered to test the SpyTag-SpyCatcher system and the trisNTA-Spy system with further MPs similar in size and constitution to the *bo₃* oxidase, as e. g. *aa₃* cytochrome *c* oxidase or *bc₁* complex, both from *Rhodobacter sphaeroides*. This would show if large, complex multi-subunit MPs are generally more difficult to be unidirectionally reconstituted into liposomes than the mono-subunit model MP pR, or if unidirectional reconstitution of the *bo₃* oxidase is exceptionally difficult to achieve.

Are there alternatives to unidirectional reconstitution? As discussed in section 1.7.2, the problem of not unidirectionally reconstituted MPs in proteoliposomes can be circumvented in some cases by imposing unidirectional function either by blocking one orientation population from interacting with the substrate, or by restricting the location of the respective membrane-impermeable substrate.[6, 171] In the case of membrane-permeable substrates (e. g. ubiquinol Q_1 for *bo₃* oxidase) however, both populations are inevitably activated.

Blocking of the interaction between substrates and one orientation population can either be achieved by inhibitors, as e. g. discussed in section 1.7.2 for Na^+/K^+-P-ATPase by ouabain or vanadate ions [6, 171], or by modification of the MP itself. Harder *et al.* [307] have reported the implementation of an on/off switch in pR based on reversible covalent chemical modification of a site-specifically introduced cysteine residue (N220C) with sodium (2-sulfonatoethyl)-methanethiosulfonate (MTSES; CAS: 184644-83-5). Treatment of proteoliposomes reconstituted with pR-N220C with MTSES resulted in substantial reduction of proton pumping activity (export), which however can be restored by reduction with β-mercaptoethanol.[307] Because MTSES is membrane-impermeable [307], addition of MTSES to the outside of proteoliposomes reconstituted with pR-N220C could be used to block activity of the proton-exporting pR population, leaving exclusively the proton-importing pR population to be active, eventually resulting in unidirectional proton pumping across the liposomal membrane.

In summary however, strategies to circumvent the issue of unidirectional reconstitution by imposing unidirectional function are very specific to the respective MP of interest. Consequently, such strategies do not really provide a valid alternative for a generally applicable strategy to unidirectionally reconstitute MPs in my opinion.

The future of unidirectional reconstitution of MPs into liposomes. Orientation of bo_3 oxidase in liposomes is still a high priority aim in our lab in order to coreconstitute an artificial respiratory chain in liposomes. However, the process of detergent-mediated reconstitution needs to be optimized for each MP of interest. Hence, efficient coreconstitution of two or more different MPs in one step is not straightforward. For this purpose, in 2016, former group members of the von Ballmoos lab published a method to deliver different separately reconstituted MPs into a common lipid bilayer by employing fusion of oppositely charged liposomes.[110] Since controlled liposome fusion preserves the orientation of the MPs in the final liposome [110], combining the methods for unidirectional reconstitution of MPs developed in this thesis with coreconstitution by charge-mediated fusion could be a giant leap towards coreconstitution of an artificial respiratory chain in liposomes, allowing investigations on consecutive processes thereof. In a first step, a proteoliposome library shall be constituted, where all required MPs of interest would be individually reconstituted unidirectionally in the desired orientations into liposomes, each by using their respective optimal reconstitution conditions. In a second step, all desired sorts of undirectionally reconstituted MPs from the previously generated proteoliposome library can be delivered into one GUV by charge-mediated fusion as described by Biner, Schick, Müller, *et al.* [110].

Investigations on (especially hereditary) diseases related to deficiencies of one or combined deficiencies of multiple enzymes of oxidative phosphorylation would benefit from having at hand such an artificial respiratiory chain. According to Mayr *et al.* [308], more than 250 gene defects related to inherited disorders of mitochondrial energy metabolism in humans have been reported. Such defects are often lethal or lead to severe disease phenotypes. Diseases related to complex III deficiencies for example are cardiomyopathy, Leber Hereditary Optic Neuropathy (LHON), GRACILE syndrome or Bjørnstad syndrome, to name a few.[309]

According to Overington *et al.* [8], in 2006 MPs constituted more than 60 % of current drug targets, and Rask-Andersen *et al.* [310] reported in 2011 that more than one-third of small-molecule drugs target proteins from the G protein-coupled receptor (GPCR) superfamily to inhibit or activate signal transduction. Consequently, the developed methods to unidirectionally reconstitute MPs in liposomes have a great potential to be applied in numerous studies beyond the research interests in our own lab.

6 Bibliography.

1. Honigmann, A. & Pralle, A. Compartmentalization of the Cell Membrane. *J Mol Biol* **428,** 4739–4748. ISSN: 0022-2836 (2016).
2. Nelson, D., Lehninger, A. & Cox, M. *Lehninger Principles of Biochemistry* Fifth edition. ISBN: 9780716771081 (W. H. Freeman, 2008).
3. Mitchell, P. Coupling of Phosphorylation to Electron and Hydrogen Transfer by a Chemi-Osmotic type of Mechanism. *Nature* **191,** 144–148. ISSN: 1476-4687 (1961).
4. Singer, S. J. & Nicolson, G. L. The fluid mosaic model of the structure of cell membranes. *Science* **175,** 720–31. ISSN: 0036-8075 (Print) 0036-8075 (1972).
5. Knol, J. PhD-Thesis - Membrane Reconstitution and Functional Analysis of a Sugar Transport System (1999).
6. Eytan, G. D. Use of liposomes for reconstitution of biological functions. *Biochim Biophys Acta* **694,** 185–202. ISSN: 0006-3002 (Print) 0006-3002 (1982).
7. Uhlen, M. *et al.* Proteomics. Tissue-based map of the human proteome. *Science* **347,** 1260419. ISSN: 0036-8075 (2015).
8. Overington, J. P., Al-Lazikani, B. & Hopkins, A. L. How many drug targets are there? *Nat Rev Drug Discov* **5,** 993–6. ISSN: 1474-1776 (Print) 1474-1776 (2006).
9. Yin, H. & Flynn, A. D. Drugging Membrane Protein Interactions. *Annual review of biomedical engineering* **18,** 51–76. ISSN: 1545-4274 1523-9829 (2016).
10. Goers, R. PhD-Thesis - A framework for the reconstitution of membrane proteins (2018).
11. Bootman, M. D., Rietdorf, K., Collins, T., Walker, S. & Sanderson, M. Ca^{2+}-sensitive fluorescent dyes and intracellular Ca^{2+} imaging. *Cold Spring Harb Protoc* **2013,** 83–99. ISSN: 1559-6095 (2013).
12. Xie, H. Activity assay of membrane transport proteins. *Acta Biochim Biophys Sin (Shanghai)* **40,** 269–77. ISSN: 1672-9145 (2008).
13. Pfleger, N. *et al.* Solid-state NMR and functional studies on proteorhodopsin. *Biochim Biophys Acta* **1787,** 697–705. ISSN: 0006-3002 (Print) 0006-3002 (2009).
14. Beja, O. *et al.* Bacterial rhodopsin: evidence for a new type of phototrophy in the sea. *Science* **289,** 1902–6. ISSN: 0036-8075 (Print) 0036-8075 (2000).

15. Sabehi, G. *et al.* New insights into metabolic properties of marine bacteria encoding proteorhodopsins. *PLoS Biol* **3,** e273. ISSN: 1544-9173 (2005).

16. Wang, W. W., Sineshchekov, O. A., Spudich, E. N. & Spudich, J. L. Spectroscopic and photochemical characterization of a deep ocean proteorhodopsin. *J Biol Chem* **278,** 33985–91. ISSN: 0021-9258 (Print) 0021-9258 (2003).

17. Dioumaev, A. K. *et al.* Proton transfers in the photochemical reaction cycle of proteorhodopsin. *Biochemistry* **41,** 5348–58. ISSN: 0006-2960 (Print) 0006-2960 (2002).

18. Lindholm, L. *et al.* Effect of lipid bilayer properties on the photocycle of green proteorhodopsin. *Biochim Biophys Acta* **1847,** 698–708. ISSN: 0006-3002 (Print) 0006-3002 (2015).

19. Friedrich, T., Geibel, S., *et al.* Proteorhodopsin is a Light-driven Proton Pump with Variable Vectoriality. *Journal of Molecular Biology* **321,** 821–838. ISSN: 0022-2836 (2002).

20. Reckel, S. *et al.* Solution NMR structure of proteorhodopsin. *Angew Chem Int Ed Engl* **50,** 11942–6. ISSN: 1433-7851 (2011).

21. Wikström, M., Krab, K. & Sharma, V. Oxygen Activation and Energy Conservation by Cytochrome *c* Oxidase. *Chemical Reviews* **118,** 2469–2490. ISSN: 0009-2665 (2018).

22. Garcia-Horsman, J. A., Barquera, B., Rumbley, J., Ma, J. & Gennis, R. B. The superfamily of heme-copper respiratory oxidases. *J Bacteriol* **176,** 5587–600. ISSN: 0021-9193 (Print) 0021-9193 (1994).

23. Calhoun, M. W., Thomas, J. W. & Gennis, R. B. The cytochrome oxidase superfamily of redox-driven proton pumps. *Trends Biochem Sci* **19,** 325–30. ISSN: 0968-0004 (Print) 0968-0004 (1994).

24. Biner, O., Schick, T., Ganguin, A. A. & von Ballmoos, C. Towards a Synthetic Mitochondrion. *Chimia (Aarau)* **72,** 291–296. ISSN: 0009-4293 (Print) 0009-4293 (2018).

25. Berg, J., Block, S., Höök, F. & Brzezinski, P. Single Proteoliposomes with *E. coli* Quinol Oxidase: Proton Pumping without Transmembrane Leaks. *Israel Journal of Chemistry* **57,** 437–445. ISSN: 0021-2148 (2017).

26. Abramson, J. *et al.* The structure of the ubiquinol oxidase from *Escherichia coli* and its ubiquinone binding site. *Nat Struct Biol* **7,** 910–7. ISSN: 1072-8368 (Print) 1072-8368 (2000).

27. Ma, J., Katsonouri, A. & Gennis, R. B. Subunit II of the cytochrome bo_3 ubiquinol oxidase from *Escherichia coli* is a lipoprotein. *Biochemistry* **36,** 11298–303. ISSN: 0006-2960 (Print) 0006-2960 (1997).

28. Rumbley, J. N., Furlong Nickels, E. & Gennis, R. B. One-step purification of histidine-tagged cytochrome bo_3 from *Escherichia coli* and demonstration that associated quinone is not required for the structural integrity of the oxidase. *Biochim Biophys Acta* **1340,** 131–42. ISSN: 0006-3002 (Print) 0006-3002 (1997).

29. Thomas, J. W. *et al.* Site-directed mutagenesis of residues within helix VI in subunit I of the cytochrome bo_3 ubiquinol oxidase from *Escherichia coli* suggests that tyrosine 288 may be a Cu_B ligand. *Biochemistry* **33,** 13013–21. ISSN: 0006-2960 (Print) 0006-2960 (1994).

30. Kawasaki, M., Mogi, T. & Anraku, Y. Substitutions of charged amino acid residues conserved in subunit I perturb the redox metal centers of the *Escherichia coli bo*-type ubiquinol oxidase. *J Biochem* **122,** 422–9. ISSN: 0021-924X (Print) 0021-924x (1997).

31. Das, T. K., Pecoraro, C., Tomson, F. L., Gennis, R. B. & Rousseau, D. L. The Post-Translational Modification in Cytochrome *c* Oxidase Is Required To Establish a Functional Environment of the Catalytic Site. *Biochemistry* **37,** 14471–14476. ISSN: 0006-2960 (1998).

32. Mogi, T. *et al.* Substitutions of conserved aromatic amino acid residues in subunit I perturb the metal centers of the *Escherichia coli bo*-type ubiquinol oxidase. *Biochemistry* **37,** 1632–9. ISSN: 0006-2960 (Print) 0006-2960 (1998).

33. Proshlyakov, D. A. *et al.* Oxygen activation and reduction in respiration: involvement of redox-active tyrosine 244. *Science* **290,** 1588–91. ISSN: 0036-8075 (Print) 0036-8075 (2000).

34. Sharma, V., Puustinen, A., Wikstrom, M. & Laakkonen, L. Sequence analysis of the cbb_3 oxidases and an atomic model for the *Rhodobacter sphaeroides* enzyme. *Biochemistry* **45,** 5754–65. ISSN: 0006-2960 (Print) 0006-2960 (2006).

35. von Ballmoos, C., Wiedenmann, A. & Dimroth, P. Essentials for ATP synthesis by F_1F_0 ATP synthases. *Annu Rev Biochem* **78,** 649–72. ISSN: 0066-4154 (2009).

36. Boyer, P. D. The ATP synthase - a splendid molecular machine. *Annual Review of Biochemistry* **66,** 717–749 (1997).

37. Berg, J. M., Stryer, L. & Tymoczko, J. L. *Biochemistry. 5th edition* ISBN: 0-7167-3051-0 (W. H. Freeman, New York, 2002).

38. Walker, J. E. The ATP synthase: the understood, the uncertain and the unknown. *Biochem Soc Trans* **41,** 1–16. ISSN: 0300-5127 (2013).

39. Igamberdiev, A. U. & Kleczkowski, L. A. Optimization of ATP synthase function in mitochondria and chloroplasts via the adenylate kinase equilibrium. *Front Plant Sci* **6,** 10. ISSN: 1664-462X (Print) 1664-462x (2015).

40. Junge, W. & Nelson, N. ATP synthase. *Annu Rev Biochem* **84,** 631–57. ISSN: 0066-4154 (2015).

41. Sobti, M. *et al.* Cryo-EM structures of the autoinhibited *E. coli* ATP synthase in three rotational states. *Elife* **5.** ISSN: 2050-084x (2016).

42. Moss, G. P., Smith, P. A. S. & Tavernier, D. *Glossary of class names of organic compounds and reactivity intermediates based on structure (IUPAC Recommendations 1995)* Generic. 1995.

43. van Meer, G., Voelker, D. R. & Feigenson, G. W. Membrane lipids: where they are and how they behave. *Nature Reviews Molecular Cell Biology* **9,** 112–124. ISSN: 1471-0080 (2008).

44. Milo, R. & Phillips, R. *Cell biology by the numbers* 1st Edition, 358. ISBN: 9780815345374 (Garland Science, 2016).

45. Chandler, D. Interfaces and the driving force of hydrophobic assembly. *Nature* **437,** 640–647. ISSN: 1476-4687 (2005).

46. Lasic, D. D. The mechanism of vesicle formation. *Biochem J* **256,** 1–11. ISSN: 0264-6021 (Print) 0264-6021 (1988).

47. De Rosa, M., Gambacorta, A. & Gliozzi, A. Structure, biosynthesis, and physicochemical properties of archaebacterial lipids. *Microbiol Rev* **50,** 70–80. ISSN: 0146-0749 (Print) 0146-0749 (1986).

48. Lichtenberg, D., Goni, F. M. & Heerklotz, H. Detergent-resistant membranes should not be identified with membrane rafts. *Trends Biochem Sci* **30,** 430–6. ISSN: 0968-0004 (Print) 0968-0004 (2005).

49. Lottspeich, F. & Engels, J. W. *Bioanalytik* 1136. ISBN: 978-3-8274-1520-2 (Spektrum Akademischer Verlag, Heidelberg, 2006).

50. Breyton, C. *et al.* Assemblies of lauryl maltose neopentyl glycol (LMNG) and LMNG-solubilized membrane proteins. *Biochim Biophys Acta Biomembr* **1861,** 939–957. ISSN: 0005-2736 (2019).

51. Chae, P. S., Rana, R. R., *et al.* Glucose-neopentyl glycol (GNG) amphiphiles for membrane protein study. *Chem Commun (Camb)* **49,** 2287–9. ISSN: 1359-7345 (2013).

52. Le Maire, M., Champeil, P. & Moller, J. V. Interaction of membrane proteins and lipids with solubilizing detergents. *Biochim Biophys Acta* **1508,** 86–111. ISSN: 0006-3002 (Print) 0006-3002 (2000).

53. Brito, R. M. & Vaz, W. L. Determination of the critical micelle concentration of surfactants using the fluorescent probe N-phenyl-1-naphthylamine. *Anal Biochem* **152,** 250–5. ISSN: 0003-2697 (Print) 0003-2697 (1986).

54. De Vendittis, E., Palumbo, G., Parlato, G. & Bocchini, V. A fluorimetric method for the estimation of the critical micelle concentration of surfactants. *Anal Biochem* **115,** 278–86. ISSN: 0003-2697 (Print) 0003-2697 (1981).

55. Chae, P. S., Rasmussen, S. G., *et al.* Maltose-neopentyl glycol (MNG) amphiphiles for solubilization, stabilization and crystallization of membrane proteins. *Nat Methods* **7,** 1003–8. ISSN: 1548-7091 (2010).

56. Yang, Z. *et al.* Membrane protein stability can be compromised by detergent interactions with the extramembranous soluble domains. *Protein Sci* **23,** 769–89. ISSN: 0961-8368 (2014).

57. Seddon, A. M., Curnow, P. & Booth, P. J. Membrane proteins, lipids and detergents: not just a soap opera. *Biochim Biophys Acta* **1666,** 105–17. ISSN: 0006-3002 (Print) 0006-3002 (2004).

58. Cesar-Razquin, A. *et al.* A Call for Systematic Research on Solute Carriers. *Cell* **162,** 478–87. ISSN: 0092-8674 (2015).

59. Tang, Y. *et al.* The Regulatory Role of MeAIB in Protein Metabolism and the mTOR Signaling Pathway in Porcine Enterocytes. *Int J Mol Sci* **19.** ISSN: 1422-0067 (2018).

60. Hoffmann, T. M. *et al.* Effects of Sodium and Amino Acid Substrate Availability upon the Expression and Stability of the SNAT2 (SLC38A2) Amino Acid Transporter. *Frontiers in Pharmacology* **9.** ISSN: 1663-9812 (2018).

61. Grewal, S. *et al.* SNAT2 amino acid transporter is regulated by amino acids of the SLC6 gamma-aminobutyric acid transporter subfamily in neocortical neurons and may play no role in delivering glutamine for glutamatergic transmission. *J Biol Chem* **284,** 11224–36. ISSN: 0021-9258 (Print) 0021-9258 (2009).

62. Skrzypek, R., Iqbal, S. & Callaghan, R. Methods of reconstitution to investigate membrane protein function. *Methods.* ISSN: 1046-2023 (2018).

63. Liao, Y., Yuan, Q., Torres, J., Tam, J. P. & Liu, D. X. Biochemical and functional characterization of the membrane association and membrane permeabilizing activity of the severe acute respiratory syndrome coronavirus envelope protein. *Virology* **349,** 264–75. ISSN: 0042-6822 (Print) 0042-6822 (2006).

64. Frenkel, E. J., Roelofsen, B., Brodbeck, U., van Deenen, L. L. & Ott, P. Lipid-protein interactions in human erythrocyte-membrane acetylcholinesterase. Modulation of enzyme activity by lipids. *Eur J Biochem* **109,** 377–82. ISSN: 0014-2956 (Print) 0014-2956 (1980).

65. Shen, H. H., Lithgow, T. & Martin, L. Reconstitution of membrane proteins into model membranes: seeking better ways to retain protein activities. *Int J Mol Sci* **14,** 1589–607. ISSN: 1422-0067 (Print) 1422-0067 (2013).

66. Aroca, J. D. *et al.* Correlation between the effect of the anti-neoplastic ether lipid 1-O-octadecyl-2-O-methyl-glycero-3-phosphocholine on the membrane and the activity of protein kinase Calpha. *Eur J Biochem* **268,** 6369–78. ISSN: 0014-2956 (Print) 0014-2956 (2001).

67. Lee, A. G. Biological membranes: the importance of molecular detail. *Trends Biochem Sci* **36,** 493–500. ISSN: 0968-0004 (Print) 0968-0004 (2011).

68. Bayburt, T. H., Grinkova, Y. V. & Sligar, S. G. Self-Assembly of Discoidal Phospholipid Bilayer Nanoparticles with Membrane Scaffold Proteins. *Nano Letters* **2,** 853–856. ISSN: 15306984 (ISSN) (2002).

69. Shoulders, C. C., Kornblihtt, A. R., Munro, B. S. & Baralle, F. E. Gene structure of human apolipoprotein A1. *Nucleic Acids Res* **11,** 2827–37. ISSN: 0305-1048 (Print) 0305-1048 (1983).

70. Denisov, I. G. & Sligar, S. G. Nanodiscs for structural and functional studies of membrane proteins. *Nature Structural & Molecular Biology* **23,** 481–486. ISSN: 1545-9985 (2016).

71. Durbin, D. M. & Jonas, A. The effect of apolipoprotein A-II on the structure and function of apolipoprotein A-I in a homogeneous reconstituted high density lipoprotein particle. *J Biol Chem* **272,** 31333–9. ISSN: 0021-9258 (Print) 0021-9258 (1997).

72. Li, L., Chen, J., *et al.* Double belt structure of discoidal high density lipoproteins: molecular basis for size heterogeneity. *J Mol Biol* **343,** 1293–311. ISSN: 0022-2836 (Print) 0022-2836 (2004).

73. Denisov, I. G. & Sligar, S. G. Nanodiscs in Membrane Biochemistry and Biophysics. *Chemical Reviews* **117,** 4669–4713. ISSN: 0009-2665 (2017).

74. Jonas, A., Steinmetz, A. & Churgay, L. The number of amphipathic alpha-helical segments of apolipoproteins A-I, E, and A-IV determines the size and functional properties of their reconstituted lipoprotein particles. *J Biol Chem* **268,** 1596–602. ISSN: 0021-9258 (Print) 0021-9258 (1993).

75. Bayburt, T. H. & Sligar, S. G. Membrane protein assembly into Nanodiscs. *FEBS Lett* **584,** 1721–7. ISSN: 0014-5793 (2010).

76. Denisov, I. G., Grinkova, Y. V., Lazarides, A. A. & Sligar, S. G. Directed self-assembly of monodisperse phospholipid bilayer Nanodiscs with controlled size. *J Am Chem Soc* **126,** 3477–87. ISSN: 0002-7863 (Print) 0002-7863 (2004).

77. Pollock, N. L., Lee, S. C., Patel, J. H., Gulamhussein, A. A. & Rothnie, A. J. Structure and function of membrane proteins encapsulated in a polymer-bound lipid bilayer. *Biochimica et Biophysica Acta (BBA) - Biomembranes* **1860,** 809–817. ISSN: 0005-2736 (2018).

78. Van Den Brink-Van Der Laan, E., Chupin, V., Killian, J. A. & De Kruijff, B. Stability of KcsA Tetramer Depends on Membrane Lateral Pressure. *Biochemistry* **43,** 4240–4250. ISSN: 00062960 (ISSN) (2004).

79. Hagn, F., Etzkorn, M., Raschle, T. & Wagner, G. Optimized Phospholipid Bilayer Nanodiscs Facilitate High-Resolution Structure Determination of Membrane Proteins. *Journal of the American Chemical Society* **135,** 1919–1925. ISSN: 0002-7863 (2013).

80. Kijac, A. Z., Li, Y., Sligar, S. G. & Rienstra, C. M. Magic-Angle Spinning Solid-State NMR Spectroscopy of Nanodisc-Embedded Human CYP3A4. *Biochemistry* **46,** 13696–13703. ISSN: 0006-2960 (2007).

81. Bayburt, T. H. & Sligar, S. G. Single-molecule height measurements on microsomal cytochrome P450 in nanometer-scale phospholipid bilayer disks. *Proc Natl Acad Sci U S A* **99,** 6725–30. ISSN: 0027-8424 (Print) 0027-8424 (2002).

82. Civjan, N. R., Bayburt, T. H., Schuler, M. A. & Sligar, S. G. Direct solubilization of heterologously expressed membrane proteins by incorporation into nanoscale lipid bilayers. *Biotechniques* **35,** 556–60, 562–3. ISSN: 0736-6205 (Print) 0736-6205 (2003).

83. Baas, B. J., Denisov, I. G. & Sligar, S. G. Homotropic cooperativity of monomeric cytochrome P450 3A4 in a nanoscale native bilayer environment. *Arch Biochem Biophys* **430,** 218–28. ISSN: 0003-9861 (Print) 0003-9861 (2004).

84. Duan, H., Civjan, N. R., Sligar, S. G. & Schuler, M. A. Co-incorporation of heterologously expressed *Arabidopsis* cytochrome P450 and P450 reductase into soluble nanoscale lipid bilayers. *Arch Biochem Biophys* **424,** 141–53. ISSN: 0003-9861 (Print) 0003-9861 (2004).

85. Davydov, D. R., Fernando, H., Baas, B. J., Sligar, S. G. & Halpert, J. R. Kinetics of dithionite-dependent reduction of cytochrome P450 3A4: heterogeneity of the enzyme caused by its oligomerization. *Biochemistry* **44,** 13902–13. ISSN: 0006-2960 (Print) 0006-2960 (2005).

86. Denisov, I. G., Grinkova, Y. V., Baas, B. J. & Sligar, S. G. The ferrous-dioxygen intermediate in human cytochrome P450 3A4. Substrate dependence of formation and decay kinetics. *J Biol Chem* **281,** 23313–8. ISSN: 0021-9258 (Print) 0021-9258 (2006).

87. Bayburt, T. H., Carlson, J. W. & Sligar, S. G. Reconstitution and Imaging of a Membrane Protein in a Nanometer-Size Phospholipid Bilayer. *Journal of Structural Biology* **123,** 37–44. ISSN: 1047-8477 (1998).

88. Bayburt, T. H., Carlson, J. W. & Sligar, S. G. Single Molecule Height Measurements on a Membrane Protein in Nanometer-Scale Phospholipid Bilayer Disks. *Langmuir* **16,** 5993–5997. ISSN: 0743-7463 (2000).

89. Bayburt, T. H. & Sligar, S. G. Self-assembly of single integral membrane proteins into soluble nanoscale phospholipid bilayers. *Protein Sci* **12,** 2476–81. ISSN: 0961-8368 (Print) 0961-8368 (2003).

90. Bayburt, T. H., Grinkova, Y. V. & Sligar, S. G. Assembly of single bacteriorhodopsin trimers in bilayer nanodiscs. *Arch Biochem Biophys* **450,** 215–22. ISSN: 0003-9861 (Print) 0003-9861 (2006).

91. Leitz, A. J., Bayburt, T. H., Barnakov, A. N., Springer, B. A. & Sligar, S. G. Functional reconstitution of Beta2-adrenergic receptors utilizing self-assembling Nanodisc technology. *Biotechniques* **40,** 601–2, 604, 606, passim. ISSN: 0736-6205 (Print) 0736-6205 (2006).

92. Boldog, T., Grimme, S., Li, M., Sligar, S. G. & Hazelbauer, G. L. Nanodiscs separate chemoreceptor oligomeric states and reveal their signaling properties. *Proc Natl Acad Sci U S A* **103,** 11509–14. ISSN: 0027-8424 (Print) 0027-8424 (2006).

93. Nath, A., Atkins, W. M. & Sligar, S. G. Applications of Phospholipid Bilayer Nanodiscs in the Study of Membranes and Membrane Proteins. *Biochemistry* **46,** 2059–2069. ISSN: 0006-2960 (2007).

94. Knowles, T. J. *et al.* Membrane Proteins Solubilized Intact in Lipid Containing Nanoparticles Bounded by Styrene Maleic Acid Copolymer. *Journal of the American Chemical Society* **131,** 7484–7485. ISSN: 0002-7863 (2009).

95. Hwang, P. M. *et al.* Solution structure and dynamics of the outer membrane enzyme PagP by NMR. *Proc Natl Acad Sci U S A* **99,** 13560–5. ISSN: 0027-8424 (Print) 0027-8424 (2002).

96. Postis, V. *et al.* The use of SMALPs as a novel membrane protein scaffold for structure study by negative stain electron microscopy. *Biochimica et Biophysica Acta (BBA) - Biomembranes* **1848,** 496–501. ISSN: 0005-2736 (2015).

97. Morrison, K. A. *et al.* Membrane protein extraction and purification using styrene-maleic acid (SMA) copolymer: effect of variations in polymer structure. *Biochem J* **473,** 4349–4360. ISSN: 0264-6021 (2016).

98. Dekker, N., Merck, K., Tommassen, J. & Verheij, H. M. In vitro folding of *Escherichia coli* outer-membrane phospholipase A. *Eur J Biochem* **232,** 214–9. ISSN: 0014-2956 (Print) 0014-2956 (1995).

99. Oluwole, A. O. *et al.* Solubilization of Membrane Proteins into Functional Lipid-Bilayer Nanodiscs Using a Diisobutylene/Maleic Acid Copolymer. *Angew Chem Int Ed Engl* **56,** 1919–1924. ISSN: 1433-7851 (2017).

100. Murakami, S., Nakashima, R., Yamashita, E. & Yamaguchi, A. Crystal structure of bacterial multidrug efflux transporter AcrB. *Nature* **419,** 587–593. ISSN: 00280836 (ISSN) (2002).

101. Smirnova, I. A., Sjöstrand, D., *et al.* Isolation of yeast complex IV in native lipid nanodiscs. *Biochimica et Biophysica Acta (BBA) - Biomembranes* **1858,** 2984–2992. ISSN: 0005-2736 (2016).

102. Smirnova, I. A., Adelroth, P. & Brzezinski, P. Extraction and liposome reconstitution of membrane proteins with their native lipids without the use of detergents. *Sci Rep* **8,** 14950. ISSN: 2045-2322 (2018).

103. Dörr, J. M. *et al.* The styrene–maleic acid copolymer: a versatile tool in membrane research. *European Biophysics Journal* **45,** 3–21. ISSN: 1432-1017 (2016).

104. Smith, A. A. A., Autzen, H. E., *et al.* Controlling Styrene Maleic Acid Lipid Particles through RAFT. *Biomacromolecules* **18,** 3706–3713. ISSN: 1525-7797 (2017).

105. Discher, B. M., Won, Y. Y., *et al.* Polymersomes: tough vesicles made from diblock copolymers. *Science* **284,** 1143–6. ISSN: 0036-8075 (Print) 0036-8075 (1999).

106. Discher, D. E. & Ahmed, F. Polymersomes. *Annu Rev Biomed Eng* **8,** 323–41. ISSN: 1523-9829 (Print) 1523-9829 (2006).

107. Rideau, E., Dimova, R., Schwille, P., Wurm, F. R. & Landfester, K. Liposomes and polymersomes: a comparative review towards cell mimicking. *Chem Soc Rev* **47,** 8572–8610. ISSN: 0306-0012 (2018).

108. Bulbake, U., Doppalapudi, S., Kommineni, N. & Khan, W. Liposomal Formulations in Clinical Use: An Updated Review. *Pharmaceutics* **9.** ISSN: 1999-4923 (Print) 1999-4923 (2017).

109. Barenholz, Y. Doxil®–the first FDA-approved nano-drug: lessons learned. *J Control Release* **160,** 117–34. ISSN: 0168-3659 (2012).

110. Biner, O., Schick, T., Müller, Y. & von Ballmoos, C. Delivery of membrane proteins into small and giant unilamellar vesicles by charge-mediated fusion. *FEBS Lett* **590,** 2051–62. ISSN: 0014-5793 (2016).

111. van Swaay, D. & deMello, A. Microfluidic methods for forming liposomes. *Lab on a Chip* **13,** 752–767. ISSN: 1473-0197 (2013).

112. Naumann, R. *et al.* Incorporation of Membrane Proteins in Solid-Supported Lipid Layers. *Angewandte Chemie International Edition in English* **34,** 2056–2058. ISSN: 0570-0833 (1995).

113. Bronder, A. M. *et al.* Oriented Membrane Protein Reconstitution into Tethered Lipid Membranes for AFM Force Spectroscopy. *Biophys J* **111,** 1925–1934. ISSN: 0006-3495 (2016).

114. Sumino, A., Uchihashi, T. & Oiki, S. Oriented Reconstitution of the Full-Length KcsA Potassium Channel in a Lipid Bilayer for AFM Imaging. *The Journal of Physical Chemistry Letters,* 785–793. ISSN: 1948-7185 (2017).

115. Carlson, M. L. *et al.* The Peptidisc, a simple method for stabilizing membrane proteins in detergent-free solution. *Elife* **7.** ISSN: 2050-084x (2018).

116. Angiulli, G. *et al.* New approach for membrane protein reconstitution into peptidiscs and basis for their adaptability to different proteins. *Elife* **9.** ISSN: 2050-084x (2020).

117. Popot, J.-L. Amphipols, Nanodiscs, and Fluorinated Surfactants: Three Non-conventional Approaches to Studying Membrane Proteins in Aqueous Solutions. *Annual Review of Biochemistry* **79,** 737–775 (2010).

118. Pocanschi, C. L. *et al.* Amphipathic polymers: tools to fold integral membrane proteins to their active form. *Biochemistry* **45,** 13954–61. ISSN: 0006-2960 (Print) 0006-2960 (2006).

119. Dahmane, T., Damian, M., Mary, S., Popot, J. L. & Baneres, J. L. Amphipol-assisted *in vitro* folding of G protein-coupled receptors. *Biochemistry* **48,** 6516–21. ISSN: 0006-2960 (2009).

120. Popot, J. L. *et al.* Amphipols from A to Z. *Annu Rev Biophys* **40,** 379–408. ISSN: 1936-122x (2011).

121. Zoonens, M. & Popot, J. L. Amphipols for each season. *J Membr Biol* **247,** 759–96. ISSN: 0022-2631 (2014).

122. Kleinschmidt, J. H. & Popot, J. L. Folding and stability of integral membrane proteins in amphipols. *Arch Biochem Biophys* **564,** 327–43. ISSN: 0003-9861 (2014).

123. Le Bon, C., Marconnet, A., Masscheleyn, S., Popot, J. L. & Zoonens, M. Folding and stabilizing membrane proteins in amphipol A8-35. *Methods* **147,** 95–105. ISSN: 1046-2023 (2018).

124. Rigaud, J. L., Pitard, B. & Levy, D. Reconstitution of membrane proteins into liposomes: application to energy-transducing membrane proteins. *Biochim Biophys Acta* **1231,** 223–46. ISSN: 0006-3002 (Print) 0006-3002 (1995).

125. Etemadi, A. H. Functional and orientational features of protein molecules in reconstituted lipid membranes. *Adv Lipid Res* **21,** 281–428. ISSN: 0065-2849 (Print) 0065-2849 (1985).

126. Rigaud, J. L. & Levy, D. Reconstitution of membrane proteins into liposomes. *Methods Enzymol* **372,** 65–86. ISSN: 0076-6879 (Print) 0076-6879 (2003).

127. Kagawa, Y. & Racker, E. Partial Resolution of the Enzymes Catalyzing Oxidative Phosphorylation. *The Journal of Biological Chemistry* **246,** 5477–5487 (1971).

128. Hinkle, P. C., Kim, J. J. & Racker, E. Ion transport and respiratory control in vesicles formed from cytochrome oxidase and phospholipids. *J Biol Chem* **247,** 1338–9. ISSN: 0021-9258 (Print) 0021-9258 (1972).

129. Racker, E. Reconstitution of a calcium pump with phospholipids and a purified Ca^{++}-adenosine triphosphatase from sacroplasmic reticulum. *J Biol Chem* **247,** 8198–200. ISSN: 0021-9258 (Print) 0021-9258 (1972).

130. Knol, J., Veenhoff, L., *et al.* Unidirectional reconstitution into detergent-destabilized liposomes of the purified lactose transport system of *Streptococcus thermophilus*. *J Biol Chem* **271,** 15358–66. ISSN: 0021-9258 (Print) 0021-9258 (1996).

131. Lichtenberg, D., Ahyayauch, H. & Goni, F. M. The mechanism of detergent solubilization of lipid bilayers. *Biophys J* **105,** 289–99. ISSN: 0006-3495 (2013).

132. Crouch, C. H. *et al.* Optimization of Detergent-Mediated Reconstitution of Influenza A M2 Protein into Proteoliposomes. *Membranes (Basel)* **8.** ISSN: 2077-0375 (Print) 2077-0375 (2018).

133. Degrip, W. J., Vanoostrum, J. & Bovee-Geurts, P. H. Selective detergent-extraction from mixed detergent/lipid/protein micelles, using cyclodextrin inclusion compounds: a novel generic approach for the preparation of proteoliposomes. *Biochem J* **330 (Pt 2),** 667–74. ISSN: 0264-6021 (Print) 0264-6021 (1998).

134. Bernat, V. *et al.* Inclusion complex of n-octyl beta-D-glucopyranoside and alpha-cyclodextrin in aqueous solutions: thermodynamic and structural characterization. *Langmuir* **24,** 3140–9. ISSN: 0743-7463 (Print) 0743-7463 (2008).

135. Hădărugă, N. G., Bandur, G. N., David, I. & Hădărugă, D. I. A review on thermal analyses of cyclodextrins and cyclodextrin complexes. *Environmental Chemistry Letters* **17,** 349–373. ISSN: 1610-3661 (2019).

136. Jones, S. T. *et al.* Modified cyclodextrins as broad-spectrum antivirals. *Science Advances* **6,** eaax9318 (2020).

137. Cagno, V., Tseligka, E. D., Jones, S. T. & Tapparel, C. Heparan Sulfate Proteoglycans and Viral Attachment: True Receptors or Adaptation Bias? *Viruses* **11.** ISSN: 1999-4915 (2019).

138. Wang, L. & Tonggu, L. Membrane protein reconstitution for functional and structural studies. *Sci China Life Sci* **58,** 66–74. ISSN: 1674-7305 (2015).

139. Dalziel, J. E., Wong, S. S., Phung, T., Zhang, Y. L. & Dunlop, J. Expression of human BK ion channels in Sf9 cells, their purification using metal affinity chromatography, and functional reconstitution into planar lipid bilayers. *Journal of Chromatography B* **857,** 315–321. ISSN: 1570-0232 (2007).

140. Wang, L. & Sigworth, F. J. Structure of the BK potassium channel in a lipid membrane from electron cryomicroscopy. *Nature* **461,** 292–295. ISSN: 1476-4687 (2009).

141. Kameyama, A., Shearman, M. S., Sekiguchi, K. & Kameyama, M. Cyclic AMP-Dependent Protein Kinase but Not Protein Kinase C Regulates the Cardiac Ca^{2+} Channel through Phosphorylation of Its α1 Subunit. *The Journal of Biochemistry* **120,** 170–176. ISSN: 0021-924X (1996).

142. Schiebler, W. & Hucho, F. Membranes Rich in Acetylcholine Receptor: Characterization and Reconstitution to Excitable Membranes from Exogenous Lipids. *European Journal of Biochemistry* **85,** 55–63. ISSN: 0014-2956 (1978).

143. Mimms, L. T., Zampighi, G., Nozaki, Y., Tanford, C. & Reynolds, J. A. Phospholipid vesicle formation and transmembrane protein incorporation using octyl glucoside. *Biochemistry* **20,** 833–840. ISSN: 0006-2960 (1981).

144. Nakao, S.-i., Ebata, H., Hamamoto, T., Kagawa, Y. & Hirata, H. Solubilization and reconstitution of voltage-dependent calcium channel from bovine cardiac muscle. Ca^{2+} influx assay using the fluorescent dye Quin2. *Biochimica et Biophysica Acta (BBA) - Biomembranes* **944,** 337–343. ISSN: 0005-2736 (1988).

145. Epstein, M. & Racker, E. Reconstitution of carbamylcholine-dependent sodium ion flux and desensitization of the acetylcholine receptor from *Torpedo californica*. *Journal of Biological Chemistry* **253,** 6660–6662. ISSN: 00219258 (ISSN) (1978).

146. Cheng, K. H., Lepock, J. R., Hui, S. W. & Yeagle, P. L. The role of cholesterol in the activity of reconstituted Ca-ATPase vesicles containing unsaturated phosphatidylethanolamine. *J Biol Chem* **261,** 5081–7. ISSN: 0021-9258 (Print) 0021-9258 (1986).

147. Young, H. S., Rigaud, J. L., Lacapère, J. J., Reddy, L. G. & Stokes, D. L. How to make tubular crystals by reconstitution of detergent-solubilized Ca^{2+}-ATPase. *Biophysical Journal* **72,** 2545–2558. ISSN: 0006-3495 (1997).

148. Lévy, D., Bluzat, A., Seigneuret, M. & Rigaud, J.-L. A systematic study of liposome and proteoliposome reconstitution involving Bio-Bead-mediated Triton X-100 removal. *Biochimica et Biophysica Acta (BBA) - Biomembranes* **1025,** 179–190. ISSN: 0005-2736 (1990).

149. Holloway, P. W. A simple procedure for removal of triton X-100 from protein samples. *Analytical Biochemistry* **53,** 304–308. ISSN: 0003-2697 (1973).

150. Zhou, X. & Graham, T. R. Reconstitution of phospholipid translocase activity with purified Drs2p, a type-IV P-type ATPase from budding yeast. *Proceedings of the National Academy of Sciences* **106,** 16586 (2009).

151. Kim, M. & Song, E. Iron transport by proteoliposomes containing mitochondrial F_1F_o ATP synthase isolated from rat heart. *Biochimie* **92,** 333–342. ISSN: 0300-9084 (2010).

152. Hatzi, P., Mourtas, S., Klepetsanis, P. G. & Antimisiaris, S. G. Integrity of liposomes in presence of cyclodextrins: effect of liposome type and lipid composition. *Int J Pharm* **333,** 167–76. ISSN: 0378-5173 (Print) 0378-5173 (2007).

153. Cliff, L., Chadda, R. & Robertson, J. L. Occupancy distributions of membrane proteins in heterogeneous liposome populations. *Biochim Biophys Acta Biomembr* **1862,** 183033. ISSN: 0005-2736 (2020).

154. Richard, P., Rigaud, J. L. & Graber, P. Reconstitution of CF_0F_1 into liposomes using a new reconstitution procedure. *Eur J Biochem* **193,** 921–5. ISSN: 0014-2956 (Print) 0014-2956 (1990).

155. Levy, D., Gulik, A., Bluzat, A. & Rigaud, J. L. Reconstitution of the sarcoplasmic reticulum Ca^{2+}-ATPase: mechanisms of membrane protein insertion into liposomes during reconstitution procedures involving the use of detergents. *Biochim Biophys Acta* **1107,** 283–98. ISSN: 0006-3002 (Print) 0006-3002 (1992).

156. Hegde, R. S. & Keenan, R. J. Tail-anchored membrane protein insertion into the endoplasmic reticulum. *Nature Reviews Molecular Cell Biology* **12,** 787–798. ISSN: 1471-0080 (2011).

157. Seppala, S., Slusky, J. S., Lloris-Garcera, P., Rapp, M. & von Heijne, G. Control of membrane protein topology by a single C-terminal residue. *Science* **328,** 1698–700. ISSN: 0036-8075 (2010).

158. Stephens, D., Kulkarni, S. & Austen, B. in *Biomembranes: A Multi-Volume Treatise* (ed Lee, A. G.) 107–135 (JAI, 1995). ISBN: 978-1-55938-659-3.

159. Van den Berg, B. *et al.* X-ray structure of a protein-conducting channel. *Nature* **427,** 36–44. ISSN: 0028-0836 (2004).

160. Tate, C. G. Biochemistry. Membrane protein gymnastics. *Science* **328,** 1644–5. ISSN: 0036-8075 (2010).

161. Xie, K. & Dalbey, R. E. Inserting proteins into the bacterial cytoplasmic membrane using the Sec and YidC translocases. *Nat Rev Microbiol* **6,** 234–44. ISSN: 1740-1526 (2008).

162. von Heijne, G. Control of topology and mode of assembly of a polytopic membrane protein by positively charged residues. *Nature* **341,** 456–8. ISSN: 0028-0836 (Print) 0028-0836 (1989).

163. Gafvelin, G. & von Heijne, G. Topological "frustration" in multispanning *E. coli* inner membrane proteins. *Cell* **77,** 401–12. ISSN: 0092-8674 (Print) 0092-8674 (1994).

164. Korkhov, V. M. & Tate, C. G. An emerging consensus for the structure of EmrE. *Acta Crystallogr D Biol Crystallogr* **65,** 186–92. ISSN: 0907-4449 (2009).

165. Woodall, N. B., Yin, Y. & Bowie, J. U. Dual-topology insertion of a dual-topology membrane protein. *Nature Communications* **6,** 8099. ISSN: 2041-1723 (2015).

166. Fluman, N., Tobiasson, V. & von Heijne, G. Stable membrane orientations of small dual-topology membrane proteins. *Proc Natl Acad Sci U S A* **114,** 7987–7992. ISSN: 0027-8424 (2017).

167. Näsvik Öjemyr, L., von Ballmoos, C., Faxen, K., Svahn, E. & Brzezinski, P. The membrane modulates internal proton transfer in cytochrome *c* oxidase. *Biochemistry* **51,** 1092–100. ISSN: 0006-2960 (2012).

168. Seigneuret, M. & Rigaud, J.-L. Partial separation of inwardly pumping and outwardly pumping bacteriorhodopsin reconstituted liposomes by gel filtration. *FEBS Letters* **228,** 79–84. ISSN: 0014-5793 (1988).

169. Wiedenmann, A., Dimroth, P. & von Ballmoos, C. $\Delta\psi$ and ΔpH are equivalent driving forces for proton transport through isolated F_0 complexes of ATP synthases. *Biochim Biophys Acta* **1777,** 1301–10. ISSN: 0006-3002 (Print) 0006-3002 (2008).

170. von Ballmoos, C., Biner, O., Nilsson, T. & Brzezinski, P. Mimicking respiratory phosphorylation using purified enzymes. *Biochim Biophys Acta* **1857,** 321–331. ISSN: 0006-3002 (Print) 0006-3002 (2015).

171. Dixon, J. F. & Hokin, L. E. The reconstituted Na,K-ATPase is electrogenic. *J Biol Chem* **255,** 10681–6. ISSN: 0021-9258 (Print) 0021-9258 (1980).

172. Li, M., Jørgensen, S. K., *et al.* Single Enzyme Experiments Reveal a Long-Lifetime Proton Leak State in a Heme-Copper Oxidase. *Journal of the American Chemical Society* **137,** 16055–16063. ISSN: 0002-7863 (2015).

173. Nilsson, T. *et al.* Lipid-mediated Protein-protein Interactions Modulate Respiration-driven ATP Synthesis. *Sci Rep* **6,** 24113. ISSN: 2045-2322 (2016).

174. Nordlund, G., Brzezinski, P. & von Ballmoos, C. SNARE-fusion mediated insertion of membrane proteins into native and artificial membranes. *Nat Commun* **5,** 4303. ISSN: 2041-1723 (2014).

175. Nomura, T., Cox, C. D., Bavi, N., Sokabe, M. & Martinac, B. Unidirectional incorporation of a bacterial mechanosensitive channel into liposomal membranes. *Faseb j* **29,** 4334–45. ISSN: 0892-6638 (2015).

176. Delcour, A. H., Martinac, B., Adler, J. & Kung, C. Modified reconstitution method used in patch-clamp studies of *Escherichia coli* ion channels. *Biophys J* **56,** 631–6. ISSN: 0006-3495 (Print) 0006-3495 (1989).

177. Hase, C. C., Le Dain, A. C. & Martinac, B. Purification and functional reconstitution of the recombinant large mechanosensitive ion channel (MscL) of *Escherichia coli*. *J Biol Chem* **270,** 18329–34. ISSN: 0021-9258 (Print) 0021-9258 (1995).

178. Verkhovskaya, M. L. *et al.* Glutamic acid 286 in subunit I of cytochrome bo_3 is involved in proton translocation. *Proc Natl Acad Sci U S A* **94,** 10128–31. ISSN: 0027-8424 (Print) 0027-8424 (1997).

179. Rigaud, J. L., Paternostre, M. T. & Bluzat, A. Mechanisms of membrane protein insertion into liposomes during reconstitution procedures involving the use of detergents. 2. Incorporation of the light-driven proton pump bacteriorhodopsin. *Biochemistry* **27,** 2677–88. ISSN: 0006-2960 (Print) 0006-2960 (1988).

180. Knol, J., Sjollema, K. & Poolman, B. Detergent-mediated reconstitution of membrane proteins. *Biochemistry* **37,** 16410–5. ISSN: 0006-2960 (Print) 0006-2960 (1998).

181. de Lima Santos, H., Lopes, M. L., Maggio, B. & Ciancaglini, P. Na,K-ATPase reconstituted in liposomes: effects of lipid composition on hydrolytic activity and enzyme orientation. *Colloids Surf B Biointerfaces* **41,** 239–48. ISSN: 0927-7765 (Print) 0927-7765 (2005).

182. Huang, H., Ge, B., *et al.* Using Fluorescence Quenching Titration to Determine the Orientation of a Model Transmembrane Protein in Mimic Membranes. *Materials (Basel)* **12.** ISSN: 1996-1944 (Print) 1996-1944 (2019).

183. Tunuguntla, R. *et al.* Lipid bilayer composition can influence the orientation of proteorhodopsin in artificial membranes. *Biophys J* **105,** 1388–96. ISSN: 0006-3495 (2013).

184. Happe, M., Teathera, R. M., Overath, P., Knobling, A. & Oesterhelt, D. Direction of proton translocation in proteoliposomes formed from purple membrane and acidic lipids depends on the pH during reconstitution. *Biochim Biophys Acta* **465,** 415–20. ISSN: 0006-3002 (Print) 0006-3002 (1977).

185. Schadauer, F. *et al.* Silica nanoparticles for the oriented encapsulation of membrane proteins into artificial bilayer lipid membranes. *Langmuir* **31,** 2511–6. ISSN: 0743-7463 (2015).

186. Geiss, A. F. *et al.* Proteo-lipobeads to encapsulate cytochrome *c* oxidase from *Paracoccus denitrificans*. *J Colloid Interface Sci* **500,** 119–125. ISSN: 0021-9797 (2017).

187. Behrens, S. H. & Grier, D. G. The charge of glass and silica surfaces. *The Journal of Chemical Physics* **115,** 6716–6721 (2001).

188. Zheng, H., Lee, S., Llaguno, M. C. & Jiang, Q.-X. bSUM: A bead-supported unilamellar membrane system facilitating unidirectional insertion of membrane proteins into giant vesicles. *The Journal of General Physiology* **147,** 77–93 (2016).

189. Ruta, V., Jiang, Y., Lee, A., Chen, J. & MacKinnon, R. Functional analysis of an archaebacterial voltage-dependent K^+ channel. *Nature* **422,** 180–5. ISSN: 0028-0836 (Print) 0028-0836 (2003).

190. Jiang, Q.-X., Wang, D.-N. & MacKinnon, R. Electron microscopic analysis of K_vAP voltage-dependent K^+ channels in an open conformation. *Nature* **430,** 806–810. ISSN: 1476-4687 (2004).

191. Friedrich, M. G., Robertson, J. W. F., Walz, D., Knoll, W. & Naumann, R. L. C. Electronic Wiring of a Multi-Redox Site Membrane Protein in a Biomimetic Surface Architecture. *Biophysical Journal* **94,** 3698–3705. ISSN: 0006-3495 (2008).

192. Ritzmann, N. *et al.* Fusion Domains Guide the Oriented Insertion of Light-Driven Proton Pumps into Liposomes. *Biophys J* **113,** 1181–1186. ISSN: 0006-3495 (2017).

193. Rumbley, J. N., Furlong Nickels, E. & Gennis, R. B. One-step purification of histidine-tagged cytochrome bo_3 from *Escherichia coli* and demonstration that associated quinone is not required for the structural integrity of the oxidase. *Biochim Biophys Acta* **1340,** 131–42. ISSN: 0006-3002 (Print) 0006-3002 (1997).

194. Bedbrook, C. N. *et al.* Genetically Encoded Spy Peptide Fusion System to Detect Plasma Membrane-Localized Proteins *In Vivo*. *Chem Biol* **22,** 1108–21. ISSN: 1074-5521 (2015).

195. Min, D., Arbing, M. A., Jefferson, R. E. & Bowie, J. U. A simple DNA handle attachment method for single molecule mechanical manipulation experiments. *Protein Sci* **25,** 1535–44. ISSN: 0961-8368 (2016).

196. Veggiani, G. *et al.* Programmable polyproteams built using twin peptide superglues. *Proc Natl Acad Sci U S A* **113,** 1202–7. ISSN: 0027-8424 (2016).

197. Yap, L. L., Samoilova, R. I., Gennis, R. B. & Dikanov, S. A. Characterization of mutants that change the hydrogen bonding of the semiquinone radical at the QH site of the cytochrome bo_3 from *Escherichia coli*. *J Biol Chem* **282,** 8777–85. ISSN: 0021-9258 (Print) 0021-9258 (2007).

198. Fairhead, M. & Howarth, M. Site-specific biotinylation of purified proteins using BirA. *Methods Mol Biol* **1266,** 171–84. ISSN: 1064-3745 (2015).

199. Huang, Z., Park, J. I., Watson, D. S., Hwang, P. & Szoka F. C., J. Facile synthesis of multivalent nitrilotriacetic acid (NTA) and NTA conjugates for analytical and drug delivery applications. *Bioconjug Chem* **17,** 1592–600. ISSN: 1043-1802 (Print) 1043-1802 (2006).

200. Huang, Z., Hwang, P., Watson, D. S., Cao, L. & Szoka F. C., J. Tris-nitrilotriacetic acids of subnanomolar affinity toward hexahistidine tagged molecules. *Bioconjug Chem* **20,** 1667–72. ISSN: 1043-1802 (2009).

201. Felpin, F. X. & Fouquet, E. A useful, reliable and safer protocol for hydrogenation and the hydrogenolysis of O-benzyl groups: the in situ preparation of an active Pd(0)/C catalyst with well-defined properties. *Chemistry* **16,** 12440–5. ISSN: 0947-6539 (2010).

202. Mandal, P. K. & McMurray, J. S. Pd-C-induced catalytic transfer hydrogenation with triethylsilane. *J Org Chem* **72,** 6599–601. ISSN: 0022-3263 (Print) 0022-3263 (2007).

203. Silverman, R. B. & Holladay, M. W. Stereospecific total syntheses of the natural antitumor agent, (αS,5S)-α-amino-3-chloro-4,5-dihydro-5-isoxazoleacetic acid, and its unnatural C-5 epimer. *Journal of the American Chemical Society* **103,** 7357–7358. ISSN: 0002-7863 (1981).

204. Fujii, N., Otaka, A., Sugiyama, N., Hatano, M. & Yajima, H. Studies on peptides. CLV. Evaluation of trimethylsilyl bromide as a hard-acid deprotecting reagent in peptide synthesis. *Chem Pharm Bull (Tokyo)* **35,** 3880–3. ISSN: 0009-2363 (Print) 0009-2363 (1987).

205. Beckett, D., Kovaleva, E. & Schatz, P. J. A minimal peptide substrate in biotin holoenzyme synthetase-catalyzed biotinylation. *Protein Sci* **8,** 921–9. ISSN: 0961-8368 (Print) 0961-8368 (1999).

206. Fall, R. R. Analysis of microbial biotin proteins. *Methods Enzymol* **62,** 390–8. ISSN: 0076-6879 (Print) 0076-6879 (1979).

207. Cronan J. E., J. Biotination of proteins *in vivo*. A post-translational modification to label, purify, and study proteins. *J Biol Chem* **265,** 10327–33. ISSN: 0021-9258 (Print) 0021-9258 (1990).

208. Diamandis, E. P. & Christopoulos, T. K. The biotin-(strept)avidin system: principles and applications in biotechnology. *Clin Chem* **37,** 625–36. ISSN: 0009-9147 (Print) 0009-9147 (1991).

209. Boucher, L. E. & Bosch, J. Development of a multifunctional tool for drug screening against plasmodial protein-protein interactions via surface plasmon resonance. *J Mol Recognit* **26,** 496–500. ISSN: 0952-3499 (2013).

210. Ng, K. & Connolly, J. E. Development of a multiplex bead-based assay to monitor dengue virus seroconversion. *Methods Mol Biol* **1138,** 53–74. ISSN: 1064-3745 (2014).

211. Niers, J. M. *et al.* Single reporter for targeted multimodal *in vivo* imaging. *J Am Chem Soc* **134,** 5149–56. ISSN: 0002-7863 (2012).

212. Jain, A., Barve, A., Zhao, Z., Jin, W. & Cheng, K. Comparison of Avidin, Neutravidin, and Streptavidin as Nanocarriers for Efficient siRNA Delivery. *Mol Pharm* **14,** 1517–1527. ISSN: 1543-8384 (2017).

213. Green, N. M. Avidin. *Adv Protein Chem* **29,** 85–133. ISSN: 0065-3233 (Print) 0065-3233 (1975).

214. Holmberg, A. *et al.* The biotin-streptavidin interaction can be reversibly broken using water at elevated temperatures. *Electrophoresis* **26,** 501–10. ISSN: 0173-0835 (Print) 0173-0835 (2005).

215. Michael Green, N. in *Methods in Enzymology* (eds Wilchek, M. & Bayer, E. A.) 51–67 (Academic Press, 1990).

216. Lesch, H. P., Kaikkonen, M. U., Pikkarainen, J. T. & Yla-Herttuala, S. Avidin-biotin technology in targeted therapy. *Expert Opin Drug Deliv* **7,** 551–64. ISSN: 1742-5247 (2010).

217. Humbert, N., Zocchi, A. & Ward, T. R. Electrophoretic behavior of streptavidin complexed to a biotinylated probe: a functional screening assay for biotin-binding proteins. *Electrophoresis* **26,** 47–52. ISSN: 0173-0835 (Print) 0173-0835 (2005).

218. Simons S. S., J. Selective covalent labeling of cysteines in bovine serum albumin and in hepatoma tissue culture cell glucocorticoid receptors by dexamethasone 21-mesylate. *J Biol Chem* **262,** 9669–75. ISSN: 0021-9258 (Print) 0021-9258 (1987).

219. Holmberg, A. *et al.* The biotin-streptavidin interaction can be reversibly broken using water at elevated temperatures. *Electrophoresis* **26,** 501–10. ISSN: 0173-0835 (Print) 0173-0835 (2005).

220. Zheng, C., Ma, G. & Su, Z. Native PAGE eliminates the problem of PEG-SDS interaction in SDS-PAGE and provides an alternative to HPLC in characterization of protein PEGylation. *Electrophoresis* **28,** 2801–7. ISSN: 0173-0835 (Print) 0173-0835 (2007).

221. Casadio, R. Measurements of transmembrane pH differences of low extents in bacterial chromatophores. *European Biophysics Journal* **19,** 189–201. ISSN: 1432-1017 (1991).

222. Mazurenko, I., Hatzakis, N. S. & Jeuken, L. J. C. Single Liposome Measurements for the Study of Proton-Pumping Membrane Enzymes Using Electrochemistry and Fluorescent Microscopy. *J Vis Exp.* ISSN: 1940-087x (2019).

223. Seigneuret, M. & Rigaud, J.-L. Use of the fluorescent pH probe pyranine to detect heterogeneous directions of proton movement in bacteriorhodopsin reconstituted large liposomes. *FEBS Letters* **188,** 101–106 (1985).

224. Overly, C. C., Lee, K. D., Berthiaume, E. & Hollenbeck, P. J. Quantitative measurement of intraorganelle pH in the endosomal-lysosomal pathway in neurons by using ratiometric imaging with pyranine. *Proc Natl Acad Sci U S A* **92,** 3156–60. ISSN: 0027-8424 (Print) 0027-8424 (1995).

225. de Wet, J. R., Wood, K. V., DeLuca, M., Helinski, D. R. & Subramani, S. Firefly luciferase gene: structure and expression in mammalian cells. *Molecular and Cellular Biology* **7,** 725 (1987).

226. Lundin, A. Optimization of the firefly luciferase reaction for analytical purposes. *Adv Biochem Eng Biotechnol* **145,** 31–62. ISSN: 0724-6145 (Print) 0724-6145 (2014).

227. Meyrat, A. & von Ballmoos, C. ATP synthesis at physiological nucleotide concentrations. *Scientific Reports* **9,** 3070. ISSN: 2045-2322 (2019).

228. Smale, S. T. Luciferase assay. *Cold Spring Harb Protoc* **2010,** pdb.prot5421. ISSN: 1559-6095 (2010).

229. Biner, O. PhD-thesis - Co-reconstitution of respiratory chain enzymes and characterisation of *Escherichia coli* cytochrome *b*561.

230. Zakeri, B. *et al.* Peptide tag forming a rapid covalent bond to a protein, through engineering a bacterial adhesin. *Proc Natl Acad Sci U S A* **109,** E690–7. ISSN: 0027-8424 (2012).

231. Li, L., Fierer, J. O., Rapoport, T. A. & Howarth, M. Structural Analysis and Optimization of the Covalent Association between SpyCatcher and a Peptide Tag. *Journal of Molecular Biology* **426,** 309–317. ISSN: 0022-2836 (2014).

232. Reddington, S. C. & Howarth, M. Secrets of a covalent interaction for biomaterials and biotechnology: SpyTag and SpyCatcher. *Current Opinion in Chemical Biology* **29,** 94–99. ISSN: 1367-5931 (2015).

233. Keeble, A. H. & Howarth, M. Insider information on successful covalent protein coupling with help from SpyBank. *Methods Enzymol* **617,** 443–461. ISSN: 0076-6879 (2019).

234. Costa, S., Almeida, A., Castro, A. & Domingues, L. Fusion tags for protein solubility, purification and immunogenicity in *Escherichia coli*: the novel Fh8 system. *Frontiers in Microbiology* **5.** ISSN: 1664-302X (2014).

235. Salema, V. & Fernandez, L. A. High yield purification of nanobodies from the periplasm of *E. coli* as fusions with the maltose binding protein. *Protein Expr Purif* **91,** 42–8. ISSN: 1046-5928 (2013).

236. Kapust, R. B. & Waugh, D. S. *Escherichia coli* maltose-binding protein is uncommonly effective at promoting the solubility of polypeptides to which it is fused. *Protein Sci* **8,** 1668–74. ISSN: 0961-8368 (Print) 0961-8368 (1999).

237. Fox, J. D., Kapust, R. B. & Waugh, D. S. Single amino acid substitutions on the surface of *Escherichia coli* maltose-binding protein can have a profound impact on the solubility of fusion proteins. *Protein Sci* **10,** 622–30. ISSN: 0961-8368 (Print) 0961-8368 (2001).

238. Nikaido, H. Maltose transport system of *Escherichia coli*: an ABC-type transporter. *FEBS Lett* **346,** 55–8. ISSN: 0014-5793 (Print) 0014-5793 (1994).

239. Pryor, K. D. & Leiting, B. High-level expression of soluble protein in *Escherichia coli* using a His_6-tag and maltose-binding-protein double-affinity fusion system. *Protein Expr Purif* **10,** 309–19. ISSN: 1046-5928 (Print) 1046-5928 (1997).

240. di Guan, C., Li, P., Riggs, P. D. & Inouye, H. Vectors that facilitate the expression and purification of foreign peptides in *Escherichia coli* by fusion to maltose-binding protein. *Gene* **67,** 21–30. ISSN: 0378-1119 (Print) 0378-1119 (1988).

241. Fox, J. D. & Waugh, D. S. in *E. coliGene Expression Protocols* (ed Vaillancourt, P. E.) 99–117 (Humana Press, Totowa, NJ, 2003). ISBN: 978-1-59259-301-9.

242. Davis, G. D., Elisee, C., Newham, D. M. & Harrison, R. G. New fusion protein systems designed to give soluble expression in *Escherichia coli*. *Biotechnol Bioeng* **65,** 382–8. ISSN: 0006-3592 (Print) 0006-3592 (1999).

243. LaVallie, E. R. *et al.* A thioredoxin gene fusion expression system that circumvents inclusion body formation in the *E. coli* cytoplasm. *Biotechnology (N Y)* **11,** 187–93. ISSN: 0733-222X (Print) 0733-222x (1993).

244. Song, J. A., Lee, D. S., Park, J. S., Han, K. Y. & Lee, J. A novel *Escherichia coli* solubility enhancer protein for fusion expression of aggregation-prone heterologous proteins. *Enzyme Microb Technol* **49,** 124–30. ISSN: 0141-0229 (2011).

245. Smith, D. B. & Johnson, K. S. Single-step purification of polypeptides expressed in *Escherichia coli* as fusions with glutathione S-transferase. *Gene* **67,** 31–40. ISSN: 0378-1119 (Print) 0378-1119 (1988).

246. Butt, T. R., Edavettal, S. C., Hall, J. P. & Mattern, M. R. SUMO fusion technology for difficult-to-express proteins. *Protein Expr Purif* **43,** 1–9. ISSN: 1046-5928 (Print) 1046-5928 (2005).

247. Marblestone, J. G. *et al.* Comparison of SUMO fusion technology with traditional gene fusion systems: enhanced expression and solubility with SUMO. *Protein Sci* **15,** 182–9. ISSN: 0961-8368 (Print) 0961-8368 (2006).

248. Costa, S. J., Almeida, A., Castro, A., Domingues, L. & Besir, H. The novel Fh8 and H fusion partners for soluble protein expression in *Escherichia coli*: a comparison with the traditional gene fusion technology. *Appl Microbiol Biotechnol* **97,** 6779–91. ISSN: 0175-7598 (2013).

249. Costa, S. J., Coelho, E., *et al.* The Fh8 tag: a fusion partner for simple and cost-effective protein purification in *Escherichia coli*. *Protein Expr Purif* **92,** 163–70. ISSN: 1046-5928 (2013).

250. Zhang, Y. B. *et al.* Protein aggregation during overexpression limited by peptide extensions with large net negative charge. *Protein Expr Purif* **36,** 207–16. ISSN: 1046-5928 (Print) 1046-5928 (2004).

251. H., K. A. *et al.* Evolving Accelerated Amidation by SpyTag/SpyCatcher to Analyze Membrane Dynamics. *Angewandte Chemie International Edition* **56,** 16521–16525 (2017).

252. Hopp, T. P. *et al.* A Short Polypeptide Marker Sequence Useful for Recombinant Protein Identification and Purification. *Bio/Technology* **6,** 1204–1210. ISSN: 1546-1696 (1988).

253. Einhauer, A. & Jungbauer, A. The FLAG peptide, a versatile fusion tag for the purification of recombinant proteins. *J Biochem Biophys Methods* **49,** 455–65. ISSN: 0165-022X (Print) 0165-022x (2001).

254. Ueda, M., Manabe, Y. & Mukai, M. The high performance of 3XFLAG for target purification of a bioactive metabolite: a tag combined with a highly effective linker structure. *Bioorg Med Chem Lett* **21,** 1359–62. ISSN: 0960-894x (2011).

255. Goers, R. *et al.* Optimized reconstitution of membrane proteins into synthetic membranes. *Communications Chemistry* **1,** 35. ISSN: 2399-3669 (2018).

256. Hatzi, P., Mourtas, S., Klepetsanis, P. G. & Antimisiaris, S. G. Integrity of liposomes in presence of cyclodextrins: effect of liposome type and lipid composition. *Int J Pharm* **333,** 167–76. ISSN: 0378-5173 (Print) 0378-5173 (2007).

257. Pick, U. Liposomes with a large trapping capacity prepared by freezing and thawing of sonicated phospholipid mixtures. *Arch Biochem Biophys* **212,** 186–94. ISSN: 0003-9861 (Print) 0003-9861 (1981).

258. Gerber, G. E., Gray, C. P., Wildenauer, D. & Khorana, H. G. Orientation of bacteriorhodopsin in *Halobacterium halobium* as studied by selective proteolysis. *Proc Natl Acad Sci U S A* **74,** 5426–30. ISSN: 0027-8424 (Print) 0027-8424 (1977).

259. Kalmbach, R. *et al.* Functional Cell-free Synthesis of a Seven Helix Membrane Protein: In situ Insertion of Bacteriorhodopsin into Liposomes. *Journal of Molecular Biology* **371,** 639–648. ISSN: 0022-2836 (2007).

260. Gerber, G. E., Gray, C. P., Wildenauer, D. & Khorana, H. G. Orientation of bacteriorhodopsin in *Halobacterium halobium* as studied by selective proteolysis. *Proc Natl Acad Sci U S A* **74,** 5426–30. ISSN: 0027-8424 (Print) 0027-8424 (1977).

261. van Dijck, P. W. M. & van Dam, K. in *Methods in Enzymology* 17–25 (Academic Press, 1982). ISBN: 0076-6879.

262. Ihara, K. & Mukohata, Y. Proteoliposomes with right-side-out oriented purple membrane/bacteriorhodopsin require cations inside for proton pumping. *FEBS Lett* **240,** 148–52. ISSN: 0014-5793 (Print) 0014-5793 (1988).

263. Vaughan, J. C., Dempsey, G. T., Sun, E. & Zhuang, X. Phosphine Quenching of Cyanine Dyes as a Versatile Tool for Fluorescence Microscopy. *Journal of the American Chemical Society* **135,** 1197–1200. ISSN: 0002-7863 (2013).

264. Cline, D. J. *et al.* New water-soluble phosphines as reductants of peptide and protein disulfide bonds: reactivity and membrane permeability. *Biochemistry* **43,** 15195–203. ISSN: 0006-2960 (Print) 0006-2960 (2004).

265. Stern, O. & Volmer, M. Über die Abklingungszeit der Fluoreszenz. *Physikalische Zeitschrift* **20,** 183–188 (1919).

266. Malhotra, A. in *Methods in Enzymology* (eds Burgess, R. R. & Deutscher, M. P.) 239–258 (Academic Press, 2009). ISBN: 0076-6879.

267. Hemdan, E. S., Zhao, Y. J., Sulkowski, E. & Porath, J. Surface topography of histidine residues: a facile probe by immobilized metal ion affinity chromatography. *Proc Natl Acad Sci U S A* **86,** 1811–5. ISSN: 0027-8424 (Print) 0027-8424 (1989).

268. Hochuli, E., Döbeli, H. & Schacher, A. New metal chelate adsorbent selective for proteins and peptides containing neighbouring histidine residues. *J Chromatogr* **411,** 177–84 (1987).

269. Bornhorst, J. A. & Falke, J. J. Purification of proteins using polyhistidine affinity tags. *Methods Enzymol* **326,** 245–54. ISSN: 0076-6879 (Print) 0076-6879 (2000).

270. Mohanty, A. K. & Wiener, M. C. Membrane protein expression and production: effects of polyhistidine tag length and position. *Protein Expr Purif* **33,** 311–25. ISSN: 1046-5928 (Print) 1046-5928 (2004).

271. Hochuli, E., Bannwarth, W., Döbeli, H., Gentz, R. & Stüber, D. Genetic Approach to Facilitate Purification of Recombinant Proteins with a Novel Metal Chelate Adsorbent. *Bio/Technology* **6,** 1321–1325. ISSN: 1546-1696 (1988).

272. Janknecht, R., de Martynoff, G., *et al.* Rapid and efficient purification of native histidine-tagged protein expressed by recombinant vaccinia virus. *Proc Natl Acad Sci U S A* **88,** 8972–6. ISSN: 0027-8424 (Print) 0027-8424 (1991).

273. Janknecht, R. & Nordheim, A. Affinity purification of histidine-tagged proteins transiently produced in HeLa cells. *Gene* **121,** 321–4. ISSN: 0378-1119 (Print) 0378-1119 (1992).

274. Wülfing, C., Lombardero, J. & Plückthun, A. An *Escherichia coli* protein consisting of a domain homologous to FK506-binding proteins (FKBP) and a new metal binding motif. *J Biol Chem* **269,** 2895–901. ISSN: 0021-9258 (Print) 0021-9258 (1994).

275. Grisshammer, R. & Tucker, J. Quantitative evaluation of neurotensin receptor purification by immobilized metal affinity chromatography. *Protein Expr Purif* **11,** 53–60. ISSN: 1046-5928 (Print) 1046-5928 (1997).

276. Lata, S., Reichel, A., Brock, R., Tampe, R. & Piehler, J. High-affinity adaptors for switchable recognition of histidine-tagged proteins. *J Am Chem Soc* **127,** 10205–15. ISSN: 0002-7863 (Print) 0002-7863 (2005).

277. Sigal, G. B., Bamdad, C., Barberis, A., Strominger, J. & Whitesides, G. M. A self-assembled monolayer for the binding and study of histidine-tagged proteins by surface plasmon resonance. *Anal Chem* **68,** 490–7. ISSN: 0003-2700 (Print) 0003-2700 (1996).

278. Gershon, P. D. & Khilko, S. Stable chelating linkage for reversible immobilization of oligohistidine tagged proteins in the BIAcore surface plasmon resonance detector. *J Immunol Methods* **183,** 65–76. ISSN: 0022-1759 (Print) 0022-1759 (1995).

279. Nieba, L. *et al.* BIACORE analysis of histidine-tagged proteins using a chelating NTA sensor chip. *Anal Biochem* **252,** 217–28. ISSN: 0003-2697 (Print) 0003-2697 (1997).

280. Dorn, I. T., Pawlitschko, K., Pettinger, S. C. & Tampé, R. Orientation and two-dimensional organization of proteins at chelator lipid interfaces. *Biol Chem* **379,** 1151–9. ISSN: 1431-6730 (Print) 1431-6730 (1998).

281. Dorn, I. T., Neumaier, K. R. & Tampé, R. Molecular Recognition of Histidine-Tagged Molecules by Metal-Chelating Lipids Monitored by Fluorescence Energy Transfer and Correlation Spectroscopy. *Journal of the American Chemical Society* **120,** 2753–2763. ISSN: 0002-7863 (1998).

282. Kapanidis, A. N., Ebright, Y. W. & Ebright, R. H. Site-specific incorporation of fluorescent probes into protein: hexahistidine-tag-mediated fluorescent labeling with (Ni^{2+}:nitrilotriacetic Acid (n)-fluorochrome conjugates. *J Am Chem Soc* **123,** 12123–5. ISSN: 0002-7863 (Print) 0002-7863 (2001).

283. Hutschenreiter, S., Neumann, L., Rädler, U., Schmitt, L. & Tampé, R. Metal-chelating amino acids as building blocks for synthetic receptors sensing metal ions and histidine-tagged proteins. *Chembiochem* **4,** 1340–4. ISSN: 1439-4227 (Print) 1439-4227 (2003).

284. Guignet, E. G., Hovius, R. & Vogel, H. Reversible site-selective labeling of membrane proteins in live cells. *Nat Biotechnol* **22,** 440–4. ISSN: 1087-0156 (Print) 1087-0156 (2004).

285. Johnson, R. D., Todd, R. J. & Arnold, F. H. Multipoint binding in metal-affinity chromatography II. Effect of pH and imidazole on chromatographic retention of engineered histidine-containing cytochromes *c*. *J Chromatogr A* **725,** 225–35. ISSN: 0021-9673 (Print) 0021-9673 (1996).

286. Lata, S. & Piehler, J. Stable and functional immobilization of histidine-tagged proteins via multivalent chelator headgroups on a molecular poly(ethylene glycol) brush. *Anal Chem* **77,** 1096–105. ISSN: 0003-2700 (Print) 0003-2700 (2005).

287. Rao, J., Lahiri, J., Isaacs, L., Weis, R. M. & Whitesides, G. M. A trivalent system from vancomycin.D-ala-D-Ala with higher affinity than avidin.biotin. *Science* **280,** 708–11. ISSN: 0036-8075 (Print) 0036-8075 (1998).

288. Wieneke, R. & Tampé, R. Multivalent Chelators for In Vivo Protein Labeling. *Angew Chem Int Ed Engl* **58,** 8278–8290. ISSN: 1433-7851 (2019).

289. Lata, S., Gavutis, M., Tampé, R. & Piehler, J. Specific and stable fluorescence labeling of histidine-tagged proteins for dissecting multi-protein complex formation. *J Am Chem Soc* **128,** 2365–72. ISSN: 0002-7863 (Print) 0002-7863 (2006).

290. Dyla, M. *et al.* Dynamics of P-type ATPase transport revealed by single-molecule FRET. *Nature* **551,** 346–351. ISSN: 0028-0836 (2017).

291. Guesdon, A. *et al.* EB1 interacts with outwardly curved and straight regions of the microtubule lattice. *Nat Cell Biol* **18,** 1102–8. ISSN: 1465-7392 (2016).

292. Chepuri, V. & Gennis, R. B. The use of gene fusions to determine the topology of all of the subunits of the cytochrome *o* terminal oxidase complex of *Escherichia coli*. *J Biol Chem* **265,** 12978–86. ISSN: 0021-9258 (Print) 0021-9258 (1990).

293. van der Oost, J., Lappalainen, P., *et al.* Restoration of a lost metal-binding site: construction of two different copper sites into a subunit of the *E. coli* cytochrome *o* quinol oxidase complex. *Embo j* **11,** 3209–17. ISSN: 0261-4189 (Print) 0261-4189 (1992).

294. van der Oost, J., Musacchio, A., *et al.* Crystallization and Preliminary X-ray Analysis of the Periplasmic Fragment of CyoA-a Subunit of the *Escherichia coli* Cytochrome *o* Complex. *Journal of Molecular Biology* **229,** 794–796. ISSN: 0022-2836 (1993).

295. Piehler, J. in *Advanced Fluorescence Reporters in Chemistry and Biology III* (ed Demchenko, P. A.) 297–310 (Springer, 2011). ISBN: 978-3-642-18034-7.

296. Yoo, J. *et al.* Click chemistry-mediated tumor-targeting of SN38-loaded nanoparticles using trastuzumab. *Biochem Biophys Res Commun* **515,** 207–213. ISSN: 0006-291x (2019).

297. Kolb, H. C., Finn, M. G. & Sharpless, K. B. Click Chemistry: Diverse Chemical Function from a Few Good Reactions. *Angewandte Chemie International Edition* **40,** 2004–2021. ISSN: 1433-7851 (2001).

298. Kenry & Liu, B. Bio-orthogonal Click Chemistry for *In Vivo* Bioimaging. *Trends in Chemistry* **1,** 763–778. ISSN: 2589-7209 (2019).

299. Lutz, J. F. & Zarafshani, Z. Efficient construction of therapeutics, bioconjugates, biomaterials and bioactive surfaces using azide-alkyne "click" chemistry. *Adv Drug Deliv Rev* **60,** 958–70. ISSN: 0169-409X (Print) 0169-409x (2008).

300. Binder, W. H. & Sachsenhofer, R. 'Click' Chemistry in Polymer and Materials Science. *Macromolecular Rapid Communications* **28,** 15–54. ISSN: 1022-1336 (2007).

301. Chen, G. *et al.* Synthesis of azide/alkyne-terminal polymers and application for surface functionalisation through a $[2+3]$ Huisgen cycloaddition process, "click chemistry". *Soft Matter* **3,** 732–739. ISSN: 1744-683X (2007).

302. Gondi, S. R., Vogt, A. P. & Sumerlin, B. S. Versatile Pathway to Functional Telechelics via RAFT Polymerization and Click Chemistry. *Macromolecules* **40,** 474–481. ISSN: 0024-9297 (2007).

303. Hawker, C. J., Fokin, V. V., Finn, M. G. & Sharpless, K. B. Bringing Efficiency to Materials Synthesis: The Philosophy of Click Chemistry. *Australian Journal of Chemistry* **60,** 381–383 (2007).

304. Zeglis, B. *et al.* A Pretargeted PET Imaging Strategy Based on Bioorthogonal Diels-Alder Click Chemistry. *Journal of nuclear medicine : official publication, Society of Nuclear Medicine* **54** (2013).

305. Merrifield, B. Solid phase synthesis. *Science* **232,** 341–7. ISSN: 0036-8075 (Print) 0036-8075 (1986).

306. Khairil Anuar, I. N. A. *et al.* Spy&Go purification of SpyTag-proteins using pseudo-SpyCatcher to access an oligomerization toolbox. *Nat Commun* **10,** 1734. ISSN: 2041-1723 (2019).

307. Harder, D. *et al.* Engineering a Chemical Switch into the Light-driven Proton Pump Proteorhodopsin by Cysteine Mutagenesis and Thiol Modification. *Angew Chem Int Ed Engl* **55,** 8846–9. ISSN: 1433-7851 (2016).

308. Mayr, J. A. *et al.* Spectrum of combined respiratory chain defects. *J Inherit Metab Dis* **38,** 629–40. ISSN: 0141-8955 (2015).

309. Benit, P., Lebon, S. & Rustin, P. Respiratory-chain diseases related to complex III deficiency. *Biochim Biophys Acta* **1793,** 181–5. ISSN: 0006-3002 (Print) 0006-3002 (2009).

310. Rask-Andersen, M., Almén, M. S. & Schiöth, H. B. Trends in the exploitation of novel drug targets. *Nat Rev Drug Discov* **10,** 579–90. ISSN: 1474-1776 (2011).

7 Supplementary Information.

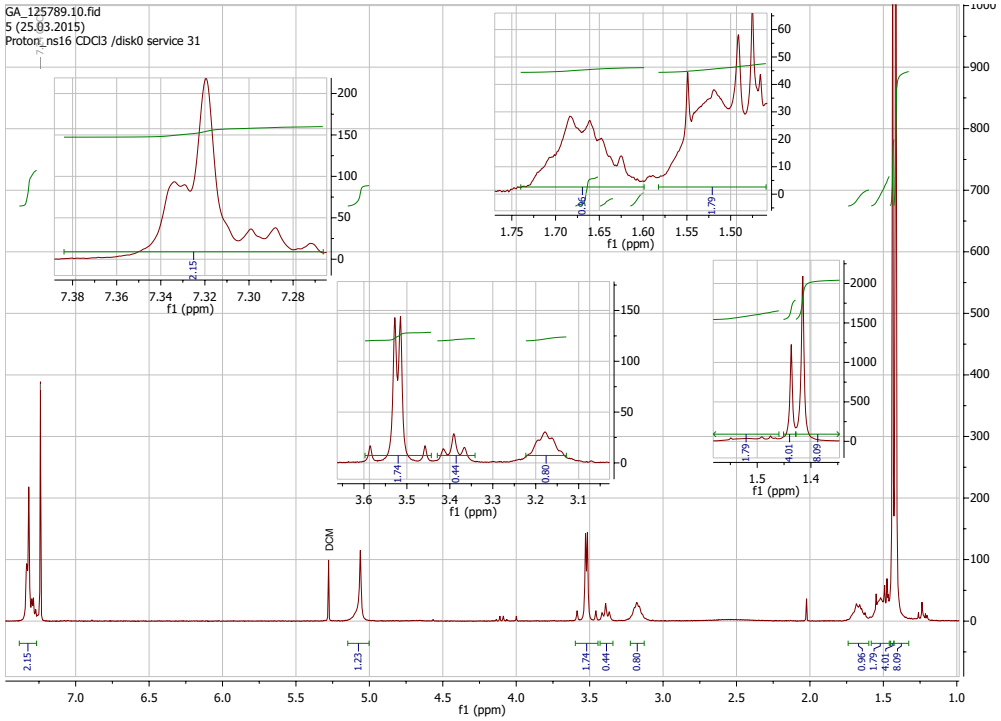

Figure S1: ^{1}H-NMR of 2. Number of scans: 16. In $CDCl_3$.

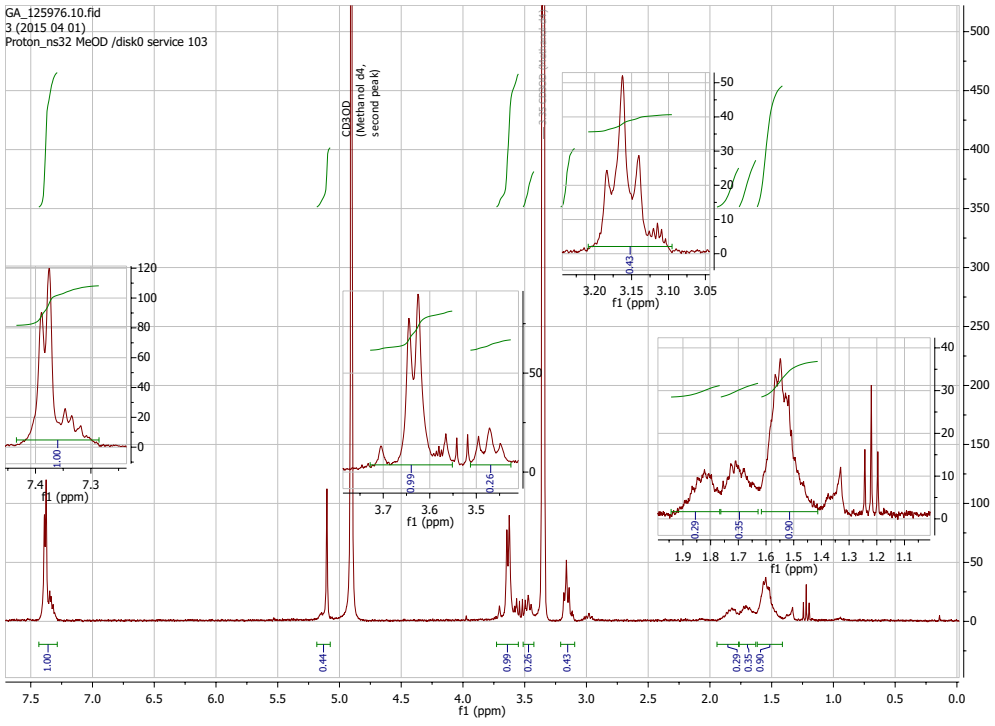

Figure S2: ^{1}H-NMR of 3. Number of scans: 32. In MeOD.

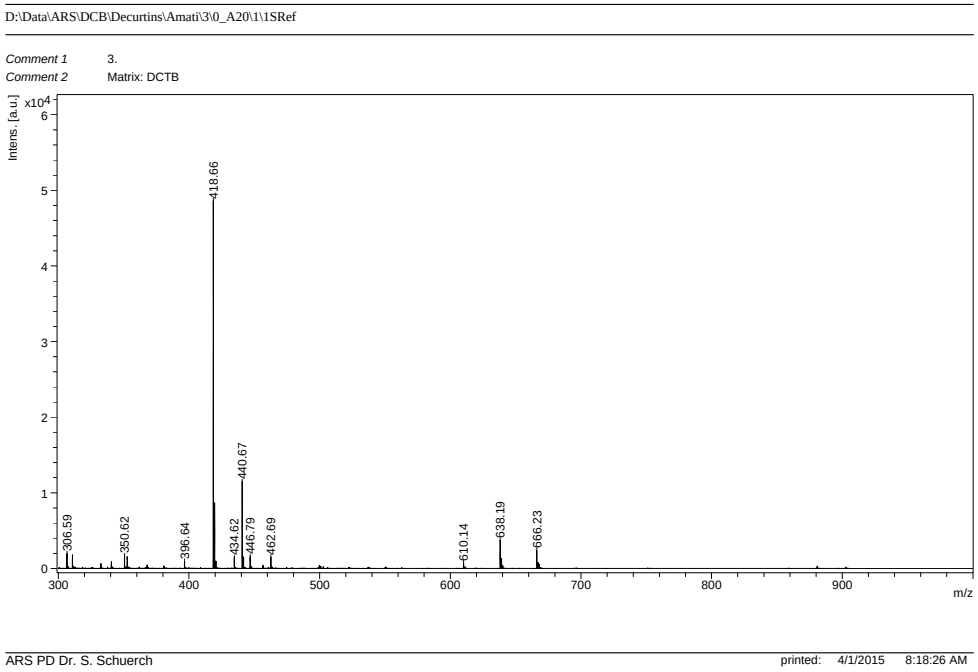

Figure S3: MALDI-TOF MS of 3. Matrix: DCTB.

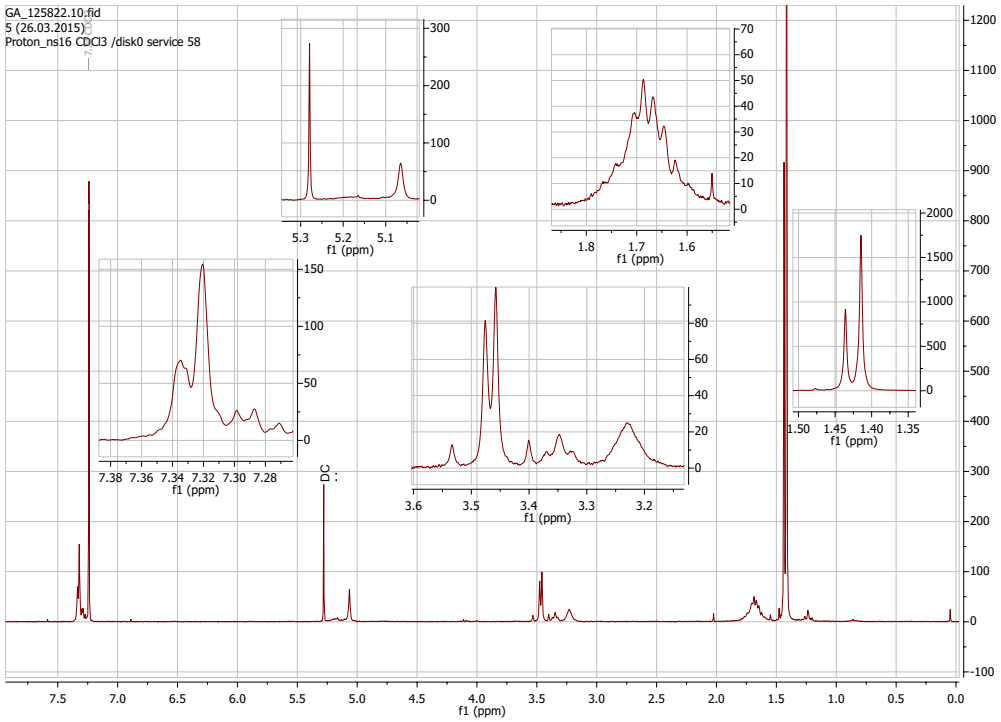

Figure S4: ^{1}H-NMR of 5. Number of scans: 16. In $CDCl_3$.

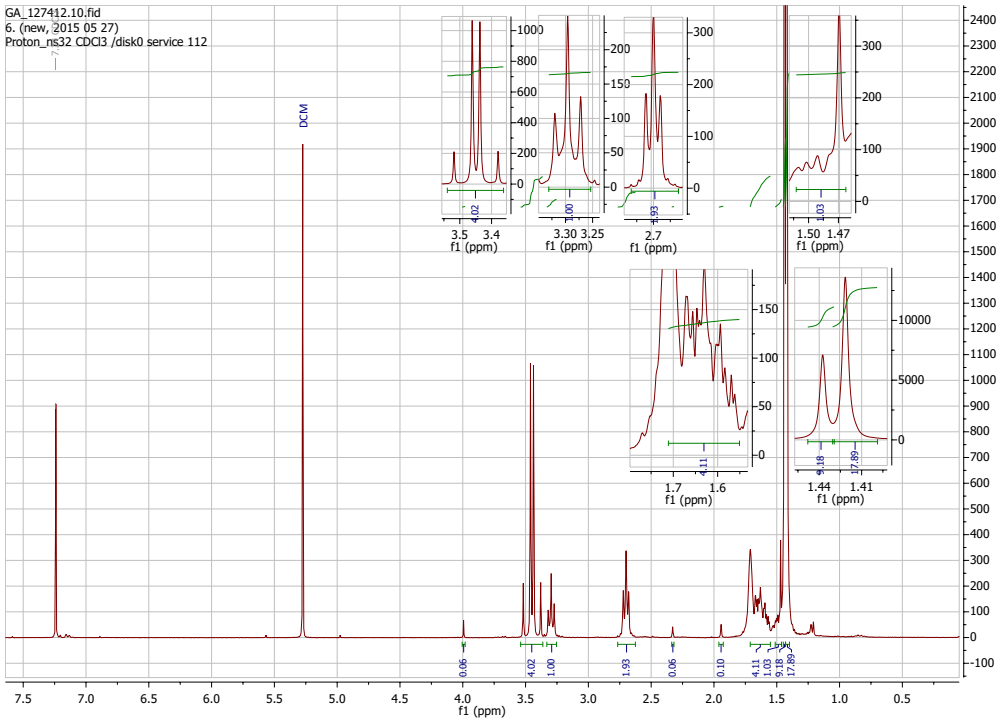

Figure S5: ^{1}H-NMR of 6. Number of scans: 32. In $CDCl_3$.

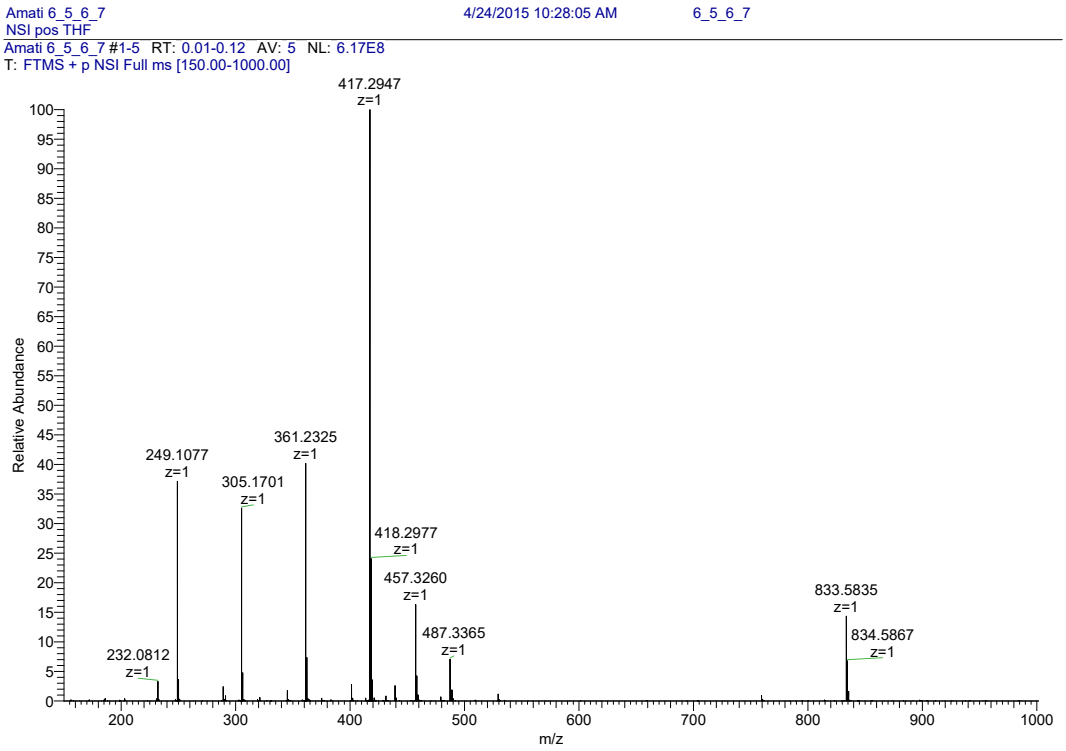

Figure S6: ESI-MS of 6. Positive ion mode.

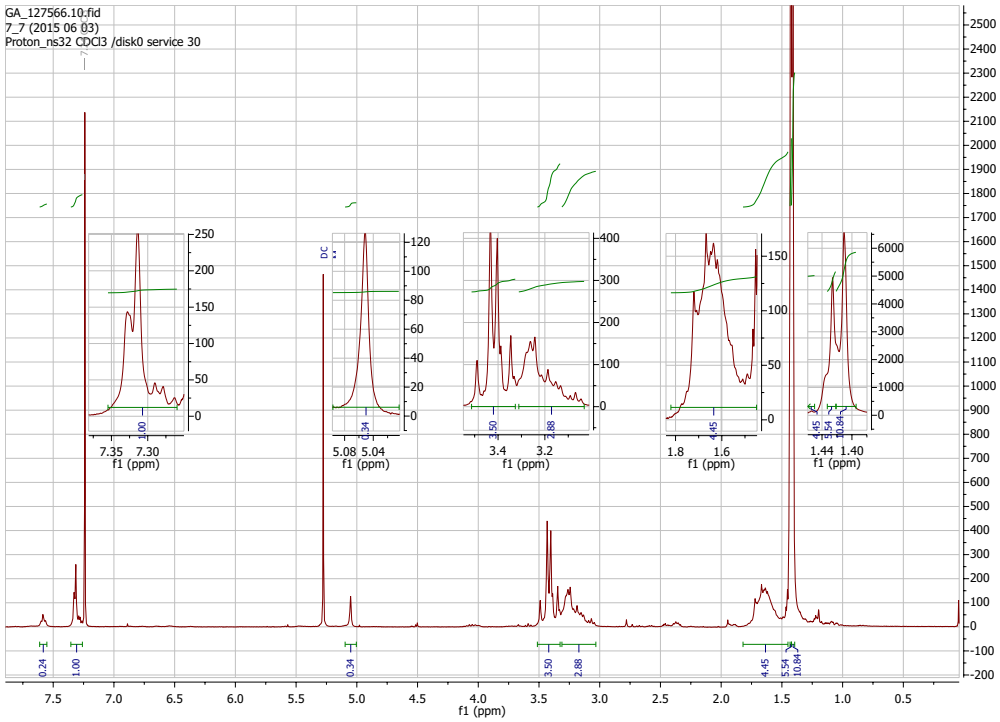

Figure S7: ^{1}H-NMR of 7. Number of scans: 32. In $CDCl_3$.

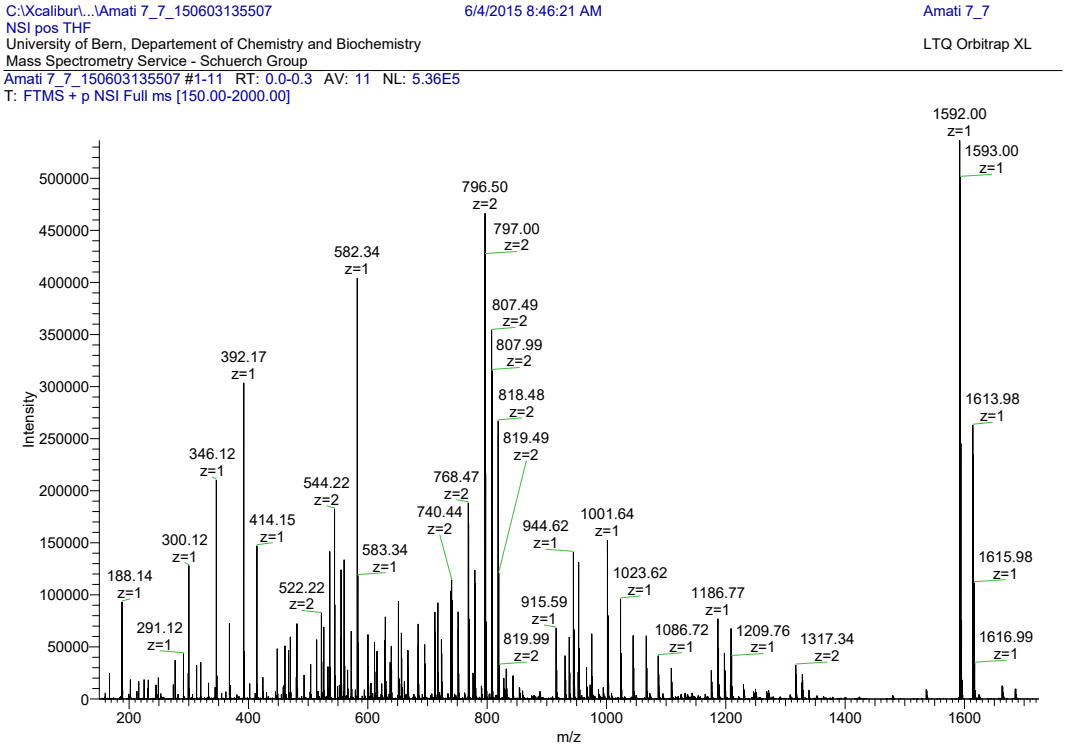

Figure S8: ESI-MS of 7. Positive ion mode.

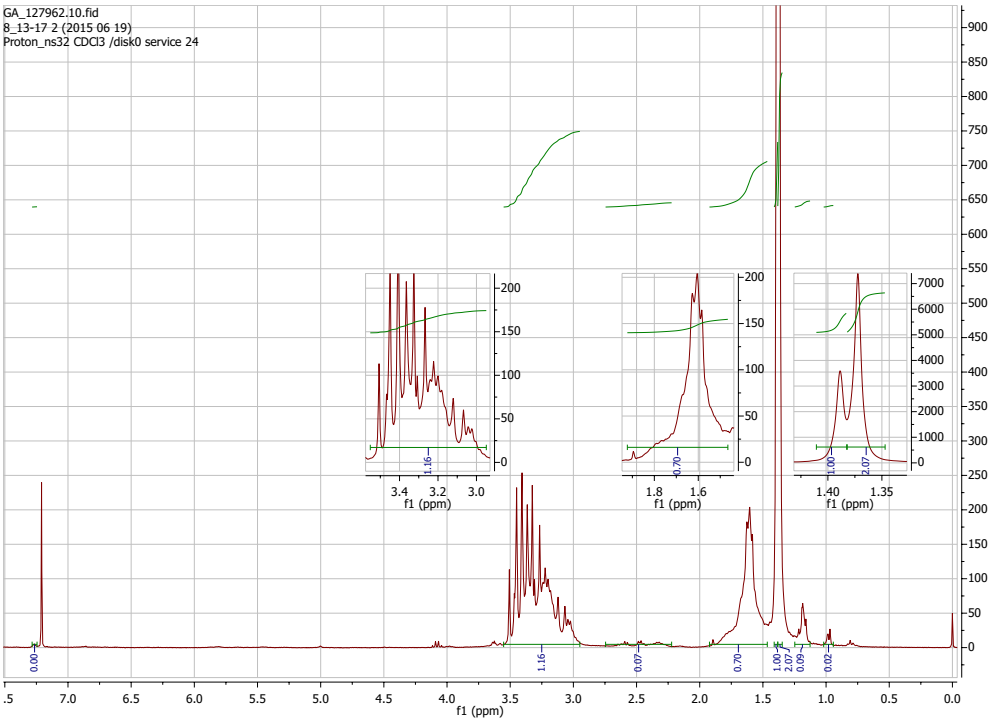

Figure S9: ^{1}H-NMR of 8. Number of scans: 32. In $CDCl_3$.

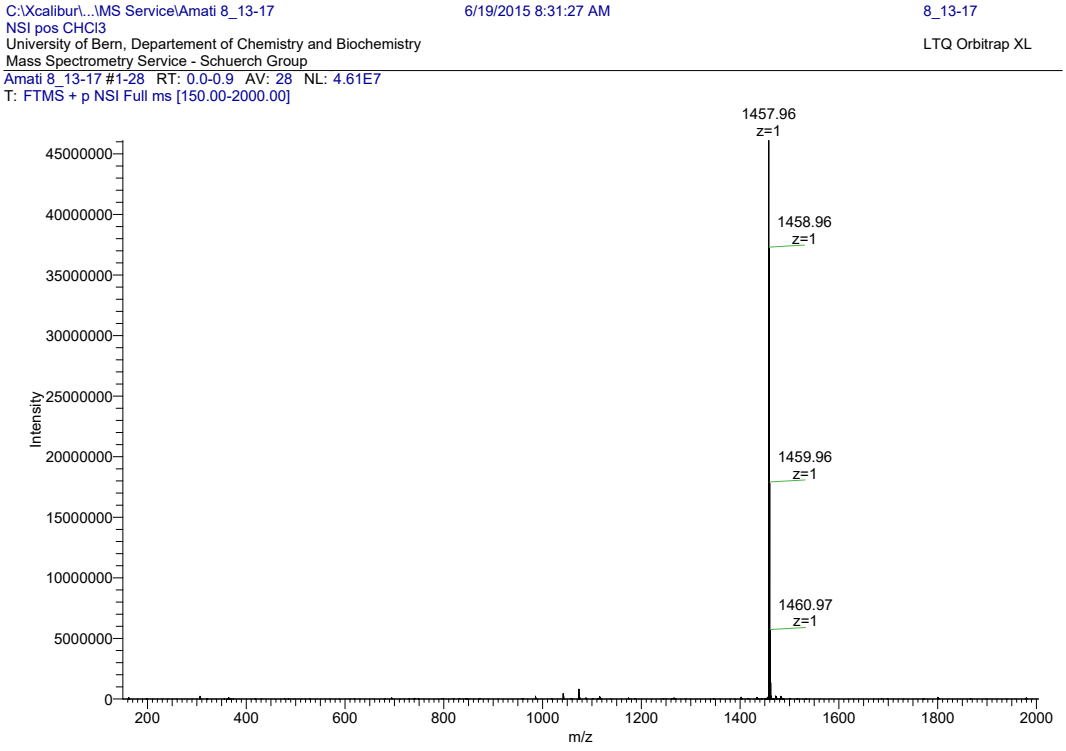

Figure S10: ESI-MS of 8. Positive ion mode.

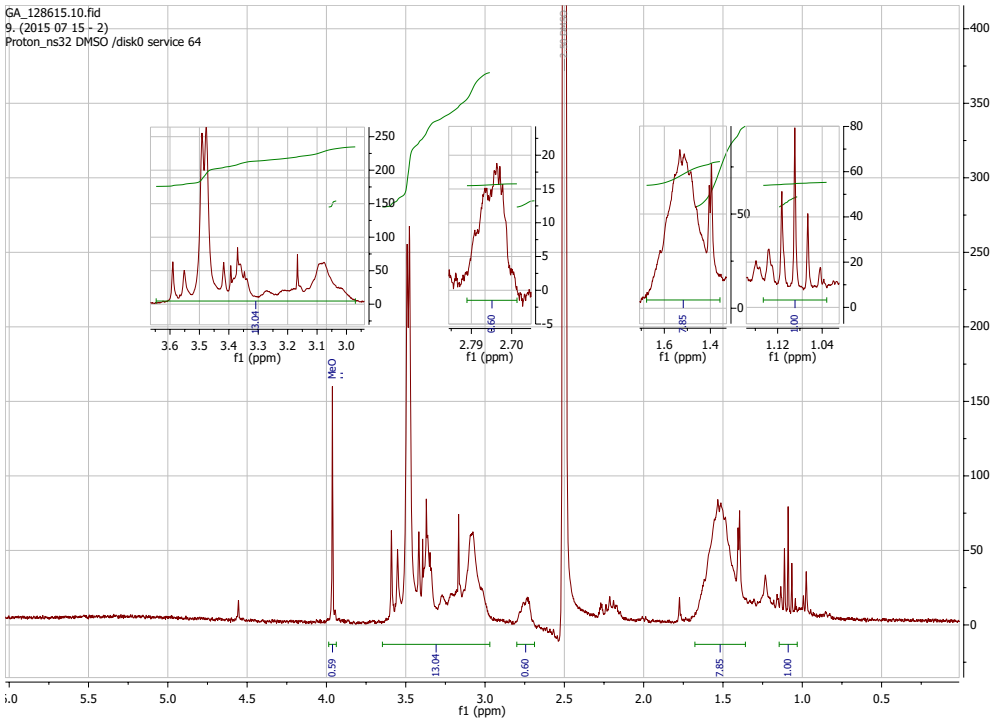

Figure S11: ^{1}H-NMR of 9. Number of scans: 32. In DMSO-d_6.

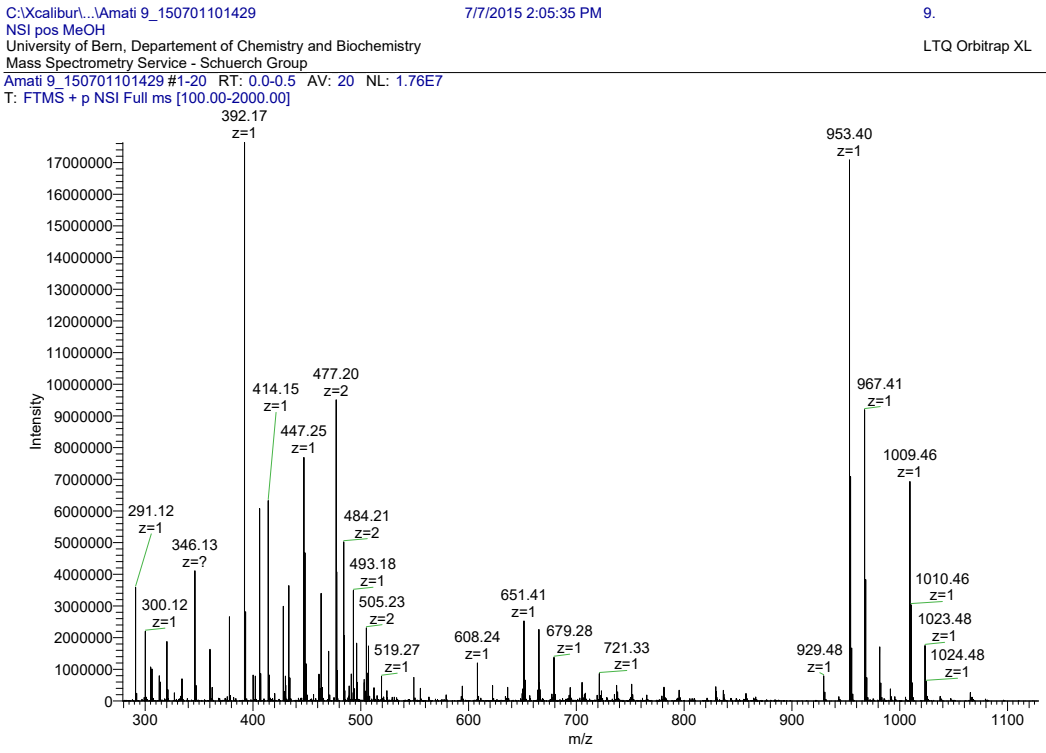

Figure S12: ESI-MS of 9. Positive ion mode.

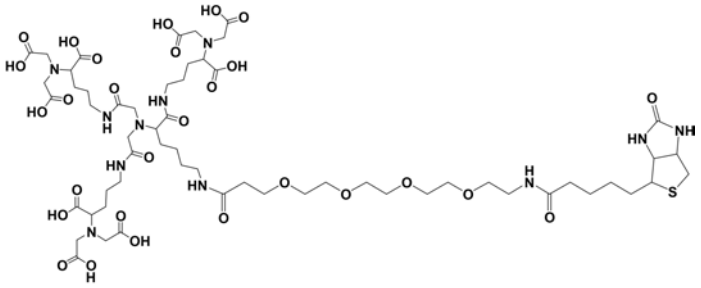

Figure S13: Structure of trisNTA-PEG$_4$-biotin. M_w: 1424.5 g mol^{-1}.

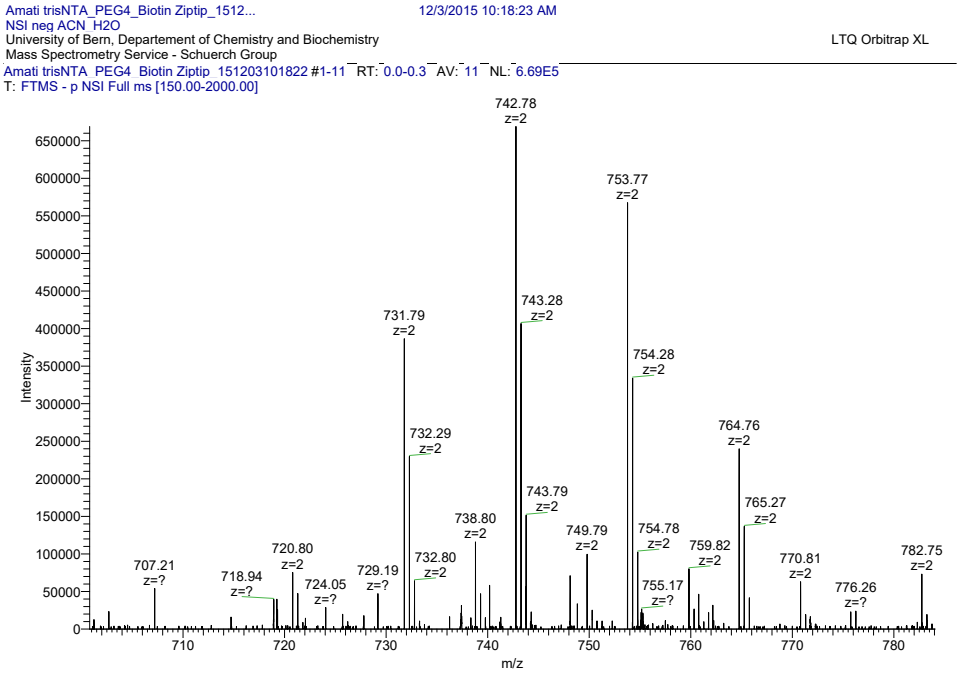

Figure S14: ESI-MS of trisNTA-PEG$_4$-biotin. Negative ion mode. M_w: 1424.54 g mol^{-1}. The respective mass in z=1 could not be detected, however in z=2, different Na^+-adducts are detected containing 2, 3, 4, or 5 Na^+ ions resulting in m/z of 731.79, 742.78, 753.77, or 764.76, respectively.

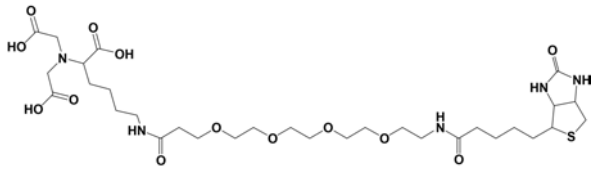

Figure S15: Structure of LysNTA-PEG$_4$-biotin. M_w: 735.3 g mol^{-1}.

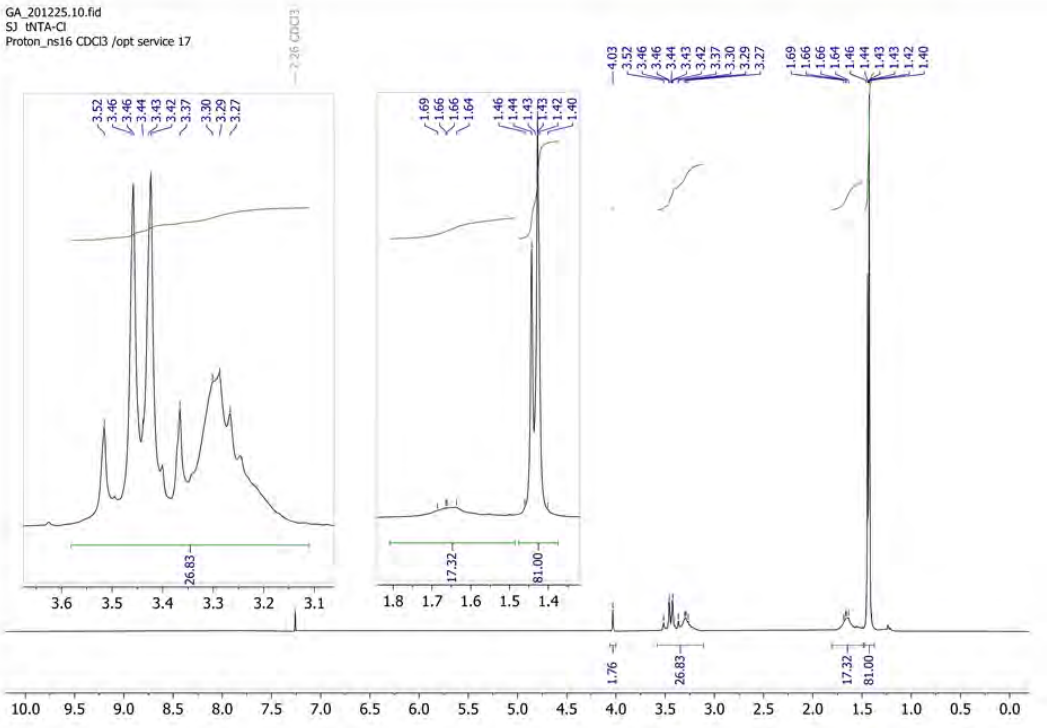

Figure S16: ^{1}H-NMR of 10. Number of scans: 16. In $CDCl_3$.

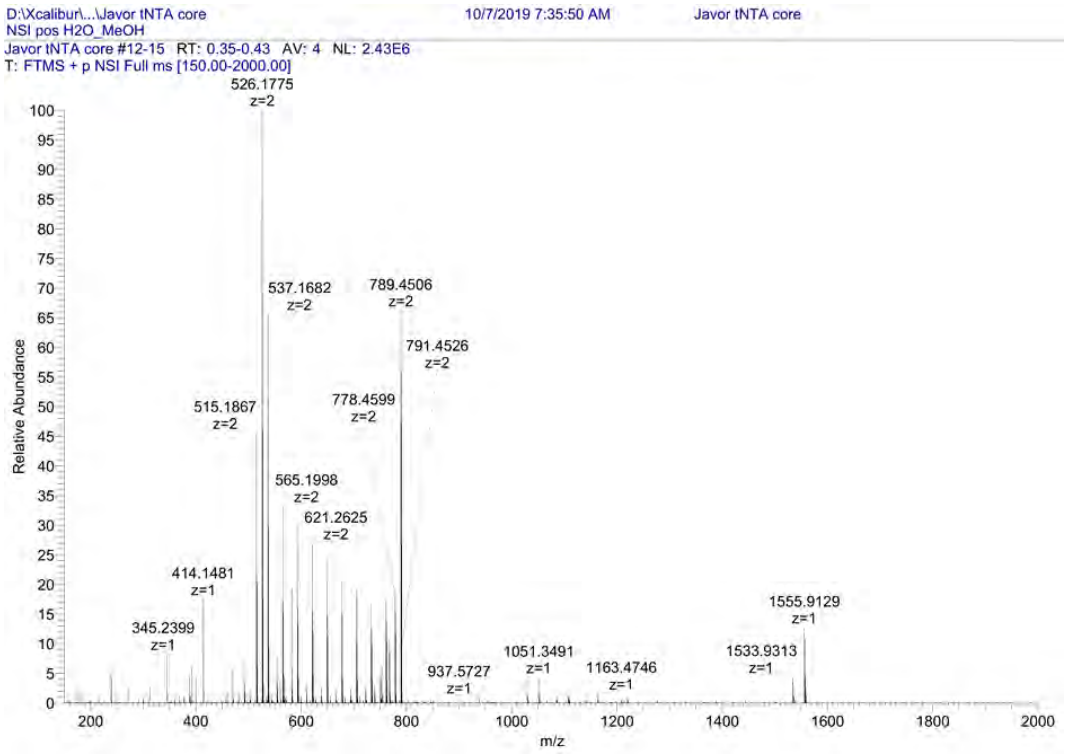

Figure S17: ESI-MS of 10. Positive ion mode.

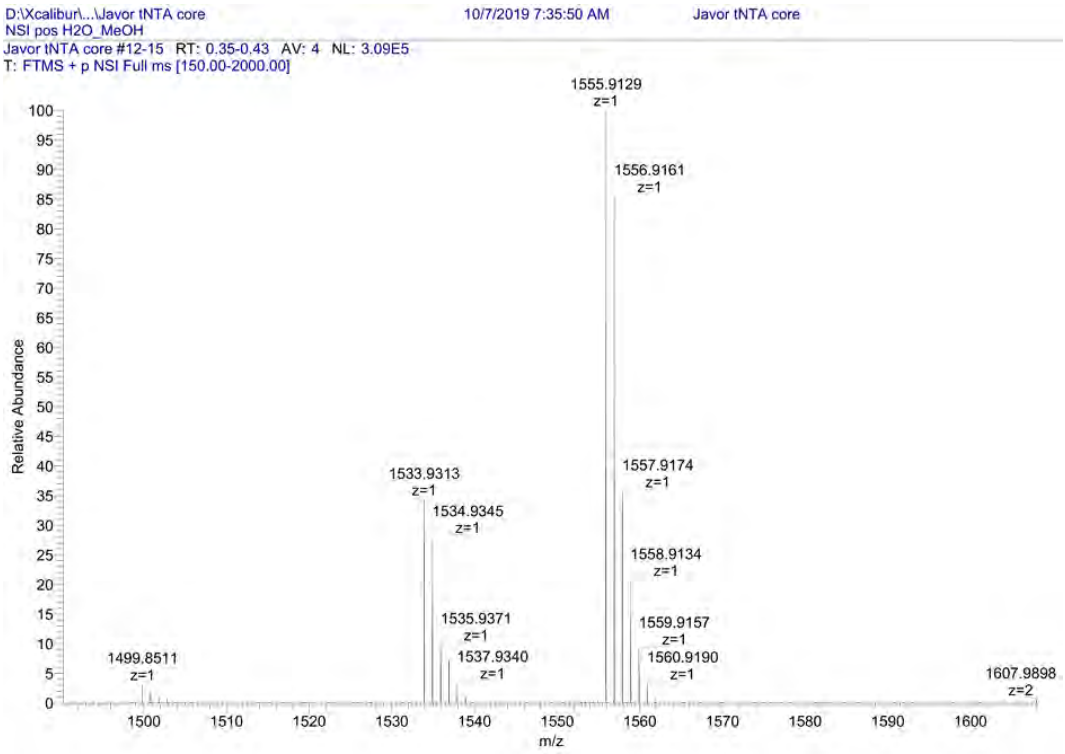

Figure S18: Zoom-in of ESI-MS of 10. Positive ion mode.

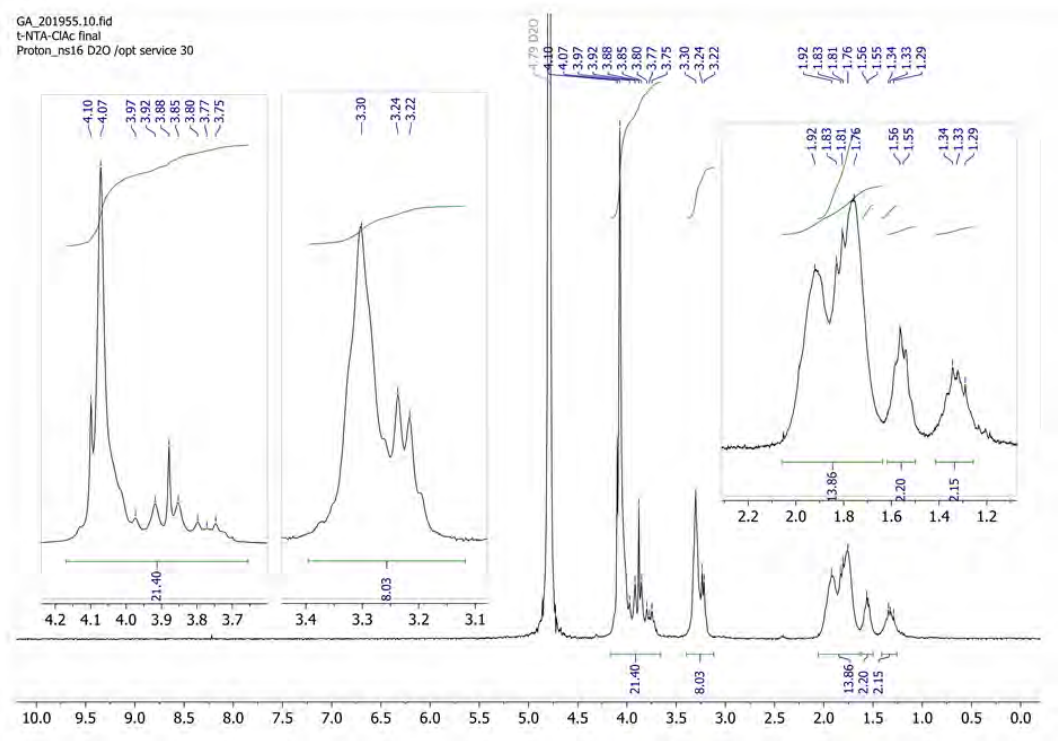

Figure S19: ^{1}H-NMR of 11. Number of scans: 16. In D_2O.

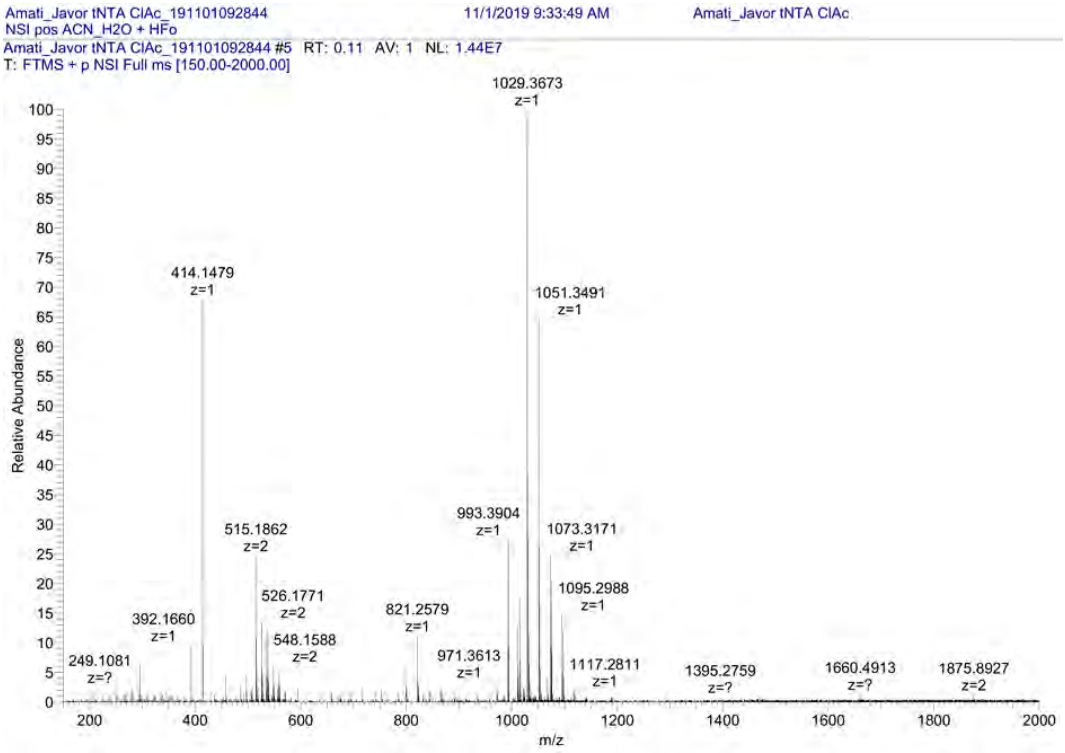

Figure S20: ESI-MS of 11. Positive ion mode.

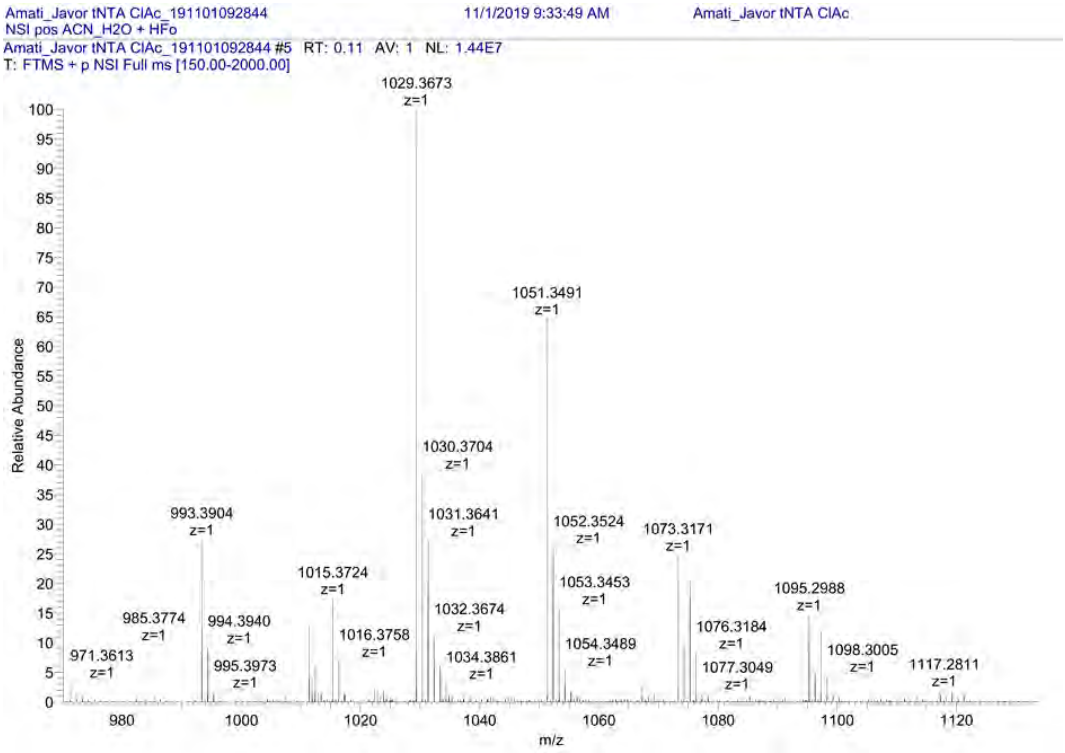

Figure S21: Zoom-in of ESI-MS of 11. Positive ion mode.

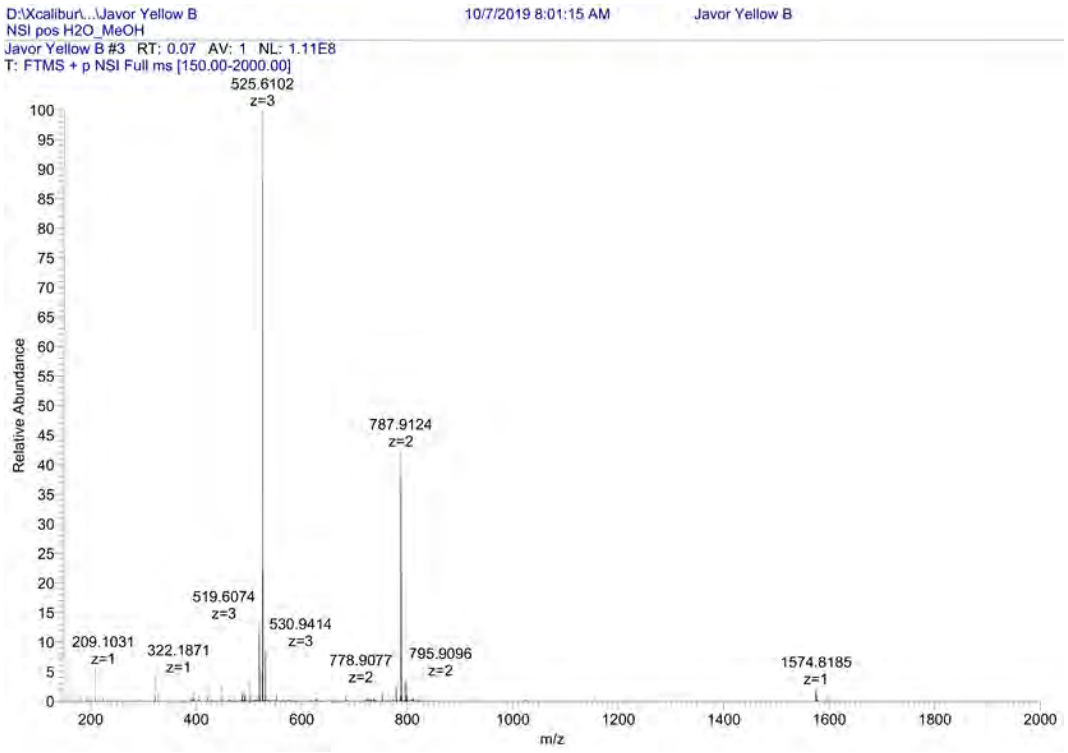

Figure S22: ESI-MS of SpyC. Positive ion mode.

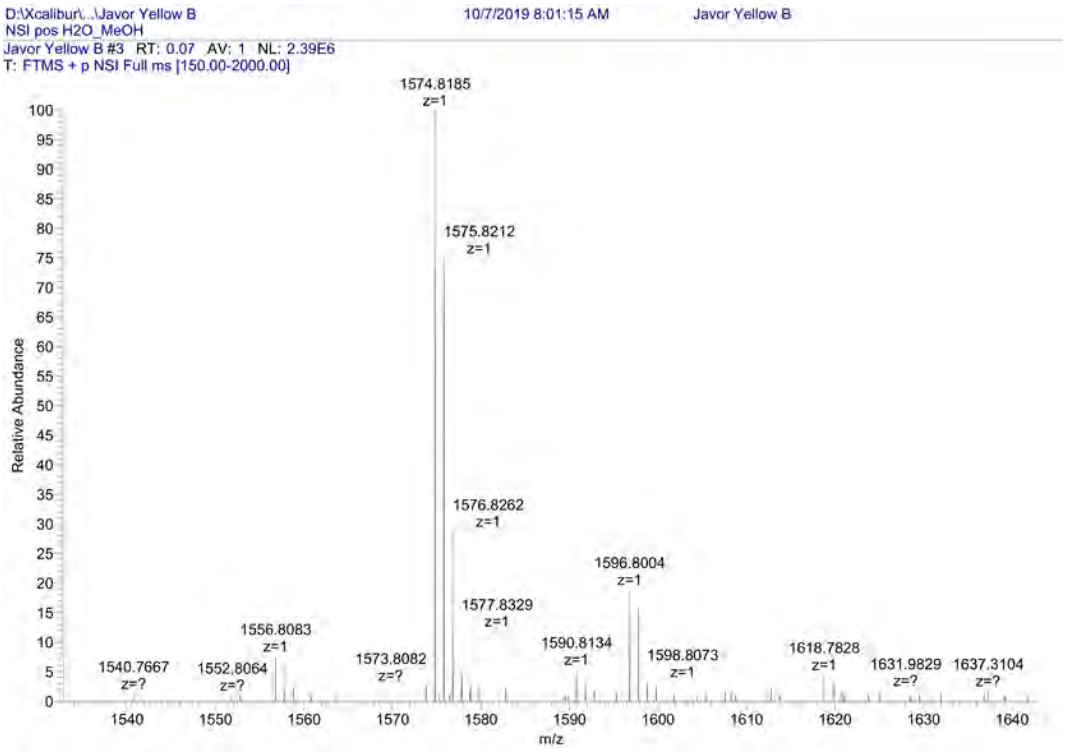

Figure S23: Zoom-in of ESI-MS of SpyC. Positive ion mode.

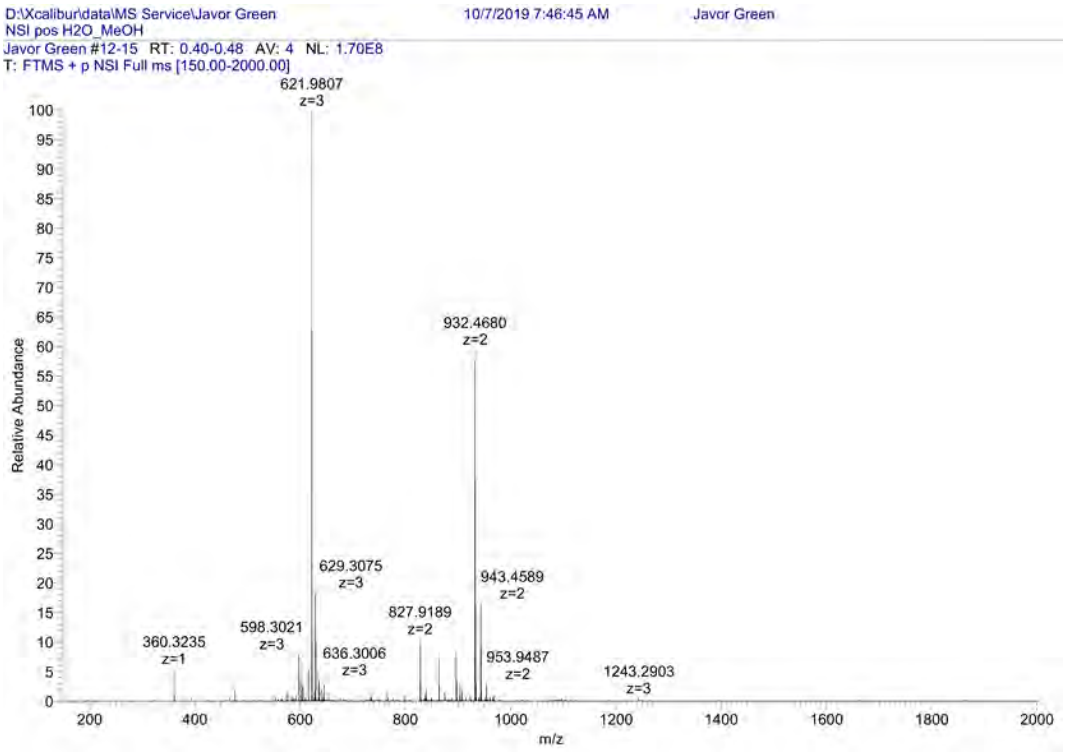

Figure S24: ESI-MS of SpyGSGSC. Positive ion mode.

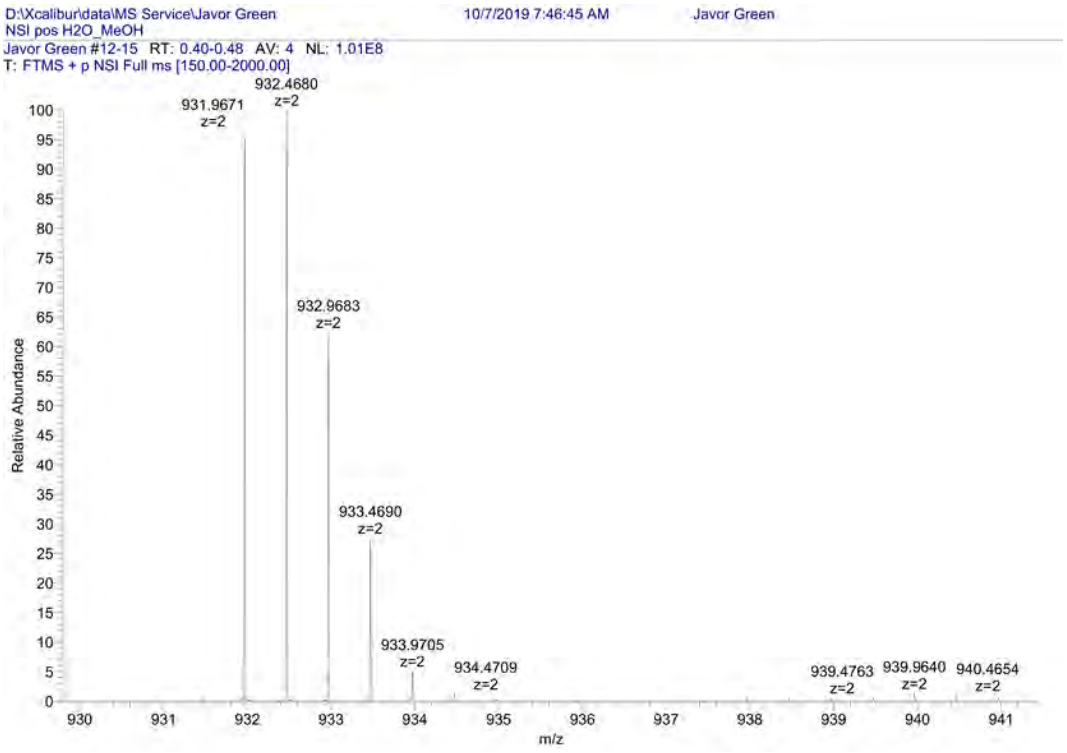

Figure S25: Zoom-in of ESI-MS of SpyGSGSC. Positive ion mode.

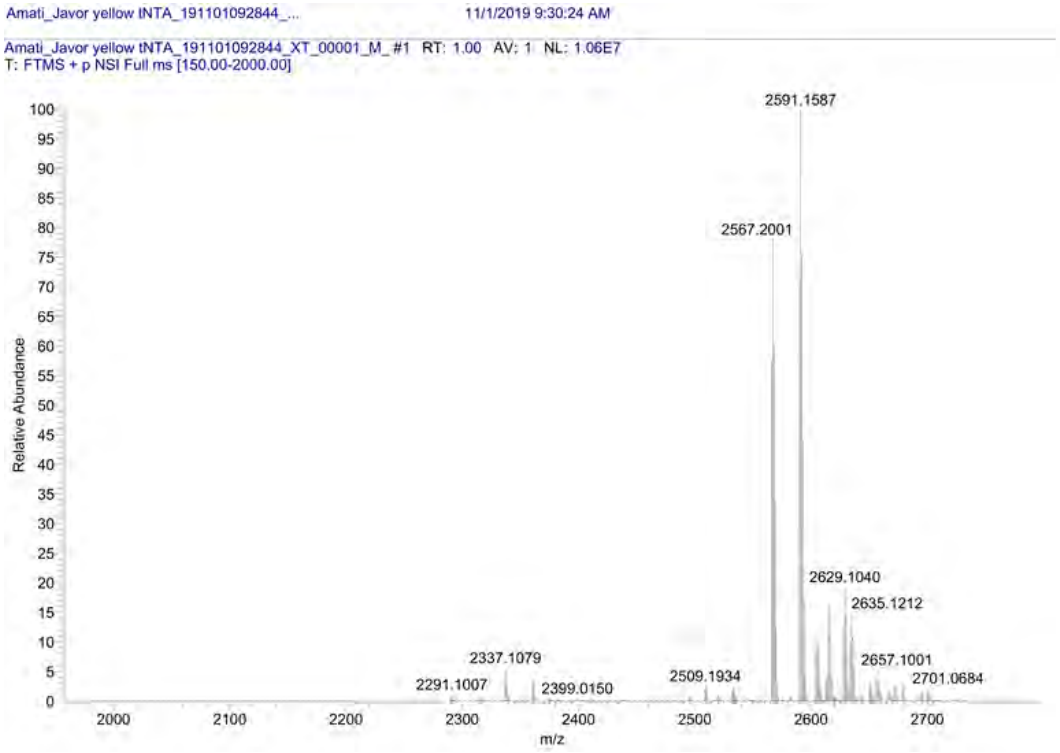

Figure S26: ESI-MS of SpyC-trisNTA. Positive ion mode.

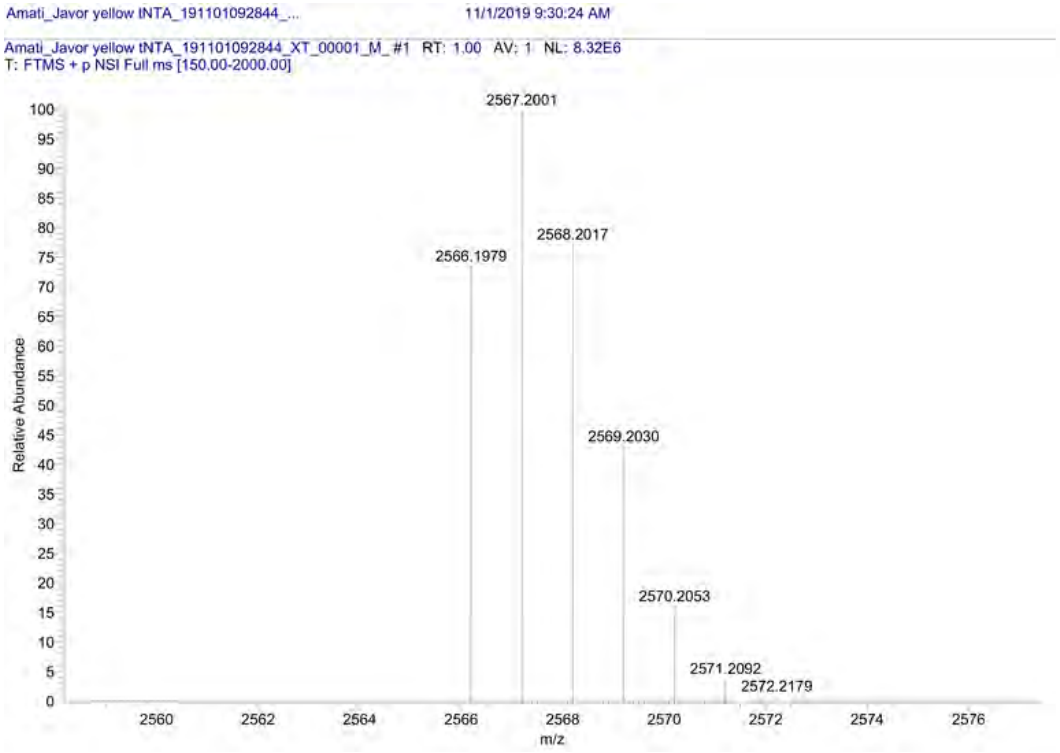

Figure S27: Zoom-in of ESI-MS of SpyC-trisNTA. Positive ion mode.

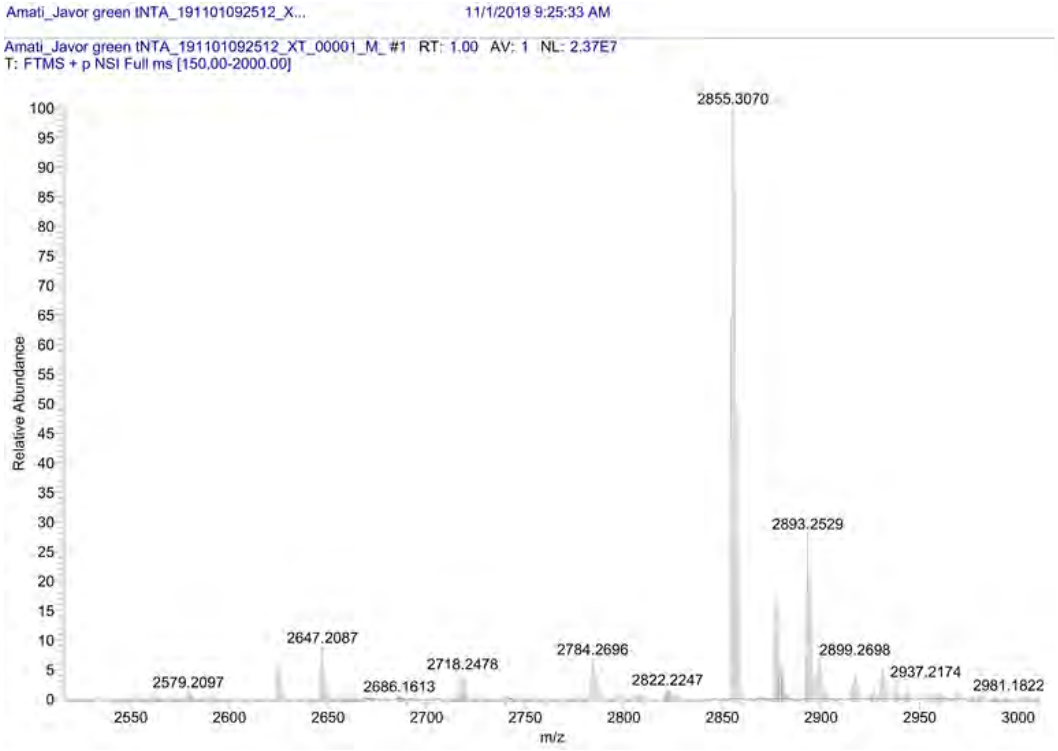

Figure S28: ESI-MS of SpyGSGSC-trisNTA. Positive ion mode.

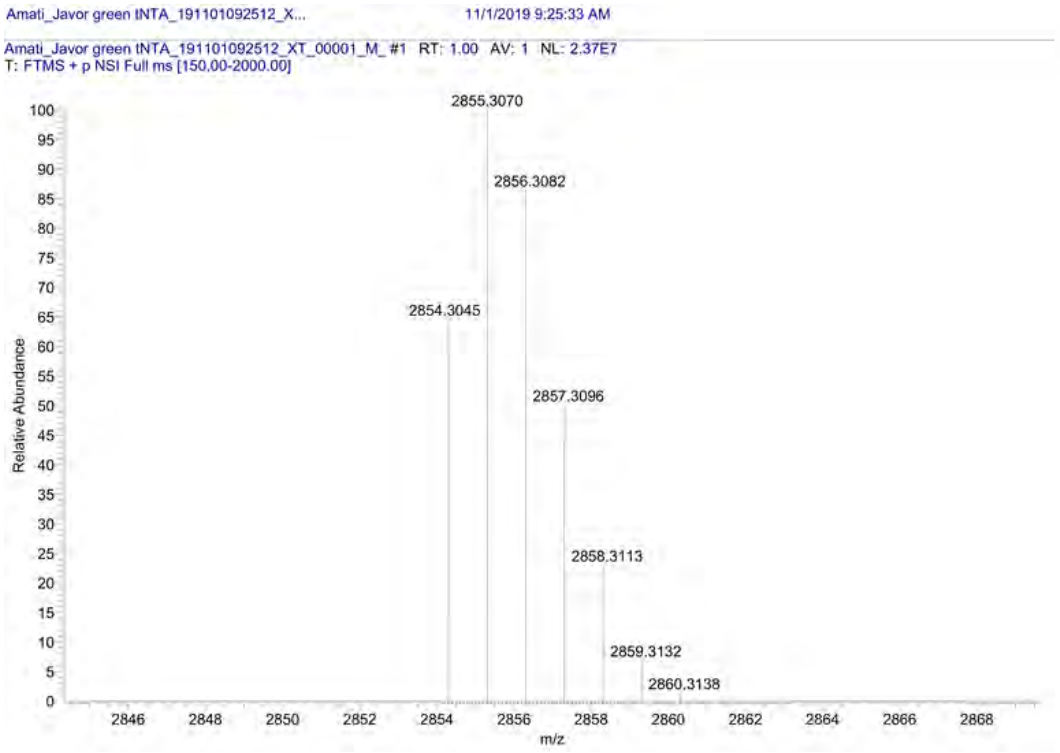

Figure S29: Zoom-in of ESI-MS of SpyGSGSC-trisNTA. Positive ion mode.

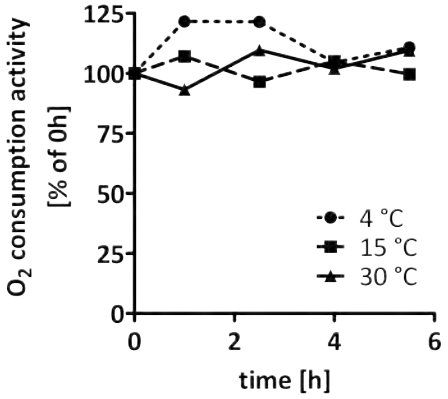

Figure S30: Thermal stability of *bo₃* oxidase wt. Purified, detergent-solubilized *bo₃* oxidase wt was incubated at different temperatures (4 °C, 15 °C, 30 °C) for 5.5 h. Oxygen consumption activity was regularly assessed using an Oxygraph+. 2 µl 20 µM *bo₃* oxidase wt were diluted into 1 ml buffer (50 mM K_2HPO_4 pH 8.3, 0.1 % DDM) containing 2 mM DTT. After a stable baseline was obtained, oxygen consumption by *bo₃* oxidase was started by addition of 200 µM ubiquinol Q_1.

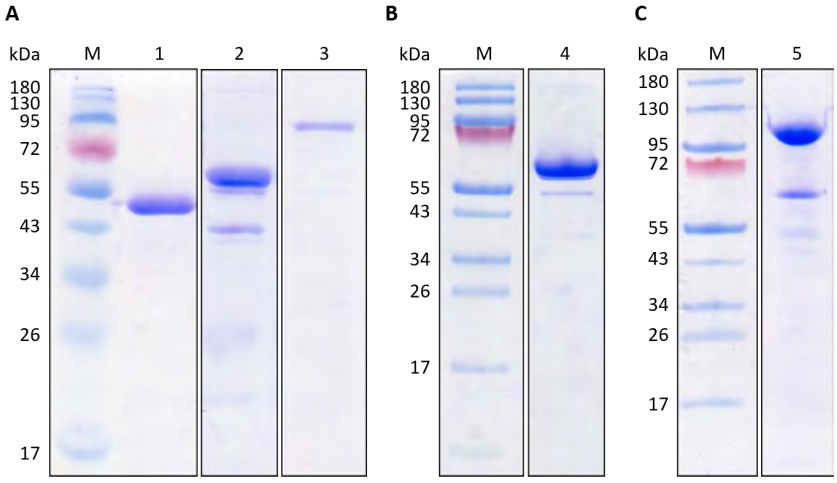

Figure S31: SDS-PAGE analysis of LSUs after expression and purification. (A) 1: SC-ELP-GFP, 49.9 kDa; 2: SC-MBP, 55.8 kDa; 3: SC-MBPx, 95.9 kDa; M: marker. (B) 4: SC-MBP-3xFLAG, 58.7 kDa; M: marker. (C): 5: SC-MBPx-3xFLAG, 99.1 kDa; M: marker.

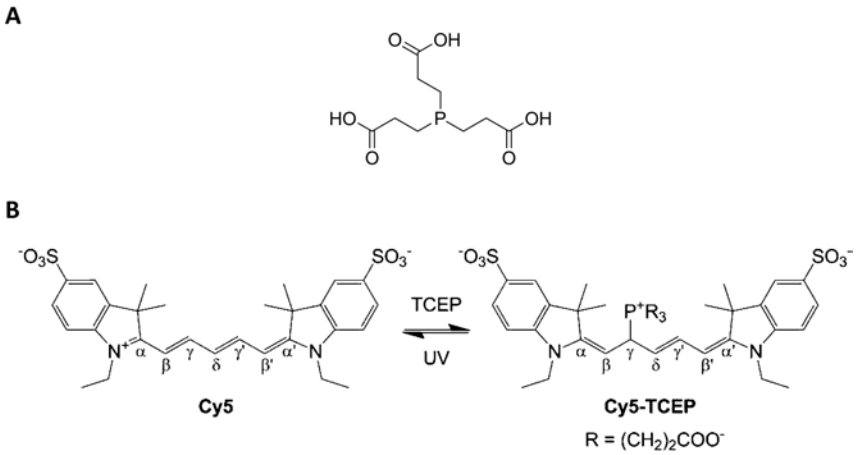

Figure S32: Formation and structure of Cy5-TCEP adduct. (A) Structure of TCEP. (B) 1,4-addition of TCEP to the polymethine bridge of Cy5 to form a covalent adduct, resulting in Cy5 quenching. Quenching can be reversed either by illumination with UV light, or by addition of an excess of the disulfide cystamine.[263] Figure (B) adapted from [263].

8 Appendix.

8.1 Curriculum Vitae.

Curriculum Vitae

PERSONAL INFORMATION

Amati, Andrea Marco

Donnerbühlweg 41, 3012 Bern (Switzerland)

+41 (0)78 810 33 21

andrea.amati@gmx.ch

Sex Male | Date of birth 17 April 1990 | Nationality Swiss

EDUCATION AND TRAINING

November 2014 – April 2020

PhD of Science in Biochemistry & Molecular Biology.

University of Bern, Bern (Switzerland)

PhD Thesis

"Towards unidirectional reconstitution of membrane proteins into liposomes."
Research group: Prof. Dr. Christoph von Ballmoos
Department of Chemistry & Biochemistry
University of Bern
Freiestrasse 3
3012 Bern
Switzerland

Education

Programming in R, chemical modifications of proteins, structural studies of membrane proteins using X-ray crystallography, applied fluorescence microscopy, environment-related diseases & nanotoxicology.

Training

Expression and purification of membrane and soluble proteins, genetic engineering, size exclusion chromatography, anion exchange chromatography, ÄKTA pure & prime, reconstitution of membrane proteins into liposomes, fluorescence spectroscopy, UV-Vis spectroscopy, Oxygraph, luminescence measurements Glomax, organic synthesis, NMR, chemical modification of proteins.

Teaching

Supervision of bachelor and master students; repeated organization and supervision of a six-days membrane protein purification course for bachelor students.

September 2012 – March 2014

Master of Science in Molecular Life Sciences, with special qualifications in Biochemistry.

University of Bern, Bern (Switzerland)

Master's Thesis

"The influence of amino acid transporter SNAT2 (SLC38A2) in colon cancer."
Research group: Prof. Dr. Matthias A. Hediger
Supervisor: Dr. Pascale Anderle
Institute for Biochemistry and Molecular Medicine (IBMM)
University of Bern
Bühlstrasse 28
3012 Bern
Switzerland

Education

Medicinal chemistry, chemical biology, applied MS & NMR spectroscopy, principles of nucleic acids, nucleic acid analogues, omics, neurochemistry, forensic chemistry & toxicology, molecular virology, pathogenesis and evolution of infectious diseases, modern methods of chemistry-information, antibiotics.

Training

Cell culture of human tumor cell lines, RNAi by siRNA transfection, cloning, protein overexpression technology (transient & stable), proliferation testing (including MTT, XTT, cell counting, FACS), migration/invasion transwell assays, total RNA isolation, RT-PCR, qPCR, western blotting, surface biotinylation assay, transport assays using radioactively labeled uptake substrates, set-up of medium-high throughput screening assay.

Curriculum Vitae

27 August 2012 – 5 September 2012

LTK Module 1: Introductory Course in Laboratory Animal Science

Institute of Laboratory Animal Sciences, University of Zürich, Zürich (Switzerland)

Education & Training

Legislation, ethics, alternatives to animal experimentation, methods to decrease anxiety in mice, biology (breeding: general aspects and transgenics; standardization: nutrition, husbandry, transport), husbandry and behaviour (standardization; practical training: mouse/rat), handling, weighting, identification, hygiene, health monitoring (management and symptoms), anesthesia, euthanasia, sample collection and application of substances, design and execution of animal experiments.
Theory total: ca. 23 hours, practical training total: ca. 21 hours

September 2009 – August 2012

Bachelor of Science in Biochemistry & Molecular Biology

University of Bern, Bern (Switzerland)

Bachelor's Thesis

"The influence of amino acid transporter SNAT2 (SLC38A2) and LAT1/4F2hc (SLC3A2) in colon cancer."
Research group: Dr. Pascale Anderle
Supervisors: Dr. Pascale Anderle & Dr. Susanne Bentz
Institute for Biochemistry and Molecular Medicine (IBMM)
University of Bern
Bühlstrasse 28
3012 Bern
Switzerland

Education

Biochemistry, methods of biochemistry, bioinformatics, genetics, immunology, molecular biology, microbiology, cell biology, organic chemistry, physical chemistry, general chemistry, physics, statistics, quantum physics, quantum chemistry, spectroscopy (IR, NMR, MS).

Training

Affinity chromatography, SDS-PAGE, western blotting, quantitative amino acid analysis, RP-HPLC, ESI-MS, MALDI-TOF-MS, Nano-ESI-Orbitrap-MS, cell culture of human derived cell lines, migration/invasion transwell assays, RNAi by siRNA transfection, total RNA extraction, RT-PCR, qPCR (ViiA7 System, Life Technologies), protein isolation, bradford assay, immunofluorescent staining and confocal microscopy, proliferation testing (including MTT, XTT, cell counting, FACS)

August 2004 – 20 June 2008

General qualification for university entrance (high school)

Mathematical & scientific high school Gymnasium Kirchenfeld Bern, Bern (Switzerland)

Focus: Physics & applied mathematics

1996 – 2004

Primary & secondary school

Elementary schools Worb BE (Switzerland)

Curriculum Vitae

WORK EXPERIENCE

1 April 2014 – 30 September 2014

Internship at Novartis Pharma AG

Novartis Institutes for Biomedical Research, Novartis Pharma AG, Basel (Switzerland)

Internship as recent master graduate scientist in the in Silico Lead Discovery (iSLD) of the Center for Proteomic Chemistry (CPC) at the Novartis Institutes for Biomedical Research (NIBR), Novartis Pharma AG, Basel.

Techniques used during internship:
Cell culture of suspended/adherent cells, calcium FLIPR assays, HTRF assays, statistical programming in "R", GraphPad Prism, Spotfire, E-WorkBook, microarrays, panomics, RNA isolation, RT-PCR, qPCR and HTS assay development (especially for calcium FLIPR assays and HTRF assays).

January 2011 – March 2019

Security Bierhübeli GmbH

Bierhübeli GmbH, Neubrückstrasse 43, 3012 Bern (Switzerland)

Crew leader & security in one of Bern's most prestigious and biggest concert halls or clubs.

During this employment I was especially trained in leadership.

January 2009 – July 2009

Substitute Teacher Middle School

Oberstufenzentrum Worbboden, Worb (Switzerland)

Taught courses: mathematics, sports, informatics, science (chemistry, biology), history, geography, french.

Levels: 7th, 8th & 9th grade

PERSONAL SKILLS

Mother tongue: German

Other languages

	UNDERSTANDING		SPEAKING		WRITING
	Listening	Reading	Spoken interaction	Spoken production	
English	C2	C2	C1	C2	C2
French	C1	C1	C1	C1	B2
Italian	C2	C1	C1	B2	B1
Spanish	A2	A2	A2	A2	A2

Levels: A1/A2: Basic user - B1/B2: Independent user - C1/C2: Proficient user
Common European Framework of Reference for Languages

Communication skills

- excellent skills in presenting planned projects, results data etc. at (local/global) meetings
- good teaching skills gained through my experience as substitute teacher at the middle school "Oberstufenzentrum Worbboden, Worb, Switzerland" for six months (taught courses: mathematics, sports, informatics, science, history, geography, french; levels: 7th, 8th, 9th year).
- good contact skills gained through my experience as water polo coach.
- excellent poster presentation skills gained through presentation of posters at several national and international conferences listed below

Curriculum Vitae

Organisational / managerial skills

- excellent leadership skills gained through my experience as crew leader of a security crew (responsibility for a team of up to 10 employees) at the concert and night club "Bierhübeli" in Bern, Switzerland.
- good organisational and administrative skills gained as person in charge for material in the water polo club.
- good team-leading skills gained as water polo coach

Computer skills

- excellent command of Microsoft Office (Word, Excel, Powerpoint, Outlook, One Note)
- good command of photo editing software as ImageJ, IrfanView, Gimp, Photoshop
- good command of scientific databases such as NCBI (including PubMed), UniProt, Reaxys, SciFinder, BLAST, etc.
- good command of GraphPad Prism
- currently improving command of statistical programming in "R"
- basic knowledge of "Spotfire"
- good command of E-WorkBook / SmartBook (electronic labjournal)
- good command of website creating tools Wix, Joomla!
- good command of Java programming language

Driving licences

A1, A, B

ADDITIONAL INFORMATION

Conferences

- Gordon Research Conference (GRC) on Bioenergetics (Integration of Structure, Mechanism and Theory of Bioenergy Conversion in Health and Disease), June 2-7 2019, Proctor Academy, Andover NH, USA. (presentation of a poster)
- European Bioenergetics Conference (EBEC) 2018, August 25-30 2018, Budapest, Hungary. (presentation of a poster)
- International Conference on Molecular Systems Engineering (ICMSE) 2017, August 27-29 2017, Basel, Switzerland. (presentation of a poster)
- Annual Meeting of the German Biophysical Society, September 25-28 2016, Erlangen, Germany. (presentation of a poster)
- Workshop on Supramolecular Interactions in the Cellular Power Plant, October 9-10 2014, Department of Biochemistry & Biophysics, Stockholm University, Sweden. (attendance only)
- NCCR TransCure Site Visit 2013, Bern, Switzerland. (presentation of a poster)
- NCCR TransCure Annual Retreat 2013, Bern, Switzerland. (presentation of a poster)
- NCCR TransCure Site Visit 2012, Bern, Switzerland. (presentation of a poster)
- Clinical Research Day 2012 of the Department of Clinical Research at the University of Bern, Bern, Switzerland. (presentation of a poster)

Continuing education

- Introduction to LaTeX, University of Bern, Switzerland, May 2019
- Lessons in leadership, University of Bern, Switzerland, September 2018

Grants

- Conference Travel Grant of the Graduate School for Cellular and Biomedical Sciences (GCB) of the University of Bern, Switzerland, for the visit of the GRC on Bioenergetics, June 2-7 2019, Andover, NH, USA.

Curriculum Vitae

Symposia

- GCB Symposium 2018: Symposium of the Graduate School for Cellular and Biomedical Sciences of the University of Bern, Switzerland, February 1 2018
- GCB Symposium 2017: Symposium of the Graduate School for Cellular and Biomedical Sciences of the University of Bern, Switzerland, February 2 2017
- GCB Symposium 2016: Symposium of the Graduate School for Cellular and Biomedical Sciences of the University of Bern, Switzerland, February 4 2016
- Attended "Symposium of Transgenic Mouse Technologies" on October 2013, 3rd & 4th at the University of Bern, Bern, Switzerland

Publications

- *Gene-signatures predict biologically relevant dose-response potencies in phenotypic assays.*
  Steffen Renner, Christian Bergsdorf, Rochdi Bouhelal, Magdalena Koziczak-Holbro, **Andrea Marco Amati**, Valerie Techer Etienne, Ludivine Flotte, Nicole Reymann, Karen Kapur, Sebastian Hoersch, Edward J. Oakeley, Ansgar Schuffenhauer, Hanspeter Gubler, Eugen Lounkine, Pierre Farmer.
  (2019) bioRxiv 799106; doi: https://doi.org/10.1101/799106
  Manuscript accepted, in print at Scientific Reports.
- *Measuring membrane protein function in unilamellar vesicles.*
  Andrea Marco Amati, Simone Sandra Graf, Sabina Deutschmann, Nicolas Dolder, Christoph von Ballmoos:
  Manuscript submitted to Biochemical Society Transactions.

References

Christoph von Ballmoos, PhD
Professor
Department for Chemistry & Biochemistry
University of Bern
Freiestrasse 3
CH-3012 Bern
christoph.vonballmoos@dcb.unibe.ch
Office: +41 (0)31 631 43 67

Pierre Farmer, PhD
Senior Investigator II
Novartis Pharma AG
Novartis Campus
Postfach
CH-4002 Basel
pierre.farmer@novartis.com

Steffen Renner, PhD
Investigator III
Novartis Pharma AG
Novartis Campus
Postfach
CH-4002 Basel
steffen.renner@novartis.com

Rochdi Bouhelal, PhD
Senior Investigator I
Novartis Pharma AG
Novartis Campus
Postfach
CH-4002 Basel
rochdi.bouhelal@novartis.com

8.2 Publications.

8.2.1 Chronological List of Publications.

I *Gene-signatures predict biologically relevant dose-response potencies in phenotypic assays*
Steffen Renner, Christian Bergsdorf, Rochdi Bouhelal, Magdalena Koziczak-Holbro, **Andrea Marco Amati**, Valerie Techer-Etienne, Ludivine Flotte, Nicole Reymann, Karen Kapur, Sebastian Hoersch, Edward J. Oakeley, Ansgar Schuffenhauer, Hanspeter Gubler, Eugen Lounkine, Pierre Farmer
(2019) bioRxiv 799106; doi: https://doi.org/10.1101/799106
Manuscript accepted, in print soon at Scientific Reports.

II *Measuring membrane protein function in unilamellar vesicles*
Andrea Marco Amati*, Simone Sandra Graf*, Sabina Deutschmann*, Nicolas Dolder*, Christoph von Ballmoos
* contributed equally
Manuscript submitted upon invitation to Biochemical Society Transactions.

8.2.2 Publication I.

Gene-signatures predict biologically relevant dose-response potencies in phenotypic assays

Steffen Renner, Christian Bergsdorf, Rochdi Bouhelal, Magdalena Koziczak-Holbro, **Andrea Marco Amati**, Valerie Techer-Etienne, Ludivine Flotte, Nicole Reymann, Karen Kapur, Sebastian Hoersch, Edward J. Oakeley, Ansgar Schuffenhauer, Hanspeter Gubler, Eugen Lounkine, Pierre Farmer

(2019) bioRxiv 799106; doi: https://doi.org/10.1101/799106

Manuscript accepted, in print soon at Scientific Reports.

This publication is off-topic; it resulted from my internship at Novartis Institutes for Biomedical Research (NIBR) prior to the start of my PhD. The manuscript however was written and reviewed during my PhD.

Gene-signatures predict biologically relevant dose-response potencies in phenotypic assays

Steffen Renner[1*], Christian Bergsdorf[1], Rochdi Bouhelal[1], Magdalena Koziczak-Holbro[2], Andrea Marco Amati[1,6], Valerie Techer-Etienne[1], Ludivine Flotte[2], Nicole Reymann[1], Karen Kapur[3], Sebastian Hoersch[3], Edward J. Oakeley[4], Ansgar Schuffenhauer[1], Hanspeter Gubler[3], Eugen Lounkine[5], Pierre Farmer[1*]

1 Chemical Biology & Therapeutics, Novartis Institutes for Biomedical Research, Basel 4056, Switzerland

2 Musculoskeletal, NIBR, Basel, Switzerland

3 NIBR Informatics, NIBR, Basel, Switzerland

4 ASI, NIBR, Basel, Switzerland

5 Chemical Biology & Therapeutics, NIBR, 181 Massachusetts Avenue, Cambridge, MA 02139, USA

6 current address: Department of Chemistry & Biochemistry, University of Bern, Freiestrasse 3, 3012 Bern, Switzerland

* Corresponding authors:

Steffen Renner: steffen.renner@novartis.com

Pierre Farmer: pierre.farmer@novartis.com

Abstract

Multiplexed gene-signature-based phenotypic assays are increasingly used for the identification and profiling of small molecule-tool compounds and drugs. Here we introduce a method (provided as R-package) for the quantification of the dose-response potency of a gene-signature as EC_{50} and IC_{50} values.

Two signaling pathways were used as models to validate our methods: beta-adrenergic agonistic activity on cAMP generation (dedicated dataset generated for this study) and EGFR inhibitory effect on cancer cell viability. In both cases, potencies derived from multi-gene expression data were highly correlated with orthogonal potencies derived from cAMP and cell growth readouts, and superior to potencies derived from single individual genes.

Our results show that gene-signature potencies are a novel valid alternative to conventional readouts for compound potency quantification, in particular in scenarios where no other established readouts are available.

Introduction

Gene expression signatures are widely used in the field of translational medicine to define disease sub-types [1], severity [2] and predict treatment outcome [3]. Bridging this technology to early drug discovery was previously proposed years ago [4, 5] but its prohibitive costs limited this approach. The recent advancement of massively parallel gene expression technologies such as RASL-seq [6], DRUG-seq [7], QIAseq [8, 9], PLATE-seq [10], or LINCS L1000 [11] are now transforming the field of compound profiling, enabling larger scale profiling and screening experiments at a more affordable cost [12-17].

In drug discovery, dose-response experiments enable researchers to compare the efficacy of various compounds to modulate biological processes of interest, finding doses for animal and human experiments and estimating windows to off-target and toxic effects. Multiple statistical methods are reported for the identification of individual genes with a dose dependent effect from dose-response gene expression data [18-23]. However, in the case of multivariate gene expression profiling there are no generally accepted methods to estimate the key pharmacological efficacy variables EC_{50} (compound concentration of half-maximal activating effect) and IC_{50} (compound concentration of half-maximal inhibitory effect) from multi-parametric readouts.

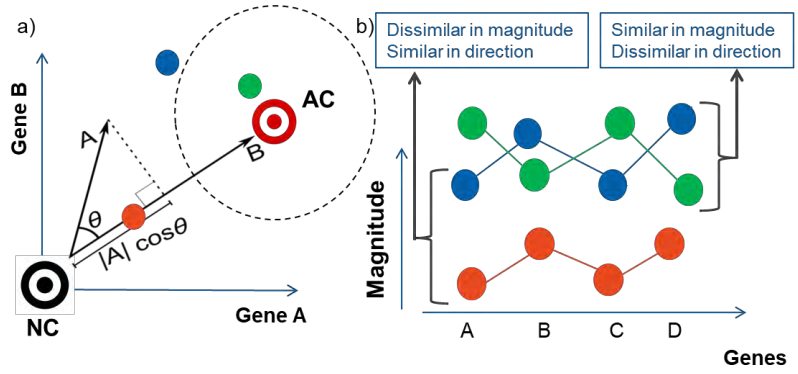

Figure 1. Introduction to gene-signature quantification methods. a) Within the manuscript, we consider methods measuring the similarity of gene-signature changes relative to an active control (AC) or a neutral control (NC). b) Two main characteristics of signature similarity can be distinguished: similar changes in magnitude or similar changes in the direction of the gene expression. The magnitude can be interpreted biologically as the efficacy, while the direction emphasizes the direction of the change of the phenotype, e.g. different pathways might result in different directions of changes in gene expression.

Connectivity Map (CMap) established the concept that compounds with similar mode of actions (MOAs) are highly similar in their differential expression profiles over many genes [4, 11, 24]. We postulate that this concept can be applied for quantifying compound potencies based on compound/pathway specific gene expression signatures. This work aims at defining and comparing several multivariate statistical summaries to enable classical compound potency estimation. In this study, we focus mainly on methods measuring the similarity of gene-signature changes relative to a gene-signature induced by an active control compound, representing a defined phenotype of interest, e.g. a tool compound for a target or pathway of interest. The overall principal relies on assessing the similarity of a compound-induced gene-signature profile relative to the one generated by an active control compound; hence, the AC profile will anchor all other measurements in the form of a global reference.

The different similarity methods explored in this paper differ by their approach to assess either the direction of the effect (as example by the geometric angle (cosine) to the AC; referred as direction-based

methods) and / or by how the magnitude of the effect is assessed (e.g. Euclidean distance to the NC, referred as magnitude-based methods). Combined, the two measures quantify the strength and direction of a phenotypic effect (see Fig. 1 and Table 1). Methods referred to as direction&magnitude-based combine both types of information into a single measure.

Table 1: Overview over gene-signature quantification methods.

Method	Description	Method class
cor_p_AC	Pearson correlation of the compound signature to the active control signature	direction
cor_s_AC	Spearman rank correlation of the compound signature to the active control signature	direction
cos_AC	Cosine of the compound signature to the active control signature	direction
cos_weight_AC	cos_AC * significance_weight. Idea: downweight cosine values for signatures with very small / non-significant amplitudes, likely caused by noise. Significance weight = weight from 0 to 1 quantifying the significance of the signal amplitude of the compound gene-signature vector. Formula: min(1, mean(abs(gene rscores)) /3). The mean of the absolute gene expression value rscores of the signature readouts divided by 3 equals 1, if on average the rscores of the signature are 3 standard deviations away from the background. This is considered the threshold from where on signals are considered strong enough not to be downweighted. This score requires the gene expression readouts to be scaled as rscores.	direction
dot_p_AC	Dot product of compound signature with the active control signature	direction&magnitude
scalar_projection_AC	Scalar projection of the signature to the active control signature	direction&magnitude
vec_norm	Norm of the compound signature vector	magnitude
euc_NC	Euclidean distance of compound signature from neutral control signature	magnitude
maha_NC	Mahalanobis distance of the compound signature from the neutral control signature	magnitude
num_readouts_changed	Number of readouts with signal different from background (abs(rscore) > 3)	magnitude
euc_AC	Euclidean distance of the compound signature to the active control signature	AC_similarity
maha_AC	Mahalanobis distance of the compounds signature to the active control signature	AC_similarity

For this study, two well-characterized biological pathways with multiple well-characterized ligands were selected: the beta-adrenergic receptor pathway for which we generated experimental biological data for this manuscript, and the EGFR pathway, which is publicly available through the LINCS L1000 project [11]. For the beta-adrenergic pathway we used cAMP EC_{50}s as functional orthogonal readout [25]. For practical purposes, we had to measure a small set of biologically relevant genes, instead of the full transcriptome like in CMap. RNA-seq was used to determine a beta-adrenergic receptor specific gene-signature that was subsequently used to quantify compound potencies on the level of gene expression. The L1000 assay is a panel of ca. 1000 measured genes, which are used to infer the differential gene expression of a total of ca. 13k genes. This allowed us to benchmark our methods using all L1000 genes, and subsets thereof specific for EGFR signaling or cell proliferation. The IC_{50}s calculated from gene expression were compared to compound potencies measuring the inhibition of cell growth rate (GR_{50}) [26].

Our results demonstrate that gene-signature-based compound EC_{50} and IC_{50} values estimated with multi-variate gene-signatures are highly related to potencies inferred with relevant but independent reference readouts. Therefore, we expect that these methods will find a wide application in gene-signature based assays in the near future. All methods in Table 1 and an EC_{50} and IC_{50} fitting method are made available in the R-package mvAC50 on github [https://github.com/Novartis/mvAC50].

Results

Generation of the beta-adrenergic receptor dataset

Vitamin-D3 differentiated THP1 cells were chosen as an experimental model for its sensitivity to beta agonists over a large dynamic range of compound concentrations and the ease of measuring cAMP [27]. To identify a gene-signature for beta agonists, a series of RNA-seq experiments were performed on THP1 cells sampled at baseline and after four hours stimulation with adrenaline, noradrenaline or isoproterenol.

Genes differentially expressed over all three treatments were identified, and prioritized for large fold change and high expression levels, for independent qPCR validation (Supplementary Fig. 1a). Our internal compound screening setup allows us to simultaneously multiplex the measurement of eight genes. Two independent sets of seven genes were defined from 14 qPCR validated genes (Supplementary Table 1, Supplementary Fig. 1b) with the eighth gene per set (TBP) serving as a baseline house keeper gene. For our analysis, we considered the two sets of genes as two independant signatures. Not all of these 14 identified genes produced a detectable signal in the QuantiGene Plex technology due to decreased sensitivity of this method compared to qPCR (Supplementary Fig. 1b). The two sets of genes contain respectively three (CD55, DOCK4, and NR4A1) and five genes (PDE4B, SGK1, THBS1, TOB1 and VEGFA) responding consistently to 10uM of isoproterenol.

Comparison of EC_{50}s from single genes, gene-signatures, and cAMP

A total of 21 beta agonists (Supplementary Table 2) covering a wide range of potencies (<10pM to ca. 5uM), were chosen for this study. Other cAMP modulators were also included in this compound set: the histamine receptor H3 antagonist N-alpha-methylhistamine and the adenylyl cyclase activator forskolin. As additional control, we added the beta-1 antagonist CGP-20712A, which, as expected, failed to increase cAMP levels. All compounds were measured in dose-response mode in the cAMP assay and for both gene signatures. An overview of dose-response curves of the genes is shown in Supplementary Fig. 2. The gene-expression data, derived gene-signature scores, and fitted EC_{50}s are presented in Supplementary Tables 3 and 4.

The relationship of EC_{50} values derived from genes and gene-signatures compared to cAMP-derived EC_{50}s depends on the gene-signature methods used. Representative examples for method classes are shown in Fig. 2a. (all methods and genes are shown in Supplementary Fig. 3). The EC_{50}s derived from direction-based methods cor_p_AC and cos_weight_AC are found almost entirely within a window of one log unit around the cAMP-derived EC_{50}s, which is very close considering the different incubation times and the different locations of the readouts in the adrenergic signaling pathway (gene expression vs cAMP). In contrast, the EC_{50}s derived from gene-signature methods containing magnitude information (scalar_projection_AC and vec_norm) and EC_{50}s from the individual genes NR4A1 and THBS1 are almost all more than one log unit above the cAMP-derived EC_{50}s. The ranking of cAMP potencies is not preserved as well (e.g. Spearman correlation for scalar_projection_AC to cAMP = 0.32).

A performance overview of all genes and gene-signature methods is given in Fig. 2b. The similarity between gene or gene-signature derived EC_{50}s with cAMP derived EC_{50}s over all tested compounds is quantified by the Pearson correlation between logged EC_{50}s. Most methods within one method-class performed equally well. While direction&magnitude and magnitude-based methods showed no significant difference to individual genes (TukeyHSD test with p-val < 0.05), direction-based methods performed significantly better than the other methods with Pearson correlations ranging between 0.6 and 0.9. All other method classes showed mean Pearson correlations < 0.5. The AC_similarity method performed significantly worse relative to others (only negative correlations).

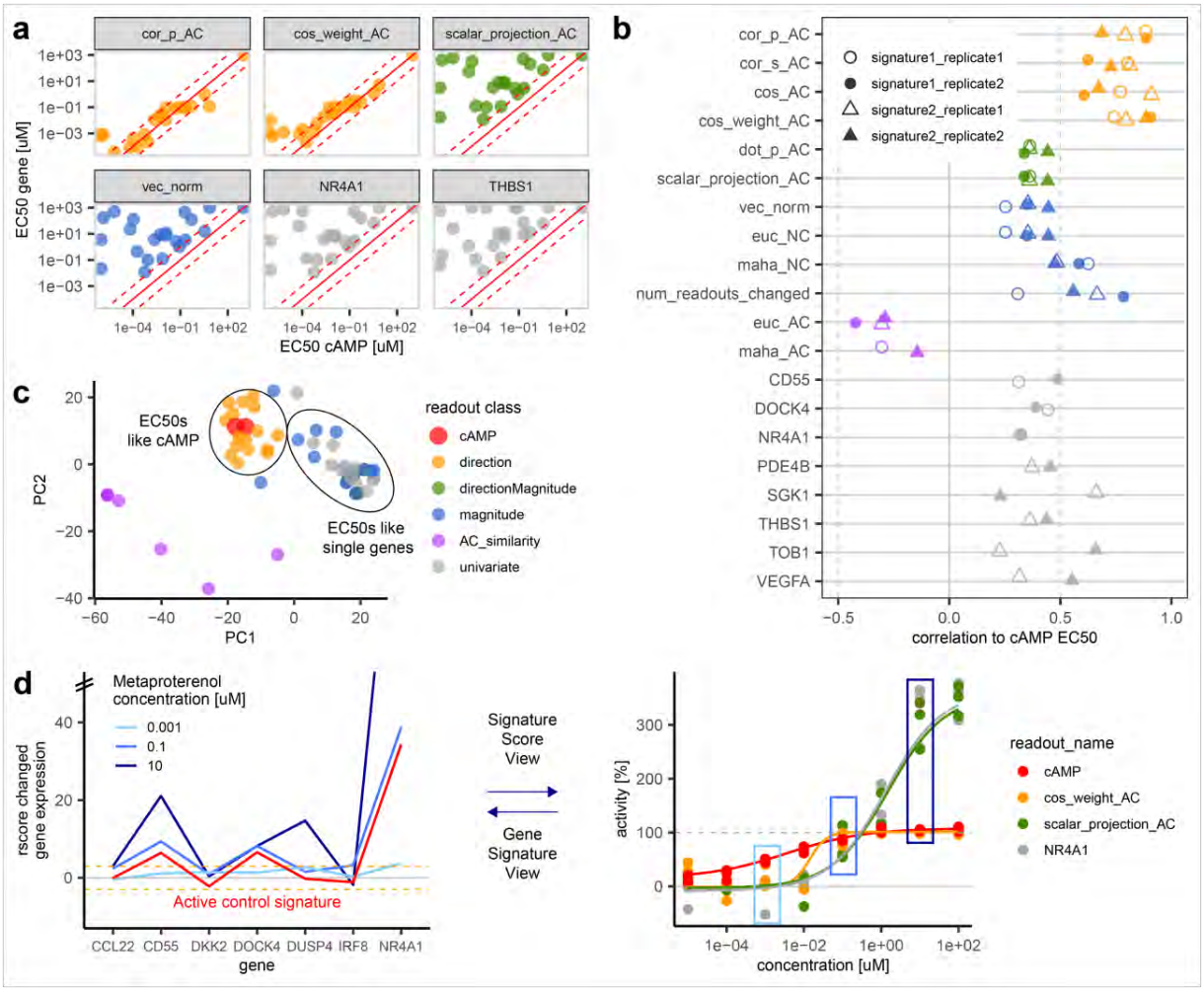

Figure 2: Comparison of EC_{50}s from gene-signatures, single-genes and cAMP for the beta agonists dataset. a) Example of gene and gene-signature EC_{50}s from representative methods compared to cAMP EC_{50}s. The dashed red lines indicates one log unit above and below the red line of equality. The shown gene and gene-signature EC_{50}s are from signature one, except THBS1 from signature two. The shown data is from replicate two. Axes are log10 transformed. b) Correlation of gene-signature and single-gene EC_{50}s with cAMP EC_{50}s. c) PCA of the cAMP, gene, and gene-signature summary methods logged EC_{50}s of all compounds in the dataset. Colors of a), b), and c) are according to the definition in c). d). Dose dependent change of the genes in the gene-signature (left panel, with y-axis values > 50 not shown, orange dashed lines at three rscores indicating significant changes from the background), compared with the dose dependent change in gene-signature summary score methods and cAMP for metaproterenol (right panel, boxes colored according concentrations shown in left panel, dashed grey line at 100% activity).

The relationship between all gene-signature methods, single genes and cAMP EC_{50}s is shown by a principle component analysis (PCA) projection of the dataset (Fig. 2c). Each data point represents the vector of logged EC_{50}s calculated by one method (for one replicate and one gene-signature) of all compounds in the dataset, Methods generating similar EC_{50}s are projected close to each other. The PCA

projection confirms that direction methods cluster together with the cAMP EC_{50}s, and all EC_{50}s containing magnitude information cluster together with single gene EC_{50}s. As mentioned above, the AC_similarity methods are outliers relative to the two major clusters.

Fig. 2d visualizes the expression levels of the individual genes over compound concentrations (left panel) and the resulting dose-response curves of derived multivariate EC_{50} methods (right panel). Increasing concentrations of metaproterenol result in increasing expression of the genes of the gene-signature. While the shape of the gene-signature remains similar to the active control signature (isoproterenol [10uM], red line), the magnitude of the metaproterenol signature exceeds the AC signature with increasing concentrations (left panel). The observed difference in gene expression magnitude between high concentrations of metaproterenol and the active control signature is only captured by metrics that make use of this information (Fig. 2d, right panel, green line). It is important to note that the difference between methods does not only lead to different maximal effect plateaus of the dose-response curve, but also to different EC_{50} values of the fitted curves.

The increase in gene expression beyond the active control also explains why AC_similarity methods cannot work in this scenario: the maximum similarity between compounds and AC signature is reached at identical magnitudes of both signatures. Both lower and larger magnitudes result in less similar signatures, resulting in bell shaped curves.

EGFR inhibitors dataset from L1000

For the L1000 EGFR ("Epidermal growth factor receptor") inhibitor dataset, we selected a set of eight EGFR inhibitors measured in six-point dose-response in MCF10A cells after 3h and 24h incubation time [11]. As reference univariate readout, the corresponding growth rate inhibition GR_{50} measured after three days was used [26]. As the LINC technology reported 12,717 genes, it was possible to test several gene-signatures: (1) a published EGFR signature [28], and (2) a published cell proliferation gene-signature [3], further referred to by the gene name "Targeting protein for Xklp2" (TPX2). As a third biologically unbiased gene-set, all genes from L1000 were used for comparison. We also investigated the performance of single gene measurements, for which we chose the 20 genes from each of the three signatures with the strongest response to the active control (gefitinib at 3.33uM).

Like with the beta agonist pathway data, gene-signature IC_{50}s of the EGFR inhibitors corresponded well to the reference GR_{50}s (Fig. 3a for representative readouts, all results in Supplementary Fig. 4-6). Results show a strong influence of the incubation time. At 24h all shown gene-signature methods over all three gene-signatures resulted in IC_{50} vs GR_{50} correlations >= 0.88, except scalar_projection_AC and vec_norm with the TPX2 gene-signature resulting in slightly lower correlations each of 0.68. The individual single gene IC_{50}s at 24h incubation showed more variance, with Pearson correlations ranging from -0.36 with the TPX2 signature to 0.9 with the EGFR signature. The individual genes from the EGFR signature resulted in the highest median correlation of 0.88. Two very similar median correlations of 0.68 and 0.69 were found for the individual genes of the TPX2 signature and from all L1000 genes, confirming the lower biological relevance for the EGFR pathway of the latter signatures. Even though all three gene-signatures contained individual genes that correlated very well with the GR_{50}s (> 0.9), all of them also contained genes with correlations to GR_{50}s < 0.5, few even around 0. It is not clear how one could reliably distinguish more relevant from less relevant genes in the absence of another orthogonal reference-readout like the GR_{50}s.

At 3h incubation time, differences between methods and gene-signatures are more pronounced, showing highest correlations for direction-based methods with the EGFR signature (both above 0.75). Again individual genes show a wide distribution of results ranging from -0.38 for TPX2 to ca. 0.85 for all three gene-sets. Like with the beta agonists, the values of gene-signature IC_{50}s are very close to the values

from GR_{50}s and more than 50% of the gene-signature IC_{50} values are within a one-log-unit window to the GR_{50}s (Fig. 3b).

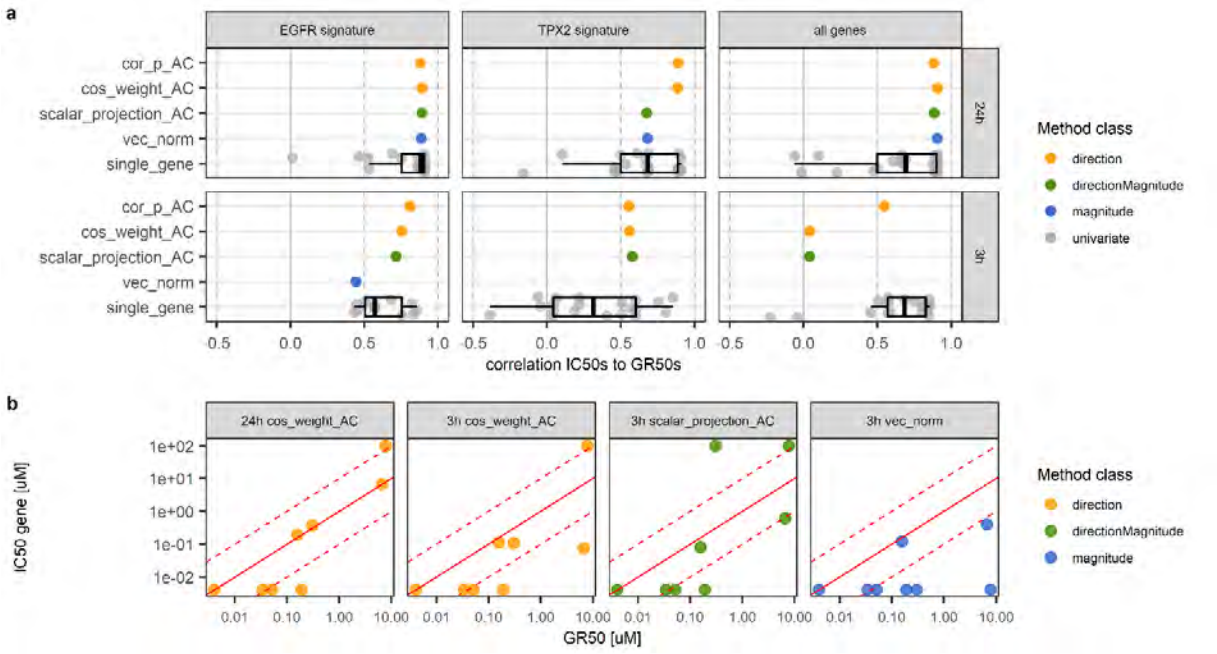

Figure 3. Comparison of gene and gene-signature IC_{50}s to growth rate inhibition GR_{50}s of EGFR inhibitors. a) Pearson correlation of representative methods and 20 individual gene IC_{50}s to GR_{50}s. b) Comparison of representative EGFR gene-signature IC_{50}s in MCF10A vs. GR_{50}s. The dashed red lines indicate one log unit above and below the red line of equality.

Discussion

The two main contributions of this work are: (1) the development and validation of an analytical framework for calculating compound potency based on multivariate readouts and (2) the provision of an open-source R-package to facilitate the application of our methods on new data by the scientific community.

The principal of this framework is to first summarize the information contained in multiple-genes into a single value and then pass it into a logistic function for potency estimation. The optimal metrics were selected based on their degree of concordance with compound potencies estimated with standard readouts (cAMP/GR_{50}).

The fact that IC_{50}/EC_{50} potency measurements are specific to a given biologic process (cAMP, gene expression, cell viability), and not a general property of the compound, is a potential challenge for comparing methods. However, choosing experimental models where gene expression is closely linked to pathway activation provides us confidence in our working model. The conservation of the compounds potency rank-order regardless of using gene expression or standard readouts supports our premise. Indeed, very close potency relationship (Pearson correlations up to 0.9) were observed for reference potency values (cAMP, GR_{50}) upstream (cAMP) and downstream (GR_{50}) of the gene expression readout, and independent of very different compound incubation times of readouts. The assessments of optimal

methods was not influenced by gene-signature composition. Indeed, all signatures used in this work were previously reported, or constructed independently of the screening datasets.

Of the five methodological classes of metrics: (1) direction-based, (2) distance based (magnitude) to the NC, (3) distance based (magnitude) to the AC, (4) magnitude and direction-based and (5) single genes, results show that magnitude-based methods to the AC clearly underperformed to other methods while direction-based methods performed consistently well in the two explored datasets. We did not find large differences in the performance of the methods within a single method class in these two datasets. Yet we recommend cos_weight_AC for direction-based methods due to its ability to down-weight signal with very small magnitude. To our surprise, adding information about the magnitude of the gene expression did not improve the results.

To this date, there is still very limited data available in the public domain that enables the comparison of multivariate EC_{50}/IC_{50} with standard readouts, hence it is impossible to generalized current findings to future situations. Nonetheless, with the raise of novel sequencing methods that enable low to medium throughput compound screening based on hundreds to thousands of genes, the need for multivariate potency estimation will be strong.

Finally, our work enables the of use gene-signatures as screening readouts and biomarkers throughout all stages of research from early cell line experiments, to animal models and clinical studies. Using the same readout will in many cases contribute to increased biological relevancy at all stage of the drug discovery process. Similar multiplexed readouts like the data from cell painting or metabolomics [29, 30] might also benefit from our multiplexed potency methods.

The publication of the first dedicated dataset to investigate the quantification of the dose-response based on gene-signatures together with the first analysis of such data and the publication of an R-package providing the methods for such analyses will enable the further exploration and application of these methods by the scientific community. The algorithms and datasets used in the publications are available in the R-package mvAC50 from https://github.com/Novartis/mvAC50 .

References

1. Perou, C.M., et al., *Molecular portraits of human breast tumours.* Nature, 2000. **406**(6797): p. 747-52.
2. Sotiriou, C., et al., *Gene expression profiling in breast cancer: understanding the molecular basis of histologic grade to improve prognosis.* J Natl Cancer Inst, 2006. **98**(4): p. 262-72.
3. Farmer, P., et al., *A stroma-related gene signature predicts resistance to neoadjuvant chemotherapy in breast cancer.* Nat Med, 2009. **15**(1): p. 68-74.
4. Lamb, J., et al., *The Connectivity Map: using gene-expression signatures to connect small molecules, genes, and disease.* Science, 2006. **313**(5795): p. 1929-35.
5. Scherf, U., et al., *A gene expression database for the molecular pharmacology of cancer.* Nat Genet, 2000. **24**(3): p. 236-44.
6. Li, H., J. Qiu, and X.D. Fu, *RASL-seq for massively parallel and quantitative analysis of gene expression.* Curr Protoc Mol Biol, 2012. **Chapter 4**: p. Unit 4 13 1-9.
7. Ye, C., et al., *DRUG-seq for miniaturized high-throughput transcriptome profiling in drug discovery.* Nat Commun, 2018. **9**(1): p. 4307.
8. Guibert, N., et al., *Amplicon-based next-generation sequencing of plasma cell-free DNA for detection of driver and resistance mutations in advanced non-small cell lung cancer.* Ann Oncol, 2018. **29**(4): p. 1049-1055.
9. Xu, C., et al., *Detecting very low allele fraction variants using targeted DNA sequencing and a novel molecular barcode-aware variant caller.* BMC Genomics, 2017. **18**(1): p. 5.

10. Bush, E.C., et al., *PLATE-Seq for genome-wide regulatory network analysis of high-throughput screens.* Nat Commun, 2017. **8**(1): p. 105.
11. Subramanian, A., et al., *A Next Generation Connectivity Map: L1000 Platform and the First 1,000,000 Profiles.* Cell, 2017. **171**(6): p. 1437-1452 e17.
12. Chen, M.H., et al., *Gene expression-based chemical genomics identifies potential therapeutic drugs in hepatocellular carcinoma.* PLoS One, 2011. **6**(11): p. e27186.
13. De Wolf, H., et al., *High-Throughput Gene Expression Profiles to Define Drug Similarity and Predict Compound Activity.* Assay Drug Dev Technol, 2018. **16**(3): p. 162-176.
14. Hahn, C.K., et al., *Proteomic and genetic approaches identify Syk as an AML target.* Cancer Cell, 2009. **16**(4): p. 281-94.
15. Hahn, C.K., et al., *Expression-based screening identifies the combination of histone deacetylase inhibitors and retinoids for neuroblastoma differentiation.* Proc Natl Acad Sci U S A, 2008. **105**(28): p. 9751-6.
16. Peck, D., et al., *A method for high-throughput gene expression signature analysis.* Genome Biol, 2006. **7**(7): p. R61.
17. Stegmaier, K., et al., *Gene expression-based high-throughput screening(GE-HTS) and application to leukemia differentiation.* Nat Genet, 2004. **36**(3): p. 257-63.
18. House, J.S., et al., *A Pipeline for High-Throughput Concentration Response Modeling of Gene Expression for Toxicogenomics.* Front Genet, 2017. **8**: p. 168.
19. Hu, J., et al., *Analysis of dose-response effects on gene expression data with comparison of two microarray platforms.* Bioinformatics, 2005. **21**(17): p. 3524-9.
20. Ji, R.R., et al., *Transcriptional profiling of the dose response: a more powerful approach for characterizing drug activities.* PLoS Comput Biol, 2009. **5**(9): p. e1000512.
21. Lin, D., et al., *Classification of Trends in Dose-Response Microarray Experiments Using Information Theory Selection Methods.* The Open Applied Informatics Journal, 2009(3): p. 34-43.
22. Lin, D., et al., *Testing for trends in dose-response microarray experiments: a comparison of several testing procedures, multiplicity and resampling-based inference.* Stat Appl Genet Mol Biol, 2007. **6**: p. Article26.
23. Pramana, S., et al., *IsoGene: An R Package for Analyzing Dose-response Studies in Microarray Experiments.* The R Journal, 2010. **2**(1): p. 5-12.
24. Duan, Q., et al., *L1000CDS(2): LINCS L1000 characteristic direction signatures search engine.* NPJ Syst Biol Appl, 2016. **2**.
25. Gabriel, D., et al., *High throughput screening technologies for direct cyclic AMP measurement.* Assay Drug Dev Technol, 2003. **1**(2): p. 291-303.
26. Hafner, M., et al., *Growth rate inhibition metrics correct for confounders in measuring sensitivity to cancer drugs.* Nat Methods, 2016. **13**(6): p. 521-7.
27. Farmer, P. and J. Pugin, *beta-adrenergic agonists exert their "anti-inflammatory" effects in monocytic cells through the IkappaB/NF-kappaB pathway.* Am J Physiol Lung Cell Mol Physiol, 2000. **279**(4): p. L675-82.
28. Creighton, C.J., et al., *Activation of mitogen-activated protein kinase in estrogen receptor alpha-positive breast cancer cells in vitro induces an in vivo molecular phenotype of estrogen receptor alpha-negative human breast tumors.* Cancer Res, 2006. **66**(7): p. 3903-11.
29. Abraham, Y., X. Zhang, and C.N. Parker, *Multiparametric Analysis of Screening Data: Growing Beyond the Single Dimension to Infinity and Beyond.* J Biomol Screen, 2014. **19**(5): p. 628-39.
30. Loo, L.H., L.F. Wu, and S.J. Altschuler, *Image-based multivariate profiling of drug responses from single cells.* Nat Methods, 2007. **4**(5): p. 445-53.
31. Liberzon, A., et al., *Molecular signatures database (MSigDB) 3.0.* Bioinformatics, 2011. **27**(12): p. 1739-40.
32. Subramanian, A., et al., *Gene set enrichment analysis: a knowledge-based approach for interpreting genome-wide expression profiles.* Proc Natl Acad Sci U S A, 2005. **102**(43): p. 15545-50.
33. Gubler, H., et al., *Helios: History and Anatomy of a Successful In-House Enterprise High-Throughput Screening and Profiling Data Analysis System.* SLAS Discov, 2018. **23**(5): p. 474-488.

Abbreviations

CMap: Connectivity Map

EC_{50} = Compound concentration of half-maximal activating effect.

IC_{50} = Compound concentration of half-maximal inhibitory effect.

AC_{50} = Compound concentration of half-maximal effect, independent of curve direction. General term including both EC_{50} and IC_{50}.

GR_{50} = Compound concentration of 50% reduction of the GR values, where the GR value is the ratio between growth rates under treated and untreated conditions normalized to a single cell division.

AC = active control.

NC = neutral control.

Methods

THP1 cells

Human promonocytic THP-1 cells (TIB-202, ATCC) were cultured at 37°C/CO_2 in medium (Hepes (72400-054, Life Technologies), with 10% FBS (2-01F16-I, Amimed/Bioconcept), 1% Pen/Strep (15140-122, Life Technologies), 1mM Sodium Pyruvate (11360-039, Life Technologies), 2mM L-Glutamine (25030-024, Life Technologies), 0.0mM Mercaptoethanol (31350-010, Life Technologies)). Before compound treatment and for all experiments, the THP1 cells were differentiated with 100nM Vitamin D_3 (Biotrend Chemicals AG, Switzerland, Cat. No. BG0684) for 3 days at 37°C/CO_2.

cAMP HTRF assay

The assay was run using the Cisbio cAMP dynamic 2 Kit (62AM4PEB), in white 384well-plates BioCoat #354661, with 20,000 cells/well in 10µL/well HBSS/HEPES/IBMX. Isoproterenol [10uM] was used as active control. Cells were incubated with compounds for 20 min. at 37°C in HBSS/HEPES, in the presence of the Phosphodiesterase (PDE) inhibitor IBMX. Then, cells were lysed and the amount of generated cAMP was quantified by HTRF (Homogeneous Time Resolved Fluorescence).

Beta agonists gene-signature.

RNASeq experiments were done comparing untreated cells with a treatment with isoproterenol, adrenaline or noradrenaline for 4h in THP1 cells.

qPCR was run in THP1 cells for 4h incubation time with isoproterenol and formoterol at 1, 10 and 100 nM. Total RNAs were isolated with MagMAX™-96 Total RNA Isolation Kit (Ambion ref#AM1830), and cDNA was made using a cDNA Synthesis Kit (Applied Biosystems™ Ref#4368813) RT-PCRs were performed in 384-well plates on an AB7900HT cycler (Applied Biosystems) using specific TaqMan probes (Applied Biosystems). Housekeeper normalization was done relative to the one of the three genes GAPDH, PPIB or TBP, which had the most similar expression level to the gene of interest, according to our DMSO qPCR data. All measurements were done in quadruplicates.

QuantiGene Plex assay

Gene expression changes were measured using a customized QuantiGene Plex assay (Thermo Fisher Scientific).

Two different eight-gene-signatures were designed (obtained from Thermo Fisher Scientific), as the internal QuantiGene process was set up to handle custom-designed signatures of eight genes. Each of the eight-gene-signatures consisted of seven target genes responding to cAMP and one housekeeper gene (TBP).

Measurements were done in THP1 cells. Compounds were measured in six replicates on the same day on different plates, and the procedure was repeated on another day using three replicates on different plates (referred to as biological replicates in the manuscript).

For the assay, 100,000 cells were seeded in a volume of 20uL in each well of a 384 well plate (Greiner PP V bottom 781280). Compounds were added in serial dilutions of 1:10 (200nL volume added per well) with maximal compound concentrations of 100uM. After 4h incubation, cells were lysed with QuantiGene lysis mixture (10uL), and after 2 min, stored at -80°C.

Targeted mRNA transcripts were captured to their respective beads by combining lysis mixture (5uL), blocking reagent (2uL), probe mix (1.125uL), water (11.25uL), and magnetic beads (0.3 uL; 500 beads/region/uL) and incubated overnight.

Signal amplification via branched DNA is added by sequential hybridization of 2.0 Pre Amplifier biotinylated label probe, and binding with Steptavidin-conjugated Phycoerythrin (SAPE). For this purpose, each 15uL/well pre-amplifier, amplifier and label probe & SAPE were added after washing followed by 1h incubation at 50°C and multitron shaking 300rpm 1h.

The amount of RNA in 90uL of probe was quantified using a Luminex Flexmap 3D instrument (Luminex). The identity of the mRNA is encoded by the hybridized Luminex beads, and the level of SAPE fluorescence is proportional to the amount of mRNA transcripts captured by the respective beads.

QuantiGene Plex data processing

The raw readout of the assay was processed as follows:

1. Fold change = 50 * $\log_2$ (mRNA count / median mRNA count for NC well)

2. Rscore = (Fold change for well – median Fold change for NC wells) / MAD (mRNA count for NC wells)

3. HKnorm = Rscore for well – HK_Rscore for well; with HK = housekeeper gene.

L1000 / GR_{50} dataset

EGFR inhibitors in MCF10A cells were selected as model system, because (1) they showed a strong GR_{50} dynamic range (Dose-response curves visualization http://www.grcalculator.org/grbrowser/.), and (2) were measured in six concentrations in L1000 (10uM, 3.33uM, 1.11uM, 0.37uM, 0.12uM, 0.04uM).

The L1000 data was obtained in two files (GSE70138_Broad_LINCS_Level4_ZSVCINF_mlr12k_n78980x22268_2015-06-30.gct.gz and GSE70138_Broad_LINCS_Level4_ZSVCINF_mlr12k_n115209x22268_2015-12-31.gct.gz) from NCBI GEO (https://www.ncbi.nlm.nih.gov/geo/query/acc.cgi?acc=GSE70138).

This version of the data contains the changed gene-expression normalized as z-scores relative to the DMSO controls on each plate, a similar normalization procedure to the one performed for the beta-

agonists expression data. When multiple probes were measured for the same gene_symbol, the probe with the highest variance was kept, for each timepoint. The gefitinib treatment at 3.33 uM was defined as the active control of the experiment. Compounds, smiles, and inchi_key were downloaded from the LINCS webpage (http://lincs.hms.harvard.edu/db/datasets/20000/).

From the 12,727 genes in the L1000 dataset, two different subsets were selected based on published gene-signatures. An EGFR (entrez gene_id 1956) signature [28] ("EGFR_UP.V1_UP" with 193 genes, "EGFR_UP.V1_DN" with 196 genes) was downloaded from msigdb [31, 32], of which a total of 381 genes could be mapped to the L1000 data. This gene-signature was derived from profiling of MCF-7 cell lines stably overexpressing ligand-activatable EGFR. A TPX2 (entrez gene_id 22974) signature (50 genes, of which 39 could be mapped to L1000) was taken from Farmer et al [3], representing a more general signature for cell proliferation.

The GR_{50} cell viability potency values after three days compound incubation time were also obtained from the LINCS consortium (http://lincs.hms.harvard.edu/db/datasets/20252/results). To make the data more comparable to the fitted IC_{50}'s from the gene-signatures, compounds with flat GR_{50} dose-response curves were set to either one log unit above or below the highest or lowest tested concentration, depending whether their fitted GRInf value was larger or smaller than 0.5.

As the files from L1000 and the GR_{50}s contained slightly different compound and cell line names, the names were set all to lowercase and whitespaces and "-" were removed. Eight known EGFR inhibitors afatinib, neratinib, pelitinib, gefitinib, erlotinib, canertinib, lapatinib, and HG-5-88-01 overlapped between the two datasets. The two EGFR/ERBB2 dual inhibitors neratinib and afatinib were considered as EGFR inhibitors for this study (even though they are annotated as ERBB2 inhibitors in the LINCS nominal target annotation).

Dose-response (DRC) fitting

Four-point parametric logistic fits were calculated with an R function included in the mvAC50 R-package [https://github.com/Novartis/mvAC50]. The fitting algorithm was adopted from our in-house HTS analysis software Helios [33]. The fits were constrained to A0 and Ainf (minimal and maximal fitted activities) between -50% and 500% of the active control effect, respectively, and a hill slope between 0.1 and 10. The IC_{50}s or EC_{50}s were constrained to one log unit above and below the experimentally measured range of concentrations, (for the beta agonists ranging from 0.00001uM to 100uM, and for the L1000 data ranging from 0.04uM to 10uM)

In the case of constant fits, IC_{50} or EC_{50} values one-log unit above or below the range of tested concentrations were assigned to the compounds to be able to use those data points as well in the correlation of calculated potencies to the reference potencies. Depending on whether the Amax of the constant fit was below or above 50%, a potency of either one log unit below or above the tested concentration range was assigned. Fitted AC_{50}s with Ainf values < 50% were set to one log unit above the highest tested concentration as well, assuming that the observed effect is not caused by the same mode of action as in the active control.

In parallel to the four-point parametric fit and constant fits, a nonparametric fit was also calculated and compared to the other fits, to allow for more unusual curve shapes, e.g. bell shaped curves. For these fits the reported potency is the concentration at which the fit crosses the line of 50% activity. The decision for the reported fit and potency was done as follows: If the non-parametric fit resulted in r2 < 0.5, the data was considered as not suitable for curve fitting and assigned as constant fit. If the curve had a bell-shape, the nonparametric potency was reported. If parametric fits had r2 < 0.5 or the absolute (amin-amax) < 30, a constant fit was reported as well, where amin and amax correspond to A0 and Ainf within the measured concentration range. For the remaining curves (the majority) parametric potencies were reported.

cAMP EC_{50}s were fitted with the same algorithm and settings, to ensure a higher consistency in the data. The fitted cAMP EC_{50}s were in agreement with the fits generated by the biologists who ran the assays. For the GR_{50} dataset this approach was not feasible, as no raw data was available, and the GR_{50} algorithm was claimed to be superior to four-point parametric fits of the same data [26].

Acknowledgment

We would like to acknowledge Stan Lazic, Xian Zhang, and Jeremy Jenkins for helpful discussions about the concept of multivariate AC_{50}s, Wendy Broom, Elaine Donohue and Jacques Hamon for help with the QuantiGene assay, Magalie Mathies for help with setting up the THP-1 assays, Pierre Rigo, Thomas Hoerter, Cornelia Mouzo and Valerie Heidinger for production of THP-1 cells, Ioannis Moutsatsos for help with the QuantigGene analysis pipeline, and Pascale Anderle for referring Andrea Amati as NIBR intern for this project.

Supplementary Information

Supplementary Table 1: Genes selected for quantification of beta agonist potencies.

Gene symbol	Gene id	Name	Set	Comment
CCL22	6367	C-C motif chemokine ligand 22	1	
CD55	1604	CD55 molecule (Cromer blood group)	1	
DKK2	27123	dickkopf WNT signaling pathway inhibitor 2	1	
DOCK4	9732	dedicator of cytokinesis 4	1	
DUSP4	1846	dual specificity phosphatase 4	1	
IRF8	3394	interferon regulatory factor 8	1	
NR4A1	3164	nuclear receptor subfamily 4 group A member 1	1	
TBP	6908	TATA-box binding protein	1	Housekeeper
NR4A3	8013	nuclear receptor subfamily 4 group A member 3	2	
PDE4B	5142	phosphodiesterase 4B	2	
PPARGC1B	133522	PPARG coactivator 1 beta	2	
SGK1	6446	serum/glucocorticoid regulated kinase 1	2	
THBS1	6908	TATA-box binding protein	2	
TOB1	7057	thrombospondin 1	2	
VEGFA	10140	transducer of ERBB2, 1	2	
TBP	7422	vascular endothelial growth factor A	2	Housekeeper

Supplementary Table 2: Overview over compounds used in THP1 experiments, comparing cAMP and QuantiGene readouts.

Compound	MOA	Inchi_key	Smiles	EC_{50} repl1	Amax repl1	EC_{50} repl2	Amax repl2
(+/-)-isoproterenol	beta agonist	JWZZKOKVBUJMES-UHFFFAOYSA-N	CC(C)NCC(O)c1ccc(O)c(O)c1	0.00008	109	< 0.00001	110
terbutaline	beta agonist	XWTYSIMOBUGWOL-UHFFFAOYSA-N	CC(C)(C)NCC(O)c1cc(O)cc(O)c1	0.713	101	0.202	98
fenoterol	beta agonist	LSLYOANBFKQKPT-UHFFFAOYSA-N	CC(Cc1ccc(O)cc1)NCC(O)c2cc(O)cc(O)c2	0.0036	106	0.0013	111
adrenaline	beta agonist	UCTWMZQNUQWSLP-VIFPVBQESA-N	CNC[C@H](O)c1ccc(O)c(O)c1	0.139	106	0.0171	115
metaproterenol	beta agonist	LMOINURANNBYCM-UHFFFAOYSA-N	CC(C)NCC(O)c1cc(O)cc(O)c1	0.0036	108	0.0141	111
isoetharine	beta agonist	HUYWAWARQUIQLE-UHFFFAOYSA-N	CCC(NC(C)C)C(O)c1ccc(O)c(O)c1	0.0012	93	0.0115	108
BRL 37344	beta agonist	ZGGNJJJYUVRADP-UHFFFAOYSA-N	CC(Cc1ccc(cc1)OCC(O)=O)NCC(O)c2cccc(Cl)c2	0.0282	84	0.0984	91
ritodrine	beta agonist	IOVGROKTTNBUGK-SJCJKPOMSA-N	C[C@H](NCCc1ccc(O)cc1)[C@H](O)c2ccc(O)cc2	0.846	91	0.51	83
norepinephrine	beta agonist	SFLSHLFXELFNJZ-QMMMGPOBSA-N	NC[C@H](O)c1ccc(O)c(O)c1	0.0002792	109	0.0005829	115
procaterol	beta agonist	FKNXQNWAXFXVNW-BLLLJJGKSA-N	CC[C@H](NC(C)C)[C@H](O)c1ccc(O)c2NC(=O)C=Cc12	0.008542	93	0.00013	102
dobutamine	beta agonist	JRWZLRBJNMZMFE-UHFFFAOYSA-N	CC(CCc1ccc(O)cc1)NCCc2ccc(O)c(O)c2	0.0008564	106	0.00242	106
abediterol	beta agonist	SFYAXIFVXBKRPK-QFIPXVFZSA-N	O[C@@H](CNCCCCCCOCC(F)(F)c1ccccc1)c2ccc(O)c3NC(=O)C=Cc23	< 0.00001	101	< 0.00001	105
olodaterol	beta agonist	COUYJEVMBVSIHV-SFHVURJKSA-N	COc3ccc(CC(C)(C)NC[C@H](O)c2cc(O)cc1NC(=O)COc12)cc3	0.00001869	97	< 0.00001	102
batefenterol	beta agonist	URWYQGVSPQJGGB-DHUJRADRSA-N	COc4cc(NC(=O)CCN1CCC(CC1)OC(=O)Nc2ccccc2c3ccccc3)c(Cl)cc4CNC[C@H](O)c5ccc(O)c6NC(=O)C=Cc56	0.0021	101	1.89E-04	101
vilanterol	beta agonist	DAFYYTQWSAWIGS-DEOSSOPVSA-N	OCc1cc(ccc1O)[C@@H](O)CNCCCCCCOCCOCc2c(Cl)cccc2Cl	0.00001721	96	< 0.00001	98
tulobuterol	beta agonist	YREYLAVBNPACJM-UHFFFAOYSA-N	CC(C)(C)NCC(O)c1ccccc1Cl	0.016	68	0.0366	50
salbutamol	beta agonist	NDAUXUAQIAJITI-UHFFFAOYSA-N	CC(C)(C)NCC(O)c1ccc(O)c(CO)c1	0.02	89	0.004285	88
zinterol	beta agonist	XJBCFFLVLOPYBV-UHFFFAOYSA-N	CC(C)(Cc1ccccc1)NCC(O)c2ccc(O)c(c2)NS(C)(=O)=O	< 0.00001	99	0.00004344	95
tretoquinol	beta agonist	RGVPOXRFEPSFGH-UHFFFAOYSA-N	COc3cc(CC1NCCc2cc(O)c(O)cc12)cc(OC)c3OC	0.00005932	101	< 0.00001	105
dopexamine	beta agonist	RYBJORHCUPVNMB-UHFFFAOYSA-N	Oc2ccc(CCNCCCCCCNCCc1ccccc1)cc2O	4.1	56	5.837	62
formoterol	beta agonist	BPZSYCZIITTYBL-YJYMSZOUSA-N	COc2ccc(C[C@@H](C)NC[C@H](O)c1ccc(O)c(c1)NC=O)cc2	0.00001267	106	0.0000231	109
forskolin	AC activator	OHCQJHSOBUTRHG-KENMSXPPSA-N	CC(=O)OC2C(O)[C@H]1C(C)(C)CC[C@H](O)[C@]1(C)[C@@]3(O)C(=O)C[C@](C)(C=C)O[C@]23C	6.283	90	3.757	104
N-alpha-methylhistamine	histamine H3 antagonist	PHSPJQZRQAJPPF-UHFFFAOYSA-N	CNCCC1=CNC=N1	0.161	98	0.199	102
CGP-20712A	beta-1 antagonist	GKJZEKSHCJELPL-UHFFFAOYSA-N	CN1C=C(N=C1c2ccc(cc2)OCC(O)CNCCOc3ccc(O)c(c3)C(N)=O)C(F)(F)F	> 100	-17	> 100	-19

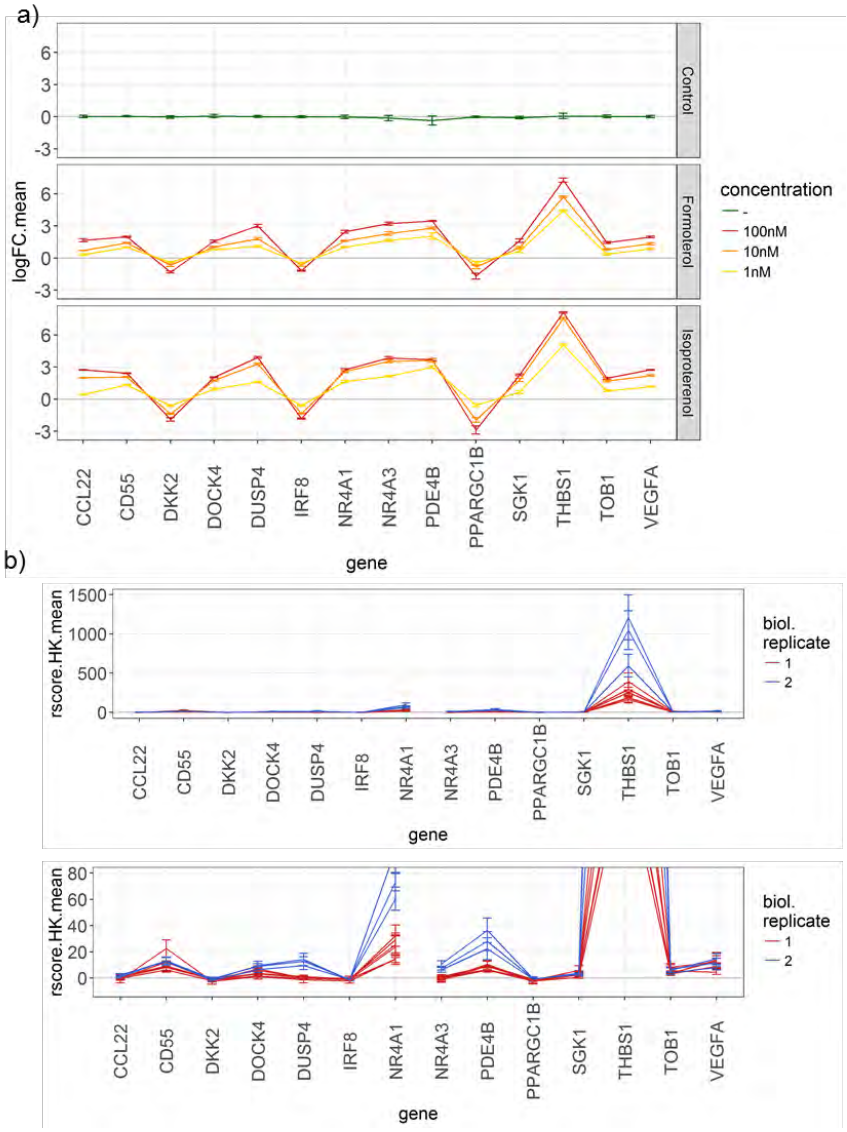

Supplementary Figure 1: Validation of the beta agonists gene-signature. a) qPCR results for DMSO, formoterol and isoproterenol demonstrate dose dependent effect on genes after 4h incubation. b) QuantiGene Plex results for the two gene-signatures for 10uM of isoproterenol after 4h incubation, shown at two different scales: upper = full scale with THBS1 having a much stronger response than the other genes, and lower = y-axis cut at 80 to visualize the genes with lower variance. Shown are mean standard deviations of the rscore_HK values of active control wells of each plate.

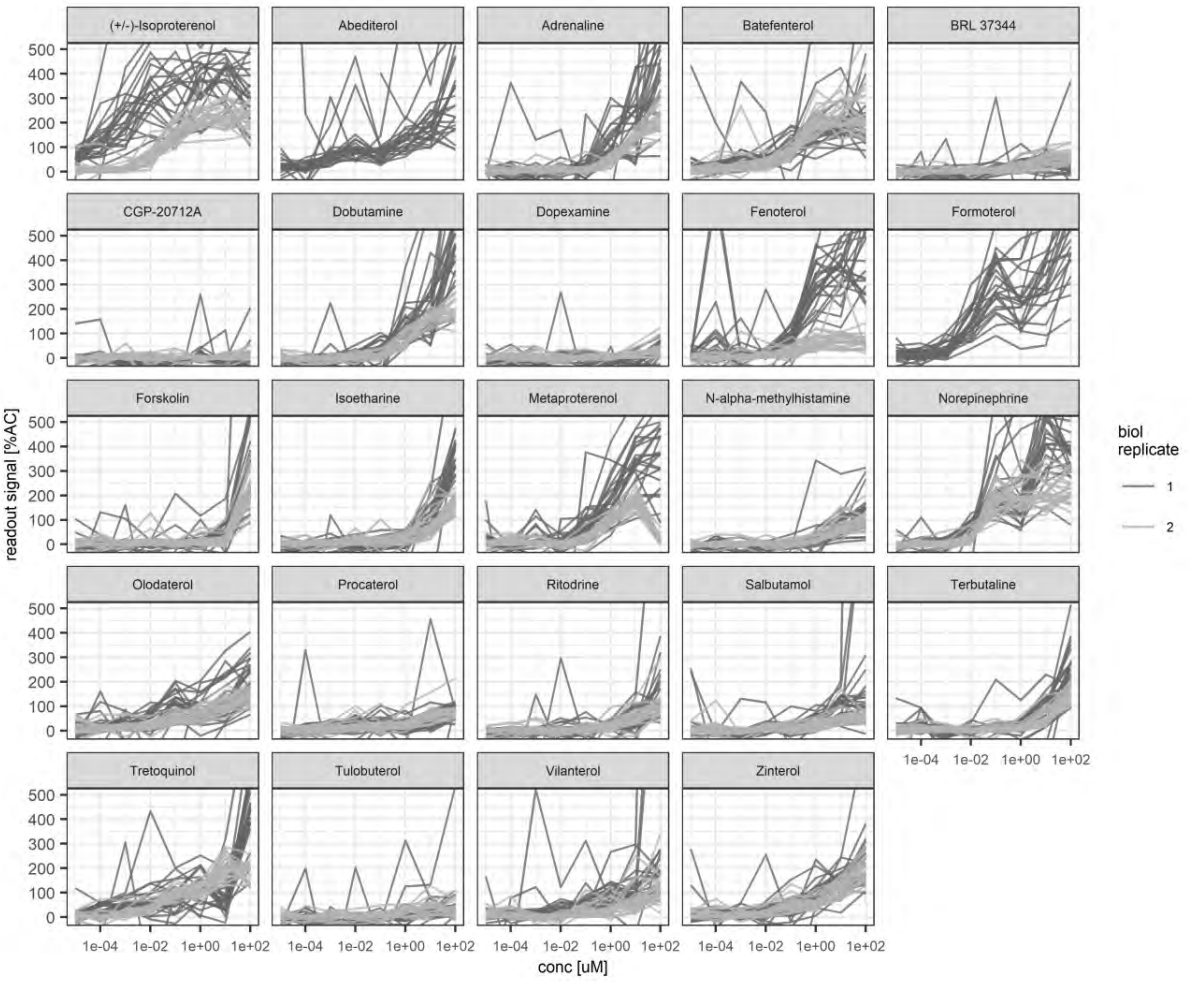

Supplementary Figure 2: Dose-response of genes for each compound in the beta agonists dataset.

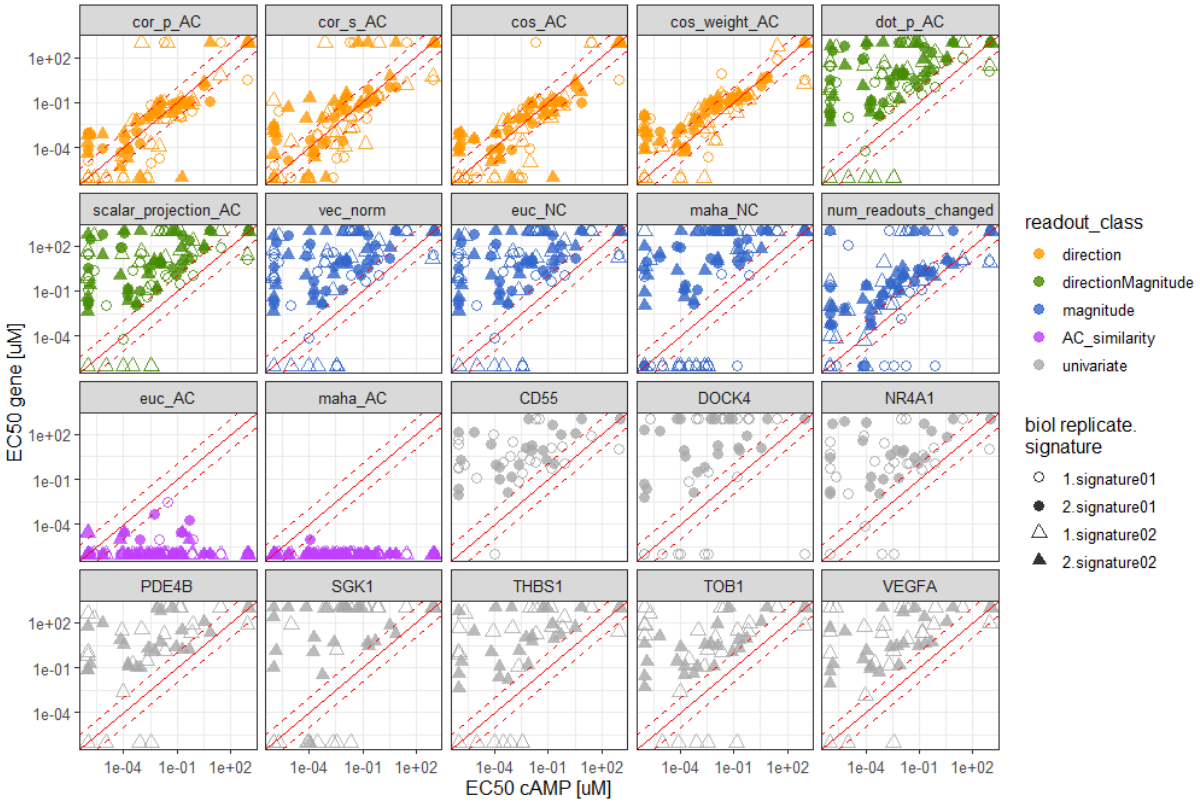

Supplementary Figure 3: Correlation of gene and gene-signature EC_{50}s with cAMP EC_{50}s of the beta agonist dataset.

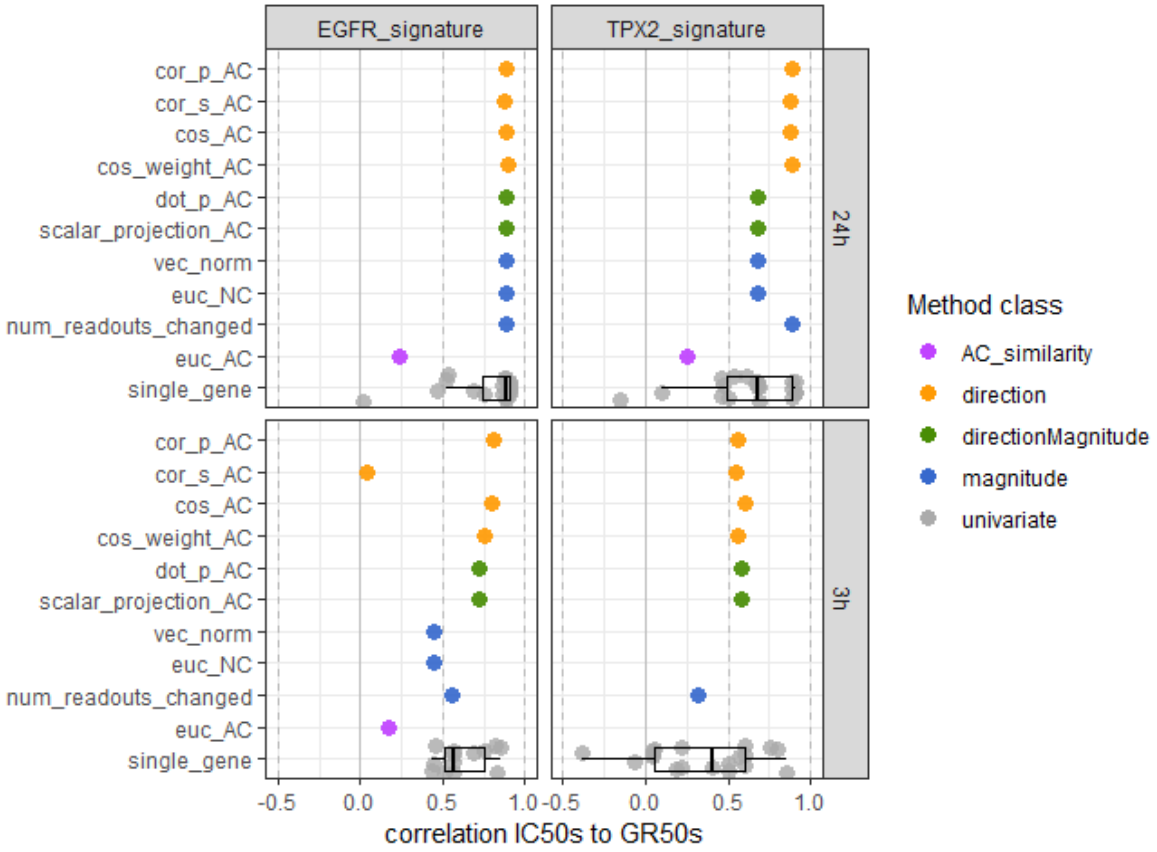

Supplementary Figure 4: Correlation of cell growth inhibition GR_{50}s with all gene and gene-signature EC_{50}s of the EGFR inhibitor dataset.

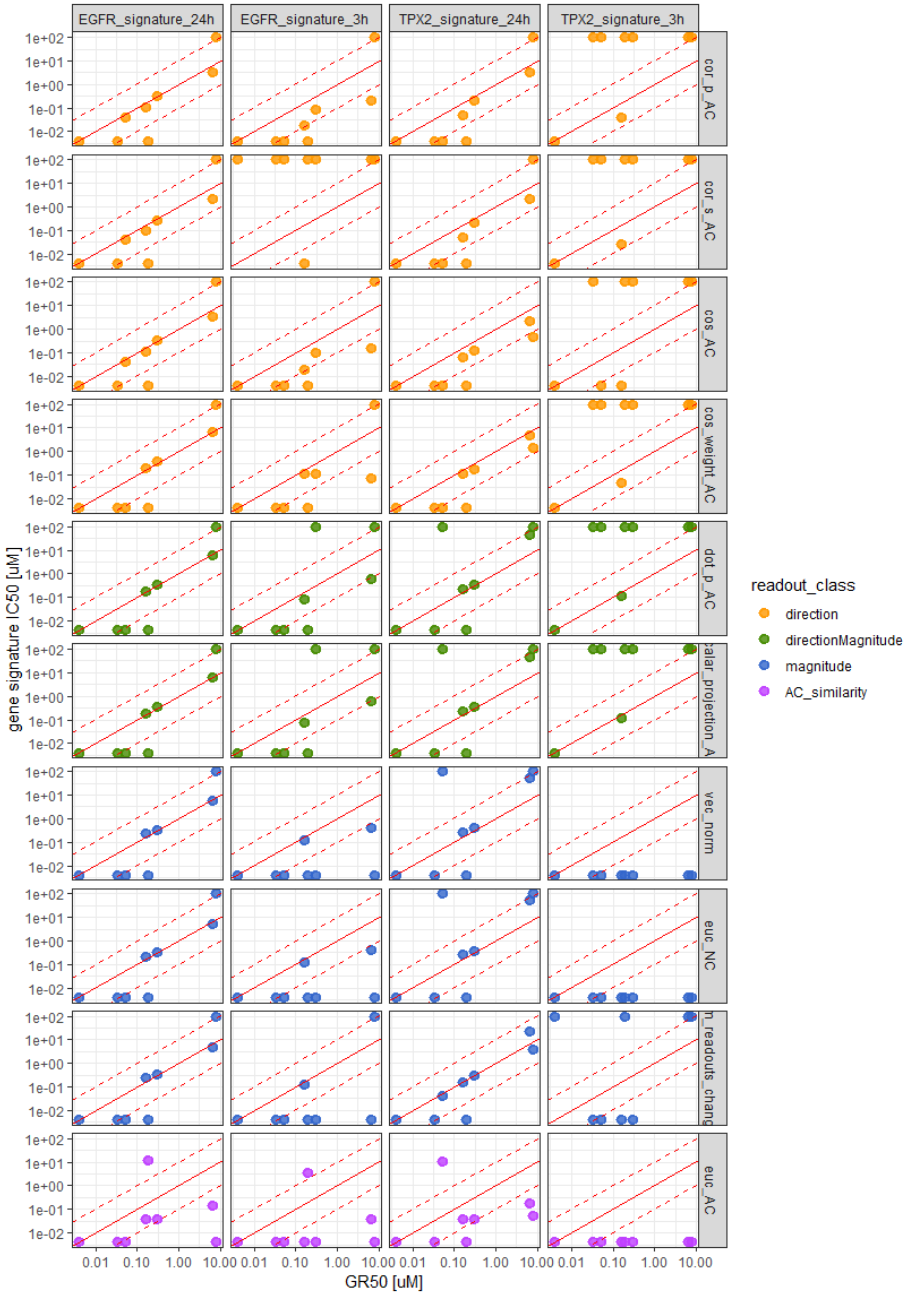

Supplementary Figure 5: Correlation of gene-signature IC_{50}s to GR_{50}s of the EGFR inhibitor dataset.

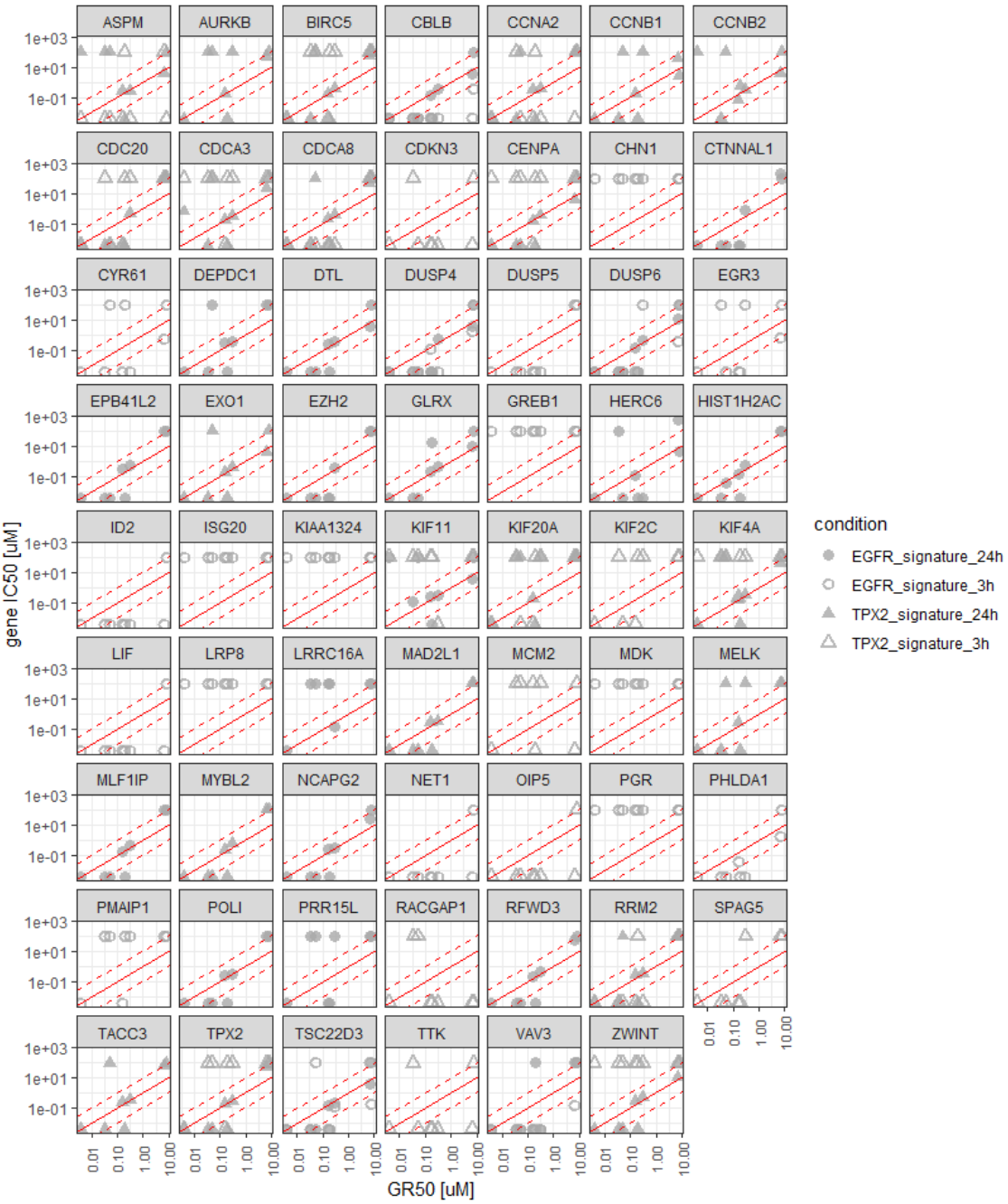

Supplementary Figure 6: Correlation of single gene IC_{50}s to GR_{50}s of the EGFR inhibitor dataset, for the 20 genes most responding to the active control from the EGFR and TPX2 signatures.

8.2.3 Publication II.

Measuring membrane protein function in unilamellar vesicles

Andrea Marco Amati*, Simone Sandra Graf*, Sabina Deutschmann*, Nicolas Dolder*, Christoph von Ballmoos

* contributed equally

Manuscript submitted upon invitation to Biochemical Society Transactions.

Manuscript will be included here asap.

8.3 Declaration of Originality.

Declaration of Originality

Last name, first name: Amati, Andrea Marco
Matriculation number: 09-106-758

I hereby declare that this thesis represents my original work and that I have used no other sources except as noted by citations.
All data, tables, figures and text citations which have been reproduced from any other source, including the internet, have been explicitly acknowledged as such.
I am aware that in case of non-compliance, the Senate is entitled to withdraw the doctorate degree awarded to me on the basis of the present thesis, in accordance with the "Statut der Universität Bern (Universitätsstatut; UniSt)", Art. 69, of 7 June 2011.

Place, date

Bern, 31.03.2020

Signature

No one will hit you harder than life itself. It doesn't matter how hard you hit back. It's about how much you can take, and keep fighting, how much you can suffer, and keep moving forward. That's how you win.
— *Sylvester Stallone*

PhD.
abbreviation [pee-eych-dee]
An academic who has learned more and more about less and less so that eventually they know everything about nothing at all.